JSCSEN 78(4)563–609(2013)

ISSN 1820-7421(Online)

Journal of the Serbian Chemical Society

Electronic Version

VOLUME 78

No 4

BELGRADE 2013

Available on line at

www.shd.org.rs/JSCS/

Journal of the Serbian Chemical Society
JSCS-info@shd.org.rs • www.shd.org.rs/JSCS

J. Serb. Chem. Soc. Vol. 78, No. 4 (2013)

CONTENTS

Published by the Serbian Chemical Society
Karnegijeva 4/III, 11000 Belgrade, Serbia
Printed by the Faculty of Technology and Metallurgy
Karnegijeva 4, P.O. Box 35-03, 11120 Belgrade, Serbia

Available online at www.shd.org.rs/JSCS/

Journal of the Serbian Chemical Society
JSCS-info@shd.org.rs • www.shd.org.rs/JSCS
J. Serb. Chem. Soc. 78 (4) 463–468 (2013) UDC 547.753/.756+542.913+546.74:544.412.3
JSCS–4429 *Original scientific paper*

A novel approach to bis(indolyl)methanes using nickel nanoparticles as a reusable catalyst under solvent-free conditions

ABOLFAZL OLYAEI[1]*, MOHSEN VAZIRI[1], REZA RAZEGHI[1], BAHAREH SHAMS[1] and HASAN BAGHERI[2]

[1]*Department of Chemistry, Payame Noor University, P. O. Box 19395–3697, Tehran, Iran and* [2]*Department of Chemistry, Takestan Branch, Islamic Azad University, Takestan, Iran*

(Received 6 May, revised 10 July 2012)

Abstract: Nano-sized nickel as a catalyst has been developed for the electrophilic substitution reactions of indole with various aromatic aldehydes under solvent-free conditions to afford the corresponding bis(indolyl)methanes in high to excellent yields. The described method has promising features, such as no hazardous organic solvents or catalysts, short reaction time, high product yields, simple work-up procedure, reusable catalyst and easy product separation without further purification with column chromatography.

Keywords: indole; aldehyde; electrophilic substitution; Nickel.

INTRODUCTION

The efficiency of heterogeneous catalysis in organic synthesis can be improved by employing nano-sized catalysts because of their extremely small size and large surface to volume ratio. It was recently demonstrated that Ni nanoparticles as catalysts offer great opportunities for a wide range of applications in organic synthesis and chemical manufacturing processes, including the chemoselective oxidative coupling of thiols,[1] reduction of aldehydes and ketones,[2–4] hydrogenation of olefins[5] and supports for hydrogen adsorption.[6] Thus, the remarkable catalytic activity and easy synthesis, simplicity and reusability of Ni nanoparticles encouraged the present utilization of them as a catalyst for the synthesis of bis(indolyl)methanes (BIM).

Development of bis(indolyl)alkane (BIA) derivatives has been of considerable interest in organic synthesis because of their wide occurrence in various natural products possessing biological activity[7] and usefulness for drug design. BIM are substances found in cruciferous plants that exhibit activity promoting beneficial estrogen metabolism and inducing apoptosis in human cancer cells.[8] Consequently, a number of synthetic methods for the preparation of BIA deri-

* Corresponding author. E-mail: Olyaei_a@pnu.ac.ir
doi: 10.2298/JSC120506076O

vatives by reaction of indole with various aldehydes and ketones in the presence of either a Lewis acid or a protic acid have been reported in the literature.[9–16] In recent years, environmentally safer synthetic methods have received considerable attention and some solvent-free protocols have been developed. The synthesis of BIM under solvent-free conditions may be performed using catalysts such as I_2[17] and $ZrOCl_2 \cdot 8H_2O$/silica gel.[18] These previous methods generally involved difficult handling, a stoichiometric amount of catalyst may be needed, and require tedious aqueous work-up, along with the use of environmentally harmful organic solvents.

In view of the importance of BIA derivatives, the use of nano-sized nickel[19] as catalyst in the reaction of indole with aromatic aldehydes under solvent-free conditions is reported herein. As such, the method provides the product *via* easy work-up and is in accord with green sustainable chemistry principles.

EXPERIMENTAL

All commercially available chemicals and reagents were used without further purification. Melting points were determined using an electrothermal model 9100 apparatus and are uncorrected. The IR spectra were recorded on a Shimadzu 4300 spectrophotometer. The ^{1}H- and ^{13}C-NMR spectra were recorded in DMSO-d_6 on Bruker DRX-500 Avance spectrometer. Chemical shifts (δ) are reported in ppm and are referenced to the NMR solvent. Mass spectra of the products were obtained with an HP 5937 (Agilent Technologies) mass selective detector. Elemental analyses were performed using a CHN–O–Rapid Heraeus elemental analyzer (Wellesley, MA, USA).

*General procedure for the synthesis of bis(indolyl)methanes **3***

To a mixture of indole (2 mmol) and aromatic aldehyde (1 mmol) was added nickel nanoparticle powder (10 mol %). The reaction mixture was magnetically stirred on a preheated oil bath at 80 °C for the appropriate time as indicated in Table I. After completion of the reaction, as indicated by TLC, the reaction mixture was cooled to room temperature. Then, ethanol (5 mL) was added. The nanoparticles were recovered by centrifuging the organic layer and reutilized for the same reaction. The solution was poured into water (50 mL). The precipitate that formed was filtered, washed with water and dried. The crude product was stirred for 5 min in boiling *n*-hexane and the resulting precipitate was filtered. The thus obtained product **3** was found to be pure upon TLC examination.

RESULTS AND DISCUSSION

In continuation of work on the development of solvent-free conditions in one-pot, multi-component reactions,[20–24] it was observed that the treatment of indole with aromatic aldehydes in the presence of nickel catalyst under solvent-free conditions afforded the corresponding BIM derivatives. As a model reaction, the reaction of indole (2 mmol) with benzaldehyde (1 mmol) was initially examined at 70–120 °C in the presence of nano-sized nickel powder (10 mol %) as catalyst under solvent-free conditions. The investigation demonstrated that the best result was obtained when the temperature was fixed at 80 °C and the reaction was completed in 1 h. Thereby, an excellent yield of bis(3-indolyl)phenyl-

methane (**3a**) was obtained (95 %). To determine the appropriate concentration of the Ni nanoparticles catalyst, the model reaction of benzaldehyde and indole was investigated at different concentrations of the catalyst. This indicated that 10 mol % of nano-sized Ni produced the best results with respect to product yield (Table I).

TABLE I. Comparison of the amount of Ni and yields for the synthesis of BIM

Entry	Catalyst amount, mol %	Time, min	Yield, %
1	1	90	55
2	2.5	90	65
3	5.0	90	70
4	7.5	60	84
5	10	60	95

In order to show the general applicability of the method for other substrates and derivatives, the same reaction conditions were applied for the reactions of 2 equiv. indole and 1 equiv. of an aromatic aldehyde **2** in the presence of nickel nanoparticle catalyst under solvent-free conditions at 80 °C for an appropriate time, which directly afforded BIM derivatives (**3a–n**) in good to excellent yields (Scheme 1). The reaction times and yields of the synthesized BIM derivatives are given in Table II, which shows that the yields were almost quantitative in most cases. It was found that aromatic aldehydes with electron donating or electron withdrawing groups were converted to the corresponding products within some hours.

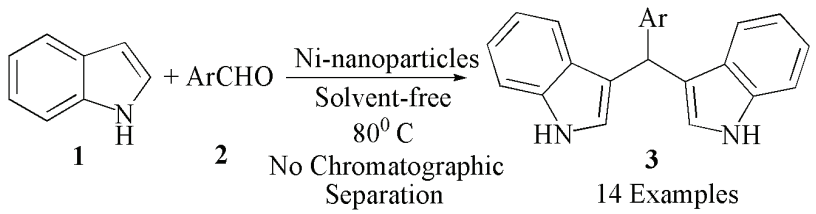

Scheme 1. Synthesis of bis(indolyl)methanes.

The recovery and reusability of the catalyst was examined. The catalyst was recovered by a simple work-up using the centrifugation method and reused during four consecutive runs without any apparent loss of activity for the same reaction. It is noteworthy that the yields of the product in the second, third, and fourth runs were almost the same as that in the first run.

All products were well characterized by ^{1}H-NMR, ^{13}C-NMR, FTIR, mass spectroscopy, elemental analyses and melting point determination. The data are given in the Supplementary material to this paper. To the best of our knowledge, the synthesis of compounds **3j**–**n** has not been previously reported in the literature. The ^{1}H-NMR spectra of compounds **3j–n** showed a sharp singlet for the

indole-NH at about δ 10.80 ppm. The methine protons appeared as a singlet at about δ 6.20 ppm and the aromatic protons were displayed in the region of 6.68–7.86 ppm. Hydroxyl protons in compounds **3k** and **3l** were observed at δ 11.30 and 9.76 ppm, respectively. The ^{13}C-NMR, FTIR, mass spectra and elemental analyses confirmed the structures of the synthesized compounds.

TABLE II. Ni nanoparticles-catalyzed synthesis of BIM under solvent-free conditions at 80 °C

Entry	Ar	Product	Time, min	Yield, %	M.p. / °C	
					Found	Reported
1	C_6H_5	**3a**	60	95	148–150	149–150[25]
2	4-$NO_2C_6H_4$	**3b**	20	92	220–222	217–220[25]
3	3-$NO_2C_6H_4$	**3c**	30	89	264–265	265–266[26]
4	2-$NO_2C_6H_4$	**3d**	60	88	137–139	139–141[27]
5	2-ClC_6H_4	**3e**	20	91	74–75	70–71[25]
6	4-ClC_6H_4	**3f**	100	90	80–82	76–77[25]
7	4-BrC_6H_4	**3g**	100	88	116–117	110–112[28]
8	4-OHC_6H_4	**3h**	120	85	136–137	122–124[25]
9	4-$CH_3C_6H_4$	**3i**	90	85	96–97	93–94[25]
10	4-Cl-3-$NO_2C_6H_3$	**3j**	70	89	183–184	–
11	2-OH-5-$NO_2C_6H_3$	**3k**	20	94	194–196	–
12	2-Br-5-OHC_6H_3	**3l**	110	88	141–142	–
13	2-Cl-6-FC_6H_3	**3m**	60	92	94–95	–
14	2-$OCH_2PhC_6H_4$	**3n**	70	88	206–208	–

CONCLUSIONS

In summary, for the first time, it was found that Ni in the form of nanoparticles is a potential alternative to the use of noble-metal-based catalysts for the synthesis of BIM derivatives. Compared to other procedures previously reported in the literature, the present method provides some advantages such as omitting an organic solvent, efficient and experimental simplicity, compatibility with various functional groups, generality, clean, easy work-up and high yields. Moreover, there is no necessity for dry solvents or protecting gas atmospheres. Product purification by column chromatography is not necessary and the catalyst could be easily recovered from the reaction mixture by simple centrifugation.

SUPPLEMENTARY MATERIAL

IR, ^{1}H- and ^{13}C-NMR data for obtained compounds are available electronically from http://www.shd.org.rs/JSCS/, or from the corresponding author on request.

Acknowledgment. The authors thank the Research Council of Payame Noor University for financial support.

И З В О Д

НОВ ПРИСТУП СИНТЕЗИ БИС(ИНДОЛИЛ)МЕТАНА УПОТРЕБОМ НАНОЧЕСТИЦА НИКЛА КАО КАТАЛИЗАТОРА БЕЗ ПРИСУСТВА РАСТВАРАЧА

ABOLFAZL OLYAEI[1], MOHSEN VAZIRI[1], REZA RAZEGHI[1], BAHAREH SHAMS[1] и HASAN BAGHERI[2]

[1]*Department of Chemistry, Payame Noor University, P. O. Box 19395–3697, Tehran, Iran* и [2]*Department of Chemistry, Takestan Branch, Islamic Azad University, Takestan, Iran*

Развијене су наночестице никла које су употребљене као катализатор у реакцији електрофилне супституције индола и различитих ароматичних алдехида у одсуству растварача. Добијени су одговарајући бис(индолил)метани у добром до одличном приносу. Предности ове методе су одсуство органских растварача, кратко реакционо време, висок принос производа реакције, једноставан поступак обраде реакционе смеше, олакшано изоловање производа и могућност регенерације и вишеструке употребе катализатора.

(Примљено 6. маја, ревидирано 10. јула 2012)

REFERENCES

1. A. Saxena, A. Kumar, S. Mujumdar, *J. Mol. Catal., A* **269** (2007) 35
2. F. Alonso, P. Riente, M. Yus, *Tetrahedron* **64** (2008) 1847
3. F. Alonso, P. Riente, M. Yus, *Tetrahedron Lett.* **49** (2008) 1939
4. F. Alonso, P. Riente, M. Yus, *Synlett* (2008) 1289
5. A. Dhakshinamoorty, K. Pitchumani, *Tetrahedron Lett.* **49** (2008) 1818
6. L. Zank, J. Zielinsky, *Appl. Catal., A* **334** (2008) 268
7. R. Bell, S. Carmeli, N. Sar, *J. Nat. Prod.* **57** (1994) 1587
8. X. Ge, S. Yannai, G. Rennert, N. Gruener, F. A. Fares, *Biochem. Biophys. Res. Commun.* **228** (1996) 153
9. B. V. Gregorovich, K. Liang, M. Clugston, S. MacDonald, *Can. J. Chem.* **46** (1968) 3291
10. A. Chatterjee, S. Manna, J. Benerji, C. Pascard, T. Prange, J. Shoolery, *J. Chem. Soc. Perkin Trans. 1* (1980) 553
11. W. E. Noland, M. R. Venkiteswaran, G. Richards, *J. Org. Chem.* **26** (1961) 4241
12. G. Babu, N. Sridhar, P. T. Perumal, *Synth. Commun.* **30** (2000) 1609
13. H. Firouzabadi, N. Iranpoor, A. A. Jafari, *J. Mol. Catal., A* **244** (2005) 168
14. M. A. Zolfigol, P. Salehi, M. Shiria, *Phosphorus, Sulfur Silicon Relat. Elem.* **179** (2004) 2273
15. P. Srinivasan, J. Amalraj, *J. Mol. Catal., A* **242** (2005) 168
16. M. Chakrabarty, A. Mukherji, S. Karmakar, S. Arima, Y. Harigaya, *Heterocycles* **68** (2006) 331
17. S. J. Ji, S. Y. Wang, Y. Zhang, T. P. Loh, *Tetrahedron* **60** (2004) 2051
18. H. Firouzabadi, N. Iranpoor, M. Jafarpour, A. Ghaderi, *J. Mol. Catal., A* **253** (2006) 249
19. S. H. Wu, D. H. Chen, *J. Colloid Interface Sci.* **259** (2003) 282
20. A. Shockravi, M. Sadeghpour, A. Olyaei, *Synth. Commun.* **39** (2009) 2347
21. A. Shockravi, M. Sadeghpour, A. Olyaei, *J. Chem. Res.* (2009) 556
22. A. Olyaei, E. Chehrehgosha Parashkuhi, S. Raoufmoghaddam, M. Sadeghpour, *Synth. Commun.* **40** (2010) 3609
23. A. Olyaei, B. Shams, M. Sadeghpour, F. Gesmati, Z. Razaziane, *Tetrahedron Lett.* **51** (2010) 6086

24. A. Olyaei, S. Raoufmoghaddam, M. Sadeghpour, B. Ebadzadeh, *Chin. J. Chem.* **28** (2010) 825
25. Z. C. Ma, Z. H. Zhang, *Synth. Commun.* **35** (2005) 1997
26. G. Penieres-Carrillo, J. G. Garcia-Estrada, J. L. Gutierrez-Ramirez, C. Alvarez-Tolendano, *Green Chem.* **5** (2003) 337
27. R. Tayebee, F. Nehzat, E. Rezaei-Seresht, F. Z. Mohammadi, E. Ezzat Rafiee, *J. Mol. Cat. A: Chem.* **351** (2011) 154
28. S. M. Vahdat, S. Khaksar, S. Baghery, *World Appl. Sci. J.* **15** (2011) 877.

Journal of the Serbian Chemical Society
JSCS@tmf.bg.ac.rs • www.shd.org.rs/JSCS
J. Serb. Chem. Soc. 78 (4) S17–S19 (2013) *Supplementary material*

SUPPLEMENTARY MATERIAL TO

A novel approach to bis(indolyl)methanes using nickel nanoparticles as a reusable catalyst under solvent-free conditions

ABOLFAZL OLYAEI[1]*, MOHSEN VAZIRI[1], REZA RAZEGHI[1], BAHAREH SHAMS[1] and HASAN BAGHERI[2]

[1]*Department of Chemistry, Payame Noor University, P. O. Box 19395–3697, Tehran, Iran and* [2]*Department of Chemistry, Takestan Branch, Islamic Azad University, Takestan, Iran*

J. Serb. Chem. Soc. 78 (4) (2013) 463–468

IR, ^{1}H- AND ^{13}C-NMR DATA FOR **3a–n**

*3,3´-(Phenylmethylene)bis-1*H-*indole* (***3a***). IR (KBr, cm^{-1}): 3416, 1630, 1460, 1371, 1090; ^{1}H-NMR (500 MHz, DMSO-d_6, δ / ppm): 5.68 (1H, s, methine-H), 6.67–7.22 (15H, *m*, Ar-H), 10.71 (2H, *s*, indole-NH); ^{13}C-NMR (125 MHz, DMSO-d_6, δ / ppm): 40.58, 112.33, 118.91, 119.03, 119.94, 121.73, 124.39, 124.66, 126.64, 127.48, 128.89, 129.15, 137.44, 145.83.

*3,3´-[(4-Nitrophenyl)methylene]bis-1*H-*indole* (***3b***). IR (KBr, cm^{-1}): 3425, 1590, 1456, 1340, 1229; ^{1}H-NMR (500 MHz, DMSO-d_6, δ / ppm): 5.89 (1H, *s*, methine-H), 6.72–8.01 (14H, *m*, Ar-H), 10.79 (2H, *s*, indole-NH); ^{13}C-NMR (125 MHz, DMSO-d_6, δ / ppm): 40.35, 112.46, 117.55, 119.29, 119.78, 121.97, 124.28, 124.73, 127.24, 130.32, 137.47, 146.63, 154.00.

*3,3´-[(3-Nitrophenyl)methylene]bis-1*H-*indole* (***3c***). IR (KBr, cm^{-1}): 3405, 1525, 1458, 1351, 1045; ^{1}H-NMR (500 MHz, DMSO-d_6, δ / ppm): 5.92 (1H, *s*, methine-H), 6.72–8.30 (14H, *m*, Ar-H), 10.77 (2H, *s*, indole-NH); ^{13}C-NMR (125 MHz, DMSO-d_6, δ / ppm): 39.97, 112.46, 117.82, 119.29, 119.79, 121.92, 121.98, 123.47, 124.75, 127.23, 130.46, 135.97, 137.49, 148.27, 148.67.

*3,3´-[(2-Nitrophenyl)methylene]bis-1*H-*indole* (***3d***). IR (KBr, cm^{-1}): 3415, 1574, 1461, 1350, 1227; ^{1}H-NMR (500 MHz, DMSO-d_6, δ / ppm): 6.41 (1H, *s*, methine-H), 6.77–7.87 (14H, *m*, Ar-H), 10.92 (2H, *s*, indole-NH); ^{13}C--NMR (125 MHz, DMSO-d_6, δ / ppm): 34.93, 112.51, 116.83, 119.37, 119.43, 122.03, 124.80, 124.99, 127.19, 128.39, 131.41, 133.38, 137.47, 138.55, 150.39.

*3,3´-[(2-Chlorophenyl)methylene]bis-1*H-*indole* (***3e***). IR (KBr, cm^{-1}): 3414, 1602, 1445, 1336, 1110; ^{1}H-NMR (500 MHz, DMSO-d_6, δ / ppm): 6.10 (1H, *s*, methine-H), 6.63–7.33 (14H, *m*, Ar-H), 10.74 (2H, *s*, indole-NH); ^{13}C-NMR

* Corresponding author. E-mail: Olyaei_a@pnu.ac.ir

(125 MHz, DMSO-d_6, δ / ppm): 37.02, 112.46, 117.39, 119.27, 119.55, 121.90, 124.88, 127.38, 127.84, 128.60, 130.10, 131.09, 133.57, 137.52, 142.73.

*3,3´-[(4-Chlorophenyl)methylene]bis-1*H-*indole (**3f**)*. IR (KBr, cm^{-1}): 3412, 1610, 1487, 1455, 1012; ^{1}H-NMR (500 MHz, DMSO-d_6, δ / ppm): 5.84 (1H, *s*, methine-H), 6.82–7.36 (14H, *m*, Ar-H), 10.91 (2H, *s*, indole-NH); ^{13}C-NMR (125 MHz, DMSO-d_6, δ / ppm): 22.94, 31.83, 112.38, 118.41, 119.11, 121.80, 124.49, 127.35, 128.85, 130.98, 131.14, 137.48, 144.89.

*3,3´-[(4-Bromophenyl)methylene]bis-1*H-*indole (**3g**)*. IR (KBr, cm^{-1}): 3409, 1600, 1468, 1409, 1335, 1225, 1100; ^{1}H-NMR (500 MHz, DMSO-d_6, δ / ppm): 5.69 (1H, *s*, methine-H), 6.68–7.31 (14H, *m*, Ar-H), 10.8 (2H, *s*, indole-NH); ^{13}C-NMR (125 MHz, DMSO-d_6, δ / ppm): 39.90, 112.39, 118.30, 119.10, 119.61, 119.87, 121.79, 124.50, 127.33, 131.41, 131.76, 137.47, 145.34.

*3,3´-[(4-Hydroxyphenyl)methylene]bis-1*H-*indole (**3h**)*. IR (KBr, cm^{-1}): 3410, 1608, 1484, 1420, 1339, 1215, 1088; ^{1}H-NMR (500 MHz, DMSO-d_6, δ / ppm): 5.57 (1H, *s*, methine-H), 6.50–7.20 (14H, *m*, Ar-H), 8.99 (1H, *br*, OH), 10.61 (2H, *s*, indole-NH); ^{13}C-NMR (125 MHz, DMSO-d_6, δ / ppm): 39.47, 112.25, 115.63, 115.79, 118.93, 119.55, 120.05, 121.64, 124.25, 127.54, 130.00, 130.12, 136.07, 137.47, 156.14.

*3,3´-[(4-Methylphenyl)methylene]bis-1*H-*indole (**3i**)*. IR (KBr, cm^{-1}): 3403, 1600, 1457, 1218, 1090; ^{1}H-NMR (500 MHz, DMSO-d_6. δ / ppm): 2.10 (3H, *s*, CH_3), 5.64 (1H, *s*, methine-H), 6.66–7.21 (14H, *m*, Ar-H), 10.64 (2H, *s*, indole-NH); ^{13}C-NMR (125 MHz, DMSO-d_6, δ / ppm): 21.49, 40.58, 112.28, 118.97, 119.08, 120.00, 121.68, 124.34, 127.50, 129.05, 129.46, 135.42, 137.46, 142.82.

*3,3´-[(4-Chloro-3-nitrophenyl)methylene]bis-1*H-*indole (**3j**)*. Yellow solid; Anal. Calcd. for $C_{23}H_{16}ClN_3O_2$: C, 68.74; H, 3.98; N, 10.46 %. Found: C, 68.83; H, 3.90; N, 10.51 %; IR (KBr, cm^{-1}): 3400, 1574, 1471, 1350, 1225; ^{1}H--NMR (500 MHz, DMSO-d_6, δ / ppm): 5.88 (1H, *s*, methine-H), 6.74–7.87 (13H, *m*, Ar-H), 10.80 (2H, *s*, indole-NH); ^{13}C-NMR (125 MHz, DMSO-d_6, δ / ppm): 39.46, 112.49, 117.41, 119.36, 119.72, 122.03, 123.23, 124.82, 125.86, 127.13, 132.25, 134.57, 137.47, 147.25, 148.24.

*3,3´-[(2-Hydroxy-5-nitrophenyl)methylene]bis-1*H-*indole (**3k**)*. Yellow solid; Anal. Calcd. for $C_{23}H_{17}N_3O_3$: C, 72.06; H, 4.43; N, 10.96. Found: C, 71.96; H, 4.52; N, 11.01 %; IR (KBr, cm^{-1}): 3412, 1588, 1491, 1333, 1275, 1205; ^{1}H-NMR (500 MHz, DMSO-d_6, δ / ppm): 6.05 (1H, *s*, methine-H), 6.68–7.86 (13H, *m*, Ar--H), 10.74 (2H, *s*, indole-NH), 11.30 (1H, *br*, OH); ^{13}C-NMR (125 MHz, DMSO-d_6, δ / ppm): 32.64, 112.46, 116.28, 117.57, 119.20, 119.51, 121.87, 124.47, 124.66, 125.78, 127.40, 133.21, 137.54, 140.24, 162.29; MS (*m*/*z*): 383 $(M)^+$, 265, 139, 130, 118, 117, 89.

*3,3´-[(2-Bromo-5-hydroxyphenyl)methylene]bis-1*H-*indole (**3l**)*. Pink solid; Anal. Calcd. for $C_{23}H_{17}BrN_2O$: C, 66.18; H, 4.07; N, 6.71 %. Found: C, 66.24; H, 4.00; N, 6.80 %; IR (KBr, cm^{-1}): 3407, 1612, 1479, 1413, 1338, 1212, 1094;

^{1}H-NMR (500 MHz, DMSO-d_6, δ / ppm): 6.14 (1H, *s*, methine-H), 6.76–7.35 (13H, *m*, Ar-H), 9.76 (1H, *s*, OH), 10.77 (2H, *s*, indole-NH); ^{13}C-NMR (125 MHz, DMSO-d_6, δ / ppm): 32.50, 110.74, 112.36, 118.10, 118.15, 119.08, 119.64, 121.78, 124.45, 127.53, 130.15, 132.30, 134.75, 137.45, 154.64; MS (*m*/*z*): 418 $(M+2)^+$, 416 $(M)^+$, 300, 298, 245, 243, 220, 117, 97.

*3,3´-[(2-Chloro-6-fluorophenyl)methylene]bis-1*H*-indole (**3m**).* Pink solid; Anal. Calcd. for $C_{23}H_{16}ClFN_2$: C, 73.69; H, 4.27; N, 7.47 %. Found: C, 73.53; H, 4.35; N, 7.40 %; IR (KBr, cm^{-1}): 3410, 1608, 1452, 1343, 1100; ^{1}H-NMR (500 MHz, DMSO-d_6, δ / ppm): 6.40 (1H, *s*, methine-H), 6.88–7.37 (13H, *m*, Ar-H), 10.89 (2H, *s*, indole-NH); ^{13}C-NMR (125 MHz, DMSO-d_6, δ / ppm): 36.45, 114.67, 117.58, 118.61, 118.79, 121.33, 121.52, 124.00, 126.82, 126.85, 128.87, 129.63, 131.92, 132.00, 133.14, 133.26, 136.52, 139.30; MS (*m*/*z*): 376 $(M+2)^+$, 374 $(M)^+$, 337, 243, 222, 194, 117, 90, 89.

*3,3´-{[2-(Benzyloxy)phenyl]methylene}bis-1*H*-indole (**3n**).* White solid; Anal. Calcd. for $C_{30}H_{24}N_2O$: C, 84.11; H, 5.60; N, 6.54 %. Found: C, 84.17; H, 5.65; N, 6.48 %; IR (KBr, cm^{-1}): 3411, 1589, 1447, 1340, 1221, 1091; ^{1}H-NMR (500 MHz, DMSO-d_6, δ / ppm): 5.14 (2H, *s*, O–CH_2–), 6.34 (1H, *s*, methine-H), 6.79––7.38 (19H, *m*, Ar-H), 10.79 (2H, *s*, indole-NH); ^{13}C-NMR (125 MHz, DMSO-d_6, δ / ppm): 34.99, 72.40, 114.52, 115.45, 120.88, 121.22, 122.01, 123.40, 123.91, 126.79, 129.89, 130.03, 130.22, 130.59, 131.29, 132.23, 136.39, 139.70, 140.50, 158.38; MS (*m*/*z*): 428 $(M)^+$, 337, 243, 130, 117, 92, 91.

Journal of the Serbian Chemical Society
JSCS-info@shd.org.rs • www.shd.org.rs/JSCS
J. Serb. Chem. Soc. 78 (4) 469–476 (2013)
JSCS–4430
UDC 546.185–323+547.269.3+
547.387'592+544.478
Original scientific paper

Phospho sulfonic acid: a novel and efficient solid acid catalyst for the one-pot preparation of indazolo[1,2-*b*]-phthalazinetriones

ALI REZA KIASAT*, ARASH MOURADZADEGUN and SEYYED JAFAR SAGHANEZHAD

Chemistry Department, College of Science, Shahid Chamran University, Ahvaz 61357-4-3169, Iran

(Received 8 May, revised 27 August 2012)

Abstract: An efficient one-pot condensation of aldehyde, dimedone and phthalhydrazide has been achieved in the presence of a catalytic amount of phospho sulfonic acid as a novel environmentally benign heterogeneous solid acid under solvent-free conditions. Diverse indazolo[1,2-*b*]phthalazinetrione derivatives were prepared in good to excellent yields in short times. The economical factors (time, cost, waste, *etc*.) for this three-component reaction hold promise for the future of organic synthesis.

Keywords: indazolo[1,2-*b*]phthalazinetrione; multicomponent reaction; phthalhydrazide; dimedone; solvent-free; phospho sulfonic acid.

INTRODUCTION

Multicomponent reactions (MCRs) are defined as one-pot processes in which three or more substrates combine either simultaneously (so-called tandem or domino reactions), or through a sequential addition procedure that does not require any change of solvent. MCRs are gaining more and more importance especially in the total synthesis of natural products and medicinal heterocyclic compounds because of their simplicity, high yield of the products and short reaction times.[1,2]

Solvent-free organic reactions have attracted much interest particularly from the viewpoint of green chemistry. Solid-state reactions (or solvent-free reactions) have many advantages, such as reduced pollution, low costs and simplicity in the process and handling.[3] The possibility of performing multicomponent reactions under solvent-free conditions with a heterogeneous catalyst could enhance their efficiency from economic and ecological points of view.[4]

* Corresponding author. E-mail: akiasat@scu.ac.ir
doi: 10.2298/JSC120508088K

The synthesis of new heterocyclic compounds has always been a subject of great interest due to their wide applicability. Among a large variety of heterocyclic compounds, heterocycles containing phthalazine moiety are of interest because they show several pharmacological and biological activities.[5–7] Phthalazine derivatives, which have two bridgehead nitrogen atoms in a fused ring system, possess cytotoxic,[8] antimicrobial,[9] anticonvulsant,[10] antifungal,[11] anticancer[12] and anti-inflammatory[13] activities. Moreover, these compounds exhibited good promise as new luminescent materials or fluorescence probes.[14]

The first synthesis of indazolo[1,2-*b*]phthalazinetriones was reported by Bazgir *et al*. using *p*-toluenesulfonic acid (*p*-TSA) as a catalyst[15]. In recent years, silica sulfuric acid,[16] H_2SO_4 in water–ethanol or an ionic liquid,[17] silica-supported polyphosphoric acid,[18] $Mg(HSO_4)_2$[19] heteropoly acids,[20] *N*-halosulfonamides,[21] sulfonated poly(ethylene glycol),[22] wet cyanuric chloride,[23] molecular iodine[24] and nanosilica sulfuric acid,[25] have been utilized for the three-component condensation of 1,3-dicarbonyls, aromatic or aliphatic aldehydes and phthalhydrazide/urazole. Moreover, there are a few reports about the four-component condensation of phthalic anhydride, hydrazinium hydroxide, aromatic aldehydes and dimedone using $Ce(SO_4)_2 \cdot 4H_2O$[26] or 1-butyl-3-methylimidazolium bromide ([Bmim]Br).[27]

The aim of this presented protocol is to highlight the synergistic effects of the combined use of MCRs and reactions under solvent-free conditions with a heterogeneous catalyst for the development of a new eco-compatible strategy for the synthesis of heterocyclics. Therefore, a straightforward convergent one-pot synthesis of indazolo[1,2-*b*]phthalazinetrione derivatives using phospho sulfonic acid as an efficient solid acid catalyst under solvent-free conditions through the domino Knoevenagel condensation/Michael addition/intramolecular cyclodehydration sequence was examined (Scheme 1).

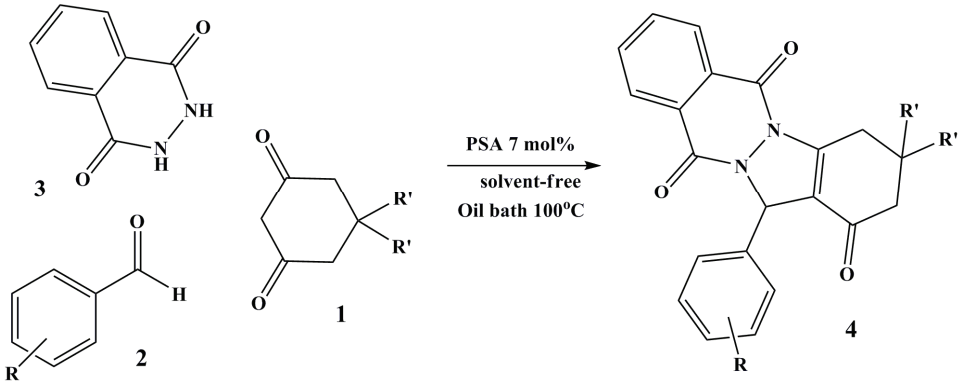

Scheme 1. Three-component reaction of dimedone, phthalhydrazide and aromatic aldehydes.

RESULTS AND DISCUSSION

Phospho sulfonic acid, PSA, was easily prepared by the simple mixing of diammonium hydrogen phosphate and chlorosulfonic acid in CH_2Cl_2 at room temperature (Scheme 2). This reaction is easy and clean because the by-products of the reaction are HCl and NH_3 gases, which are immediately evolved from the reaction vessel.

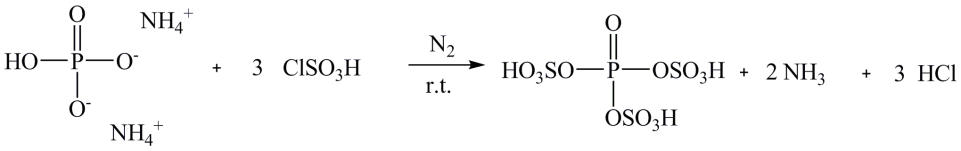

Scheme 2. Preparation of the catalyst.

To evaluate the catalytic activity of PSA in the preparation of indazolo[1,2--*b*]phthalazine-1,6,11-trione derivatives, a model three-component coupling reaction of phthalhydrazide (1 mmol), dimedone (1 mmol) and benzaldehyde (1.1 mmol) under solvent-free conditions at 100 °C in the absence and presence of PSA were examined. It was found that in the absence of solid acid catalyst, only trace amount of the desired product was observed on TLC plate even after 1 h of heating (Table I). When the reaction was performed in the presence of PSA, it proceeded rapidly to give the desired product.

TABLE I. Optimization of the conditions for the three-component condensation reaction of phthalhydrazide (1 mmol), dimedone (1 mmol) and benzaldehyde (1.1 mmol) under thermal (100 °C) solvent-free conditions

Entry	Catalyst amount, mol %	Temperature, °C	Time, min	Yield, %
1	–	100	60	–
2	3.5	100	45	85
3	7	100	10	91
4	9.5	100	8	90
5	7	25	60	–
6	7	60	60	40

In order to evaluate the appropriate catalyst loading, a model reaction was performed using 3.5 to 9.5 mol % catalyst at different temperatures without solvent (Table I). It was found that 7 mol % of the catalyst resulted in the maximum yield in the minimum time. A higher percentage of loading of the catalyst (9.5 mol %) neither increased the yield nor shortened the conversion time. Next, the effect of temperature was evaluated for the model reaction. It was observed that the reaction did not proceed at room temperature. Elevating the reaction temperature proved helpful, and the yield of desired product increased considerably. It was gratifying to find that the reaction proceeded smoothly and almost

complete conversion to the product was observed at 100 °C, affording 2,3,4,13--tetrahydro-3,3-dimethyl-13-phenyl-1*H*-indazolo[1,2-*b*]phthalazine-1,6,11-trione in 91 % yield within a short time.

Subsequently, with optimal conditions at hand, *i.e.*, 1.1:1:1 molar ratios of aldehyde, dimedone and phthalhydrazide and 7 mol % of PSA at 100 °C under solvent-free conditions, the generality and synthetic scope of this coupling protocol were demonstrated by synthesizing a series of 1*H*-indazolo[1,2-*b*]phthalazine-1,6,11-triones (Table II). Gratifyingly, a wide range of aromatic aldehydes was well tolerated under the optimized reaction conditions. The time taken for complete conversion (monitored by TLC) and the isolated yields are presented in Table II. All new compounds were characterized by their satisfactory spectral (IR, ^{1}H-NMR and ^{13}C-NMR) studies, and the known compounds by comparison of their physical and spectral data with those reported.

TABLE II. The one-pot preparation of 1*H*-indazolo[1,2-*b*]phthalazine-1,6,11-trione derivatives promoted by PSA under solvent-free conditions at 100 °C

Product	R	R′	Time, min	Yield, %	Melting point, °C	
					Found	Lit.
4a	H	CH_3	10	91	208–210	207–209[15]
4b	4-NO_2	CH_3	4	89	220–222	223–225[15]
4c	3-NO_2	CH_3	5	98	269–272	270–272[15]
4d	2-Cl	CH_3	11	88	265–267	264–266[15]
4e	4-CH_3	CH_3	10	94	227–228	227–229[15]
4f	4-Cl	CH_3	5	92	262–264	262–264[15]
4g	4-OCH_3	CH_3	10	95	218–220	218–220[17]
4h	2,4-Cl_2	CH_3	15	86	220	219–221[18]
4i	3-CF_3	CH_3	8	98	214	213–215[20]
4j	3-CH_3	CH_3	10	91	232	232–233[20]
4k	4-CF_3	H	15	75	265	–

As shown in Table II, aromatic aldehydes having electron-releasing, as well as electron-withdrawing, groups were uniformly transformed into the corresponding indazolo[1,2-*b*]phthalazinetriones in high to excellent yields within 4–15 min. Substituents on the aromatic ring had no obvious effect on yield or reaction time under the above optimal conditions.

A plausible mechanistic rationale portraying a sequence of events for this coupling reaction is postulated in Scheme 3. The first step is believed to be the acid-catalyzed Knoevenagel condensation between the aldehyde and dimedone to generate adduct A, which acts as a Michael acceptor. The phthalhydrazide attacks adduct A in a Michael-type fashion to produce an open chain intermediate B. Intermediate B undergoes intramolecular cyclization by the reaction of nucleophilic amino function to carbonyl group followed by dehydration to form indazolo[1,2-*b*]phthalazinetriones.

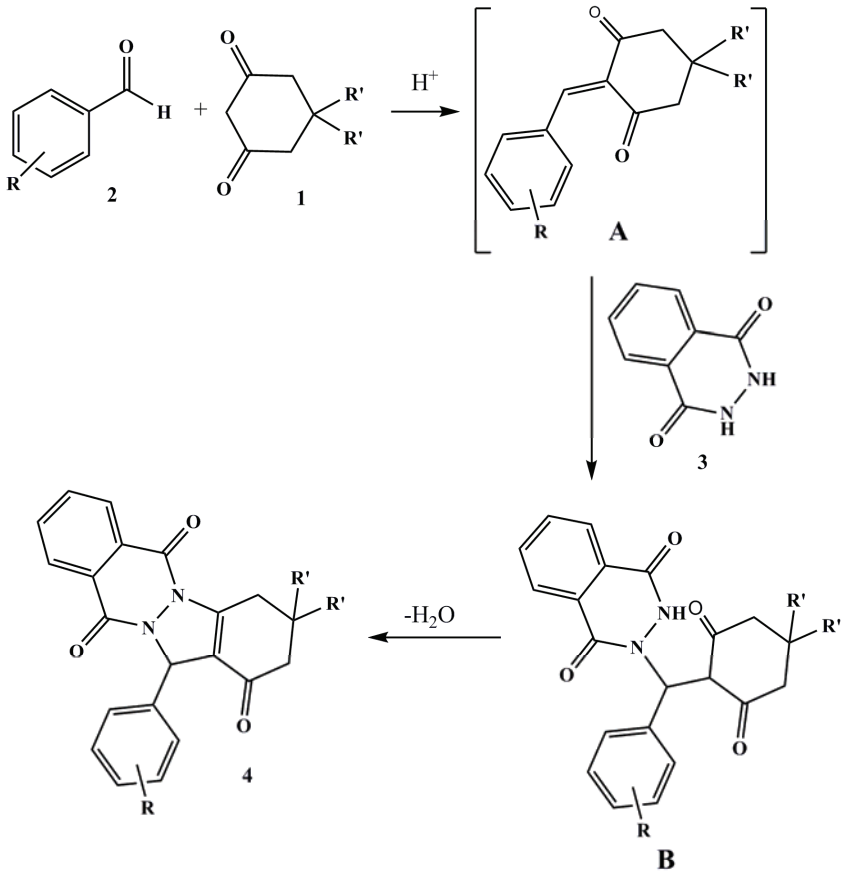

Scheme 3. A plausible reaction mechanism.

The reusability of the catalyst in the reaction of dimedone, phthalhydrazide, and benzaldehyde, under solvent-free conditions at 100 °C was evaluated. In this procedure, after completion of each reaction, hot ethanol was added and the catalyst was filtered. The recovered catalyst was washed with ethanol, dried and reused five times. A mild depression in the catalytic activity of the catalyst was observed after the 5th time of reuse (Table III).

To compare the advantages of the employment of PSA over other reported catalysts, the model reaction of dimedone, phthalhydrazide and benzaldehyde was considered as a representative example (Table IV). While in most of these cases, comparative yields of the desired product were obtained as when the PSA--catalyzed procedure was followed, the reported procedures required high catalyst loading (entries 1, 2 and 4), or long reaction times (entries 3 and 5). These results clearly demonstrate that PSA is an equally or more efficient catalyst for this three-component reaction.

TABLE III. The reusability of the catalyst in five cycles for the reaction of dimedone, phthalhydrazide and benzaldehyde, under solvent-free conditions at 100 °C

Run	Time, min	Yield, %
1	10	91
2	10	90
3	11	88
4	12	85
5	13	82

TABLE IV. Comparison of PSA with reported catalysts in the reaction of dimedone, phthalhydrazide and benzaldehyde, under solvent-free conditions

Entry	Catalyst/temperature, °C	Catalyst loading mol %	Time, min	Yield, %	Ref.
1	*p*-Toluenesulfonic acid/80	30	10	86	15
2	Silica-supported PPA/80	0.1 g	7	91	18
3	Cyanuric chloride/100	3	15	96	23
4	$Mg(HSO_4)_2$/100	11.5	10	85	19
5	$H_4SiW_{12}O_{40}$/100	1	16	92	20
6	PSA/100	7	10	91	This work

EXPERIMENTAL

All commercially available chemicals were purchased from Fluka or Merck and used without further purification. The IR spectra were recorded on a BOMEM MB-Series 1998 FT-IR spectrophotometer. The ^{1}H- and ^{13}C-NMR spectra were recorded in $CDCl_3$ on a Bruker Advanced DPX 400 MHz spectrometer using TMS as an internal standard. The obtained spectral data are given in the Supplementary material to this paper. Reaction monitoring was accomplished by TLC on silica gel polygram SILG/UV 254 plates.

Preparation of phospho sulfonic acid

A 50 mL suction flask was equipped with a constant-pressure dropping funnel. The gas outlet was connected to a vacuum system through an alkali solution trap. Diammonium hydrogen phosphate (2 g, 15 mmol) was charged into the flask and chlorosulfonic acid (5.24 g, *ca.* 3 mL, 45 mmol) in CH_2Cl_2 (10 mL) was added dropwise over a period of 30 min at room temperature. After completion of the addition, the mixture was shaken for 2 h, while the residual HCl was eliminated by suction. Then the mixture was washed with excess dried CH_2Cl_2. Finally, a solid white powder (4.2 g) was obtained. The FT-IR spectrum of the catalyst (KBr disk), showed O=S=O asymmetric and symmetric stretching peaks at 1124 and 1075 cm^{-1}, respectively, and the S–O stretching peak at 678 cm^{-1}, which strictly confirmed the sulfonic group linkage.

*Typical procedure for the preparation of indazolo[1,2-*b*]phthalazinetriones*

A mixture of dimedone (0.14 g, 1.0 mmol), phthalhydrazide (0.16 g, 1.0 mmol), an aromatic aldehyde (1.1 mmol) and PSA (0.05 g) was heated at 100 °C for 10 min. Completion of the reaction was indicated by TLC [TLC acetone/*n*-hexane (3:10)]. After completion of the reaction, the insoluble crude product was dissolved in hot ethanol and phospho sulfuric acid was filtered off. The crude product was purified by recrystallization from ethanol to afford the pure product.

CONCLUSIONS

In summary, a simple and facile protocol has been described for the synthesis of indazolo[1,2-*b*]phthalazinetrione derivatives from a one-pot, three-component condensation reaction of aromatic aldehydes, phthalhydrazide and dimedone under solvent-free conditions using phospho sulfonic acid as a novel environmentally safe heterogeneous solid acid catalyst. The method offers several advantages, including high yields, application of an inexpensive catalyst, short reaction times, easy workup and performing a multicomponent reaction under solvent-free conditions that is considered relatively environmentally benign.

SUPPLEMENTARY MATERIAL

Spectral data for obtained compounds are available electronically from http://www.shd.org.rs/JSCS/, or from the corresponding author on request.

Acknowledgement. We gratefully acknowledge the support of this work by Shahid Chamran University Research Council, Iran.

ИЗВОД

ФОСФО-СУЛФОНСКА КИСЕЛИНА: НОВ И ЕФИКАСАН КИСЕЛИ КАТАЛИЗАТОР У ЧВРСТОЈ ФАЗИ ЗА СИНТЕЗУ ИНДАЗОЛО[1,2-*b*]ФТАЛАЗИН-ТРИОНА У ЈЕДНОМ РЕАКЦИОНОМ КОРАКУ

ALI REZA KIASAT, ARASH MOURADZADEGUN и SEYYED JAFAR SAGHANEZHAD

Chemistry Department, College of Science, Shahid Chamran University, Ahvaz 61357-4-3169, Iran

Постигнута је ефикасна кондензација, у једном реакционом кораку, алдехида, димедона и фталхидразида, у присуству каталитичких количина фосфо-сулфонске киселине као новог, еколошки прихватљивог хетерогеног катализатора у одсуству органских растварача. Добијена је серија деривата индазоло[1,2-*b*]фталазин-триона у добром до одличном приносу за кратко реакционо време. Економски показатељи (време, цена и губици) за ову трокомпонентну реакцију пружају основ за даљи развој поступка.

(Примљено 8. маја, ревидирано 27. августа 2012)

REFERENCES

1. B. B. Toure, D. G. Hall, in *Multicomponent Reactions*, J. Zhu, H. Bienayme, Eds., Wiley-VCH, Weinheim, Germany, 2005, p. 342
2. N. Shajari, A. R. Kazemizadeh, A. Ramazani, *J. Serb. Chem. Soc.* **77** (2012) 1175
3. K. Tanaka, F. Toda, *Chem. Rev.* **100** (2000) 1025
4. A. Kumar, R. A. Maurya, *Tetrahedron* **63** (2007) 1946
5. F. Al-Assar, K. N. Zelenin, E. E. Lesiovskaya, I. P. Bezhan, B. A. Chakchir, *Pharm. Chem. J.* **36** (2002) 598
6. R. P. Jain, J. C. Vederas, *Bioorg. Med. Chem. Lett.* **14** (2004) 3655
7. R. W. Carling, K. W. Moore, L. J. Street, D. Wild, C. Isted, P. D. Leeson, S. Thomas, D. O'Conner, R. M. McKernan, K. Quirk, S. M. Cook, J. R. Atack, K. A. Wafford, S. A. Thompson, G. R. Dawson, P. Ferris, J. L. Castro, *J. Med. Chem.* **47** (2004) 1807
8. J. S. Kim, H. K. Rhee, H. J. Park, S. K. Lee, C. O. Lee, H. Y. Park Choo, *Bioorg. Med. Chem.* **16** (2008) 4545

9. S. S. El-Sakka, A. H. Soliman, A. M. Imam, *Afinidad* **66** (2009) 167
10. L. Zhang, L. P. Guan, X. Y. Sun, C. X. Wei, K. Y. Chai, Z. S. Quan, *Chem. Biol. Drug Design* **73** (2009) 313
11. C. K. Ryu, R. E. Park, M. Y. Ma, J. H. Nho, *Bioorg. Med. Chem. Lett.* **17** (2007) 2577
12. J. Li, Y. F. Zhao, X. Y. Yuan, J. X. Xu, P. Gong, *Molecules* **11** (2006) 574
13. J. Sinkkonen, V. Ovcharenko, K. N. Zelenin, I. P. Bezhan, B. A. Chakchir, F. Al-Assar, K. Pihlaja, *Eur. J. Org. Chem.* (2002) 2046
14. H. Wu, X. M. Chen, Y. Wan, H. Q. Xin, H. H. Xu, R. Ma, C. H. Yue, L. L. Pang, *Lett. Org. Chem.* **6** (2009) 219
15. M. Sayyafi, M. Seyyedhamzeh, H. R. Khavasi, A. Bazgir, *Tetrahedron* **64** (2008) 2375
16. H. R. Shaterian, M. Ghashang, M. Feyzi, *Appl. Catal., A* **345** (2008) 128
17. J. M. Khurana, D. Magoo, *Tetrahedron Lett.* **50** (2009) 7300
18. H. R. Shaterian, A. Hosseinian, M. Ghashang, *ARKIVOC* (2009) 59
19. H. R. Shaterian, F. Khorami, A. Amirzadeh, R. Doostmohammadi, M. Ghashang, *J. Iran. Chem. Res.* **2** (2009) 57
20. H. J. Wang, X. N. Zhang, Z. H. Zhang, *Monatsh. Chem.* **141** (2010) 425
21. R. Ghorbani-Vaghei, R. Karimi-Nami, Z. Toghraei-Semiromi, M. Amiri, M. Ghavidel, *Tetrahedron* **67** (2011) 1930
22. A. Hasaninejad, A. Zare, M. Shekouhy, *Tetrahedron* **67** (2011) 390
23. X. Wang, W. Ma, L. Wu, F. L. Yan, *J. Chin. Chem. Soc.* **57** (2010) 1341
24. X. Wang, G. Lu, W. Ma, L. Wu, *E-J. Chem.* **8** (2011) 1000
25. H. Hamidian, S. Fozooni, A. Hassankhani, S. Z. Mohammadi, *Molecules* **16** (2011) 9041
26. E. Mosaddegh, A. Hassankhani, *Tetrahedron Lett.* **52** (2011) 488
27. M. Shekouhy, A. Hasaninejad, *Ultrason. Sonochem.* **19** (2012) 307.

Journal of the Serbian Chemical Society
JSCS@tmf.bg.ac.rs • www.shd.org.rs/JSCS
J. Serb. Chem. Soc. 78 (4) S20–S22 (2013) *Supplementary material*

SUPPLEMENTARY MATERIAL TO

Phospho sulfonic acid: a novel and efficient solid acid catalyst for the one-pot preparation of indazolo[1,2-*b*]-phthalazine-triones

ALI REZA KIASAT*, ARASH MOURADZADEGUN and SEYYED JAFAR SAGHANEZHAD

Chemistry Department, College of Science, Shahid Chamran University, Ahvaz 61357-4-3169, Iran

J. Serb. Chem. Soc. 78 (4) (2013) 469–476

*2,3,4,13-Tetrahydro-3,3-dimethyl-13-phenyl-1*H-*indazolo[1,2-*b*]phthalazine-1,6,11-trione (**4a**)*. Yellow powder; IR (KBr, cm^{-1}): 2959, 1662, 1576; ^{1}H-NMR (400 MHz, $CDCl_3$, δ / ppm): 7.33–8.37 (9H, *m*, Ar-H), 6.47 (1H, *s*, CHN), 3.26 and 3.44 (2H, AB system, J = 18.6 Hz, CH_aH_bCO), 2.35 (2H, *s*, CH_2C), 1.23 (6H, *s*, 2Me); ^{13}C-NMR (100 MHz, $CDCl_3$, δ / ppm): 28.5, 28.7, 34.7, 38.1, 50.9, 64.9, 118.6, 127.1, 127.7, 127.9, 128.7, 128.9, 129.1, 133.6, 134.5, 136.4, 150.9, 154.3, 156.1, 192.2.

*2,3,4,13-Tetrahydro-3,3-dimethyl-13-(4-nitrophenyl)-1*H-*indazolo[1,2-*b*]-phthalazine-1,6,11-trione (**4b**)*. Yellow powder; IR (KBr, cm^{-1}): 2923, 1695, 1659, 1615; ^{1}H-NMR (400 MHz, $CDCl_3$, δ / ppm): 7.61–8.41 (8H, *m*, Ar-H), 6.52 (1H, *s*, CHN), 3.26 and 3.43 (2H, AB system, J = 19.2 Hz, CH_aH_bCO), 2.33 and 2.38 (2H, AB system, J = 16.5 Hz, CH_aH_bC), 1.23 (3H, *s*, Me), 1.21 (3H, *s*, Me); ^{13}C-NMR (100 MHz, $CDCl_3$. δ / ppm): 28.4, 28.7, 34.7, 38.0, 50.8, 64.2, 117.3, 124.1, 127.8, 128.1, 128.3, 128.6, 128.9, 133.9, 134.9, 143.4, 147.9, 151.7, 154.6, 155.9, 192.1.

*2,3,4,13-Tetrahydro-3,3-dimethyl-13-(3-nitrophenyl)-1*H-*indazolo[1,2-*b*]-phthalazine-1,6,11-trione* (**4c**). Yellow powder; IR (KBr, cm^{-1}): 2926, 1660, 1625; ^{1}H-NMR (400 MHz, DMSO-d_6, δ / ppm): 7.60–8.37 (8H, *m*, Ar-H), 6.46 (1H, *s*, CHN), 3.23 (2H, *br s*, CH_2CO), 2.27 (2H, *s*, CH_2C), 1.12 (6H, *s*, 2Me); ^{13}C-NMR (100 MHz, DMSO-d_6, δ / ppm): 28.3, 28.9, 34.6, 38.2, 51.5, 64.2, 116.9, 127.3, 127.3, 128.4, 128.7, 129.2, 129.8, 131.5, 132.7, 133.1, 133.6, 134.5, 135.5, 151.8, 154.4, 156.4, 192.2.

*13-(2-Chlorophenyl)-2,3,4,13-tetrahydro-3,3-dimethyl-1*H-*indazolo[1,2-*b*]-phthalazine-1,6,11-trione (**4d**)*. Yellow powder; IR (KBr, cm^{-1}): 2956, 1663,

* Corresponding author. E-mail: akiasat@scu.ac.ir

1625; ^{1}H-NMR (400 MHz, $CDCl_3$, δ / ppm): 7.25–8.40 (8H, *m*, Ar-H), 6.69 (1H, *s*, CHN), 3.24 and 3.42 (2H, AB system, J = 19.1 Hz, CH_aH_bCO), 2.33 (2H, *s*, CH_2C), 1.23 (3H, *s*, Me), 1.22 (3H, *s*, Me); ^{13}C-NMR (100 MHz, $CDCl_3$, δ / / ppm): 28.4, 28.8, 34.6, 38.0, 50.9, 64.0, 116.7, 127.2, 127.6, 128.0, 128.7, 129.0, 129.9, 130.5, 132.6, 133.0, 133.6, 134.5, 151.9, 154.2, 156.2, 192.1.

*2,3,4,13-Tetrahydro-3,3-dimethyl-13-(4-methylphenyl)-1*H-*indazolo[1,2*-b*]-phthalazine-1,6,11-trione (**4e**)*. Yellow powder; IR (KBr, cm^{-1}) 2956, 1663, 1621; ^{1}H-NMR (400 MHz, $CDCl_3$, δ / ppm): 7.12–8.38 (8H, *m*, Ar-H), 6.43 (1H, *s*, CHN), 3.24 and 3.43 (2H, AB system, *J* = 18.5 Hz, CH_aH_bCO), 2.35 (2H, *s*, CH_2C), 2.30 (3H, *s*, CH_3), 1.23 (6H, *s*, 2Me); ^{13}C-NMR (100 MHz, $CDCl_3$, δ / / ppm): 21.3, 28.5, 28.8, 34.7, 38.1, 50.9, 64.9, 118.7, 127.1, 127.7, 127.9, 128.9, 129.2, 129.5, 133.4, 133.5, 134.5, 138.5, 150.8, 154.2, 156.1, 192.2.

*13-(4-Chloro-2,3,4,13-Tetrahydro-3,3-dimethyl-1*H-*indazolo[1,2*-b*]phthalazine-1,6,11-trione (**4f**)*. Yellow powder; IR (KBr, cm^{-1}): 2957, 1656, 1623; ^{1}H--NMR (400 MHz, $CDCl_3$, δ / ppm): 7.31–8.39 (8H, *m*, Ar-H), 6.43 (1H, *s*, CHN), 3.25 and 3.43 (2H, AB system, *J* = 19.1 Hz, CH_aH_bCO), 2.35 (2H, *s*, CH_2C), 1.23 (3H, *s*, Me), 1.22 (3H, *s*, Me); ^{13}C-NMR (100 MHz, $CDCl_3$, δ / / ppm): 28.5, 28.7, 34.7, 38.0, 50.9, 64.3, 118.1, 127.7, 128.1, 128.5, 128.8, 128.9, 129.0, 133.7, 134.5, 134.6, 134.9, 151.1, 154.3, 156.0, 192.2.

*2,3,4,13-Tetrahydro-3,3-dimethyl-13-(4-methoxyphenyl)-1*H-*indazolo[1,2*--b*]phthalazine-1,6,11-trione (**4g**)*. Yellow powder; IR (KBr, cm^{-1}) 2959, 1655, 1626; ^{1}H-NMR (300 MHz, $CDCl_3$, δ / ppm): 8.25–8.35 (2H, *m*, Ar-H), 7.82––7.85 (2H, *m*, Ar-H), 6.84–7.35 (4H, *m*, Ar-H), 6.42 (1H, *s*, CHN), 3.76 (3H, *s*, OMe), 3.23 and 3.42 (2H, AB system, *J* = 19.2 Hz, CH_aH_bCO), 2.34 (2H, *s*, CH_2C), 1.21 (s, 6H, 2Me); ^{13}C-NMR (100 MHz, $CDCl_3$, δ / ppm): 28.51, 28.71, 34.65, 38.07, 50.99, 55.21, 64.59, 114.14, 118.58, 127.71, 127.93, 128.36, 128.51, 128.98, 129.18, 133.47, 134.47, 150.75, 154.28, 156.07, 159.74, 192.23.

*13-(2,4-Dichlorophenyl-2,3,4,13-tetrahydro-1*H-*indazolo[1,2*-b*]phthalazine--1,6,11-trione (**4h**)*. Yellow powder; IR (KBr, cm^{-1}): 2964, 1660, 1628; ^{1}H-NMR (300 MHz, $CDCl_3$, δ / ppm): 8.37 (1H, *dd*, *J* = 3.3, 5.6 Hz,Ar-H), 8.27 (1H, *dd*, *J* = 3.2, 5.4 Hz, Ar-H), 7.26–7.88 (5H, *m*, Ar-H), 6.64 (1H, *s*, CHN), 3.40 (1H, *d*, *J* = 19.1 Hz, CH_aH_bCO), 3.24 (1H, *d*, *J* = 19.2 Hz, CH_aH_bCO), 2.34 (2H, *s*, CH_2C), 1.22 (3H, *s*, Me), 1.21 (3H, *s*, Me); ^{13}C-NMR (100 MHz, $CDCl_3$, δ / ppm): 28.4, 28.8, 34.6, 38.0, 50.8, 63.6, 127.6, 127.7, 128.1, 128.6, 129.0, 130.4, 131.8, 133.3, 133.7, 134.6, 135.1, 152.1, 154.3, 156.1, 192.1.

*2,3,4,13-Tetrahydro-3,3-dimethyl-13-[3-(trifluoromethyl)phenyl]-1*H-*indazolo[1,2*-b*]phthalazine-1,6,11-trione (**4i**)*. Yellow powder; IR (KBr, cm^{-1}) 1635, 1616; ^{1}H-NMR (400 MHz, $CDCl_3$, δ / ppm) 8.36–8.39 (1H, *m*, Ar-H), 8.25–8.28 (1H, *m*, Ar-H), 7.85–7.89 (2H, *m*, Ar-H), 7.68 (1H, *d*, *J* = 8.0 Hz, Ar-H), 7.60 (1H, *s*, Ar-H), 7.55 (1H, *d*, J = 8.0 Hz, Ar-H), 7.48 (1H, *t*, *J* = 8.0 Hz, Ar-H), 6.49 (1H, *s*, CHN), 3.24 and 3.43 (AB system, *J* = 19.0 Hz, 2H, CH_aH_bCO), 2.34 (2H,

s, CH_2C), 1.22 (3H, *s*, Me), 1.21 (s, 3H, Me); ^{13}C-NMR (100 MHz, $CDCl_3$, *δ* / ppm) 28.3, 28.8, 34.7, 38.1, 50.9, 64.3, 117.1, 123.5, 123.6 (*q*, *J* = 3.7 Hz), 125.6 (*q*, *J* = 3.6 Hz), 126.5 (*q*, *J* = 270.8 Hz), 127.8, 128.2, 128.9, 129.0, 129.2, 131.1, 131.2 (*q*, *J* = 37.5 Hz), 133.8, 134.7, 137.5, 151.4, 154.6, 156.1, 192.1.

*2,3,4,13-Tetrahydro-3,3-dimethyl-13-(3-methylphenyl)-1*H-*indazolo[1,2*-b*]-phthalazine-1,6,11-trione (**4j**)*. Yellow powder; IR (KBr, cm^{-1}) 1639, 1616; ^{1}H--NMR (400 MHz, $CDCl_3$, δ / ppm): 8.34–8.37 (1H, *m*, Ar-H), 8.26–8.30 (1H, *m*, Ar-H), 7.83–7.87 (2H, *m*, Ar-H), 7.18–7.23 (3H, *m*, Ar-H), 7.08 (1H, *d*, *J* = 7.5 Hz, Ar-H), 6.40 (1H, *s*, CHN), 3.23 and 3.41 (AB system, *J* = 19.0 Hz, 2H, CH_aH_bCO), 2.33 (2H, *s*, CH_2C), 2.32 (3H, *s*, Ar-Me), 1.21 (3H, *s*, Me), 1.20 (3H, *s*, Me); ^{13}C-NMR (100 MHz, $CDCl_3$, *δ* / ppm): 21.5, 28.5, 28.6, 34.9, 38.1, 51.0, 65.0, 118.8, 124.1, 127.7, 127.9, 128.0, 128.6, 129.0, 129.2, 129.6, 133.4, 134.4, 136.3, 138.3, 150.7, 154.2,156.1, 192.1

*13-(Trifluoromethyl)-2,3,4,13-tetrahydro-1*H-*indazolo[1,2*-b*]phthalazine--1,6,11-trione (**4k**)*. Yellow powder; IR (KBr, cm^{-1}) 2972, 2958, 1695, 1660; ^{1}H-NMR (400 MHz, $CDCl_3$, *δ* / ppm): 8.27–8.40 (2H, *m*, Ar-H), 7.88–7.90 (2H, *m*, Ar-H), 7.5-7.6 (4H, *m*, Ar-H), 6.50 (1H, *s*, CHN), 3.33–3.61 (2H, *m*, CH_2CO), 2.47–2.50 (2H, *m*, CH_2), 2.25–2.27 (2H, *m*, CH_2); ^{13}C-NMR (100 MHz, $CDCl_3$, *δ* / ppm) 22.25, 24.53, 36.85, 64.46, 118.94, 122.54, 125.73, 125.80, 127.53, 127.79, 128.16, 128.80, 128.932, 133.83, 134.74, 140.27, 152.77, 154.44, 156.03, 192.48.

Journal of the Serbian Chemical Society
JSCS-info@shd.org.rs • www.shd.org.rs/JSCS

J. Serb. Chem. Soc. 78 (4) 477–482 (2013) UDC 542.9+547.571+547.551:542.913:547.673
JSCS–4431 *Short communication*

SHORT COMMUNICATION

An efficient synthesis and spectroscopic characterization of Schiff bases containing the 9,10-anthracenedione moiety

GHULAM FAREED[1,2]*, MUHAMMAD ALI VERSIANI[2], NIGHAT AFZA[1], NAZIA FAREED[2], MUHAMMAD IRFAN ALI[1] and MAHBOOB ALI KALHORO[1]

[1]*Pharmaceutical Research Center, PCSIR Laboratories Complex Karachi, Shahrah-e-Dr. Salim-uz-Zaman Siddiqui, Karachi-75280, Sindh, Pakistan and* [2]*Department of Chemistry, Federal Urdu University of Arts, Science and Technology, Ghulshan-e-Iqbal, Karachi-75300, Sindh, Pakistan*

(Received 9 April, revised 28 August 2012)

Abstract: A new method was developed for the synthesis of novel Schiff bases containing the anthraquinone moiety using dodecatungstosilicic acid/P_2O_5 under solvent-free conditions at room temperature. The reaction was completed in 1–3 minutes with excellent yields. This method was found to be very efficient, easy and hazardous-free for the synthesis of azomethines. The development of these types of methodologies in synthetic chemistry may contribute to green chemistry. The structures of synthesized novel Schiff bases were elucidated using ^{1}H-NMR, ^{13}C-NMR, LC–MS, FTIR and CHN analysis.

Keywords: azomethine; dodecatungstosilicic acid; P_2O_5; anthraquinone.

INTRODUCTION

Schiff bases, a versatile class of organic compounds synthesized by the condensation of primary amines with aromatic carbonyl compounds, bear many pharmaceutical properties, including anticancer, antitumor, antibacterial, antifungal, antioxidant, herbicidal, antiproliferative, antimalarial and anticovulsant activities.[1–16] Schiff bases act as ligands in coordination chemistry[17] and are considered a subject of interest due to their industrial and biological applications.[18]

Similarly 9,10-anthracenediones are a very important class of compounds having some remarkable *in vivo* biological activities, such as antibacterial, antifungal, antimalarial, antioxidant, antileukemic, hypotensive, mutagenic functions, and analgesic activity.[19–27]

Moreover, in the recent era, the use environmentally benign, facile and low costing method for the synthesis of biologically active compounds has received

* Corresponding author. E-mail: fareedchm@yahoo.com
doi: 10.2298/JSC120409092F

great attention of synthetic chemists. Based on green chemistry and facile methodologies, numerous methods have been used for the synthesis of Schiff bases, *e.g.*, catalyzed by $TiCl_2$,[28] $ZnCl_2$,[29] $Mg(ClO_4)_2$,[30] P_2O_5/SiO_2,[31] $Ni(NO_3)_2{\cdot}6H_2O$, $Cu(NO_3)_2{\cdot}6H_2O$, $Fe(NO_3)_2{\cdot}6H_2O$, $Mn(NO_3)_2{\cdot}6H_2O$ and $Co(NO_3)_2{\cdot}6H_2O$,[32] montmorilonite K-10[33] and $MgSO_4$–pyridinium *p*-toluenesulfonate (PPTL).[34]

In view of the above facts, results concerning the syntheses of novel Schiff bases using dodecatungstosilicic acid/P_2O_5 as a catalyst are reported herein. The employed method was found to be very efficient and environmentally friendly.

EXPERIMENTAL

Melting points were measured in open glass capillaries using a Gallenkamp MF-370 melting point apparatus. The IR spectra were recorded on a Nicolet Avatar 300 DTGS instrument. The ^{1}H- and ^{13}C-NMR were recorded on Bruker A V-300 instrument operating at 300 and 75 MHz, respectively, using deuterated dimethyl sulfoxide (DMSO-d_6) as the solvent and trimethylsilane (TMS) as an internal standard. The mass spectra were recorded on a Finnigan LCQ Advantage Max instrument. The CHN analyses were realized on a Carlo Erba instrument – Mod-1106. The purity of the products were determined by TLC using silica gel $60F_{254}$ precoated cards (0.2 mm thickness) and visualized under UV light (254 and 366 nm) and by iodine vapors. All chemicals were of AR grade. Analytical and spectral data for the synthesized compounds are given in the Supplementary material.

*General method for the synthesis of Schiff bases **1**–**25***

A mixture of 1-aminoanthraquinone (1 mmol), a substituted aromatic aldehyde or ketone (1 mmol) and dodecatungstosilicic acid/P_2O_5 (0.2 g, 1 mol % of 1-aminoanthraquinone/P_2O_5) as a catalyst was ground in a mortar with a pestle under solvent-free conditions at room temperature for 1–3 min, Scheme 1. The reaction mixture turned to a pasty material that

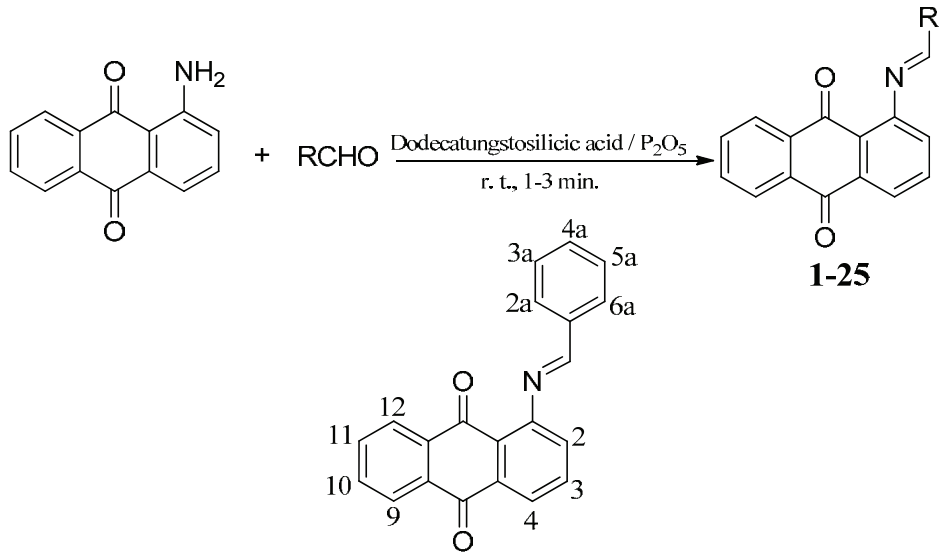

Scheme 1. Preparation of Schiff bases.

indicated the completion of the reaction. Crushed ice was added to afford precipitates of the Schiff bases. In order to remove the catalyst, the product was washed several times with ice-cold water. The solid products were obtained in excellent yield.

RESULTS AND DISCUSSION

The aim of this work was to develop a new facile method for the preparation of Schiff bases. To the best of our knowledge and a literature search, the synthesis of novel Schiff bases using dodecatungstosilicic acid/P_2O_5 has not been previously reported.

An efficient methodology was established using an acidic catalyst for the synthesis of novel Schiff bases by the condensation of 1-aminoanthraquinone with aromatic carbonyl compounds under solvent free conditions at room temperature. The reactions were completed in 1–3 minutes and the products were obtained in high yield after simple work-up (Table I). In order to develop optimum conditions for this synthesis, varying amounts of dodecatungstosilicic acid/P_2O_5 were used using 4-hydroxybenzaldehyde and 1-aminoanthraquinone under solvent-free conditions at room temperature as a model reaction (Table II). The method is very simple and contributes to the hazardous-free synthesis. The catalyst dodecatungstosilicic acid/P_2O_5 was found to be very efficient compared to other catalysts used for the synthesis of imines (Table III).

TABLE I. Synthesis of Schiff bases using *dodeca*-tungstosilicic acid/P_2O_5 as a catalyst

Entry	Substrate	*t* / min	Entry	Substrate	*t* / min
1	3-Hydroxybenzaldehyde	2	14	2,4-Dihydroxybenzaldehyde	2
2	4-Hydroxybenzaldehyde	1	15	4-(Diethylamino)benzaldehyde	3
3	3-Chlorobenzaldehyde	2	16	α-Bromocinnamaldehyde	3
4	Furfural	1	17	3,5-Dibromo-4-hydroxy-benzaldehyde	2
5	4-Hydroxy-3-methoxy-benzaldehyde	2	18	4-(Dimethylamino)cinnam-aldehyde	3
6	3-Bromo-4-hydroxy-benzaldehyde	2	19	2-Ethoxybenzaldehyde	3
7	4-Nitrobenzaldehyde	2	20	4-(Dimethylamino)benzaldehyde	2
8	3-Bromobenzaldehyde	1	21	2-Hydroxyacetophenone	1
9	3-Nitrobenzaldehyde	3	22	3,5-Dimethoxybenzaldehyde	2
10	2-Nitrobenzaldehyde	3	23	4-Methoxycinnamaldehyde	1
11	4-Methoxybenzaldehyde	1	24	4-Ethoxybenzaldehyde	1
12	4-Chlorobenzaldehyde	2	25	4-Methylbenzaldehyde	2
13	4-Chloro-3-nitro-benzaldehyde	1			

Moreover, the structures of the products were elucidated by LC–MS, ^{1}H-NMR, ^{13}C-NMR, IR, and CHN analysis. The ^{1}H-NMR spectra of all the compounds was quite simple and the azomethine group (–N=CH–Ar) of all the synthesized Schiff bases was found in the region of 7.4–8.9 ppm. The aromatic protons ap-

peared as a multiplet in the region of 6.74–7.90 ppm depending on the aromatic substituent. In IR spectrum, –N=C– appears in the region 1511–1545 cm^{-1}.

TABLE II. Effect of different amounts of catalyst on the yield of 1-{[(4-hydroxyphenyl)-methylidene]amino}-9,10-anthraquinone

Entry	Catalyst, mol %	Reaction time, min	Yield, %
1	Free	20	50
2	0.5	10	70
3	1	1	87
4	1.5	1	87

TABLE III. Comparison with other catalysts used for the synthesis of Schiff base

Entry	Catalyst	Solvent	Reaction Time	Yield, %	Ref.
1	$Mg(ClO_4)_2$	1,2-Dichloroethane	8 h	80	30
2	SiO_2/P_2O_5	–	13–26 min	88	31
3	$Ni(NO_3)_2 \cdot 6H_2O$	MeOH/EtOH/DMF	20–30 min	60–88	32
4[a]	Montmorilonite K-10	–	1–3 min	80	33
5	$ZnCl_2$	1,2-Dichloroethane	8 h	46	30
6	$CuSO_4 \cdot H_2O$	1,2-Dichloroethane	8 h	65	30
7	$TiCl_2$	1,2-Dichloroethane	8 h	35	30

[a]Under microwave conditions

CONCLUSION

Based of the excellent yields, short reaction time, easy work-up, solvent-free facile and environment greener reaction, it could be concluded that dodecatungstosilicic acid/P_2O_5 is a very useful catalyst for the synthesis of Schiff bases.

SUPPLEMENTARY MATERIAL

Analytical and spectral data for the synthesized compounds are available electronically from http://www.shd.org.rs/JSCS/, or from the corresponding author on request.

Acknowledgement: All authors are grateful to the Pharmaceutical Research Center, PCSIR Laboratories Complex, Karachi, Pakistan, for the financial and technical support of this research work.

ИЗВОД

ЕФИКАСНА СИНТЕЗА И СПЕКТРОСКОПСКА КАРАКТЕРИЗАЦИЈА ШИФОВИХ БАЗА КОЈЕ САДРЖЕ 9,10-АНТРАЦЕНДИОНСКИ СТРУКТУРНИ ФРАГМЕНТ

GHULAM FAREED[1,2], MUHAMMAD ALI VERSIANI[2], NIGHAT AFZA[1], NAZIA FAREED[2], MUHAMMAD IRFAN ALI[1] и MAHBOOB ALI KALHORO[1]

[1]*Pharmaceutical Research Center, PCSIR Laboratories Complex Karachi, Shahrah-e-Dr.Salim-uz-Zaman Siddiqui, Karachi-75280, Sindh, Pakistan* и [2]*Department of Chemistry, Federal Urdu University of Arts, Science and Technology, Ghulshan-e-Iqbal, Karachi-75300, Sindh, Pakistan*

Развијен је нов поступак за синтезу Шифових база које садрже антрахинонски фрагмент, употребом додекаволфрамсилицијумове киселине/P_2O_5, у одсуству органских растварача, на собној температури. Реакција је готова у периоду 1–3 min у одличном

приносу. Утврђено је да је поступак ефикаснији, једноставнији и безбеднији. Структуре синтетисаних Шифових база одређене су ^{1}H-NMR, ^{13}C-NMR, LC–MS, FT-IR и CHN анализама.

(Примљено 9. априла, ревидирано 28. августа 2012)

REFERENCES

1. A. Faizul, S. Satendra, L. K. Sukhbir, P. Om, *J. Zhejiang Univ. Sci., B* **8** (2007) 446
2. P. G. More, R. B. Bhalvankar, S. C. Pattar, *J. Indian Chem. Soc.* **78** (2001) 474
3. A. H. El-Masry, H. H. Fahmy, S. H. A. Abdelwahed, *Molecules* **5** (2000) 1429
4. M. A. Baseer, V. D. Jadhav, R. M. Phule, Y. V. Archana, Y. B. Vibhute, *Orient. J. Chem.* **16** (2000) 553
5. S. N. Pandeya, D. Sriram, G. Nath, E. De Clercq, *Farmaco* **54** (1999) 624
6. W. M. Singh, B. C. Dash, *Pesticides* **22** (1988) 33
7. E. M. Hodnett, W. J. Dunn, *J. Med. Chem.* **13** (1970) 768
8. S. B. Desai, P. B. Desai, K. R. Desai, *Heterocycl. Commun.* **7** (2001) 83
9. S. Samadhiya, A. Halve, *Orient. J. Chem.* **17** (2001) 119
10. W. P. Narocka, B. Sztuba, A. Drys, J. Wietrzyk. J. Ietrzyk, J. Kosendiak, A. Opolski, *Pol. J. Chem*. **80** (2006) 279
11. J. P. Kaplan, B. M. Rizon, *J. Med. Chem.* **23** (1980) 702
12. M. Verma, S. N. Pandeya, K. N. Singh, J. P. Stables, *Acta Pharm*. **54** (2004) 49
13. B. Rada, T. L. Leto, *Contrib. Microbiol*. **15** (2008) 164
14. A. Almasirad, R. Hosseini, H. Jalalizadeh, Z. Rahimi-Moghaddam, N. Abeian, M. Janafrooz, M. Abbaspour, V. Ziaee, A. Dalvandi, A. Shafiee, *Biol. Pharm. Bull*. **29** (2006) 1180
15. C. J. Clarke, J. W. Eaton, *Clin. Res.* **38** (1990) 300A
16. A. Tsafack, M. Loyevski, P. Ponks, Z. I. Cabantchik, *J. Lab. Clin. Med*. **127** (1996) 575
17. J. C. Pessoa, J. Cavaco, J. Covreia, D. Costa, R. T. Henriques, R. D. Gillard, *Inorg. Chim. Acta* **305** (2000) 7
18. Z. M. Zaki, S. S. Haggag, A. A. Soayed, *Spectrosc. Lett*. **31** (1998) 757
19. N. W. Alcock, D. F. Cook, E. D. McKenzie, J. M. Worthington, *Inorg. Chem. Acta* **38** (1980) 107
20. M. K. Adwankar, M. P. Chitnis,. *Chemotherapy* **28** (1982) 291
21. A. A. Sittie, E. Lemmich, C. E. Olsen, L. Hviid, A. Kharazmi, F. K. Nkrumah, S. B Christensen, *Planta Med.* **65** (1999) 259
22. G. Bath, M. Ndonzao, K. Hostettmann, *Int. J. Pharmacog.* **33** (1995) 107
23. C. Younos, A. Rolland, M. Fleurentin, M.-C. Lanhers, R. Misslin, F. Mortier, *Planta Med.* **56** (1990) 430
24. K. Koumaglo, M. Gbeassor, O. Nikabu, C. D. Souza, W. Werner, *Planta Med.* **58** (1992) 533
25. Y. B. Tripathi, M. Sharma, M. Manickam, *Indian J. Biochem. Biophys.* **34** (1997) 302
26. P. Chang, C. Chen, *Chin. Pharm. J. (Taipei)* **47** (1995) 347
27. N. H. Ismail, A. M. Ali, N. Aimi, M. Kitajima, H. Takayama, N. H. Lajja, *Phytochemistry* **45** (1997) 1723
28. H. Weingart, J. P. Chupp, W. A. White, *J. Org. Chem.* **32** (1967) 213
29. J. H. Billman, K. M. Tai, *J. Org. Chem*. **23** (1958) 535
30. A. K. Chakraborti, S. Bhagat, S. Rudrawar, *Tetrahedron Lett.* **45** (2004) 7641

31. S. M. Devidas, S. H. Quadri, S. A. Kamble, F. M. Syed, D. Y. Vyavhare, *J. Chem. Pharm. Res.* **3** (2011) 489
32. A. Mobinikhaledi, N. Fourughifar, M. Kalhor, *Turk. J. Chem.* **34** (2010) 367
33. R. S. Vass, J. Dudas, R. S. Varma, *Tetrahedron Lett.* **40** (1999) 4951
34. B. P. Branchaud, *J. Org. Chem.* **48** (1983) 3531.

Journal of the Serbian Chemical Society
JSCS@tmf.bg.ac.rs • www.shd.org.rs/JSCS
J. Serb. Chem. Soc. 78 (4) S23–S29 (2013) *Supplementary material*

SUPPLEMENTARY MATERIAL TO

An efficient synthesis and spectroscopic characterization of Schiff bases containing the 9,10-anthracenedione moiety

GHULAM FAREED[1,2]*, MUHAMMAD ALI VERSIANI[2], NIGHAT AFZA[1], NAZIA FAREED[2], MUHAMMAD IRFAN ALI[1] and MAHBOOB ALI KALHORO[1]

[1]Pharmaceutical Research Center, PCSIR Laboratories Complex Karachi, Shahrah-e-Dr. Salim-uz-Zaman Siddiqui, Karachi-75280, Sindh, Pakistan and [2]Department of Chemistry, Federal Urdu University of Arts, Science and Technology, Ghulshan-e-Iqbal, Karachi-75300, Sindh, Pakistan

J. Serb. Chem. Soc. 78 (4) (2013) 477–482

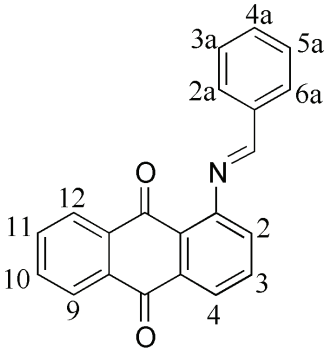

Fig. S-1. Atomic numbering of the prepared Schiff bases.

1-{[(3-Hydroxyphenyl)methylidene]amino -9,10-anthraquinone (***1***). Orange solid; Yield: 82 %; m.p. 312 °C; Anal. Calcd. for $C_{21}H_{13}NO_3$: C, 77.05; H, 4.00; N, 4.28 %. Found: C, 77.00; H, 3.92 ; N, 4.21 %; IR (KBr, cm^{-1}): 3425, 3331, 1666, 1635, 1600, 1542,1280; ^{1}H-NMR (300 MHz, DMSO-d_6, δ / ppm): 11.20 (1H, *bs*, OH), 8.64 (1H, *s*, N=CH–Ar), 8.01–7.99 (3H, *m*, H-4/H-9/H-12), 7.70––7.56 (4H, *m*, H-2/H-3/H-10/H-11), 7.34–6.79 (4H, *m*, Ar–H); ^{13}C-NMR (75 MHz, DMSO-d_6, δ / ppm): 184.90, 182.80, 159.52 (N=C), 156.01, 147.01, 136.89, 135.90, 134.33, 133.71, 133.25, 133.15, 131.65, 131.10, 130.30, 126.36, 126.30, 125.51, 122.39, 122.09 121.59, 115.89; LC–MS Mass (*m*/*z*): 327.

1-{[(4-Hydroxyphenyl)methylidene]amino}-9,10-anthraquinone (***2***). Orange solid; Yield: 87 %; m.p. 306 °C; Anal. Calcd. for $C_{21}H_{13}NO_3$: C, 77.05; H, 4.00;

* Corresponding author. E-mail: fareedchm@yahoo.com

N, 4.28 %. Found: C, 77.01; H, 3.98; N, 4.29 %; IR (KBr, cm^{-1}): 3427, 3312, 1666, 1635, 1600, 1542, 1282; ^{1}H-NMR (300 MHz, DMSO-d_6, δ / ppm): 11.26 (1H, *bs*, OH), 8.51 (1H, *s*, N=CH–Ar), 8.01–7.99 (3H, *m*, H-4/H-9/H-12), 7.70-7.56 (4H, *m*, H-2/H-3/H-10/H-11), 7.39 (2H, *d*, $J_{2a,3a} = J_{6a,5a}$ = 8.7 Hz, H-2a/H--6a), 6.75 (2H, *d*, $J_{3a,2a} = J_{5a,6a}$ = 8.7 Hz, H-3a/H-5a); ^{13}C-NMR (75 MHz, DMSO-d_6, δ / ppm): 184.90, 182.80, 161.01, 159.40 (N=C), 147.01, 135.90, 134.33, 133.71, 133.25, 133.15, 132.61, 131.65, 130.30, 127.11, 126.36, 126.30, 125.51, 122.39, 116.29; LC–MS Mass (*m*/*z*): 327.

1-{[(3-Chlorophenyl)methylidene]amino}-9,10-anthraquinone (***3***). Red solid; Yield: 82 %; m.p. 289 °C; Anal. Calcd. for $C_{21}H_{12}ClNO_2$: C, 72.94; H, 3.50; N, 4.05 %. Found: C, 72.96; H, 3.48; N, 4.01 %; IR (KBr, cm^{-1}): 1665, 1636, 1603, 1589, 1542, 1279, 706, 650; ^{1}H-NMR (300 MHz, DMSO-d_6, δ / ppm): 8.54 (1H, *s*, N=CH–Ar), 8.01–7.99 (3H, *m*, H-4/H-9/H-12), 7.70–7.56 (4H, *m*, H--2/H-3/H-10/H-11), 7.52–7.20 (4H, *m*, Ar–H); ^{13}C-NMR (75 MHz, DMSO-d_6, δ / ppm): 184.90, 182.80, 159.52 (N=C), 147.01, 136.10, 135.90, 134.33, 133.71, 133.41, 133.25, 133.15, 132.10, 131.74, 130.11, 130.01, 129.84, 127.20, 126.36, 126.30, 125.52, 122.39; LC–MS Mass (*m*/*z*): M^+, 345.5; M^{2+}, 347.5.

1-{[(2-Furylmethylidene]amino}-9,10-anthraquinone (***4***). Red solid; Yield: 92 %; m.p. 321 °C; Anal. Calcd. for $C_{19}H_{11}NO_3$: C, 75.74; H, 3.68; N, 4.65 %. Found: C, 75.71; H, 3.62; N, 4.66 %; IR (KBr, cm^{-1}): 1666, 1635, 1604, 1590, 1542, 1281; ^{1}H-NMR (300 MHz, DMSO-d_6, δ / ppm): 8.68 (1H, *s*, N=CH–Ar), 8.09–8.01 (3H, *m*, H-4/H-9/H-12), 7.87 (1H, *d*, $J_{4a,3a}$ = 5.6 Hz, H-4a), 7.75–7.61 (4H, *m*, H-2/H-3/H-10/H-11), 6.75 (1H, *d*, $J_{2a,3a}$ = 5.6 Hz, H-2a), 6.55 (1H, *t*, $J_{3a(2a,4a)}$ = 7.5 Hz, H-3a); ^{13}C-NMR (75 MHz, DMSO-d_6, δ / ppm): 184.90, 182.80, 148.70, 147.01, 145.35 (N=C), 144.92, 135.90, 134.33, 133.71, 133.25, 133.15, 131.72, 130.30, 126.36, 126.30, 125.50, 122.39, 116.92, 112.84; LC–MS Mass (*m*/*z*): 301.

1-{[(4-Hydroxy-3-methoxyphenyl)methylidene]amino}-9,10-anthraquinone (***5***). Red solid; Yield: 85 %; m.p. 306 °C; Anal. Calcd. for $C_{22}H_{15}NO_4$: C, 73.94; H, 4.23; N, 3.92 %. Found: C, 73.89; H, 4.20; N, 3.89 %; IR (KBr, cm^{-1}): 3434, 3312, 1667, 1635, 1605, 1590, 1542, 1282; ^{1}H-NMR (300 MHz, DMSO-d_6, δ / / ppm): 11.40 (1H, *bs*, OH), 8.64 (1H, *s*, N=CH–Ar), 8.01–7.99 (3H, *m*, H-4/H--9/H-12), 7.70–7.56 (4H, *m*, H-2/H-3/ H-10/H-11), 7.30 (1H, *s*, H-2a), 7.00 (1H, *d*, $J_{5a,6a}$ = 8.4 Hz, H-5a), 6.68 (1H, *d*, $J_{6a,5a}$ = 8.4 Hz, H-6a), 3.79 (3H, *s*, OCH_3); ^{13}C-NMR (75 MHz, DMSO-d_6, δ / ppm): 184.90, 182.80, 159.31 (N=C), 150.80, 148.76, 147.01, 135.90, 134.61, 134.33, 133.71, 133.25, 133.15, 131.71, 130.30, 126.36, 126.30, 125.49, 125.30, 122.39, 114.92, 113.26, 56.78; LC–MS Mass (*m*/*z*): 357.

1-{[(3-Bromo-4-hydroxyphenyl)methylidene]amino}-9,10-anthraquinone (***6***). Orange solid; Yield: 83 %; m.p. 324 °C; Anal. Calcd. for $C_{21}H_{12}BrNO_3$: C, 62.09; H, 2.98; N, 3.45 %. Found: C, 73.75; H, 3.11; N, 3.42 %; IR (KBr, cm^{-1}):

1666, 1605, 1542, 1282, 708, 633; ^{1}H-NMR (300 MHz, DMSO-d_6, δ / ppm): 12.10 (1H, *bs*, OH), 8.54 (1H, *s*, N=CH–Ar), 8.01–7.99 (3H, *m*, H-4/H-9/H-12), 7.70-7.56 (4H, *m*, H-2/H-3/H-10/H-11), 7.40 (1H, *s*, H-2a), 7.34 (1H, *d*, $J_{5a,6a}$ = = 8.4 Hz, H-5a), 6.68 (1H, *d*, $J_{6a,5a}$ = 8.4 Hz, H-6a); ^{13}C-NMR (75 MHz, DMSO-d_6, δ / ppm): 184.90, 182.80, 159.31 (N=C), 156.40, 147.01, 135.90, 134.33, 133.71, 133.25, 133.15, 131.71, 131.56, 130.30, 129.46, 128.10, 126.36, 126.30, 125.49, 122.39, 116.48, 109.40; LC–MS Mass (*m*/*z*): M^+, 406; M^{2+}, 408.

1-{[(4-Nitrophenyl)methylidene]amino}-9,10-anthraquinone ***(7)***. Red solid; Yield: 94 %; m.p. 345 °C; Anal. Calcd. for $C_{21}H_{12}N_2O_4$: C, 70.78; H, 3.39; N, 7.86 %. Found: C, 70.93; H, 3.15; N, 7.80 %; IR (KBr, cm^{-1}): 1665, 1636, 1602, 1541, 1279; ^{1}H-NMR (300 MHz, DMSO-d_6, δ / ppm): 8.64 (1H, *s*, N=CH–Ar), 8.15 (2H, *d*, $J_{2a,3a}$ = $J_{6a,5a}$ = 8.4 Hz, H-2a/H-6a), 8.01–7.99 (3H, *m*, H-4/H-9/H-12), 7.90 (2H, *d*, $J_{3a,2a}$ = $J_{5a,6a}$ = 8.4 Hz, H-3a/H-5a), 7.70–7.56 (4H, *m*, H-2/H--3/H-10/H-11); ^{13}C-NMR (75 MHz, DMSO-d_6, δ / ppm): 184.90, 182.80, 159.51 (N=C), 151.70, 147.01, 139.97, 135.90, 134.33, 133.71, 133.25, 133.15, 131.71, 131.20, 130.30, 126.36, 126.30, 125.51, 124.59, 122.39; LC–MS Mass (*m/z*): 356.

1-{[(3-Bromophenyl)methylidene]amino}anthra-9,10-quinone ***(8)***. Red solid; Yield: 74 %; m.p. 340 °C; Anal. Calcd. for $C_{21}H_{12}BrNO_2$: C, 64.63; H, 3.10; N, 3.59 %. Found: C, 64.60; H, 3.02; N, 7.89 %; IR (KBr, cm^{-1}): 1671, 1605, 1587, 1542, 1291, 916, 795, 705, 645; ^{1}H-NMR (300 MHz, DMSO-d_6, δ / ppm): 8.54 (1H, *s*, N=CH–Ar), 8.01–7.99 (3H, *m*, H-4/H-9/H-12), 7.70–7.56 (4H, *m*, H--2/H-3/H-10/H-11), 7.52–7.44 (3H, *m*, H-2a/H-4a/H-6a), 7.20 (1H, *t*, $J_{5a(4a,6a)}$ = 7.2 Hz, H-5a); ^{13}C-NMR (75 MHz, DMSO-d_6, δ / ppm): 184.90, 182.80, 159.52 (N=C), 147.01, 136.10, 135.90, 134.33, 133.71, 133.25, 133.15, 132.10, 131.74, 130.11, 130.30, 129.84, 127.20, 126.36, 126.30, 125.52, 122.39; LC-MS Mass (*m/z*): M^+, 390; M^{2+}, 392.

1-{[(3-Nitrophenyl)methylidene]amino}-9,10-anthraquinone ***(9)***. Red solid; Yield: 87 %; m.p. 290 °C; Anal. Calcd. for $C_{21}H_{12}N_2O_4$: C, 70.78; H, 3.39; N, 7.86 %. Found: C, 70.72; H, 3.34; N, 7.89 %; IR (KBr, cm^{-1}): 1665, 1635, 1603, 1589, 1542, 1279; ^{1}H-NMR (300 MHz, DMSO-d_6, δ / ppm): 8.75 (1H, *s*, H-2a), 8.70 (1H, *s*, N=CH–Ar), 8.26 (1H, *d*, $J_{4a,5a}$ = 8.4 Hz, H-4a), 8.01–7.99 (3H, *m*, H-4/H-9/H-12), 7.90 (1H, *d*, $J_{6a,5a}$ = 8.4 Hz, H-6a), 7.70–7.56 (4H, *m*, H-2/H--3/H-10 /H-11), 7.50 (1H, *t*, $J_{5a(4a,6a)}$ = 7.2 Hz, H-5a); ^{13}C-NMR (75 MHz, DMSO-d_6, δ / ppm): 184.90, 182.80, 159.62 (N=C), 148.72, 147.01, 135.90, 135.30, 134.33, 133.71, 133.25, 133.15, 131.70, 130.80, 130.30, 129.39, 126.36, 126.30, 125.51, 123.65, 122.39, 117.96; LC–MS Mass (*m*/*z*): 356.

1-{[(2-Nitrophenyl)methylidene]amino}-9,10-anthraquinone ***(10)***. Red solid; Yield: 87 %; m.p. 299 °C; Anal. Calcd. for $C_{21}H_{12}N_2O_4$: C, 70.78; H, 3.39; N, 7.86 %. Found: C, 70.77; H, 3.41; N, 7.84 %; IR (KBr, cm^{-1}): 1665, 1635, 1603, 1589, 1542, 1279; ^{1}H-NMR (300 MHz, DMSO-d_6, δ / ppm): 8.82 (1H, *s*,

N=CH–Ar), 8.21 (1H, *d*, $J_{3a\ 4a}$ = 8.4 Hz, H-3a), 8.01–7.99 (3H, *m*, H-4/H-9/H--12), 7.81 (1H, *d*, $J_{6a,5a}$ = 8.4 Hz, H-6a), 7.70–7.54, (5H, *m*, H-2/H-3/H-10/H--11/H-6a), 7.50 (1H, *t*, $J_{5a(4a,6a)}$ = 7.2 Hz, H-5a); ^{13}C-NMR (75 MHz, DMSO-d_6, δ / ppm): 184.90, 182.80, 155.32 (N=C), 149.30, 147.01, 135.90, 134.33, 133.72, 133.71, 133.60, 133.25, 133.15, 131.80, 131.71, 130.30, 128.70, 126.36, 126.30, 125.50, 124.79, 122.39; LC–MS Mass (*m*/*z*): 356.

1-{[(4-Methoxyphenyl)methylidene]amino}-9,10-anthraquinone ***(11)***. Blood red solid; Yield: 91 %; m.p. 289 °C; Anal. Calcd. for $C_{22}H_{15}NO_3$: C, 77.41; H, 4.43; N, 4.10 %. Found: C, 77.39; H, 4.46; N, 4.07 %; IR (KBr, cm^{-1}): 1677, 1597, 1573, 1511, 1259, 1161; ^{1}H-NMR (300 MHz, DMSO-d_6, δ / ppm): 8.51 (1H, *s*, N=CH–Ar), 8.01–7.99 (3H, *m*, H-4/H-9/H-12), 7.70–7.56 (4H, *m*, H-2/H--3/H-10/H-11), 7.50 (2H, *d*, $J_{2a,3a}$ = $J_{6a,5a}$ = 8.7 Hz, H-2a/H-6a), 6.85 (2H, *d*, $J_{3a,2a}$ = $J_{5a,6a}$ = 8.7 Hz, H-3a/H-5a), 3.74 (3H, *s*, OCH_3); ^{13}C-NMR (75 MHz, DMSO-d_6, δ / ppm): 184.90, 182.80, 164.06, 159.82 (N=C), 147.01, 135.90, 134.33, 133.71, 133.25, 133.15, 132.30, 131.72, 128.31, 130.30, 126.36, 126.30, 125.42, 122.39, 114.46, 56.04; LC–MS Mass (*m*/*z*): 341.

1-{[(4-Chlorophenyl)methylidene]amino}-9,10-anthraquinone ***(12)***. Red solid; Yield: 90 %; m.p. 305 °C; Anal. Calcd. for $C_{21}H_{12}ClNO_2$: C, 72.49; H, 3.50; N, 4.05 %. Found: C, 72.56; H, 4.45; N, 4.01 %; IR (KBr, cm^{-1}): 1668, 1573, 1517, 1280, 1171; ^{1}H-NMR (300 MHz, DMSO-d_6, δ / ppm): 8.64 (1H, *s*, N=CH–Ar), 8.01–7.99 (3H, *m*, H-4/H-9/H-12), 7.70–7.56 (4H, *m*, H-2/H-3/H--10/H-11), 7.50 (2H, *d*, $J_{2a,3a}$ = $J_{6a,5a}$ = 8.4 Hz, H-2a/H-6a), 7.28 (2H, *d*, $J_{3a,2a}$ = = $J_{5a,6a}$ = 8.4 Hz, H-3a/H-5a); ^{13}C-NMR (75 MHz, DMSO-d_6, δ / ppm): 184.95, 182.80, 160.01 (N=C), 147.01, 138.36, 135.90, 134.61, 134.33, 133.71, 133.25, 133.15, 131.71, 131.20, 130.30, 129.21, 126.36, 126.30, 125.51, 122.39; LC–MS Mass (*m*/*z*): M^+, 345.5; M^{2+}, 347.5.

1-{[(4-Chloro-3-nitrophenyl)methylidene]amino}-9,10-anthraquinone ***(13)***. Red solid; Yield: 74 %; m.p. 312 °C; Anal. Calcd. for $C_{21}H_{11}ClN_2O_4$: C, 64.54; H, 2.84; N, 4.05 %. Found: C, 64.58; H, 2.79; N, 7.11 %; IR (KBr, cm^{-1}): 1665, 1632, 1602, 1589, 1542, 1279, 707; ^{1}H-NMR (300 MHz, DMSO-d_6, δ / ppm): 8.69 (1H, *s*, N=CH–Ar), 8.66 (1H, *s*, H-2a), 8.01–7.99 (3H, *m*, H-4/H-9/H-12), 7.88 (1H, *d*, $J_{6a,5a}$ = 8.6 Hz, H-6a), 7.70–7.56 (4H, *m*, H-2/H-3/H-10/H-11), 7.50 (1H, *d*, $J_{5a,6a}$ = 8.6 Hz, H-5a); ^{13}C-NMR (75 MHz, DMSO-d_6, δ / ppm): 184.95, 182.80, 159.62 (N=C), 147.92, 147.01, 137.85, 136.58, 135.90, 134.33, 133.71, 133.25, 133.15, 131.72, 130.30, 129.65, 128.70, 126.36, 126.30, 122.55, 124.36, 122.39; LC–MS Mass (*m*/*z*): M^+, 390.5; M^{2+}, 392.5.

1-{[(2,4-Dihydroxyphenyl)methylidene]amino}-9,10-anthraquinone ***(14)***. Red solid; Yield: 72 %; m.p. 330 °C; Anal. Calcd. for $C_{21}H_{13}NO_4$: C, 73.46; H, 3.82; N, 4.08 %. Found: C, 73.50; H, 3.79; N, 7.05 %; IR (KBr, cm^{-1}): 3412, 3311, 1666, 1605, 1542, 1281; ^{1}H-NMR (300 MHz, DMSO-d_6, δ / ppm): 12.10 (1H, *bs*, OH), 10.23 (1H, *bs*, OH), 8.01–7.99 (3H, *m*, H-4/H-9/H-12), 7.70–7.56

(4H, *m*, H-2/H-3/H-10/H-11), 7.20 (1H, *d*, $J_{6a,5a}$ = 8.4 Hz, H-6a), 7.10 (1H, *s*, N=CH–Ar), 6.55 (1H, *d*, $J_{5a,6a}$ = 8.4 Hz, H-5a), 6.44 (1H, *s*, H-3a); ^{13}C-NMR (75 MHz, DMSO-d_6, δ / ppm): 184.90, 181.98, 164.90, 162.40, 159.52 (N=C), 147.01, 135.90, 134.33, 133.71, 133.31, 133.25, 133.15, 131.70, 130.30, 126.36, 126.30, 125.50, 122.39, 113.70, 108.95, 103.55; LC–MS Mass (*m*/*z*): 343.

1-{[(4-(Diethylamino)phenyl)methylidene]amino}-9,10-anthraquinone (***15***). Brownish red solid; Yield: 83 %; m.p. 346 °C; Anal. Calcd. for $C_{25}H_{22}N_2O_2$: C, 78.51; H, 5.80; N, 7.29 %. Found: C, 78.49; H, 5.85; N, 7.29 %; IR (KBr, cm^{-1}): 1665, 1602, 1573, 1535; ^{1}H-NMR (300 MHz, DMSO-d_6, δ / ppm): 8.81 (1H, *s*, N=CH–Ar), 8.01–7.99 (3H, *m*, H-4/H-9/H-12), 7.70–7.56 (4H, *m*, H-2/H-3/H--10/H-11), 7.48 (2H, *d*, $J_{\boldsymbol{2a,3a}}$ = $J_{6a,5a}$ = 8.7 Hz, H-2a/H-6a), 6.65 (2H, *d*, $J_{3a,2a}$ = = $J_{5a,6a}$ = 8.7 Hz, H-3a/H-5a), 3.50 (4H, *q*, *J* = 6.5 Hz, N(C**H**$_2$CH$_3$)$_2$), 1.18 (6H, *t*, *J* = 6.5 Hz, N(CH$_2$C**H**$_3$)$_2$), ^{13}C-NMR (75 MHz, DMSO-d_6, δ / ppm): 184.90, 182.80, 159.46 (N=C), 151.82, 147.01, 135.90, 134.33, 133.71, 133.25, 133.15, 132.92, 131.74, 130.30, 126.36, 126.30, 123.81, 122.39, 125.50, 109.48, 46.30, 13.02; LC–MS Mass (*m*/*z*): 382.

1-[(2-Bromo-3-phenyl-2-propenylidene)amino]-9,10-anthraquinone (***16***). Orangish red solid; Yield: 87 %; m.p. 315 °C; Anal. Calcd. for $C_{23}H_{14}BrNO_2$: C, 66.36; H, 3.39; N, 3.36 %. Found: C, 66.37; H, 3.35; N, 3.33 %; IR (KBr, cm^{-1}): 1665, 1602, 1573, 1535, 916, 784, 707; ^{1}H-NMR (300 MHz, DMSO-d_6, δ / / ppm): 9.40 (1H, *s*, N=CH), 8.42 (1H, *s*, CH–Ar), 8.01–7.99 (3H, *m*, H-4/H-9/H--12), 7.70–7.56 (4H, *m*, H-2/H-3/H-10/H-11), 7.56–7.19 (5H, *m*, Ar–H); ^{13}C--NMR (75 MHz, DMSO-d_6, δ / ppm): 184.90, 182.80, 149.82 (N=C), 147.01, 140.71, 135.90, 134.33, 133.76, 133.71, 133.25, 133.15, 131.70, 130.30, 129.81, 128.70, 128.01, 126.36, 126.30, 125.49, 122.42, 122.35; LC–MS Mass (*m*/*z*): M^+, 416; M^{2+}, 418.

1-{[(3,5-Dibromo-4-hydroxyphenyl)methylidene]amino}-9,10-anthraquinone (***17***). Orangish red solid; Yield: 86 %; m.p. 346 °C; Anal. Calcd. for $C_{21}H_{11}Br_2NO_3$: C, 51.99; H, 2.29; N, 2.89 %. Found: C, 51.89; H, 2.35; N, 2.85 %; IR (KBr, cm^{-1}): 3433, 3311, 1670, 1636, 1604, 1589, 1543, 1280, 879, 707; ^{1}H-NMR (300 MHz, DMSO-d_6, δ / ppm): 12.10 (1H, *bs*, OH), 8.67 (1H, *s*, N=CH–Ar), 8.01–7.99 (3H, *m*, H-4/H-9/H-12), 7.73–7.56 (6H, *m*, H-2/H-3/H--10/H-11/H-2a/H-6a); ^{13}C-NMR (75 MHz, DMSO-d_6, δ / ppm): 184.90, 182.80, 159.26 (N=C), 153.61, 147.01, 135.90, 134.33, 133.71, 133.25, 133.15, 131.74, 131.45, 130.30, 128.72, 126.36, 126.30, 125.48, 122.39, 109.92; LC–MS Mass (*m*/*z*): 485.

1-{[3-(4-(Dimethylamino)phenyl)-2-propenylidene]amino}-9,10-anthraquinone (***18***). Black solid; Yield: 94 %; m.p. 296 °C; Anal. Calcd. for $C_{25}H_{20}N_2O_2$: C, 78.93; H, 5.30; N, 7.36 %. Found: C, 78.90; H, 5.35; N, 7.33 %; IR (KBr, cm^{-1}): 1672, 1602, 1529, 1156; ^{1}H-NMR (300MHz, DMSO-d_6, δ / ppm): 8.47 (*d*, 1H, N=C**H**, *J*= 7.8 Hz), 8.01–7.99 (*m*, 3H, H-4/H-9/H-12), 7.70–7.56 (*m*, 4H, H-2/H-

-3/H-10/H-11), 7.01 (*d*, 2H, $J_{2a,3a} = J_{6a,5a}$ = 8.7 Hz, H-2a/H-6a), 6.95 (*dd*, 1H, *J* = = 7.8 Hz and *J* = 14.5 Hz, CH=C**H**-CH), 6.79 (*d*, 1H, *J* = 14.5 Hz, CH=C**H**), 6.52 (*d*, 2H, $J_{3a,2a} = J_{5a,6a}$ = 8.7 Hz, H-3a/H-5a), 2.88 (*s*, 6H, $N(CH_3)_2$); ^{13}C-NMR (75 MHz, DMSO-d_6, δ / ppm): 184.90, 182.80, 155.12 (N=C), 150.72, 146.88, 146.46, 134.98, 134.33, 133.71, 133.25, 133.15, 131.11, 131.06, 129.54, 127.99, 126.36, 126.30, 124.96, 124.04, 121.88, 112.52, 41.81; LC–MS Mass (*m*/*z*): 380.

1-{[(2-Ethoxyphenyl)methylidene]amino}-9,10-anthraquinone ***(19)***. Orange solid; Yield: 79 %; m.p. 300 °C; Anal. Calcd. for $C_{23}H_{17}NO_3$: C, 77.73; H, 4.82; N, 3.94 %. Found: C, 77.70; H, 4.85; N, 3.93 %; IR (KBr, cm^{-1}): 1683, 1621, 1604, 1562, 1286; ^{1}H-NMR (300 MHz, DMSO-d_6, δ / ppm): 8.54 (1H, *s*, N=CH–Ar), 8.01–7.99 (3H, *m*, H-4/H-9/H-12), 7.70–7.54 (4H, *m*, H-2/H-3/H--10/H-11), 7.52 (1H, *d*, $J_{3a,4a}$ = 8.4 Hz, H-3a), 7.51 (1H, *d*, $J_{6a,5a}$ = 8.4 Hz, H--6a), 6.90 (1H, *t*, $J_{4a(3a,5a)}$ = 7.2 Hz, H-4a), 6.70 (1H, *t*, $J_{5a(4a,6a)}$ = 7.2 Hz, H-5a), 3.99 (2H, *q*, *J* = 6.5 Hz, O**C**$\mathbf{H}_2$$CH_3$), 1.32 (3H, *t*, *J* = 6.5 Hz, C$\mathbf{H}_3$$CH_2O$); ^{13}C-NMR (75 MHz, DMSO-d_6, δ / ppm): 184.90, 182.80, 160.62, 160.22 (N=C), 147.01, 135.90, 134.33, 133.71, 133.25, 133.15, 133.12, 131.71, 131.68, 130.30, 126.36, 126.30, 125.49, 121.47, 121.75, 121.39, 114.35, 64.42, 13.84; LC–MS Mass (*m*/*z*): 355.

1-{{[4-(Dimethylamino)phenyl]methylidene}amino}-9,10-anthraquinone ***(20)***. Brownish red solid; Yield: 71 %; m.p. 310 °C; Anal. Calcd. for $C_{23}H_{18}N_2O_2$: C, 77.95; H, 5.12; N, 7.90 %. Found: C, 77.90; H, 5.16; N, 7.88 %; IR (KBr, cm^{-1}): 1665, 1602, 1542, 1282; ^{1}H-NMR (300 MHz, DMSO-d_6, δ / ppm): 8.51 (1H, *s*, N=CH–Ar), 8.01–7.99 (3H, *m*, H-4/H-9/H-12), 7.70–7.56 (4H, *m*, H-2/H-3/H--10/H-11), 7.50 (2H, *d*, $J_{2a,3a} = J_{6a,5a}$ = 8.7 Hz, H-2a/H-6a), 6.85 (2H, *d*, $J_{3a,2a}$ = = $J_{5a,6a}$ = 8.7 Hz, H-3a/H-5a), 3.74 (6H, *s*, $N(CH_3)_2$); ^{13}C-NMR (75 MHz, DMSO-d_6, δ / ppm): 184.90, 182.80, 159.46 (N=C), 154.82, 147.01, 135.90, 134.33, 133.71, 133.25, 133.15, 131.74, 130.30, 126.36, 126.30, 125.50, 123.81, 122.95, 122.39, 111.51, 41.85; LC–MS Mass (*m*/*z*): 354.

1-{[1-(2-Hydroxyphenyl)ethylidene]amino}-9,10-anthraquinone ***(21)***. Orangish red solid; Yield: 82 %; m.p. 330 °C; Anal. Calcd. for $C_{22}H_{15}NO_3$: C, 77.41; H, 4.43; N, 4.10 %. Found: C, 77.39; H, 4.46; N, 4.07 %; IR (KBr, cm^{-1}): 3442, 3310, 1664, 1635, 1602, 1589, 1542, 1280; ^{1}H-NMR (300 MHz, DMSO-d_6, δ / / ppm): 11. 59 (1H, *bs*, OH), 8.01–7.99 (3H, *m*, H-4/H-9/H-12), 7.70–7.54 (4H, *m*, H-2/H-3/H-10/H-11), 7.52 (1H, *d*, $J_{3a,4a}$ = 8.4 Hz, H-3a), 7.51 (1H, *d*, $J_{6a,5a}$ = = 8.4 Hz, H-6a), 6.90 (1H, *t*, $J_{4a(3a,5a)}$ = 7.2 Hz, H-4a), 6.70 (1H, *t*, $J_{5a(4a,6a)}$ = = 7.2 Hz, H-5a), 2.79 (3H, *s*, CH_3); ^{13}C-NMR (75 MHz, DMSO-d_6, δ / ppm): 184.90, 182.80, 166.22 (N=C), 159.55, 145.01, 134.33, 133.72, 133.71, 133.25, 133.15, 132.80, 132.54, 132.36, 129.02, 126.36, 126.30, 125.10, 121.47, 120.94, 120.15, 117.24, 21.36; LC–MS Mass (*m*/*z*): 341.

1-{[(3,4-Dimethoxyphenyl)methylidene]amino}-9,10-anthraquinone ***(22)***. Red solid; Yield: 89 %; m.p. 303 °C; Anal. Calcd. for $C_{23}H_{17}NO_4$: C, 74.38; H,

4.61; N, 3.77 %. Found: C, 74.35; H, 4.66; N, 3.72 %; IR (KBr, cm^{-1}): 1665, 1636, 1603, 1590, 1542, 1280; ^{1}H-NMR (300 MHz, DMSO-d_6, δ / ppm): 8.64 (1H, *s*, N=CH–Ar), 8.01–7.99 (3H, *m*, H-4/H-9/H-12), 7.70–7.56 (4H, *m*, H-2/H--3/H-10/H-11), 7.46 (1H, *s*, H-2a), 7.18 (1H, *d*, $J_{6a,5a}$ = 8.4 Hz, H-6a), 6.80 (1H, *d*, $J_{5a,6a}$ = 8.4 Hz, H-5a), 3.79 (6H, *s*, OCH_3); ^{13}C-NMR (75 MHz, DMSO-d_6, δ / / ppm): 184.90, 182.80, 159.72 (N=C), 154.86, 149.62, 147.01, 135.90, 134.33, 133.71, 133.25, 133.15, 131.71, 130.46, 130.30, 126.36, 126.30, 125.51. 125.36, 122.39, 112.88, 112.01, 56.76; LC–MS Mass (*m*/*z*): 371.

1-{[3-(4-Methoxyphenyl)-2-propenylidene]amino}-9,10-anthraquinone (***23***). Red solid; Yield: 88 %; m.p. 305 °C; Anal. Calcd. for $C_{24}H_{17}NO_3$: C, 78.46; H, 4.66; N, 3.81. Found: C, 78.40; H, 4.62; N, 3.85; IR (KBr, cm^{-1}): 1665, 1599, 1545, 1270, 1160; ^{1}H-NMR (300 MHz, DMSO-*d*6, δ / ppm): 8.60 (*d*, 1H, N=CH, *J*= 7.6 Hz), 8.01–7.99 (m, 3H, H-4/H-9/ H-12), 7.70–7.56 (4H, *m*, H-2/ /H-3/H-10/H-11), 7.16 (2H, *d*, $J_{2a,3a}$ = $J_{6a,5a}$ = 8.7 Hz, H-2a/H-6a), 6.92 (*dd*, 1H, *J* = 7.6 Hz and *J* = 14.5 Hz, CH=C**H**–CH)), 6.83 (1H, *d*, *J* = 14.5 Hz, CH=CH), 6.68 (2H, *d*, $J_{3a,2a}$ = $J_{5a,6a}$ = 8.7 Hz, H-3a/H-5a), 3.81 (3H, *s*, OCH_3); ^{13}C-NMR (75 MHz, DMSO-d_6, δ / ppm): 184.90, 182.80, 159.94, 154.12 (N=C), 146.88, 146.46, 134.98, 134.33, 133.71, 133.25, 133.15, 131.11, 131.06, 129.44, 128.72, 127.99, 126.36, 126.30, 124.92, 121.54, 114.52, 56.01; LC–MS Mass (*m*/*z*): 367.

1-{[(4-Ethoxyphenyl)methylidene]amino}-9,10-anthraquinone (***24***). Red solid; Yield: 88 %; m.p. 297 °C; Anal. Calcd. for $C_{23}H_{17}NO_3$: C, 73.73; H, 4.82; N, 3.94 %. Found: C, 73.69; H, 4.78; N, 3.97 %; IR (KBr, cm^{-1}): 1666, 1605, 1543, 1282; ^{1}H-NMR (300 MHz, DMSO-d_6, δ / ppm): 8.53 (1H, *s*, N=CH–Ar), 8.06–7.99 (3H, *m*, H-4/H-9/H-12), 7.70–7.56 (4H, *m*, H-2/H-3/H-10/H-11), 7.54 (2H, *d*, $J_{2a,3a}$ = $J_{6a,5a}$ = 8.7 Hz, H-2a/H-6a), 6.95 (2H, *d*, $J_{3a,2a}$ = $J_{5a,6a}$ = 8.7 Hz, H-3a/H-5a), 3.99 (2H, *q*, O**C**$H_2$$CH_3$), 1.32 (3H, *t*, C**H**$_3$$CH_2$O); ^{13}C-NMR (75 MHz, DMSO-d_6, δ / ppm): 184.90, 182.80, 162.06, 159.82 (N=C), 147.01, 135.90, 134.33, 133.71, 133.25, 133.15, 132.30, 131.70, 130.36, 130.30, 126.36, 126.30, 125.42, 122.39, 114.36, 63.98, 13.82; LC–MS Mass (*m*/*z*): 355.

1-{[(4-Methylphenyl)methylidene]amino}-9,10-anthraquinone (***25***). Orange solid; Yield: 81 %; m.p. 290 °C; Anal. Calcd. for $C_{22}H_{15}NO_2$: C, 81.21; H, 4.65; N, 4.30 %. Found: C, 81.19; H, 4.68; N, 4.27 %; IR (KBr, cm^{-1}): 1672, 1628, 1600, 1571, 1516, 1174; ^{1}H-NMR (300 MHz, DMSO-d_6, δ / ppm): 8.61 (1H, *s*, N=CH–Ar), 8.01–7.99 (3H, *m*, H-4/H-9/H-12), 7.70–7.56 (4H, *m*, H-2/H-3/H-10/H-11), 7.50 (2H, *d*, $J_{2a,3a}$ = $J_{6a,5a}$ = 8.7 Hz, H-2a/H-6a), 7.11 (2H, *d*, $J_{3a,2a}$ = = $J_{5a,6a}$ = 8.7 Hz, H-3a/H- 5a), 2.31 (3H, *s*, CH_3); ^{13}C-NMR (75 MHz, DMSO--d_6, δ / ppm): 184.90, 182.80, 159.40 (N=C), 147.01, 143.61, 135.90, 134.33, 133.71, 133.25, 133.15, 133.85, 131.61, 130.30, 130.16, 129.48, 126.36, 126.30, 125.51, 122.39, 21.19; LC–MS Mass (*m*/*z*): 325.

Journal of the Serbian Chemical Society
JSCS-info@shd.org.rs • www.shd.org.rs/JSCS
J. Serb. Chem. Soc. 78 (4) 483–494 (2013)
JSCS–4432
UDC 66.095.253+546.16+547.313.3–31
Original scientific paper

Theoretical study on the nucleophilic fluoroalkylation of propylene oxide with fluorinated sulfones

LING-LI HAN[1] and TAO LIU[1,2]*

[1]*Department of Chemistry and Chemical Engineering, Key Laboratory of Inorganic Chemistry in Universities of Shandong, Jining University, Qufu 273155, Shandong, China and* [2]*School of Chemistry and Chemical Engineering, Shandong University, Jinan 250010, Shandong, China*

(Received 31 August, revised 18 September 2012)

Abstract: The paths of nucleophilic fluoroalkylation reaction of propylene oxide with $PhSO_2CYF^-$ (Y = F, H, and $PhSO_2$, respectively) in the gas phase and in Et_2O solvent were studied theoretically. The nucleophilic fluoroalkylation of propylene oxide with fluorinated carbanions was probed by comparison of the reactivities (phenylsulfonyl)monofluoromethyl anion ($PhSO_2CHF^-$), the (phenylsulfonyl)difluoromethyl anion ($PhSO_2CF_2^-$), and the bis(phenylsulfonyl)monofluoromethyl anion ($(PhSO_2)_2CF^-$). The nucleophilicity reactivity order of $PhSO_2CYF^-$ (Y = F, H, and $PhSO_2$) is $(PhSO_2)_2CF^-$ > $PhSO_2CHF^-$ > > $PhSO_2CF_2^-$, which indicates that the introduction of another electron-withdrawing phenylsulfonyl group is an effective way to significantly increase the nucleophilicity of fluorinated carbanions. For comparison, the nucleophilic addition reaction of propylene oxide with the chlorine-substituted carbanion $PhSO_2CHCl^-$ was investigated. The calculated results show that the nucleophilicity of $PhSO_2CYF^-$ is better than that of $PhSO_2CHCl^-$ in the ring opening reaction with propylene oxide. The calculated results are in good agreement with the available experimental ones.

Keywords: nucleophilic fluoroalkylation; propylene oxide; $PhSO_2CYF^-$ (Y = F, H and $PhSO_2$).

INTRODUCTION

Nucleophilic fluoroalkylation, typically involving the transfer of a fluorine-bearing carbanion to an electrophile, has been widely studied and applied to synthesize fluorine-containing materials and bioactive molecules.[1–7] The nucleophilic fluoroalkylation of simple epoxides with fluorinated sulfones was achieved to give *α*-fluoroalkyl alcohols in one-step. Although there are a variety of examples of nucleophilic fluoroalkylation of various substrates,[6,7] the study of nucleophilic fluoroalkylation of simple epoxides is rare. The possible reason could be

* Corresponding author. E-mail: liutao3569@gmail.com
doi: 10.2298/JSC120831097H

attributed to the intrinsic properties of fluorine-bearing carbanions and weak nucleophilicity toward epoxides.[1]

The exploration of the ring-opening reactions of epoxides from various sources of carbanions can be fully employed in drug design, organic synthesis and other fields. In the present work, the ring-opening mechanisms of epoxides by some sources of carbanions, *i.e.*, $PhSO_2CYF^-$ (Y = F, H or $PhSO_2$), applied in the literature[1] were theoretically investigated (as shown in Scheme 1). Propylene oxide (C_3H_6O) was selected as a model molecule of epoxides to study the nucleophilic fluoroalkylations. Correspondingly, the nucleophilic chloroalkylation of propylene oxide with $PhSO_2CHCl^-$ was also studied. The following reaction of propylene oxide with $PhSO_2CYF^-$ (Y = F, H, and $PhSO_2$) was considered:

$$C_3H_6O + PhSO_2CYF^- \rightarrow \textit{gauche}\text{-product} \rightarrow \textit{anti}\text{-product}$$

In the above equation, Y is F, H, or $PhSO_2$; the *gauche*-product anion and *anti*-product anion (Scheme 1) for the reaction are distinguished by the F atom being in the *gauche*-conformation or *anti*-conformation to the O atom in this conformer.

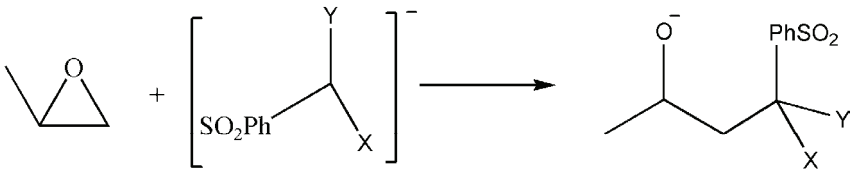

X=F, Y=F, H, and $PhSO_2$
X=Cl, Y=H

Scheme 1. The ring opening reaction of propylene oxide by nucleophilic alkylation with halogenated sulfones.

COMPUTATIONAL METHODS

The reactions were studied using the MP2 and B3LYP methods for the calculations of the reaction path in gas phase, which included geometry optimization, frequency analysis, and IRC (intrinsic reaction coordinate)[8,9] calculations.

Due to the high computational cost required for the full optimization of the large system, investigation of the reaction pathways was realized using the ONIOM approach.[10-13] The ONIOM methodology has been shown to be quite successful in the description of computationally time-consuming systems, by allowing the partitioning of a large cluster computation into various levels of accuracy, for example the active region treated with an advanced level of theory and the remaining region treated with an inexpensive, less accurate method. In the present work, the DFT-B3LYP, two layer ONIOM (MP2:B3LYP) and MP2 levels of theory were used. In the ONIOM (MP2:B3LYP) method, the extended framework environment (benzene ring) was considered with a less expensive level of B3LYP/6-311+g(d,p), while the remainder was treated with the high-level method of MP2/6-311+g(d,p) level.

In order to verify the reliability of the basis set used, BP91/6-311+g(d,p) calculations were also performed for the extended framework environment (benzene ring) of several representative intermediates and transition states, including IM1-2, TS1-2, *s-gauche*, and TS2 for the reaction of $PhSO_2CF_2^-$ with C_3H_6O. It was found that the energy barriers from IM1-2 to TS1-2, and from *s-gauche* to TS2, are 20.62 and 7.68 kcal mol^{-1}, respectively. These results are comparative with corresponding ones obtained using B3LYP/6-311+g(d,p) (20.53 and 7.44 kcal mol^{-1}), meaning that using BP91 does not change the conclusions obtained using B3LYP. Therefore, it can be assumed with confidence that the basis set used in the manuscript can give a reliable potential energy surface of the reaction.

In the gas phase, the geometry optimization calculations were performed for stationary points located along the reaction paths. The frequency analysis calculations were performed at the same level for characterizing stationary points as intermediates (IMn) or transition states (TSn). The reported energies are the zero-point energy (*ZPE*) corrected Gibbs free energies in the gas phase (ΔG_{gas}). The nature of a given transition state was analyzed by IRC computations at the same level.

For locating and characterizing the stationary points along the reaction coordinates of the reaction in diethyl ether (Et_2O) solvent, Gibbs free energy calculations in solution (ΔG_{sol}) were performed based on the gas-phase optimized geometries and calculations using the CPCM model (conductor-like polarizable continuum model)[14,15] of the self-consistent reaction field theory were used to simulate the solution effects. Unless otherwise noted, all discussed relative energies in the subsequent sections are referred to ΔG_{sol}. All the calculations were realized using Gaussian 03 program.[16] The atom labelings used are shown in Fig. 1.

RESULTS AND DISCUSSIONS

Nucleophilic fluoroalkylation of propylene oxide with $PhSO_2CYF^-$ (Y = F, H and $PhSO_2$)

The calculations predicted the same reaction path (the same mechanism) for nucleophilic fluoroalkylation of propylene oxide with $PhSO_2CYF^-$ (Y = F, H, and $PhSO_2$) in the gas phase and in Et_2O solvent. The obtained potential energy curve is shown in Fig. 2, along which there are two transition states (TS1 and TS2) and one intermediate (IM1). The relative free energies (in gas phase and in Et_2O solvent) of the corresponding species involved in Fig. 2 are given in Table I. Two conformations for IM1, TS1, and *s-anti*, respectively, differing in the position of the benzene ring, were found, but optimization of TS1-1 was unsuccessful. The relative energies to the reactants ($PhSO_2CYF^-$ + C_3H_6O) were used in the discussions in the sections unless otherwise noted. The optimized structures of IM1 (IM1-1 and IM1-2), TS1 (TS1-2), *s-gauche*, TS2, and *s-anti* for $PhSO_2CYF^-$ (Y = F, H, and $PhSO_2$, respectively) are shown in Fig. 1, and the important geometric parameters are given in Table II.

The calculations indicated that the reaction involves the formation of IM1-1 and IM1-2, followed by a decomposition process of the C_2–O_3 bond in IM1-1 and IM1-2 *via* TS1-1 and TS1-2 (a stable structure for TS1-1 could not be obtained), respectively, leading to the *gauche*-product (*s-gauche*), which transformed into the more stable *anti*-product (*s-anti*) *via* TS2. Therefore, the reaction

is considered to consist of steps 1 and 2. In the decomposition process of IM1 (step 1), the C_2–O_3 bond breaks and the C_1–C_2 bond forms. With the C_2–C_3 bond rotating along the C_1–C_2 bond, a conformational isomer of the product (s-*gauche*) transforms to another more stable isomer of the product *s-anti via* TS2 (step 2).

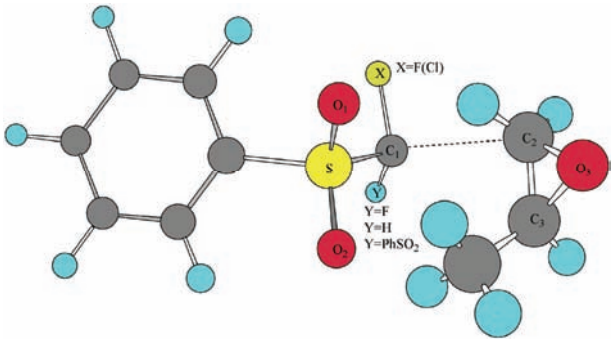

IM1-1

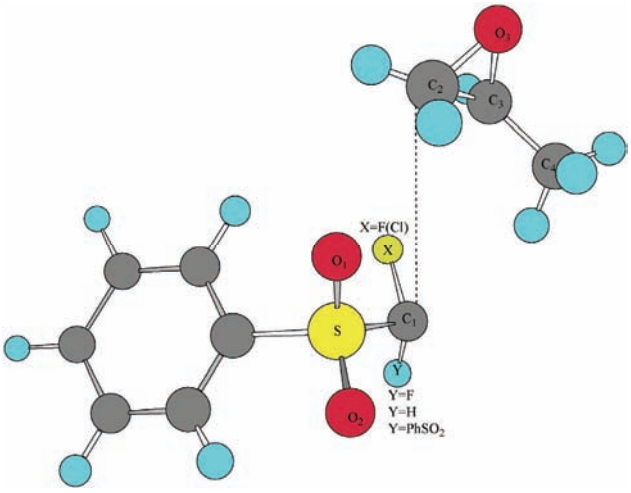

IM1-2

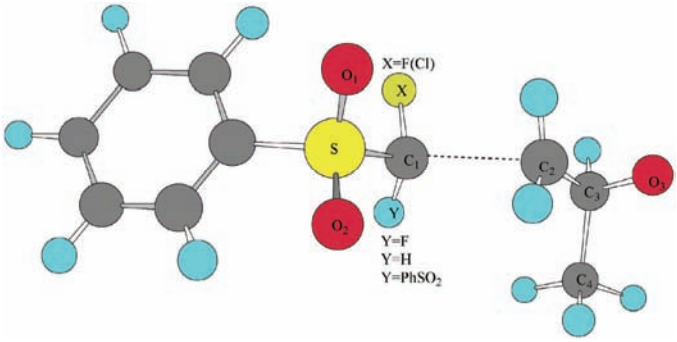

TS1-2

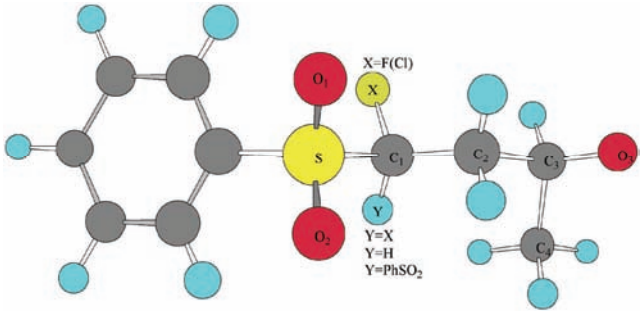

s-gauche

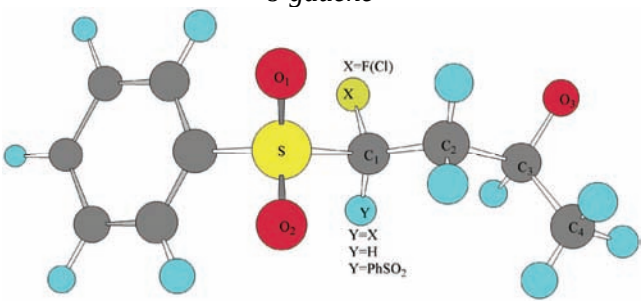

TS2

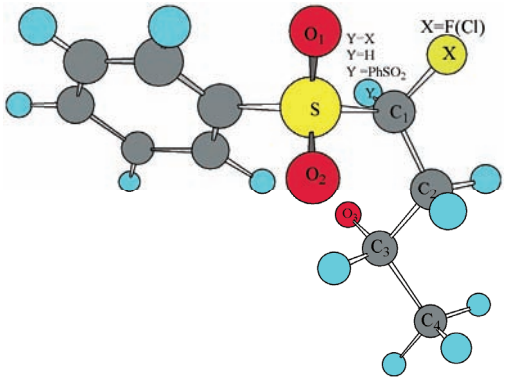

s-anti

Fig. 1. The gas phase structures of the intermediate complexes (IM1-1 and IM1-2), transition states (TS1-2 and TS2) and products (*s-gauche* and *s-anti*) for $PhSO_2CYF^-$ (Y = F, H and $PhSO_2$, respectively) and $PhSO_2CHCl^-$ along the reaction coordinates optimized using the ONIOM method.

The C_2–O_3 bond distances in the structure of IM1-1 and IM1-2 for $PhSO_2CYF^-$ (Y = F, H, and $PhSO_2$) are all significantly longer than the normal C_2–O_3 single-bond length of 1.434 Å in the free propylene oxide (Table II). The primary difference between the structures of IM1-1 and IM1-2 is the relative position of the propylene oxide part to the benzene ring, as shown in Fig. 1. As given in Table II,

the $C_3C_2C_1F$ dihedral angle values of IM1-1 in $PhSO_2CYF^-$ (Y = F, H or $PhSO_2$) are 173.8, –178.1 and –177.6°, respectively, while the corresponding values for IM1-2 are –88.6, –66.4 and 68.7°, respectively.

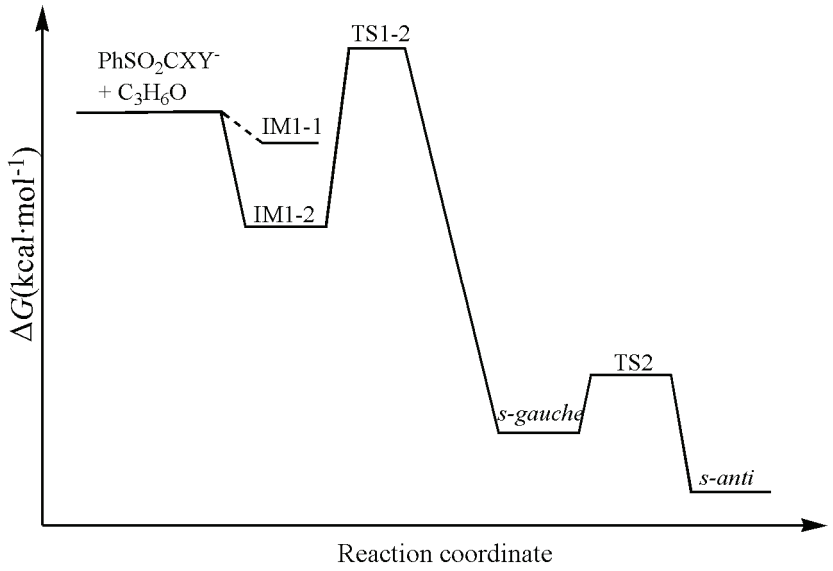

Fig. 2. Schematic diagram of the potential energy curves along the reaction coordinates for the nucleophilic halogenalkylation of propylene oxide with $PhSO_2CXY^-$ (X = F, Y = F, H and $PhSO_2$; X = Cl, Y = H) in the gas phase.

TABLE I. The relative free energies (kcal* mol^{-1}) of the intermediate complexes (IM1-1 and IM1-2), transition states (TS1-2 and TS2), and products (*s-gauche* and *s-anti*), to the reactant ($PhSO_2CYF^-$ (Y = F, H and $PhSO_2$) + C_3H_6O) or the reactant ($PhSO_2CHCl^-$ + C_3H_6O) in the gas phase and Et_2O solvent; the values in parentheses are the relative free energies in the Et_2O solvent based on the geometrical considerations

Reactant	IM1-1	IM1-2	TS1-2	*s-gauche*	TS2	*s-anti*
$PhSO_2CF_2^-$ + C_3H_6O	–8.12	–8.15	12.38	–36.61	–29.17	–43.00
	(–2.26)	(–2.45)	(18.79)	(–23.10)	(–16.35)	(–35.21)
$PhSO_2CHF^-$ + C_3H_6O	–8.82	–8.97	7.86	–38.16	–33.88	–51.92
	(–3.08)	(–3.73)	(14.33)	(–26.99)	(–22.96)	(–41.72)
$(PhSO_2)_2CF^-$ + C_3H_6O	–7.39	–8.33	6.96	–38.93	–35.47	–67.95
	(–2.01)	(–2.65)	(13.11)	(–27.52)	(–24.29)	(–61.49)
$PhSO_2CHCl^-$ + C_3H_6O	–9.06	–9.22	14.01	–30.53	–27.34	–41.20
	(–2.85)	(–3.13)	(21.72)	(–17.17)	(–14.21)	(–36.45)

The IRC calculations indicated that TS1-2 is connected to IM1-2. The barrier heights for step 1 of reaction (1) (the relative free energies of TS1-2 to IM1-2)

* 1 kcal = 4.184 kJ

were predicted to be 21.24, 18.06, and 15.76 kcal mol^{-1} for $PhSO_2CYF^-$ (Y = F, H or $PhSO_2$), respectively, in Et_2O solvent.

TABLE II. Geometric parameters (ONIOM calculations, see text for details; for labelings, see Fig. 1) of the intermediate complex (IM1–1 and IM1–2), the transition states (TS1–2 and TS2), and the products (*s–gauche* and *s–anti*) for $PhSO_2CYF^-$ (Y = F, H and $PhSO_2$) and $PhSO_2CHCl^-$; bond distances are given in Å, and dihedral angles in degrees

Bond or angle	IM1–1	IM1–2	TS1–2	*s-gauche*	TS2	*s-anti*
C_1–X	1.411;	1.417;	1.395;	1.370;	1.387;	1.377;
	1.434;	1.441;	1.421;	1.398;	1.390;	1.394;
	1.441;	1.396;	1.430;	1.401;	1.392;	1.411;
	1.828	1.835	1.817	1.818	1.809	1.816
C_1–C_2	3.860;	4.391;	2.282;	1.481;	1.486;	1.509;
	4.014;	4.371;	2.319;	1.496;	1.490;	1.506;
	4.086;	3.787;	2.323;	1.512;	1.493;	1.505;
	4.059	4.342	2.281	1.508	1.500	1.515
C_2–C_3	1.460;	1.460;	1.467;	1.653;	1.646;	1.570;
	1.460;	1.458;	1.462;	1.615;	1.639;	1.568;
	1.460;	1.460;	1.463;	1.616;	1.635;	1.566;
	1.459	1.459	1.466	1.611	1.638	1.569
C_2–O_3	1.450;	1.447;	1.818;	–	–	–
	1.451;	1.448;	1.809			
	1.452;	1.448;	1.812;			
	1.449	1.447	1.842			
$\angle C_1C_2C_3C_4$	–91.2;	–65.6;	–67.9;	–63.1;	–131.3;	–179.7;
	–84.4;	–68.7;	–69.6;	–59.7;	–125.5;	168.0;
	–82.7;	–69.7;	–68.8;	–56.6;	–123.4;	172.3;
	–98.0	–67.5	–68.0	–58.2	–125.9	169.1
$\angle C_3C_2C_1X$	173.8;	–88.6;	–63.1;	–61.2;	–61.2;	172.7;
	–178.1;	–66.4;	–73.2;	–70.9;	–70.9;	–165.4;
	–177.6;	68.7;	–76.7;	–72.7;	–72.7;	–158.9;
	–161.2	–84.4	–78.0	–68.7	–68.7	–161.3
$\angle O_3C_3C_2C_1$	163.4;	171.2;	178.1;	172.2;	103.3;	56.4;
	170.2;	–174.3;	176.6;	176.0;	109.2;	43.2;
	173.1;	–175.6;	178.3;	176.2;	113.1;	41.7;
	156.7	–173.2	177.6	177.6	108.8	44.4

The low free energies of *s-gauche* for $PhSO_2CYF^-$ (–23.10, –26.99, and –27.52 kcal mol^{-1}) in the Et_2O solvent indicate that the *s-gauche* is a stable product. In the structures of *s-gauche* for $PhSO_2CYF^-$, the C_2–O_3 and C_2–C_3 bond distances are longer and the C_1–C_2 distance is shorter than the corresponding values in the structure of TS1-2 (as shown in Table II). The O_3, C_3, C_2, and C_1 atoms in the structures of $PhSO_2CYF^-$ are almost co-planar (see the $O_3C_3C_2C_1$ dihedral angle values given in Table II).

With the C_2–C_3 bond rotating along the C_1–C_2 bond, *s-gauche* transforms to *s-anti via* TS2. The most obvious differences in the structures of *s-gauche*, TS2,

and *s-anti* are the values of the $C_1C_2C_3C_4$ and $O_3C_3C_2C_1$ dihedral angle. For example, the $O_3C_3C_2C_1$ dihedral angle value in the structure of *s-gauche* for $PhSO_2CYF^-$ is almost 180.0° (176.0°), while the corresponding values in the structures of TS2 and *s-anti* are 109.2° and 43.2°, respectively. The IRC calculations indicated that TS2 is connected to *s-gauche* in the back direction and to the *s-anti* product in the forward direction.

The product *s-anti* is predicted to be lower in energy than the reactant ($PhSO_2CYF^- + C_3H_6O$) by 35.21, 41.72 and 61.49 kcal mol^{-1} for $PhSO_2CYF^-$ (Y = F, H, and $PhSO_2$), respectively, in Et_2O solvent, which demonstrates the reactions are exothermic. The barrier heights for step 2 of the reaction (the relative energies of TS2 to *s-gauche*) were predicted to be 6.75, 4.03, and 3.46 kcal mol^{-1}, for $PhSO_2CYF^-$ (Y = F, H or $PhSO_2$, respectively) in Et_2O solvent. Since TS1 is obviously higher in energy than TS2, the relative free energies of TS1-2 to the IM1-2 are the overall barrier heights for the reaction. The overall barrier heights for the reaction of $PhSO_2CYF^-$ (Y = F, H or $PhSO_2$) in the Et_2O solvent are predicted to be 21.24, 18.06, and 15.76 kcal mol^{-1}, respectively.

The nucleophilicity order of $PhSO_2CYF^-$ ($PhSO_2CF_2^-$, $PhSO_2CHF^-$ and $(PhSO_2)_2CF^-$) can be estimated by the thermodynamic fact (the relative energies of *s-anti* to the reactant) and the kinetic fact (the overall barrier heights for reaction).

The relative free energies of *s-anti* of monofluoro-substituted carbanion, (phenylsulfonyl)monofluoromethyl ($PhSO_2CHF^-$) to the reactant ($PhSO_2CHF^- + C_3H_6O$) are 8.92 and 6.51 kcal mol^{-1} lower than the corresponding values of *s-anti* of (phenylsulfonyl)difluoromethyl anion ($PhSO_2CF_2^-$) to $PhSO_2CF_2^- + C_3H_6O$ in the two phases. The overall barrier heights of 20.53 and 21.24 kcal mol^{-1} for the reaction of $PhSO_2CF_2^-$ are higher than the overall barrier height of 16.83 and 18.06 kcal mol^{-1} for the reaction of $PhSO_2CHF^-$. All these results indicate that the $PhSO_2CHF^-$ has better nucleophilicity than $PhSO_2CF_2^-$ for the ring opening reaction with propylene oxide, confirming that the fluorine substitution of a carbanion will decrease the nucleophilicity of the latter (negative fluorine effect).[1]

To study further the nucleophilicity of a fluorinated carbanion toward epoxides, the reactivity of the bis(phenylsulfonyl)monofluoromethyl anion ($(PhSO_2)_2CF^-$) was analyzed from the thermodynamic the kinetic viewpoint. The relative energies of *s-anti* of $PhSO_2CHF^-$ to the reactant ($PhSO_2CHF^- + C_3H_6O$) are 16.03 and 19.77 kcal mol^{-1} higher than the corresponding value of *s-anti* of $(PhSO_2)_2CF^-$ to $[(PhSO_2)_2CF^- + C_3H_6O]$ in the gas phase and Et_2O solvent. In addition, the overall barrier heights for the reaction of $(PhSO_2)_2CF^-$ are lower than the overall barrier height for the reaction of $PhSO_2CHF^-$ (as shown in Table I). From the results above, it could be concluded that ($(PhSO_2)_2CF^-$) has a better nucleophilicity than $PhSO_2CHF^-$. A possible reason for this is that the phenylsul-

fonyl functionality is able to delocalize the electron density from the carbanion center; bis(phenylsulfonyl) substitution on a fluorinated carbanion can thus increase its stability and nucleophilicity by diminishing the electron repulsion between the electron pairs on the small fluorine atom and the electron lone pair occupying the p-orbital of the carbanion center.[1] The calculated nucleophilicity reactivity order of $PhSO_2CYF^-$ (Y = F, H, and $PhSO_2$, respectively) is $(PhSO_2)_2CF^- > PhSO_2CHF^- > PhSO_2CF_2^-$, which is exactly consistent with the experimental order.[1]

Nucleophilic chloroalkylation of propylene oxide with $PhSO_2CHCl^-$

For comparison, the nucleophilic addition reactions of propylene oxide with chlorine-substituted carbanion $PhSO_2CHCl^-$ were also studied (see Scheme 1). The reaction path for the nucleophilic chloroalkylation of propylene oxide with $PhSO_2CHCl^-$ is shown in Fig. 2, together with the relative free energies of respective species for the reaction in the gas phase (with *ZPE* corrections) and in the solvent Et_2O. The optimized structures of IM1 (IM1-1 and IM1-2), TS1 (TS1-2, the stable structure of TS1-1 could not be found in the present calculation), *s-gauche*, TS2, and *s-anti* for $PhSO_2CHCl^-$ are shown in Fig. 1 and important geometric parameters are given in Table II.

The reaction mechanism for the nucleophilic chloroalkylation of propylene oxide with $PhSO_2CYCl^-$ is similar to that with $PhSO_2CYF^-$ as shown in Fig. 2: $PhSO_2CHCl^- + C_3H_6O \rightarrow$ IM1 (IM1-1 and IM1-2) $\rightarrow$ TS1-2 $\rightarrow$ *s-gauche* $\rightarrow$ $\rightarrow$ TS2 $\rightarrow$ *s-anti*.

IRC calculations indicated that TS1-2 is connected to IM1-2. The relative free energy of TS1-2 to IM1-2 for $PhSO_2CHCl^-$ was predicted to be 23.23 and 24.85 kcal mol^{-1} in gas phase and in Et_2O solvent, respectively. As shown in Table II, the C_2–O_3 bond distance in TS1-2 for $PhSO_2CHCl^-$ (1.842 Å) is longer than that (1.809 Å) in TS1-2 for $PhSO_2CHF^-$, while the C_1–C_2 distances are 2.281 and 2.319 Å in $PhSO_2CHCl^-$ and $PhSO_2CHF^-$, respectively.

Comparing with the relative free energy of *s-gauche* for $PhSO_2CHF^-$ (–26.99 kcal mol^{-1}) in the Et_2O solvent, the relative free energy of *s-gauche* for $PhSO_2CHCl^-$ of –17.17 kcal mol^{-1} indicates that $PhSO_2CHCl^-$ is not as thermodynamically stable as $PhSO_2CHF^-$.

The structure of *s-gauche* transforms to *s-anti via* TS2 with the C_2–C_3 bond rotating along the C_1–C_2 bond, which could be found by examining the $C_1C_2C_3C_4$ and $O_3C_3C_2C_1$ dihedral angle values (see Table II). The IRC calculations indicate that TS2 is connected to *s-gauche* in the back direction and to *s-anti* product of the reaction in the forward direction.

The *s-anti* products of the reaction are predicted to be lower in energy than the reactant ($PhSO_2CHCl^- + C_3H_6O$) by 36.45 kcal mol^{-1} in Et_2O solvent and that the reaction is also exothermic. The barrier heights for this step (the relative

energies of TS2 to *s-gauche*) are predicted to be 3.19 and 2.96 kcal mol^{-1} in the two phases. The relative free energy of TS1-2 is considered as the overall barrier height for the reaction.

The relative free energy of *s-anti* of $PhSO_2CHCl^-$ to the reactant ($PhSO_2CHCl^-$ + C_3H_6O) is 5.27 kcal mol^{-1} higher than the corresponding value of *s-anti* of $PhSO_2CHF^-$ to ($PhSO_2CF_2^-$ + C_3H_6O) in the Et_2O solvent. On the other hand, the overall barrier height for the reaction of $PhSO_2CHCl^-$ is higher than the overall barrier height for the reaction of $PhSO_2CHF^-$ in the Et_2O solvent (see Table I). Estimated from the thermodynamic and the kinetic facts, the nucleophilicity of $PhSO_2CYF^-$ is better than that of $PhSO_2CHCl^-$ for the ring opening reaction with propylene oxide, although negative fluorine effects exist for $PhSO_2CYF^-$. These calculated results are in agreement with the experiment phenomena that the reaction provided satisfactory to good product yields for alkyl monosubstituted epoxides.[1] On the other hand, as stated in the experimental study,[1] the reaction yields dropped in the cases of aryl monosubstituted and disubstituted epoxides. It is supposed that a possible reason is that there is a competition between the negative fluorine effect and the size effect of the chlorine atom. For nucleophilic reactions with alkyl monosubstituted epoxides, such as propylene oxide, the size effect of chlorine atom is more obvious and the nucleophilicity for $PhSO_2CHF^-$ is better. However, the better nucleophilicity of $PhSO_2CHCl^-$ and the negative fluorine effect are primarily important in nucleophilic reactions with aryl monosubstituted and other disubstituted epoxides. Therefore, it can be concluded that the nucleophilicity of $PhSO_2CHCl^-$ is better in nucleophilic reactions with aryl-substituted epoxides, while the nucleophilicity of $PhSO_2CHF^-$ is better in nucleophilic reaction with alkyl-substituted epoxides.

Comparing with a previous study,[17] it could be stated that the nucleophilicity of CH_2F^- is better than that of $PhSO_2CHF^-$, although the electron-withdrawing phenylsulfonyl group is an effective way to increase the nucleophilicity. The reason could be attributed to the fact that the steric hindrance of the phenylsulfonyl group decreases nucleophilicity in nucleophilic fluoroalkylation reactions.

CONCLUSIONS

The path of nucleophilic fluoroalkylation reaction of propylene oxide with $PhSO_2CYF^-$ (Y = F, H or $PhSO_2$) in gas phase and in Et_2O solvent were studied. The nucleophilic fluoroalkylation of propylene oxide with fluorinated carbanions was probed by a reactivity comparison between $PhSO_2CHF^-$, $PhSO_2CF_2^-$ and $(PhSO_2)_2CF^-$. As stated in an experimental study,[1] introducing another electron-withdrawing phenylsulfonyl group is an effective way to increase significantly the nucleophilicity of fluorinated carbanions. The present theoretical calculations confirmed the experiment results and the nucleophilicity reactivity order of $PhSO_2CYF^-$ (Y = F, H or $PhSO_2$) is $(PhSO_2)_2CF^-$ > $PhSO_2CHF^-$ > $PhSO_2CF_2^-$.

For comparison, the nucleophilic addition reaction of propylene oxide with chlorine-substituted carbanion $PhSO_2CHCl^-$ was also studied. Although the negative fluorine effect exists for $PhSO_2CYF^-$, the nucleophilicity of $PhSO_2CYF^-$ is better than that of $PhSO_2CHCl^-$ for the ring opening reaction with propylene oxide.

Acknowledgments. This work was supported by the Natural Science Foundation of Shandong Province (No. ZR2010BQ031), the China Postdoctoral Science Foundation Funded Project (No. 2011M500724), the Shandong Province Postdoctoral Innovation Foundation Funded Project China (No. 201102019), the Advanced Project for National Fund (No. 2011YYJJ05), and the Youth Fund of Jining University (2011QNKJ03).

И З В О Д

ТЕОРИЈСКА СТУДИЈА НУКЛЕОФИЛНОГ ФЛУОРОАЛКИЛОВАЊА ПРОПИЛЕН-ОКСИДА ФЛУОРОВАНИМ СУЛФОНИМА

LING-LI HAN[1] и TAO LIU[2]

[1]*Department of Chemistry and Chemical Engineering, Key Laboratory of Inorganic Chemistry in Universities of Shandong, Jining University, Qufu 273155, Shandong, China и* [2]*School of Chemistry and Chemical Engineering, Shandong University, Jinan, China*

Теоријски је проучаван ток нуклеофилне реакције пропилен-оксида са $PhSO_2CYF^-$ (Y = F, H и $PhSO_2$) у гасној фази и у Et_2O као растварачу. Нуклеофилно флуороалкиловање пропилен-оксида са флуорованим карбањонима је испитивана упоређивањем реактивности (фенилсулфонил)монофлуорметил ($PhSO_2CHF^-$), (фенилсулфонил)дифлуорметил ($PhSO_2CF_2^-$) и бис(фенилсулфонил)монофлуорметил анјона (($PhSO_2)_2CF^-$). Редослед нуклеофилности за $PhSO_2CYF^-$ (Y = F, H или $PhSO_2$) је $(PhSO_2)_2CF^- > PhSO_2CHF^- > PhSO_2CF_2^-$, што указује на то да је увођење додатне електрон-привлачне фенилсулфонилне групе, начин да се знатно појача нуклеофилност флуорованих карбанјона. Резултати прорачуна и постојећи експерименти се добро слажу.

(Примљено 31. августа, ревидирано 18. септембра 2012)

REFERENCES

1. C. Ni, Y. Li, J. Hu, *J. Org. Chem.* **71** (2006) 6829
2. C. Ni, J. Hu, *Tetrahedron Lett.* **46** (2005) 8273
3. Y. Li, J. Hu, *Angew. Chem. Int. Ed.* **44** (2005) 5882
4. Y. Li, C. Ni, J. Liu, L. Zhang, J. Zheng, L. Zhu, J. Hu, *Org. Lett.* **8** (2006) 1693
5. B. R. Langlois, T. Billard, *Synthesis* **2003** (2003) 185
6. G. K. S. Prakash, M. Mandal, *J. Fluorine Chem.* **112** (2001) 123
7. G. K. S. Prakash, J. Hu, *New Nucleophilic Fluoroalkylation Chemistry*, in *Fluorine-Containing Synthons*, V. A. Soloshonok, Ed., American Chemical Society, Washington D. C., 2005
8. C. Gonzalez, H. B. Schlegel, *J. Chem. Phys.* **90** (1989) 2154
9. C. Gonzalez, H. B. Schlegel, *J. Phys. Chem.* **94** (1990) 5523
10. S. Dapprich, I. Komaromi, K. S. Byun, K. Morokuma, M. J. Frisch, *J. Mol. Struct. THEOCHEM* **461** (1999) 1
11. X. Solans-Monfort, M. Sodupe, V. Branchadell, J. Sauer, R. Orlando, P. Ugliengo, *J. Phys. Chem., B* **109** (2005) 3539

12. D. Lesthaeghe, V. van Speybroeck, G. B. Marin, M. Waroquier, *Chem. Phys. Lett.* **417** (2006) 309
13. D. K. Papayannis, A. M. J. Kosmas, *J. Mol. Struct. THEOCHEM* **957** (2010) 47
14. V. Barone, M. Cossi, *J. Phys. Chem., A* **102** (1998) 1995
15. M. Cossi, N. Rega, G. Scalmani, V. Barone, *J. Comput. Chem.* **24** (2003) 669
16. *Gaussian 03*, revision A.1; Gaussian, Inc.: Pittsburgh, PA, 2004
17. T. Liu, X. C. Yin, G. D. Liu, Z. Y. Yu, *J. Chem. Sci.* **122** (2010) 901.

Journal of the Serbian Chemical Society
JSCS-info@shd.org.rs • www.shd.org.rs/JSCS
J. Serb. Chem. Soc. 78 (4) 495–506 (2013)
JSCS–4433
UDC 616.98:578.828:547.568–36+
547.854.4:615.37
Original scientific paper

A quantitative structure–activity relationships study for the anti-HIV-1 activities of 1-[(2-hydroxyethoxy)methyl]-6--(phenylthio)thymine derivatives using the multiple linear regression and partial least squares methodologies

DANIELA IVAN, LUMINITA CRISAN*, SIMONA FUNAR-TIMOFEI and MIRCEA MRACEC

Institute of Chemistry of Romanian Academy, Department of Computational Chemistry, 24 Mihai Viteazul Bvd., 300223, Timisoara, Romania

(Received 13 July 2012)

Abstract: A quantitative structure–activity relationships (QSAR) study using Multiple Linear Regression (MLR) and Partial Least Squares (PLS) methodologies was performed for a series of 127 derivatives of 1-[(2-hydroxyethoxy)methyl]-6-(phenylthio)thymine (HEPT), a potent inhibitor of the of the human immunodeficiency virus type 1, HIV-1 reverse transcriptase (RT). The MLR and PLS methods were employed to explore the relationship between the descriptors (as independent variables) of a pool of HEPT derivative and anti-HIV-1 activity, expressed as log ($1/EC_{50}$) (as dependent variables). Using Dragon descriptors, the present study was aimed at developing a predictive and robust QSAR model for predicting anti-HIV activity of HEPT derivatives for a better understanding of the molecular features of these compounds important for their biological activity. According to the squared correlation coefficients, which had values between 0.826 and 0.809 for the MLR and PLS methods, the results demonstrated almost identical qualities and good predictive ability for both the MLR and PLS models. After dividing the dataset into training and test sets, the model predictability was tested by several parameters, including the Golbraikh–Tropsha external criteria and the goodness of fit, tested using the *Y*-randomization test.

Keywords: Golbraikh–Tropsha criteria; Dragon descriptors; *Y*-randomization.

INTRODUCTION

Infection with the human immunodeficiency virus type-1 (HIV-1) causes increasing destruction of immunity, which finally results in the development of the immunodeficiency syndrome (AIDS). HIV-1 reverse transcriptase (RT) is one of the enzymes responsible for the replication of HIV-1.[1] The majority of com-

* Corresponding author. E-mail: lumi_crisan@acad-icht.tm.edu.ro
doi: 10.2298/JSC120713085I

pounds used in the treatment of the HIV-1 infections are inhibitors of the reverse transcriptase. They belong to two main classes: 1) analogues of 2′,3′-dideoxynucleoside (ddNs), such as: zidovudine, didanosine, lamivudine and 2) non-nucleoside RT inhibitors (NNRTs), such as nevirapine, delavirdine, tivirapine, MKC-442 and 1-[(2-hydroxyethoxy)methyl]-6-(phenylthio)thymine (HEPT) derivatives.[2–4] The HEPT derivatives are among the most selective non-nucleoside drugs discovered and were tested on MT-4 cells by Tanaka and coworkers.[5,6] Due to their high specificity and low toxicity, these inhibitors are promising candidates for the treatment of AIDS, having been extensively studied for many years.[7]

Quantitative structure–activity relationships (QSAR) studies were previously performed on HEPT derivatives used as HIV-1 reverse transcriptase inhibitors by several methods, *i.e.*, Artificial Neural Networks (ANN) and Multiple Linear Regression (MLR) applied to 90[8] and 103[9] HEPT derivatives, respectively, Minimum Steric Difference (MTD) to 34 compounds,[10] Neural Networks (NN) to 80[11] and 103[12] compounds, Particle Swarm Optimization (PSO) and Support Vector Machine (SVM) to 40 compounds,[13] Partial Least Squares (PLS) to 107 compounds,[14] Genetic Programming (GP) to 80 compounds,[15] MLR to 79[16] and 71[17] HEPT derivatives and Comparative Molecular Field Analysis (CMFA) to 44 derivatives[18]. In QSAR, molecular descriptors are correlated with the biological activity of different series of compounds, with the purpose of investigating their binding mechanism. QSAR analysis can indicate which features of a given molecule enable the design of new and more potent compounds with strengthened biological activities.[19] The MLR and the PLS approaches are the most used computational methods in QSAR studies. These techniques can be employed to better interpret the pharmacological data and to predict new biologically active compounds.[20]

An analysis using the MLR and PLS methods applied to a series of 127[12,14] HEPT derivatives with known biological activity has not yet been published in the literature. In this study, these approaches were applied to these compounds and it was found that the anti-HIV-1 activities could be significantly described by Dragon descriptors.[21] The purpose of this paper is to offer a contribution to the understanding of the influence of the molecular features of these 127 HEPT derivatives on their anti-HIV-1 activity using QSAR procedures.

MATERIAL AND METHODS

Compounds studied

A set of 127 HEPT compounds (having the common skeleton presented in Fig. 1) with known biological activity (presented in Table S-I, Supplementary material to this paper) was analyzed in this study. The anti-HIV activity data (A_{obs}), expressed as log ($1/EC_{50}$), where EC_{50} represents the concentration that produces a 50 % protection of MT-4 cells against the cytopathic effect of HIV-1, were taken from the literature.[12,14]

Structural calculations

In the first step, the structures of the 127 investigated molecules were pre-optimized using the (MM+) Molecular Mechanics Force Field included in the HyperChem 7.52 package.[22] In the next step, the minimized structures were refined using the semi-empirical AM1 Hamiltonian also implemented in HyperChem. For geometry optimization, a gradient norm limit of 0.01 kcal $Å^{-1}$ was set. To display the "real" spatial orientation of the substituents of the HEPT derivatives, all compounds investigated were superposed on the X-ray coordinates of 1-[(2-hydroxyethoxy)methyl]-6-(phenylthio)thymine (http://www.rcsb.org/pdb/explore/ /explore.do?structureId=1RTI). The RMS fit criterion was calculated for the superposition of three atoms included in the rigid skeleton, namely N3, C6, C1' (Fig. 1, atom numbering as per the IUPAC convention).

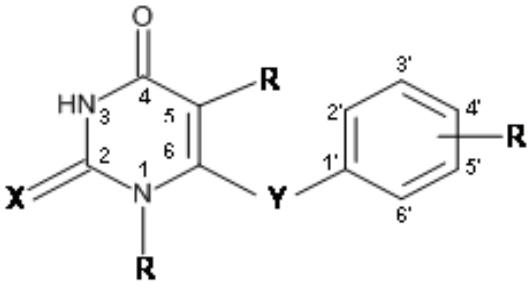

Fig. 1. General structure of the HEPT derivatives.

Molecular descriptors

1217 molecular descriptors (0D, 1D, 2D, 3D) were used to characterize the set of 127 potent inhibitors of the HIV-1 reverse transcriptase. The descriptors calculated using the DRAGON[23] software were analyzed to check and remove constant or near-constant variables. The remaining descriptors were used to build the *X*-matrix in the MLR and PLS analysis, as follows:[21] 35 constitutional descriptors, 92 topological descriptors, 42 walk and path counts, 31 connectivity indices, 47 information indices, 92 2D autocorrelations, 63 Burden eigenvalue descriptors, 18 topological charge indices, 40 eigenvalue-based indices, 41 Randic molecular profiles, 53 geometrical descriptors, 133 RDF descriptors, 160 3D-MoRSE descriptors, 99 Weighted Holistic Invariant Molecular (WHIM) descriptors, 195 Geometry, Topology and Atom-Weights Assembly (GETAWAY) descriptors, 22 functional group counts, 35 atom-centered fragments, 14 charge descriptors, and 5 molecular properties.

Training and test set generation

The clustering technique is intensively applied to split data sets into training and test sets to perform further QSAR modeling.[24] Therefore the calculated Dragon descriptors were normalized and introduced in the R package[25] for clustering. The HEPT derivatives were divided into training and test sets by means of the partition against medoids (PAM) algorithm.[26] The diversity criteria used to estimate the dissimilarity of molecules was the Euclidean distance. The initial dataset of 127 HEPT derivatives was split into fifteen clusters following the maximum silhouette value criteria. The training/test sets were built taking randomly 25 % of each cluster as the test set, while the remaining 75 % were used as the training set. In the situation of singletons, the compounds have been designated for the training set, but the equilibration of the test set was performed by the inclusion of supplementary compounds from larger clusters.

MLR method

As the number of calculated descriptors of 1217 is too high compared to the number of compounds (N = 127), an appropriate variable selection method was necessary. The Genetic Algorithm (GA) is a reliable and extensively used variable selection method.[27,28] GA uses a stochastic algorithm that elucidates the optimization issues illustrated by fitness criteria, involving the evolution assumption of Darwin and various genetic functions, including crossover and mutation. The MobyDigs[29] package uses GAs to select the significant descriptors that influence the variation of biological activity of the compounds studied in this work. In MobyDigs, the following parameters were used: the RQK fitness function[30] with leave-one-out cross-validation[31] correlation coefficient as constrained function to be optimized, a crossover/mutation trade-off parameter of T = 0.5 and a model population size of P = 50.

PLS method

The PLS method is a statistical modeling technique that simultaneously works with two matrices, **X** (dependent variables, *e.g.*, molecular descriptors) and **Y** (independent variables, *e.g.*, biological activity) to model the relationship between them.[32] The relationship between the **X** and **Y** matrices is described as a latent variable approach and is preferable for large data sets.[33] The main advantage of this method in comparison to MLR is that interrelated variables can be included in the model. This could lead to a stable and highly predictive model.[34] Using the SIMCA-P+ 12.0 package,[35] the QSAR matrix (including the **X** and **Y** matrices) was analyzed in the first step by Principal Component Analysis (PCA),[36] and subsequently by Partial Least Squares (PLS)[37] approaches. The PLS method is especially useful for larger data sets. The squared correlation regression coefficient R^2, and the squared cross-validated correlation coefficient, Q^2, are the most important statistical parameters that provide a measure of the quality and validity for the final PLS model, while the Variables Importance in the Projection (VIP) values and the sign of the coefficients of the variables are more relevant in explaining the activity mechanism. The significant principal components were selected by 7 cross-validation groups.

Model validity

The predictability of the model was tested with the Golbraikh–Tropsha[38-40] criteria and the goodness of fit with the *Y*-randomization test.[41] The following Golbraikh–Tropsha conditions should be satisfied to certify the predictive ability of the MLR and PLS models:

i) $Q^2 > 0.5$ (squared cross-validation correlation coefficient);

ii) $R^2 > 0.6$ (the squared correlation coefficient R between the predicted and observed activities);

iii) $(R^2 - R_0^2) / R^2 < 0.1$ or $(R^2 - R_0'^2) / R^2 < 0.1$ and $0.85 \le k \le 1.15$ or $0.85 \le k' \le 1.15$ (concerning the coefficients of determination for the predicted *vs*. the observed activities R_0^2, and the observed *vs*. predicted activities $R_0'^2$ through the origin and slopes k and k' of the regression lines through the origin);

iv) $\left|R_0^2 - R_0'^2\right| < 0.3$.

The predictive power of QSAR models is frequently judged based on the predictive parameter R^2 (R_{pred}^2).[42] For a predictive QSAR model, the value of R_{pred}^2 (presented in Eq. (1)) should be higher than 0.5:[24,42]

$$R_{\text{pred}}^2 = 1 - \frac{\sum\left(Y_{\text{pred(test)}} - Y_{\text{(test)}}\right)^2}{\sum\left(Y_{\text{(test)}} - \bar{Y}_{\text{training}}\right)^2} \quad (1)$$

The *Y*-randomization test is a widely used technique that displays the robustness of a QSAR model, being a measure of the model overfit. The dependent variable (biological activity) is randomly shuffled and a QSAR model is built using the same descriptor matrix. The obtained MLR and PLS models (after 500 randomizations) must have the minimal R^2 and Q^2 values.[42]

RESULTS AND DISSCUSION

MLR analysis

Using the above-mentioned genetic algorithm, the best MLR Equation (2) was obtained:

$$A_i = 33.915(\pm 5.594) - 0.155(\pm 0.011)DELS - 43.507(\pm 8.332)X0A + 3.724(\pm 0.254)GGI3 + 5.056(\pm 1.072)GATS1v - 3.075(\pm 0.649)R4u \quad (2)$$

$$N_{\text{training}} = 95, N_{\text{test}} = 32; R^2 = 0.826; Q^2_{\text{LOO}} = 0.802; Q^2_{\text{boot}} = 0.788;$$

$$Q^2_{\text{ext}} = 0.618; a(R^2) = 0.156; a(Q^2) = 0.039; R^2_{\text{adj}} = 0.816; SDEC = 0.66;$$

$$F = 84.4; s = 0.682; AIC = 0.528; Kx = 32.21; Kxy = 38.06$$

where R^2 represents the correlation coefficient, Q^2_{LOO} – leave-one-out cross-validation parameter, Q^2_{boot} – bootstrapping parameter,[31] Q^2_{ext} – external Q^2,[31] $a(R^2)$ and $a(Q^2)$ – *Y*-scrambling variables,[31] R^2_{adj} – adjusted R^2, *SDEP* – standard deviation error in the prediction, *SDEC* – standard deviation error in the calculation,[31] *F* – Fischer test, *s* – standard error of estimate, *AIC* – Akaike information criterion,[31] the multivariate *K* – correlation indices (*Kx* – the multivariate correlation index of the matrix of *X* descriptors and *Kxy* – the multivariate correlation index of the matrix of *X* descriptors and *Y* response variables).[31]

In the present study, the best MLR model had five parameters. A higher or lower number of molecular descriptors did not have any significant effect on the accuracy of the model. Additionally, the predictive R^2 (leave-one-out cross validation parameter, Q^2_{LOO}) and external Q^2 (Q^2_{ext}) values were calculated and are presented in Table I. The most important descriptors (Table S-II in the Supple-

TABLE I. Correlation matrix of the five selected descriptors included in E 2; *DELS* represents the molecular electrotopological variation; *X*0*A* represents the average connectivity index of order 0; *GGI*3 represents the topological charge index of order 3; *GATS*1*v* represents the Geary autocorrelation of lag 1 weighted by the van der Waals volume; *R*4*u* represents the *R* autocorrelation of lag 4 / unweighted

	DELS	*X*0*A*	*GGI*3	*GATS*1v	*R*4*u*
DELS	1.000				
*X*0*A*	0.182	1.000			
*GGI*3	0.056	0.477	1.000		
*GATS*1*v*	–0.099	0.295	0.119	1.000	
*R*4*u*	–0.215	0.261	0.372	0.512	1.000

mentary material to this paper), selected by a genetic algorithm, which influence the anti-HIV activity are the topological *DELS* descriptor (which describes the molecular electrotopological variation), the *X0A* (average connectivity index chi-0) connectivity index, the *GGI*3 (topological charge index of order 3 topological charge index, the *GATS*1*v* (Geary autocorrelation of lag 1/weighted by the van der Waals volume) 2D autocorrelations and the *R*4*u* (*R* autocorrelation of lag 4/unweighted) GETAWAY descriptors.[21]

An intercorrelation analysis of the selected molecular descriptors performed with the Statistica software[43] is presented in Eq. (2) (Table I). The five selected descriptors are not intercorrelated.

The statistical results and intercorrelation coefficients presented in Eq. (2) and Table I, which the MLR method associated with a proper variable selection procedure, generates an efficient QSAR model for predicting the anti-HIV-1 activity of the different HEPT derivatives.

PLS analysis

A PCA model was built with the SIMCA-P+ version 12.0[35] software for the whole **X** matrix (including N = 127 compounds and X = 1217). From the 63 significant principal components resulting from this analysis, the first three components already explained 58.2 % of the information content of the descriptor matrix. PLS calculations were also performed by the same program using 95 HEPT derivatives as a training set and 32 compounds as a test set. The statistical results of the PLS model: R^2_Y(CUM) = 0.864 and Q^2(CUM) = 0.794 obtained for the four principal components demonstrated the model overfit. This inconvenience was overcome by excluding the noise variables from this model (*i.e.*, the variables with coefficient values insignificantly different from 0). Thus, a robust model, M17 (N = 95 and X = 63) with one latent variable (Table II) was obtained. Thus, the predictive power of the final PLS model was tested in the next step using the Golbraikh–Tropsha criteria, and the R^2_{pred} tests.

TABLE II. Statistical characteristics of the final PLS model; $R^2_{X\,(\text{CUM})}$ and $R^2_{Y(\text{CUM})}$ are the cumulative sum of squares of all the X and Y values, respectively, explained by all extracted principal components; $Q^2_{(\text{CUM})}$ is the fraction of the total variation of the Y values that can be predicted for all the A extracted principal components in the cross-validation procedure (7 rounds) used to establish the number of significant principal components, A

PLS model	$R^2_{X\,(\text{CUM})}$	$R^2_{Y(\text{CUM})}$	Q^2(CUM)	N	A	X
M17	0.471	0.809	0.803	95	1	63

The descriptors summarized by the significant first principal component in M17 explain 47.1 % of the variation. 31 of the 63 selected variables in M17 (Table III) had *VIP* values greater than 1 and were considered to be the most relevant for the model.

TABLE III. The coefficients in descending order of *VIP* values for the first principal component of the M17 model

No.	Variable ID	*CoefCS* [1]	*VIP* [1]	Descriptor significance
1	MATS5e[a]	–0.0271	1.303	Moran autocorrelation of lag 5 weighted by the Sanderson electronegativity
2	PW4[b]	0.0262	1.257	Path/walk 4 – Randic shape index
3	GATS5e[a]	0.0256	1.231	Geary autocorrelation of lag 5 weighted by the Sanderson electronegativity
4	X3A[c]	–0.0248	1.190	Average connectivity index of order 3
5	Ms[d]	–0.0247	1.186	Mean electrotopological state
6	Me[c]	–0.0242	1.162	Mean atomic Sanderson electronegativity (scaled on the carbon atom)
7	CIC3[e]	0.0241	1.157	Complementary Information Content index (neighborhood symmetry of 3rd order)
8	SPAM[f]	–0.0238	1.143	average span *R*
9	SIC3[e]	–0.0238	1.141	Structural Information Content index (neighborhood symmetry of 3rd order)
10	ATS5p[a]	0.0237	1.139	Broto–Moreau autocorrelation of lag 5 (log function) weighted by polarizability
11	BIC4[e]	–0.0236	1.131	Bond Information Content index (neighborhood symmetry of 4th order)
12	CIC4[e]	0.0235	1.129	Complementary Information Content index (neighborhood symmetry of 4th order)
13	AlogP[g]	0.0234	1.123	Ghose–Crippen octanol–water partition coeff. (log *P*)
14	MATS7e[a]	–0.0233	1.117	Moran autocorrelation of lag 7 weighted by the Sanderson electronegativity
15	MATS5m[a]	–0.0233	1.117	Moran autocorrelation of lag 5 weighted by mass
16	GATS5m[a]	0.0232	1.115	Geary autocorrelation of lag 5 weighted by mass
17	MATS6e[a]	0.0232	1.113	Moran autocorrelation of lag 6 weighted by the Sanderson electronegativity
18	nHAcc[h]	–0.0232	1.113	Number of acceptor atoms for H-bonds (N,O,F)
19	SIC4[e]	–0.0231	1.108	Structural Information Content index (neighborhood symmetry of 4th order)
20	GATS7e[a]	0.0230	1.105	Geary autocorrelation of lag 7 weighted by the Sanderson electronegativity
21	SEigv[i]	0.0229	1.101	Eigenvalue sum from the van der Waals weighted distance matrix
22	R8p[j]	0.0227	1.090	*R* autocorrelation of lag 8 / weighted by polarizability
23	BIC5[e]	–0.0227	1.088	Bond Information Content index (neighborhood symmetry of 5th order)
24	SEigp[i]	0.0225	1.081	Eigenvalue sum from polarizability weighted distance matrix

TABLE III. Continued

No.	Variable ID	*CoefCS* [1]	*VIP* [1]	Descriptor significance
25	ATS5v[a]	0.0225	1.079	Broto–Moreau autocorrelation of lag 5 (log function) weighted by the van der Waals volume
26	SEige[i]	–0.0223	1.072	Eigenvalue sum from electronegativity weighted by the distance matrix
27	Mor04m[k]	–0.0223	1.071	signal 04 / weighted by mass
28	ATS4v[a]	0.0221	1.061	Broto–Moreau autocorrelation of lag 4 (log function) weighted by the van der Waals volume
29	Mor04p[k]	–0.0220	1.056	signal 04 / weighted by the polarizability
30	nO[b]	–0.022	1.055	Number of oxygen atoms
31	Hy[g]	–0.021	1.040	Hydrophilic factor

[a]2D autocorrelations; [b]topological descriptors; [c]connectivity indices; [d]constitutional descriptors; [e]information indices; [f]geometrical descriptors; [g]molecular properties; [h]functional group counts; [i]eigenvalue-based ondices; [j]GETAWAY descriptors; [k]3D-Morse descriptors

Model validation results

The predictive abilities of the best MLR and PLS models were tested (Table IV) using the Golbraikh–Tropsha criteria and the R^2_{pred} test (see Model Validity section). All the calculated parameters indicated that both models showed a good predictive power.

TABLE IV. Predictive power results for the external test set; Golbraikh and Tropsha criteria were used

Model	M1 (MLR)	M17 (PLS)
R^2	0.675	0.717
R_0^2	0.655	0.714
R'^2_0	0.635	0.952
k	1.000	0.937
k'	0.974	1.000
$\lvert R_0^2 - R'^2_0 \rvert$	0.02	0.238
$\frac{R^2 - R_0^2}{R^2}$	0.029	0.042
$\frac{R^2 - R'^2_0}{R^2}$	0.059	–0.61
R^2_{pred}	0.663	0.715

Analyzing the results of the external test set listed in Table IV, it could be observed that all the Golbraikh–Tropsha criteria were fulfilled.

The dependence between the observed (A_{obs}) *vs.* predicted (A_{pred}) anti-HIV activity values is presented in Fig. 2a for the final MLR model and in Fig. 2b for the final PLS model.

The *Y*-randomization procedure was applied to the test set by SIMCA-P+ +12.0 software[35] (for the final PLS model) and by the MobyDigs program[29] (for the final MLR model). This gave the following intercept (PLS/MLR) values of the regression lines obtained by the correlation between the calculated R^2, respectively Q^2 values of the original *Y*-variable and the shuffled *Y*-variable, respectively: –0.00267/0.159 for the R_Y^2 line and –0.125/0.039 for the Q_Y^2 line. The slope values close to zero indicate stable models.

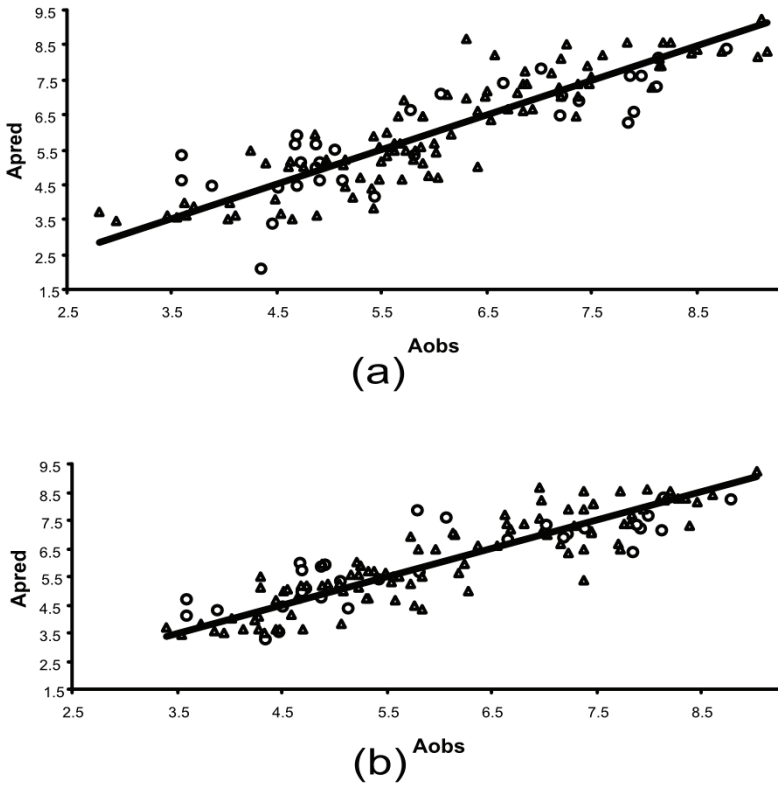

Fig. 2. Plots of the predicted (A_{pred}) *vs.* observed (A_{obs}) anti-HIV activity for the training set (triangles) and the test set (circles) for the final MLR (a) and PLS (b) model.

CONCLUSIONS

The final models obtained using the MLR and PLS methods had good statistical parameters and excellent predictive capacity.

The most important molecular descriptors included in the final MLR and PLS models are related to the geometric representation of the molecules, providing information on the interatomic distances, topological distances, types of atoms (in case of 2D-autocorrelation descriptors), information derived from the molecular graph in 2D space, *i.e.*, the connectivity, counting paths, walks, vertex

degree of the atoms, *etc*. (expressed by connectivity indices and topological descriptors) and 3D information (by the GETAWAY parameters).

SUPPLEMENTARY MATERIAL

The chemical structure of the studied HEPT derivatives, predicted anti-HIV-1 activity values and the selected molecular descriptors included in the final MLR model, and predicted activity value obtained by the PLS method, are available electronically from http://www.shd.org.rs/JSCS/, or from the corresponding author on request.

Acknowledgements. This project was financially supported by Project 1.1 and 1.2 of the Institute of Chemistry of the Romanian Academy. Statistica, MobyDigs and Simca-P+ acquisition was funded by Ministerul Educatiei, Cercetarii si Tineretului – Autoritatea Nationala pentru Cercetare Stiintifica (MedC-ANCS), Romania, Contract Grant No.: 71GR/2006.

ИЗВОД

QSAR МОДЕЛОВАЊЕ АНТИ-HIV-1 АКТИВНОСТИ ДЕРИВАТА 1-[(2-ХИДРОКСИЕТОКСИ)МЕТИЛ]-6-(ФЕНИЛТИО)ТИМИНА ПРИМЕНОМ МЕТОДОЛОГИЈА ВИШЕСТРУКЕ ЛИНЕАРНЕ РЕГРЕСИЈЕ И ПАРЦИЈАЛНИХ НАЈМАЊИХ КВАДРАТА

DANIELA IVAN, LUMINITA CRISAN, SIMONA FUNAR-TIMOFEI и MIRCEA MRACEC

Institute of Chemistry of Romanian Academy, Timisoara, Romania

Изведено је QSAR моделовање применом методологије вишеструке линеарне регресије (MLR) и парцијалних најмањих квадрата (PLS) на серији од 127 деривата 1-[(2-хидроксиетокси)метил]-6-(фенилтио)тимина (HEPT), који су моћни инхибитори реверсне транскриптазе (RT) вируса хумане имунодефициенције типе HIV-1. Да би се истражила веза између дескриптора структуре HEPT деривата (као независних променљивих) и анти-HIV-1 активности, изражене преко $\log(1/EC_{50})$ вредности, примењене су MLR и PLS методе. На основу квадрата коефицијената корелације, чије вредности леже између 0,826 и 0,809, закључено је да обе методе (MLR и PLS) имају скоро идентичну моћ предвиђања.

(Примљено 13. јула 2012)

REFERENCES

1. M. E. Goldman, J. H. Nunberg, J. A. O'Brien, J. C. Quintero, W. A. Schleif, K. F. Freund, S. Lee Gaul, W. S. Saari, J. S. Wai, J. M. Hoffman, P. S. Anderson, D. J. Hupe, E. A. Emin, *Proc. Natl. Acad. Sci. U.S.A.* **88** (1991) 6863
2. E. De Clercq, *Pure Appl. Chem.* **73** (2001) 55
3. M. Baba, H. Tanaka, E. De Clercq, R. Pauwels, J. Balzarini, D. Schols, H. Nakashima, C. F. Perno, R. T. Walker, T. Miyasaka, *Biochem. Biophys. Res. Commun.* **165 (**1989) 1375
4. T. Miyasaka, H. Tanaka, R. T. Walker, J. Balzarini, E. De Clercq, *J. Med. Chem.* **32** (1989) 2507
5. H. Tanaka, H. Takashima, M. Ubasawa, K. Sekiya, I. Nitta, M. Baba, S. Shigeta, R. T. Walker, E. DeClercq, T. Miyasaka, *J. Med. Chem.* **35** (1992) 337
6. H. Tanaka, H. Takashima, M. Ubasawa, K. Sekiya, I. Nitta, M. Baba, S. Shigeta, R. T. Walker, E. DeClercq, T. Miyasaka, *J. Med. Chem.* **35** (1992) 4713

7. H. Tanaka, H. Takashima, M. Ubasawa, K. Sekiya, N. Inouye, M. Baba, S. Shigeta, R. T. Walker, E. DeClercq, T. Miyasaka, *J. Med. Chem.* **38** (1995) 2860
8. H. Bazoui, M. Zahouily, S. Sebti, S. Boulajaaj, D. Zakarya, *J. Mol. Modell.* **8** (2002) 1
9. H. Bazoui, M. Zahouily, S. Boulajaaj, S. Sebti, D. Zakarya, *SAR QSAR Environ. Res.* **13** (2002) 567
10. M. Mracec, D. Ivan, M. Mracec, *Rev. Roum. Chim.* **49** (2004) 431
11. L. Douali, D. Villemin, A. Zyad, D. Cherqaoui, *Mol. Diversity* **8** (2004) 1
12. M. Zahouily, J. Rakik, M. Lazar, M. A. Bahlaoui, A. Rayadh, N. Komiha, *ARKIVOC* (2007) 245
13. L. Lawtrakul, C. Prakasvudhisarn, *Monatsh. Chem.* **136** (2005) 1681
14. A. Bak, J. Polanski, *Bioorg. Med. Chem.* **14** (2006) 273
15. M. Arakawa , K. Hasegawa , K. Funatsu, *Chemom. Intell. Lab. Syst.* **83** (2006) 91
16. C. Duda-Seiman, D. Duda-Seimana, M. V. Putz, D. Ciubotariu, *Dig. J. Nanomater. Bios.* **2** (2007) 207
17. V. Ravichandran, V. K. Mourya, R. K. Agrawal, *Dig. J. Nanomater. Bios.* **3** (2008) 9
18. R. S. Latha, R. Vijayaraj, E. R. Singam, K. Chitra, V. Subramanian, *Chem. Biol. Drug. Des.* **78** (2011) 418
19. A. Afantitis, G. Melagraki, H. Sarimveis, O. Igglessi-Markopoulou, J. Markopoulos, P.A. Koutentis, *Mol. Diversity* **10** (2006) 405
20. A. Ganjee , X. Lin, *J. Med. Chem.* **48** (2005) 1448
21. R. Todeschini, V. Consonni, *Molecular Descriptors for Chemoinformatics*, Wiley-VCH, New York, USA, 2009
22. HYPERCHEM 7.52, release for windows; hypercube, Inc., Gainesville, FL, USA, http://www.hyper.com
23. DRAGON, version 3.0, 2003 for windows (software for molecular descriptor calculations), http://www.talete.mi.it
24. J. T. Leonard, K. Roy, *SAR Comb. Sci.* **25** (2006) 235
25. R Development Core Team 2010, ISBN 3-900051-07-0, available at www.r-project.org
26. L. Kaufman, P. J. Rousseeuw, *Finding Groups in Data: An Introduction to Cluster Analysis*, Wiley, New York, 1990
27. U. Depczynski, V. J. Frost, K. Molt, *Anal. Chim. Acta* **420** (2000) 217
28. B. K. Alsberg, N. Marchand-Geneste, R. D. King, *Chemom. Intell. Lab. Syst.* **54** (2000) 75
29. R. Todeschini, V. Consonni, A. Mauri, M. Pavan, in *Nature-inspired Methods in Chemometrics: Genetic Algorithms and Artificial Neural Networks*, R. Leardi, Ed., Elsevier, Amsterdam, 2004, p.141
30. R. Todeschini, V. Consonni, A. Mauri, M. Pavan, *Anal. Chim. Acta* **515** (2004) 199
31. D. M. Hawkins, S. C. Basak, D. Mills, *J. Chem. Inf. Comput. Sci.* **43** (2003) 579
32. H. Wold, in *Multivariate analysis*, P. R. Krishnaiah, Ed., Academic Press, New York, 1966, p. 391
33. L. Eriksson, J. Gottfries, E. Johansson, S. Wold, *Chemom. Intell. Lab. Syst.* **73** (2004) 73
34. A. Höskuldsson, *J. Chemom.* **2** (1988) 211
35. SIMCA-P+, version 12.0, Umetrics AB: Umea, Sweden, http://www.umetrics.com
36. M. Daszykowski, K. Kaczmarek, V. Heyden, B. Walczak, *Chemom. Intell. Lab. Syst.* **85** (2007) 203
37. H. Wold, in *Encyclopedia of Statistical Sciences*, Vol. 6, S. Kotz, N. L. Johnson, Eds., Wiley, New York, 1985, p. 581

38. A. Golbraikh, A. Tropsha, *J. Comput.-Aided Mol. Des.* **16** (2002) 357
39. A. Golbraikh, A. Tropsha, *J. Comput.-Aided Mol. Des.* **20** (2002) 269
40. A. Golbraikh, M. Shen, Z. Xiao, K. H. Lee, A. Tropsha, *J. Comput.-Aided Mol. Des.* **17** (2003) 241
41. F. Lindgren, B. Hansen, W. Karcher, M. Sjöström, L. Eriksson, *J. Chemom.* **10** (1996) 521
42. P. P. Roy, S. Paul, I. Mitra, K. Roy, *Molecules* **14** (2009) 1660
43. Statistica 7.1, StatSoft Inc., Tulsa, OK, USA.

Journal of the Serbian Chemical Society
JSCS@tmf.bg.ac.rs • www.shd.org.rs/JSCS
J. Serb. Chem. Soc. 78 (4) S30–S36 (2013) *Supplementary material*

SUPPLEMENTARY MATERIAL TO

A quantitative structure–activity relationships study for the anti-HIV-1 activities of 1-[(2-hydroxyethoxy)methyl]-6--(phenylthio)thymine derivatives using the multiple linear regression and partial least squares methodologies

DANIELA IVAN, LUMINITA CRISAN*, SIMONA FUNAR-TIMOFEI and MIRCEA MRACEC

Institute of Chemistry of Romanian Academy, Department of Computational Chemistry, 24 Mihai Viteazul Bvd., 300223, Timisoara, Romania

J. Serb. Chem. Soc. 78 (4) (2013) 495–506

TABLE S-I. The chemical structure of the studied HEPT derivatives (Fig. 1 in the native paper) and the observed (A_{obs}) anti-HIV-1 activity values

No.	R_1	R_2	R_3	X	Y	A_{obs}
1	$CH_2OCH_2CH_2OH$	CH_3	2-CH_3	O	S	4.15
2	$CH_2OCH_2CH_2OH$	CH_3	2-NO_2	O	S	3.85
3	$CH_2OCH_2CH_2OH$	CH_3	2-OCH_3	O	S	4.72
4	$CH_2OCH_2CH_2OH$	CH_3	3-CH_3	O	S	5.59
5	$CH_2OCH_2CH_2OH$	CH_3	3-CH_2CH_3	O	S	5.57
6[a]	$CH_2OCH_2CH_2OH$	CH_3	3-$C(CH_3)_3$	O	S	4.92
7[a]	$CH_2OCH_2CH_2OH$	CH_3	3-CF_3	O	S	4.35
8	$CH_2OCH_2CH_2OH$	CH_3	3-F	O	S	5.48
9[a]	$CH_2OCH_2CH_2OH$	CH_3	3-Cl	O	S	4.89
10	$CH_2OCH_2CH_2OH$	CH_3	3-Br	O	S	5.24
11	$CH_2OCH_2CH_2OH$	CH_3	3-I	O	S	5.00
12[a]	$CH_2OCH_2CH_2OH$	CH_3	3-NO_2	O	S	4.47
13	$CH_2OCH_2CH_2OH$	CH_3	3-OH	O	S	4.09
14	$CH_2OCH_2CH_2OH$	CH_3	3-OCH_3	O	S	4.66
15	$CH_2OCH_2CH_2OH$	CH_3	3,5-$(CH_3)_2$	O	S	6.59
16	$CH_2OCH_2CH_2OH$	CH_3	3,5-Cl_2	O	S	5.89
17[a]	$CH_2OCH_2CH_2OH$	CH_3	3,5-$(CH_3)_2$	S	S	6.66
18	$CH_2OCH_2CH_2OH$	CH_3	3-$COOCH_3$	O	S	5.10
19[a]	$CH_2OCH_2CH_2OH$	CH_3	3-$COCH_3$	O	S	5.14
20	$CH_2OCH_2CH_2OH$	CH_3	3-CN	O	S	5.00
21	$CH_2OCH_2CH_2OH$	$CH_2CH{=}CH_2$	H	O	S	5.60
22	$CH_2OCH_2CH_2OH$	CH_2CH_3	H	S	S	6.96
23	$CH_2OCH_2CH_2OH$	$CH_2CH_2CH_3$	H	S	S	5.00

* Corresponding author. E-mail: lumi_crisan@acad-icht.tm.edu.ro

TABLE S-I. Continued

No.	R_1	R_2	R_3	X	Y	A_{obs}
24[a]	$CH_2OCH_2CH_2OH$	$CH(CH_3)_2$	H	S	S	7.23
25	$CH_2OCH_2CH_2OH$	CH_2CH_3	3,5-$(CH_3)_2$	S	S	8.11
26	$CH_2OCH_2CH_2OH$	$CH(CH_3)_2$	3,5-$(CH_3)_2$	S	S	8.30
27	$CH_2OCH_2CH_2OH$	CH_2CH_3	3,5-Cl_2	S	S	7.37
28	$CH_2OCH_2CH_2OH$	CH_2CH_3	H	O	S	6.92
29	$CH_2OCH_2CH_2OH$	$CH_2CH_2CH_3$	H	O	S	5.47
30	$CH_2OCH_2CH_2OH$	$CH(CH_3)_2$	H	O	S	7.20
31	$CH_2OCH_2CH_2OH$	CH_2CH_3	3,5-$(CH_3)_2$	O	S	7.89
32	$CH_2OCH_2CH_2OH$	$CH(CH_3)_2$	3,5-$(CH_3)_2$	O	S	8.57
33[a]	$CH_2OCH_2CH_2OH$	CH_2CH_3	3,5-Cl_2	O	S	7.85
34	$CH_2OCH_2CH_2OH$	CH_3	4-CH_3	O	S	3.66
35	$CH_2OCH_2CH_2OH$	CH_3	H	O	S	5.15
36	$CH_2OCH_2CH_2OH$	CH_3	H	S	S	6.01
37[a]	$CH_2OCH_2CH_2OH$	I	H	O	S	5.44
38	$CH_2OCH_2CH_2OH$	$CH=CH_2$	H	O	S	5.69
39	$CH_2OCH_2CH_2OH$	$CH=CHC_6H_5$	H	O	S	5.22
40	$CH_2OCH_2CH_2OH$	$CH_2C_6H_5$	H	O	S	4.37
41[a]	$CH_2OCH_2CH_2OH$	$CH=C(C_6H_5)_2$	H	O	S	6.07
42[a]	$CH_2OCH_2CH_2OCH_3$	CH_3	H	O	S	5.06
43	$CH_2OCH_2CH_2OCOOCH_3$	CH_3	H	O	S	5.17
44	$CH_2OCH_2CH_2OCOC_6H_5$	CH_3	H	O	S	5.12
45	$CH_2OCH_2CH_3$	CH_3	H	O	S	6.48
46[a]	$CH_2OCH_2CH_2Cl$	CH_3	H	O	S	5.82
47	$CH_2OCH_2CH_2N_3$	CH_3	H	O	S	5.24
48	$CH_2OCH_2CH_2F$	CH_3	H	O	S	5.96
49	$CH_2OCH_2CH_2CH_3$	CH_3	H	O	S	5.48
50	$CH_2OCH_2C_6H_5$	CH_3	H	O	S	7.06
51	$CH_2OCH_2CH_3$	CH_2CH_3	H	O	S	7.72
52	$CH_2OCH_2CH_3$	CH_2CH_3	H	S	S	7.58
53	$CH_2OCH_2CH_3$	CH_2CH_3	3,5-$(CH_3)_2$	O	S	8.24
54	$CH_2OCH_2CH_3$	CH_2CH_3	3,5-$(CH_3)_2$	S	S	8.30
55	$CH_2OCH_2C_6H_5$	CH_2CH_3	H	O	S	8.23
56	$CH_2OCH_2C_6H_5$	CH_2CH_3	3,5-$(CH_3)_2$	O	S	8.55
57	$CH_2OCH_2C_6H_5$	CH_2CH_3	H	S	S	8.09
58	$CH_2OCH_2C_6H_5$	CH_2CH_3	3,5-$(CH_3)_2$	S	S	8.14
59[a]	$CH_2OCH_2CH_3$	$CH(CH_3)_2$	H	O	S	7.99
60	$CH_2OCH_2C_6H_5$	$CH(CH_3)_2$	H	O	S	8.51
61	$CH_2OCH_2CH_3$	$CH(CH_3)_2$	H	S	S	7.89
62[a]	$CH_2OCH_2C_6H_5$	$CH(CH_3)_2$	H	S	S	8.14
63	CH_2OCH_3	CH_3	H	O	S	5.68
64	$CH_2OCH_2CH_2CH_2CH_3$	CH_3	H	O	S	5.33
65	CH_2CH_3	CH_3	H	O	S	5.66
66	$CH_2CH_2CH_2CH_3$	CH_3	H	O	S	5.92
67	$CH_2OCH_2CH_3$	CH_2CH_3	3,5-Cl_2	S	S	7.89
68	$CH_2OCH(CH_3)_2$	CH_2CH_3	H	S	S	6.66
69[a]	CH_2O-*c*-C_6H_{11}	CH_2CH_3	H	S	S	5.79

TABLE S-I. Continued

No.	R_1	R_2	R_3	X	Y	A_{obs}
70	CH_2OCH_2-*c*-C_6H_{11}	CH_2CH_3	H	S	S	6.45
71	$CH_2OCH_2C_6H_4$(4-CH_3)	CH_2CH_3	H	S	S	7.11
72[a]	$CH_2OCH_2C_6H_4$(4-Cl)	CH_2CH_3	H	S	S	7.92
73	$CH_2OCH_2CH_2C_6H_5$	CH_2CH_3	H	S	S	7.04
74[a]	$CH_2OCH_2CH_3$	CH_2CH_3	3,5-Cl_2	O	S	8.13
75	$CH_2OCH(CH_3)_2$	CH_2CH_3	H	O	S	6.47
76	CH_2O-*c*-C_6H_{11}	CH_2CH_3	H	O	S	5.40
77	CH_2OCH_2-*c*-C_6H_{11}	CH_2CH_3	H	O	S	6.35
78	$CH_2OCH_2CH_2C_6H_5$	CH_2CH_3	H	O	S	7.02
79[a]	$CH_2OCH_2CH_3$	*c*-C_3H_5	H	S	S	7.02
80	$CH_2OCH_2CH_3$	*c*-C_3H_5	H	O	S	7.00
81	$CH_2OCH_2CH_2O$-*n*-C_5H_{11}	CH_3	H	O	S	4.46
82[a]	$CH_2OCH_2CH_2OH$	CH_3	2-Cl	O	S	3.89
83	$CH_2OCH_2CH_2OH$	CH_3	3-CH_2OH	O	S	3.53
84	$CH_2OCH_2CH_2OH$	CH_3	4-F	O	S	3.60
85	$CH_2OCH_2CH_2OH$	CH_3	4-Cl	O	S	3.60
86	$CH_2OCH_2CH_2OH$	CH_3	4-NO_2	O	S	3.72
87	$CH_2OCH_2CH_2OH$	CH_3	4-CN	O	S	3.60
88	$CH_2OCH_2CH_2OH$	CH_3	4-OH	O	S	3.56
89[a]	$CH_2OCH_2CH_2OH$	CH_3	4-OCH_3	O	S	3.60
90	$CH_2OCH_2CH_2OH$	CH_3	4-$COCH_3$	O	S	3.96
91	$CH_2OCH_2CH_2OH$	CH_3	4-COOH	O	S	3.45
92	$CH_2OCH_2CH_2OH$	CH_3	3-$CONH_2$	O	S	3.51
93	$CH_2OCH_2CH_2OH$	$COOCH_3$	H	O	S	5.18
94	$CH_2OCH_2CH_2OH$	$CONHC_6H_5$	H	O	S	4.74
95[a]	$CH_2OCH_2CH_2OH$	SC_6H_5	H	O	S	4.68
96[a]	$CH_2OCH_2CH_2OH$	CCH	H	O	S	4.74
97	$CH_2OCH_2CH_2OH$	CCC_6H_5	H	O	S	5.47
98	$CH_2OCH_2CH_2OH$	CH_3	3-NH_2	O	S	3.60
99[a]	$CH_2OCH_2CH_2OH$	$COCH(CH_3)_2$	H	O	S	4.92
100[a]	$CH_2OCH_2CH_2OH$	COC_6H_5	H	O	S	4.89
101	$CH_2OCH_2CH_2OH$	$CCCH_3$	H	O	S	4.72
102	$CH_2OCH_2CH_2OH$	F	H	O	S	4.00
103[a]	$CH_2OCH_2CH_2OH$	Cl	H	O	S	4.52
104[a]	$CH_2OCH_2CH_2OH$	Br	H	O	S	4.70
105[a]	$CH_2OCH_2CH_2OCH_2C_6H_5$	CH_3	H	O	S	4.70
106[a]	H	CH_3	H	O	S	3.60
107	CH_3	CH_3	H	O	S	3.82
108	$CH_2OCH_2CH_2OH$	CH_2CH_3	H	O	CH_2	6.45
109[a]	$CH_2OCH_2CH_2OH$	CH_2CH_3	CH_3	O	CH_2	7.88
110	$CH_2OCH_2CH_3$	CH_2CH_3	H	O	CH_2	7.38
111[a]	$CH_2OCH_2CH_3$	CH_2CH_3	CH_3	O	CH_2	8.79
112[a]	$CH_2OCH_2CH_2OH$	$CH(CH_3)_2$	H	O	CH_2	7.20
113	$CH_2OCH_2CH_2OH$	$CH(CH_3)_2$	CH_3	O	CH_2	8.56
114	$CH_2OCH_2CH_3$	$CH(CH_3)_2$	H	O	CH_2	7.37
115	$CH_2OCH_2CH_3$	$CH(CH_3)_2$	CH_3	O	CH_2	9.22

TABLE S-I. Continued

No.	R_1	R_2	R_3	X	Y	A_{obs}
116	$CH_2CH_2CH_2CH_3$	CH_2CH_3	H	O	CH_2	6.67
117	$CH_2CH_2CH_2CH_3$	$CH(CH_3)_2$	H	O	CH_2	7.37
118	$CH_2CH_2OCH_3$	CH_2CH_3	H	O	CH_2	6.60
119	$CH_2CH_2OCH_3$	$CH(CH_3)_2$	H	O	CH_2	7.28
120	$CH_2OCH_2OCH_3$	CH_3	H	O	CH_2	4.63
121	CH_2SCH_3	CH_2CH_3	H	O	CH_2	8.68
122[a]	$CH_2SCH_2CH_3$	CH_2CH_3	H	O	CH_2	7.39
123	CH_2SCH_3	CH_2CH_3	CH_3	O	CH_2	7.30
124	$CH_2SCH_2CH_3$	CH_2CH_3	CH_3	O	CH_2	8.39
125	CH_2SCH_3	$CH(CH_3)_2$	H	O	CH_2	7.69
126	$CH_2SCH_2CH_3$	$CH(CH_3)_2$	H	O	CH_2	8.22
127	$CH_2OCH_2CH_2OH$	CH_3	H	O	O	5.05

[a]Compounds used as the test set

TABLE S-II. The predicted (A_{pred}MLR) anti-HIV-1 activity values and the selected molecular descriptors included in the final MLR model, and predicted activity value obtained by the PLS method (A_{pred}PLS)

No.	A_{pred}MLR[a]	*DELS*	*X*0*A*	*GGI*3	*GATS*1*v*	*R*4*u*	A_{pred}PLS[a]
1	5.23	28.795	0.732	1.688	1.688	1.688	4.59
2	3.71	45.114	0.737	2.063	2.063	2.063	3.72
3	5.3	32.565	0.731	1.688	1.688	1.688	4.65
4	5.6	28.698	0.732	1.813	1.813	1.813	5.16
5	5.88	29.301	0.731	1.813	1.813	1.813	5.23
6[b]	5.09	30.645	0.745	2.188	2.188	2.188	5.89
7[b]	2.05	57.318	0.745	2.188	2.188	2.188	3.25
8	4.25	38.722	0.732	1.813	1.813	1.813	4.30
9[b]	4.98	32.197	0.732	1.813	1.813	1.813	4.72
10	4.97	29.913	0.732	1.813	1.813	1.813	4.94
11	4.75	28.856	0.732	1.813	1.813	1.813	5.08
12[b]	3.36	43.993	0.737	1.938	1.938	1.938	3.48
13	4.48	35.366	0.732	1.813	1.813	1.813	4.27
14	5.69	32.199	0.731	1.813	1.813	1.813	4.45
15	6.84	29.204	0.738	2.25	2.25	2.25	6.36
16	5.42	36.155	0.738	2.25	2.25	2.25	5.24
17[b]	7.37	23.668	0.738	2.25	2.25	2.25	6.82
18	4.4	40.726	0.736	1.938	1.938	1.938	4.29
19[b]	4.62	37.93	0.737	1.938	1.938	1.938	4.37
20	4.61	34.556	0.731	1.813	1.813	1.813	4.51
21	5.47	30.928	0.724	1.625	1.625	1.625	5.49
22	6.31	23.231	0.725	1.625	1.625	1.625	6.14
23	6.42	23.897	0.724	1.625	1.625	1.625	6.27
24[b]	7	23.945	0.731	2	2	2	6.97
25	8.14	24.613	0.737	2.375	2.375	2.375	7.46
26	8.75	25.361	0.742	2.75	2.75	2.75	8.28

TABLE S-II. Continued

No.	A_{pred}MLR[a]	*DELS*	*X*0*A*	*GGI*3	*GATS*1*v*	*R*4*u*	A_{pred}PLS[a]
27	6.85	31.142	0.737	2.375	2.375	2.375	6.65
28	5.71	29.198	0.725	1.625	1.625	1.625	5.73
29	5.63	29.835	0.724	1.625	1.625	1.625	5.84
30	6.51	29.986	0.731	2	2	2	6.67
31	7.46	30.179	0.737	2.375	2.375	2.375	7.22
32	8.25	31.002	0.742	2.75	2.75	2.75	7.97
33[b]	6.23	37.167	0.737	2.375	2.375	2.375	6.32
34	4.53	28.629	0.732	1.563	1.563	1.563	4.69
35	4.98	28.322	0.726	1.5	1.5	1.5	4.74
36	5.54	22.389	0.726	1.5	1.5	1.5	5.21
37[b]	4.14	28.291	0.726	1.5	1.5	1.5	5.40
38	5.63	30.149	0.725	1.625	1.625	1.625	5.32
39	5.81	31.438	0.706	1.563	1.563	1.563	5.72
40	5.41	31.526	0.706	1.563	1.563	1.563	5.83
41[b]	7.07	33.87	0.699	2	2	2	7.54
42[b]	5.46	26.413	0.725	1.5	1.5	1.5	5.28
43	4.62	35.504	0.729	1.625	1.625	1.625	4.68
44	5.9	37.708	0.712	1.938	1.938	1.938	5.23
45	5.9	22.957	0.727	1.5	1.5	1.5	5.80
46[b]	5.34	26.066	0.726	1.5	1.5	1.5	5.61
47	5.16	28.585	0.724	1.5	1.5	1.5	5.04
48	4.86	30.71	0.726	1.5	1.5	1.5	4.89
49	5.82	23.545	0.726	1.5	1.5	1.5	5.56
50	6.13	24.845	0.706	1.563	1.563	1.563	6.13
51	6.87	23.74	0.726	1.625	1.625	1.625	6.62
52	7.5	17.916	0.726	1.625	1.625	1.625	6.96
53	8.46	24.877	0.738	2.375	2.375	2.375	8.08
54	9.18	19.399	0.738	2.375	2.375	2.375	8.35
55	6.57	25.628	0.706	1.688	1.688	1.688	6.98
56	7.84	25.912	0.718	2.313	2.313	2.313	7.37
57	7.2	19.529	0.706	1.688	1.688	1.688	7.47
58	9.09	21.051	0.718	2.438	2.438	2.438	8.46
59[b]	7.57	24.445	0.732	2	2	2	7.63
60	7.27	26.333	0.712	2.063	2.063	2.063	7.73
61	8.16	18.594	0.732	2	2	2	7.95
62[b]	8.09	20.232	0.712	2.063	2.063	2.063	8.26
63	5.67	22.002	0.728	1.5	1.5	1.5	5.38
64	5.54	24.118	0.725	1.5	1.5	1.5	5.55
65	6	18.73	0.729	1.5	1.5	1.5	6.18
66	6.16	19.75	0.727	1.5	1.5	1.5	6.23
67	8.14	25.745	0.738	2.375	2.375	2.375	7.38
68	6.71	18.578	0.732	1.625	1.625	1.625	7.70
69[b]	6.61	20.26	0.706	1.563	1.563	1.563	7.83
70	7.35	20.081	0.706	1.688	1.688	1.688	7.73

TABLE S-II. Continued

No.	A_{pred}MLR[a]	*DELS*	*X*0*A*	*GGI*3	*GATS*1*v*	*R*4*u*	A_{pred}PLS[a]
71	6.8	20.26	0.712	1.75	1.75	1.75	7.45
72[b]	6.54	23.036	0.712	1.75	1.75	1.75	7.15
73	7.2	20.04	0.706	1.688	1.688	1.688	7.44
74[b]	7.28	31.681	0.738	2.375	2.375	2.375	7.09
75	5.9	24.499	0.732	1.625	1.625	1.625	7.38
76	6.02	26.237	0.706	1.563	1.563	1.563	7.38
77	6.55	26.066	0.706	1.688	1.688	1.688	7.22
78	6.48	25.919	0.706	1.688	1.688	1.688	6.97
79[b]	7.78	18.887	0.706	1.556	1.556	1.556	7.30
80	7.38	24.606	0.706	1.556	1.556	1.556	7.02
81	5.16	28.833	0.722	1.5	1.5	1.5	5.76
82[b]	4.44	32.593	0.732	1.688	1.688	1.688	4.26
83	4.65	35.144	0.731	1.813	1.813	1.813	4.33
84	3.45	38.107	0.732	1.563	1.563	1.563	4.13
85	4.1	31.953	0.732	1.563	1.563	1.563	4.45
86	2.81	43.235	0.737	1.813	1.813	1.813	3.39
87	3.64	34.215	0.731	1.563	1.563	1.563	4.28
88	3.54	34.942	0.732	1.563	1.563	1.563	3.87
89[b]	4.58	31.967	0.731	1.563	1.563	1.563	4.09
90	4.05	37.465	0.737	1.813	1.813	1.813	4.24
91	2.97	42.161	0.737	1.813	1.813	1.813	3.54
92	4.04	39.868	0.737	1.938	1.938	1.938	3.94
93	5.49	41.535	0.73	2	2	2	4.88
94	5.95	43.411	0.712	2.188	2.188	2.188	5.33
95[b]	5.64	31.439	0.706	1.563	1.563	1.563	5.98
96[b]	5.09	31.372	0.725	1.625	1.625	1.625	5.05
97	5.73	32.936	0.706	1.563	1.563	1.563	5.61
98	4.89	32.011	0.732	1.813	1.813	1.813	4.47
99[b]	4.62	41.287	0.736	2	2	2	5.91
100[b]	5.63	43.404	0.712	2.188	2.188	2.188	5.81
101	6.03	30.251	0.724	1.625	1.625	1.625	5.31
102	3.62	38.773	0.726	1.5	1.5	1.5	4.02
103[b]	4.39	31.557	0.726	1.5	1.5	1.5	4.43
104[b]	4.43	29.031	0.726	1.5	1.5	1.5	4.89
105[b]	5.87	28.993	0.706	1.563	1.563	1.563	5.69
106[b]	5.32	17.216	0.721	1.188	1.188	1.188	4.69
107	5.43	18.036	0.73	1.375	1.375	1.375	5.06
108	5.66	29.288	0.725	1.625	1.625	1.625	5.97
109[b]	7.57	30.498	0.737	2.375	2.375	2.375	7.33
110	6.89	23.82	0.726	1.625	1.625	1.625	6.80
111[b]	8.37	25.185	0.738	2.375	2.375	2.375	8.21
112[b]	6.47	30.077	0.731	2	2	2	6.86
113	8.18	31.321	0.742	2.75	2.75	2.75	8.19
114	7.48	24.525	0.732	2	2	2	7.75

TABLE S-II. Continued

No.	A_{pred}MLR[a]	*DELS*	*X*0*A*	*GGI*3	*GATS*1*v*	*R*4*u*	A_{pred}PLS[a]
115	9.12	25.924	0.744	2.75	2.75	2.75	9.03
116	6.93	20.619	0.726	1.625	1.625	1.625	7.16
117	7.38	21.277	0.732	2	2	2	7.81
118	6.41	23.286	0.726	1.625	1.625	1.625	6.55
119	7.19	23.974	0.732	2	2	2	7.28
120	5.47	25.661	0.726	1.5	1.5	1.5	5.57
121	6.3	19.966	0.727	1.625	1.625	1.625	6.95
122[b]	6.85	20.477	0.726	1.625	1.625	1.625	7.19
123	8.08	21.4	0.74	2.375	2.375	2.375	8.38
124	8.51	21.955	0.738	2.375	2.375	2.375	8.61
125	7.11	20.619	0.734	2	2	2	7.84
126	7.61	21.135	0.732	2	2	2	8.14
127	5.14	32.136	0.726	1.5	1.5	1.5	4.55

[a]Predicted activity values obtained by the MLR (A_{pred}MLR) and PLS (A_{pred}PLS) approaches; *DELS* represents the molecular electrotopological variation; *X*0*A* represents the average connectivity index of order 0; *GGI*3 represents the topological charge index of order 3; *GATS*1*v* represents the Geary autocorrelation of lag 1 weighted by the van der Waals volume; *R*4*u* represents the *R* autocorrelation of lag 4 / unweighted; [b]compounds used as the test set

Journal of the Serbian Chemical Society
JSCS-info@shd.org.rs • www.shd.org.rs/JSCS
J. Serb. Chem. Soc. 78 (4) 507–521 (2013)
JSCS–4434
UDC 678.01+537.311.1:544.174.5:535.37+547.21.024+547.733
Original scientific paper

Spectroscopic analysis of the structure and stability of two electrochemically synthesized poly(3-alkylthiophene)s

ELAINE CRISTINA RODRIGUES MAIA[1], DANIELLY CRISTINA BENTO[1], EDSON LAURETO[2], DIMAS AUGUSTO MOROZIN ZAIA[1], ERALCI MOREIRA THERÉZIO[3], GREGORY J. MOORE[4] and HENRIQUE DE SANTANA[1]*

[1]Departamento de Química, Universidade Estadual de Londrina, 86051-990, Londrina, PR, Brazil, [2]Departamento de Física, Universidade Estadual de Londrina, 86051-990, Londrina, PR, Brazil, [3]Instituto de Física, Universidade Federal de Uberlândia, 38400-902, Uberlândia, MG, Brazil and [4]Yardney Technical Products, Inc. Pawcatuck, Stonington, CT, USA

(Received 27 March, revised 3 September 2012)

Abstract: In this work, poly (3-methylthiophene) (P3MT) and poly (3-octylthiophene) (P3OT) films were electrochemically synthesized in non-aqueous media through the oxidation of the monomers, (3-methylthiophene and 3-octylthiophene) using a standard three-electrode cell in acetonitrile with 0.100 mol L^{-1} $LiClO_4$. The polymeric thin films were deposited on platinum plates for optimal quality control of the process. It was observed that the material as-prepared by anodic electropolymerization undergoes a natural process of de-protonation as a function of time. Moreover, the partial de-doped form obtained in NH_4OH solution presents a good chemically stable form but becomes unstable again when radiated with blue light. Films obtained by these methods were characterized by cyclic voltammetry, Raman and photoluminescence spectroscopy. Both Raman and photoluminescence (PL) spectra led to the characterization of two structures (pristine and non-pristine forms of the thiophene rings), which formed the P3MT and P3OT polymer chains. These results were associated with the stabilization of pristine chains and mixed chains (non-pristine structures), radical cation and dication forms, in the polymeric film. Their bands in the Raman and PL spectra were broad and asymmetric and their adjustments by Gaussian functions indicated that there were three distinct contributions to the vibration and two to the emission spectra in the formed polymeric material.

Keywords: conducting polymers; Raman; photoluminescence; poly(alkylthiophenes).

* Corresponding author. E-mail: hensan@uel.br
doi: 10.2298/JSC120327111R

INTRODUCTION

Interest in poly(3-methylthiophene) (P3MT) and poly(3-octylthiophene) (P3OT), among the poly(3-alkylthiophene)s (P3ATs), is due mainly to the environmental stability of these materials that usually produces interfaces with metallic electrodes used in electronics.[1–5] In addition, the structural changes that accompany the electrochemical switching reaction, *i.e.*, the reversible cycling between the oxidized conducting state and the neutral insulating state, suggest the applicability of electro-active polymers in passive display devices.[6,7] However, Koizumi *et al.*[8] showed that a natural de-doping of poly(3-octylthiophene) occurs in time. This is caused by the instability of the material due to the presence of the alkyl side chains and other factors, such as the nature of the doping, the length of the alkyl side chain, temperature, humidity and the atmospheric conditions. This chemical stability was recently studied by submitting these materials to a de-doping process after their electrochemical synthesis.[9,10]

Since compounds such as P3ATs have a non-degenerate ground state, they carry the possibility of self-localized excitations, such as polarons (radical cations) and bipolarons (dications).[11] The two possible situations for counter ion-polymer interactions with the studied P3ATs, on simulating the doping of the polymeric chains of P3MT and P3OT, are shown in Fig. 1. The association of the

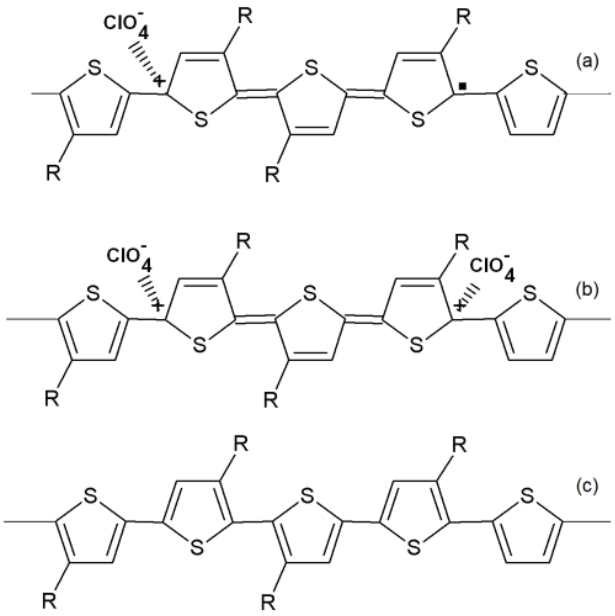

Fig. 1. Probable structures of P3MT and P3OT in the radical cation form (a), dication form (b), both doped with ClO_4^- (non-pristine forms) and pristine form (c). R represents the alkyl side chain.

counter ion (ClO_4^-) with the carbon atom in position 2 or 5 of the thiophene ring, which occurs due to coulombic interaction, forms a radical cation in the polymeric chain (Fig. 1a). However, the action of an electrochemical potential enables the formation of structures in the dication form (Fig. 1b). Through doping, the polymeric chain can present two different structures, the pristine and non-pristine forms. The formation of the non-pristine structure will only occur when a doping ion is associated with the polymeric chain. Polymeric chains like this are called mixed chains. In this context, the de-doping consists of removal of anions from the formed polymer; when that transpires, the polymer is called pristine and only pristine thiophene rings are present, Fig. 1c.[12]

In this paper, studies on the formation of P3MT and P3OT thin films on a platinum surface and the typical voltammograms of these systems are reported. Different experimental conditions were considered during the preparation of the samples, such as the electrochemical profile of the polymers, which were characterized by *ex situ* Raman and photoluminescence spectroscopy to verify the pristine and non-pristine forms present in the material. An increase in PL intensity was verified in irradiated partially de-doped P30T to obtain the PL spectrum, indicating the instability of the sample.

EXPERIMENTAL

Chemicals

The 3-methylthiophene (C_5H_7S) and the 3-octylthiophene ($C_{12}H_{20}S$) monomers were purchased from Acros-Organics – 99.0 %; lithium perchlorate ($LiClO_4$) from Acros-Organics – 99.0 % was used as the supporting electrolyte. All these reagents were used without further purification. Acetonitrile (CH_3CN) of 99.5% purity was obtained from J. T. Baker and used as supplied.

Electrochemical polymerization and samples

A standard three-electrode cell was used for cyclic voltammetry. A platinum plate (25 × 30 × 0.5 mm) acted as the working electrode and a platinum plate (10 × 10 × 0.5 mm) was used as the auxiliary electrode. The area of the working electrode covered with the film was maintained constant at 3.0 cm^2. All potentials were determined with reference to Ag/AgCl into a Luggin-Haber capillary, using a 0.100 mol L^{-1} solution of $LiClO_4$ in acetonitrile as the supporting electrolyte. The current *versus* time curve and cyclic voltammograms were obtained with a MQPG-01: Microquimica potentiostat–galvanostat controlled by a personal computer.

The polymerizations of 3-methylthiophene (0.035 mol L^{-1}) and 3-octylthiophene (0.040 mol L^{-1}) were realized at a fixed potential. The polymer synthesized on the electrode surface was obtained by taking the working electrode out of the cell and keeping it for some days under ambient conditions (referred to as “as-prepared”). The film was oxidized at 1.70 V for 1 min, using 0.100 mol L^{-1} $LiClO_4$ in acetonitrile as the supporting electrolyte (referred to as “oxidized”). The films labeled “partially de-doped” were obtained by submitting them to a concentrated basic solution (ammonium hydroxide).

Spectroscopic characterization

The Raman spectra were obtained from thin film samples using a portable Raman spectrometer DeltaNu with 785 nm laser line and a spectral resolution of 8 cm^{-1}. DeltaNu software was employed to remove background fluorescence using the baseline features.

Photoluminescence (PL) analysis

The PL spectra were recorded using a 0.5 m monochromator, a GaAs photomultiplier tube and a conventional lock-in technique for signal processing. The PL spectra were also recorded using a USB4000 Ocean Optics minispectrometer. The excitation source was a diode laser emitting at 405 nm, with a power density of 0.2 W cm^{-2}.

RESULTS AND DISCUSSION

The current *versus* oxidation time curves of 3-methylthiophene and 3-octylthiophene on a platinum electrode in a 0.100 mol L^{-1} solution of $LiClO_4$ in acetonitrile are shown in Fig. 2A. The electrochemical syntheses of the respective monomers were accomplished with current densities of 1.03 and 1.11 mA cm^{-2}, as employed by Louarn *et al.*[13] It was observed that during the 3.5 min application of the fixed potential, an abrupt current increase occurred in both systems.

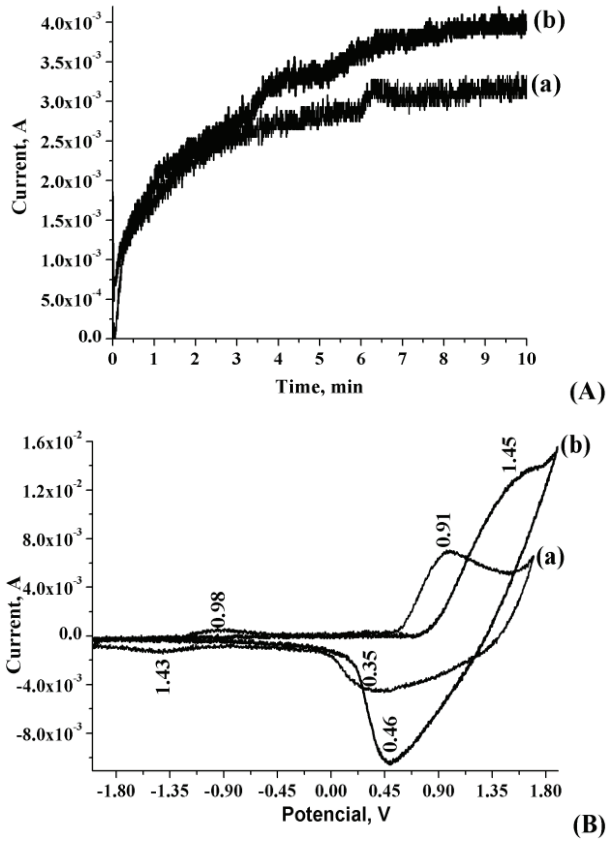

Fig. 2. A) Current *versus* time curves of the oxidation of the monomers, a) 3-methylthiophene, 0.035 mol L^{-1} and b) 3-octylthiophene, 0.040 mol L^{-1}, on a platinum electrode in a solution of 0.100 mol L^{-1} $LiClO_4$ in acetonitrile, applying fixed potentials of a) 1.55 and b) 1.70 V, respectively; B) cyclic voltammograms of the polymer thin films of a) P3MT and b) P3OT on a platinum electrode in a solution of 0.100 mol L^{-1} $LiClO_4$ in acetonitrile, at a scan rate of 50 mV s^{-1}.

Subsequently, the two systems had individual behavior, due to the different concentrations and potentials applied. Thin films of better morphological quality were obtained at 10.0 min. These behaviors could be explained by the formation of thin films through nucleation and growth mechanisms during the anodic electropolymerization, under charge transfer control.[14]

For the films formed under other synthesis conditions, *i.e.*, under potentials or concentrations below or above those mentioned above, for each different system, they presented low homogeneity and, most of the time, formed a "packed grain" morphology with an substantial amount of empty space on the electrode. It was observed that under these syntheses conditions, the initial abrupt increase in the oxidation current did not occur, as shown previously.

The cyclic voltammograms of the polymer thin films in a 0.100 mol L^{-1} solution of $LiClO_4$ in acetonitrile are shown in Fig. 2B. Peaks at –0.60 and –1.28 V were observed for this electrolytic solution, relative to the oxidation and reduction of the electrolyte, respectively, on a platinum electrode. For surfaces formed by thin films prepared in $LiClO_4$, these peaks were shifted to –0.98 and –1.43 V, corresponding to the electrochemical dynamics of the supporting electrolyte in the polymer matrix.[15]

The thin films obtained soon after the electrochemical synthesis under conditions of anodic potentials were not immediately electro-active. Cyclic voltammograms were only obtained after a period of up to three days, demonstrating that, under ambient conditions, spontaneous processes modifying the chemical structure of the material occur with time. The as-prepared films showed oxidation peaks at 0.91 and 1.45 V and of reduction at 0.35 and 0.46 V for the P3MT and P3OT, respectively. However, the bands were well formed, not just shoulders in this potential area, due to an initial sweeping of the potential to –2.00 V, and subsequent acquisition of the voltammograms. This effect could be understood taking into consideration the function of the electrolyte as a dopant, which, after sweeping to negative potentials, reorganizes the chemical structure of the thin film on platinum electrode and the doping, stimulated by the applied potential, probably leads to the formation of structured polymer layers.[16]

The two polymers used are members of the P3AT homologous series, and they differ only by their lateral chain. It could be observed that the displacements in the potentials showed a characteristic electrochemical behavior, under conditions of this study. Bazzaoui *et al.*[17] electrochemically synthesized the same P3ATs as thin films on a gold electrode in a 0.100 mol L^{-1} solution of $N(Bu)_4ClO_4$ in acetonitrile. For this study, oxidation/reduction peaks were observed at approximately 0.70 and 0.55 V (P3MT) and at 1.00 and 0.70 V (P3OT).

Attempts were made to prepare some extremely thin films under the conditions shown in Fig. 2A, but at shorter times (3 and 5 min) for P3MT and P3OT, respectively. These films showed different behaviors three days after synthesis,

the oxidation and reduction peaks were not obtained as shown in Fig. 2B. The oxidation/reduction peaks were observed at 0.35 and –0.45 V (P3MT) and at 0.37 and –0.53 V (P3OT). Probably, under these conditions, oligomeric structures were formed on the surface of the platinum electrode.

The *ex situ* Raman spectra for P3MT and P3OT, as-prepared and oxidized, are shown in Fig. 3. Bands assigned to the normal vibrations modes of the thiophene ring were observed.[13] Some small frequency displacements in relation to the bands observed in the study of Louarn were also observed, due to differences in the synthesis conditions, the thin thickness of the films and the excitation radiation used for spectra registration. The bands in the P3MT Raman spectra were of larger intensity than those in the P3OT spectra. In the latter spectra, some bands were associated with the presence of the electrolyte creating material doping.

The Raman spectra for the as-prepared samples were compared to the oxidized samples with bands at 1409 and 1423 cm^{-1}, related to P3MT and P3OT, and shifted to 1421 and 1428 cm^{-1}, respectively. In the P3MT spectrum, the

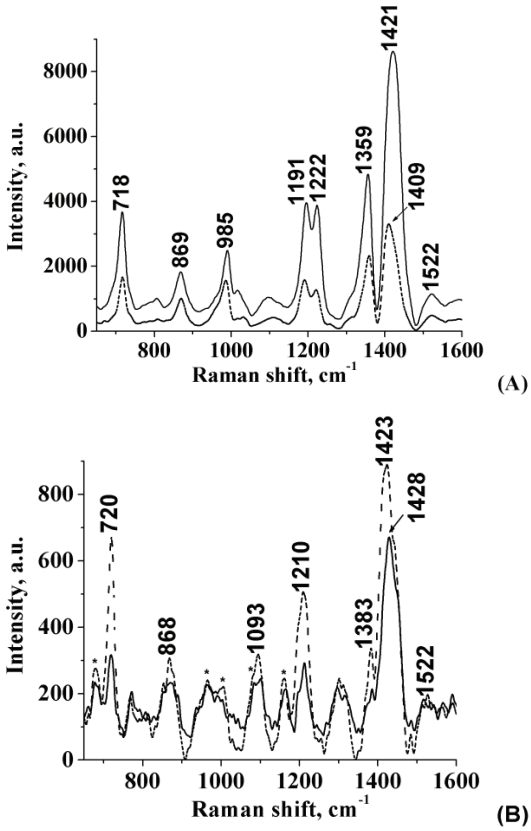

Fig. 3. *Ex situ* Raman spectra of A) P3MT and B) P3OT, obtained as-prepared (---) and oxidized (—). *) Characteristic $LiClO_4$ frequencies.

intensity of the frequency for bands at 1191 and 1222 cm^{-1} increased after the polymer oxidation, while in the P3OT, there was a broadening of the band centered at 1210 cm^{-1}. The bands associated with these compositions restrict the discussion of the spectra to these two areas of interest, in other words, at 1140––1250 cm^{-1} and 1378–1480 cm^{-1}, due to changes observed in the widths of the bands obtained under different preparation conditions. These bands are due to (C–C) inter-ring stretching and (C=C) aromatic symmetric ring stretching, respectively.[13]

Hernandez *et al.*[18] and López-Elvira *et al.*[19] obtained spectra for P3MT and P3OT in the pristine form and more intense Raman bands at 1450 and 1443 cm^{-1}, respectively. However, at 1190–1205 cm^{-1} (P3MT) and 1188 cm^{-1} (P3OT), these bands presented a certain broadening. López-Elvira *et al.*[19] observed that the (C=C) aromatic symmetric and antisymmetric ring stretching of samples degraded with UV radiation showed band broadening and a 60 cm^{-1} shift to higher frequencies. It was considered that the broadening observed in the spectra in Fig. 3 was due to structural changes in the thiophene ring during the electropolymerization process. In other words, Raman lines originating from both aromatic and quinoid structured rings could be detected.[17] It was observed that electrochemically synthesized polydiphenylamine showed a band shift at 1609 to 1618 cm^{-1}, due to the polymeric de-doping.[20] This was the consequence of the presence of different mixed segments that formed in the polydiphenylamine in the reduced state, mainly aromatic and quinoid structures.

The deconvoluted Raman spectra in the range from 1378 to 1480 cm^{-1} for the as-prepared, oxidized and partially de-doped samples are presented in Fig. 4. The spectra showed three features on deconvolution, probably from the assigned symmetric stretch of aromatic, semi-quinoid and quinoid structures. The presence of semi-quinoid species was considered based on the results obtained previously by EPR spectroscopy.[9,10] For P3OT prepared using a $LiClO_4$ containing supporting electrolyte, referred to as doped (oxidized) and partially de-doped samples, a free radical was detected, demonstrating that the polymer was not totally de-doped.

For the as-prepared P3MT, bands were observed at 1403, 1423 and 1457 cm^{-1}; the oxidized polymer bands were observed at 1405, 1429 and 1463 cm^{-1}; and for partially de-doped polymer at 1405, 1431 and 1460 cm^{-1}, with relative frequency intensities that varied with the preparation of the materials. For the as-prepared P3OT, bands were observed at 1413, 1428 and 1447 cm^{-1}; for the oxidized polymer, bands were observed at 1417, 1432 and 1451 cm^{-1}; and for partially de-doped polymer at 1414, 1429 and 1453 cm^{-1}. The Raman spectrum of the partially de-doped P3OT had a drastic intensity loss, probably due to the fluorescence effect, which will be discussed later. This spectrum variation made a more precise analysis of the intensity variations impossible.

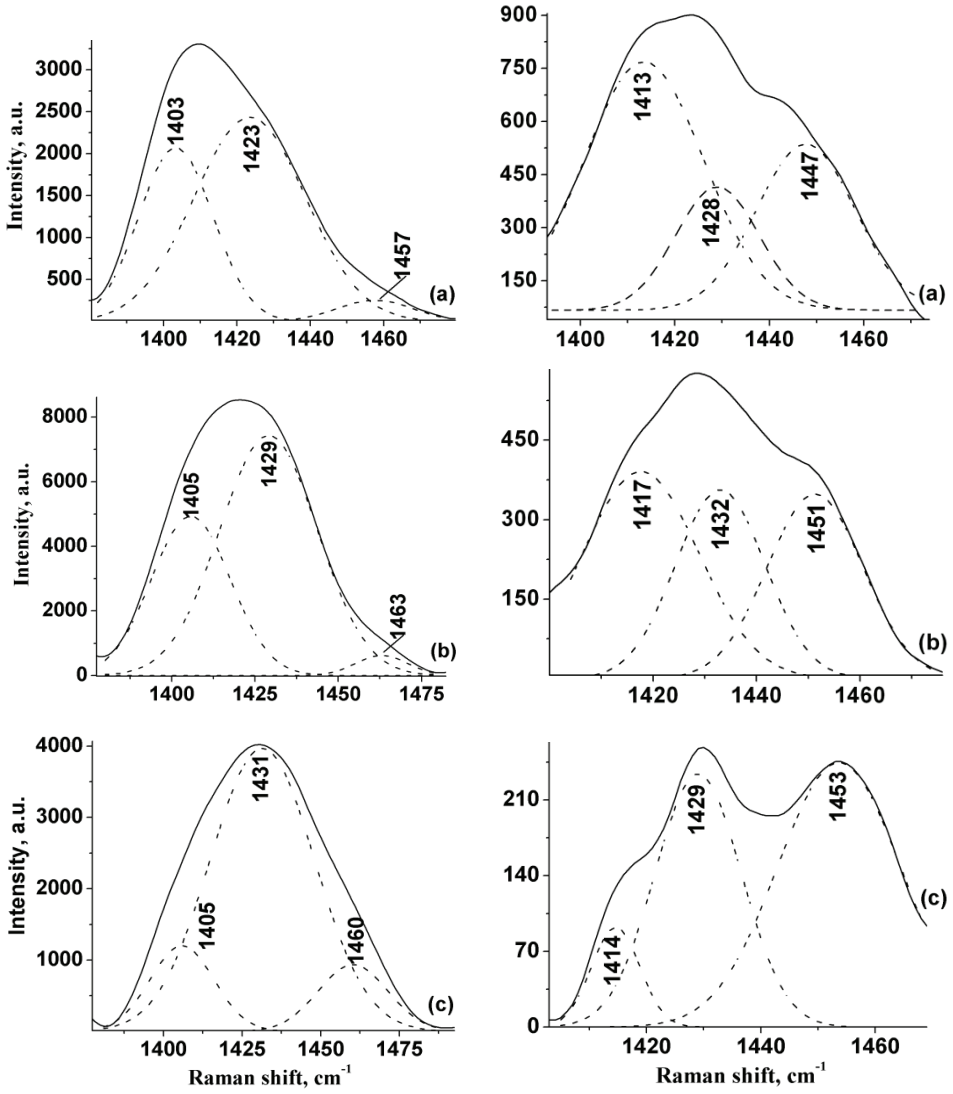

(A) (B)

Fig. 4. Deconvoluted Raman spectra from 1378–1480 cm^{-1} of A) P3MT and B) P3OT; a) as-prepared, b) oxidized and c) partially de-doped.

The bands obtained from the deconvoluted Raman spectra (Fig. 4), at 1403––1405 cm^{-1} and 1413–1419 cm^{-1}, were attributed to the aromatic species of P3MT and P3OT, respectively, based on the characteristic frequency of the pristine form.[18,19] The results indicated that there were changes in the aromatic character of thiophene rings to quinone upon electrochemical oxidation, and that the remaining aromatic rings in the polymer chains were slightly disturbed. After

deprotonation of the samples, there was an intensity increase in these bands but, even so, the predominant form was the quinone structure that had the highest intensity in the spectra. The bands obtained in the deconvoluted Raman spectra at 1423–1431 cm^{-1} and 1428–1435 cm^{-1} were attributed to quinoid species. This assignment was based on the results of Therezio *et al.*[10], who demonstrated that the polymer chain could exist in quinone and semi-quinone forms that are stabilized by the presence the electrolyte as a dopant. After removal of the electrolyte in the de-doping process, the quinone form is favored, and radical species destabilize in the chain. The frequencies at 1457–1463 cm^{-1} and 1447–1453 cm^{-1} were considered characteristics of semi-quinoid segments of representative polyalkylthiophenes, considering that these species can usually appear at higher frequencies. [21]

The frequencies obtained in the deconvoluted Raman spectra from 1189–1195 cm^{-1} and 1191–1196 cm^{-1} are shown in Fig. 5, which are attributed to the aromatic species of the P3MT and P3OT, respectively, based on the characteristic frequency of the pristine form.[18,19] Hernandez *et al.*[18] also associated a band at 1205 cm^{-1} to the aromatic form. However, an increase in the intensity of the bands in the range of 1211–1228 cm^{-1} (P3MT) and 1204–1227 cm^{-1} (P3OT) was observed. Casado *et al.*[22] observed spectral differences between the pristine and oxidized molecules for oligothiophenes related to the intensity of the bands at 1217–1226 cm^{-1}, which were related to the radical cation and dication forms. These authors considered that the assignment of these bands was not straightforward, but it could be expected that the modes have a collective character and are assignable to mixtures of (C–C) inter-ring and (C=C) aromatic symmetric ring vibrations, with the probable involvement of stretching vibrations of the alkyl side chain.

The spectra frequencies for P3MT and P3OT were different from each other, as can be seen in Fig. 5. Considering the assignment of the frequencies to (C=C) of symmetric aromatic ring and their possible collective character, the frequencies at 1211–1228 cm^{-1} and 1204–1227 cm^{-1}, respectively, could probably be characteristic of the dication form. In the same way, the bands at 1222–1228 cm^{-1} and 1221–1227 cm^{-1} are characteristic of the radical cation.

The PL spectra of P3MT and P3OT for the as-prepared, oxidized and partially de-doped samples are shown in Fig. 6. It was observed that the PL intensity of the as-prepared and oxidized samples for both films presented the same behavior. In other words, the as-prepared samples exhibited a greater intensity than the oxidized samples, indicating that the species present in the oxidized samples could be causing the loss of luminescence quenching by diminishing the exciton recombination process. Compared to these samples, the PL spectra of the partially de-doped P3MT and P3OT thin films exhibited significantly higher intensities.

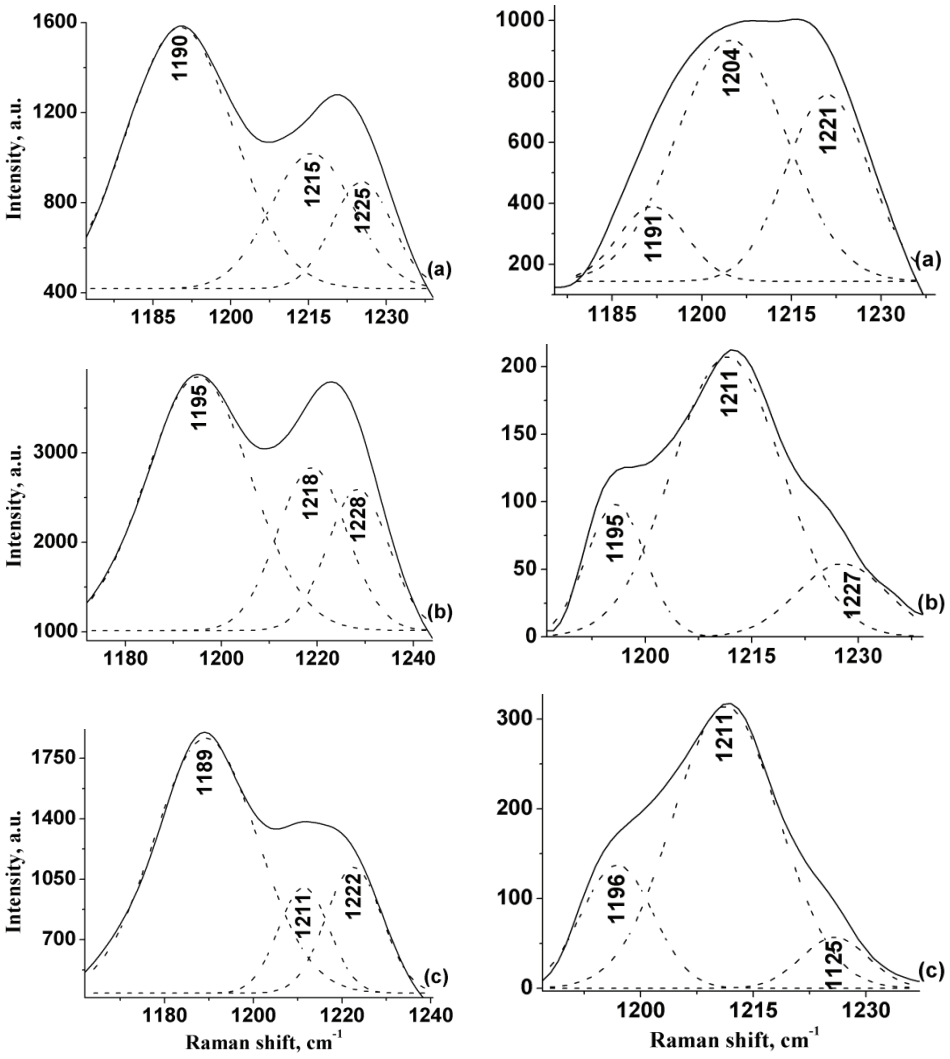

(A) (B)

Fig. 5. Deconvoluted Raman spectra from 1140–1250 cm^{-1} of A) P3MT and B) P3OT; a) as-prepared, b) oxidized and c) partially de-doped.

As verified by Yoshino *et al.*[23] and Ohmori *et al.*[24], the intensity of the luminescence emission band in P3ATs increases considerably with the nature of the alkyl chain of these materials, being related directly to the increase in the number of carbon atoms. This intensity increase was explained by confinement of the carriers caused by the alkyl chain length,[23,25] which favors carrier recombination in the chain and, consequently, the emission intensity increases.

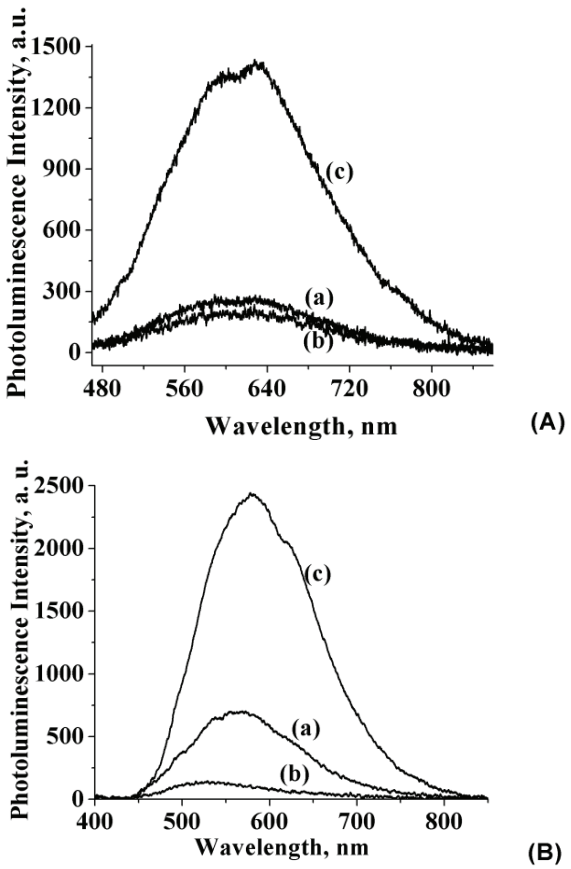

Fig. 6. PL Spectra of A) P3MT and B) P3OT; a) as-prepared; b) oxidized; c) partially de-doped.

The deconvoluted PL spectra for the partially de-doped samples are presented in Fig. 7, from which it can be seen that the fitting of data show two main contributions to the formation of the spectra of the partially de-doped P3MT and P3OT. Deconvoluted PL spectral peaks were observed at 603 and 656 nm for P3MT and 557 and 626 nm for P3OT. Singh *et al.*[26] showed the spectrum of pristine P3OT, *i.e.*, the spectrum of P3OT constituted of pristine chains, presented a band centered at 640 nm, while Wang *et al.*[27] presented a PL spectrum in which, despite having the main band at 642 nm, a small band appeared at 575 nm. Its origin was not explained. The spectra of partially de-doped samples from dos Reis *et al.*[9] and Therezio *et al.*[10] show emission bands centered very close to 599 and 678 nm for P3MT, and 575 and 640 nm for P3OT, similar to the bands discussed in this work. The bands at 599 for P3MT and 575 nm for P3OT were attributed to the formation of mixed chains, composed of pristine and non-pristine structures, in the chains of the polymeric film synthesized by the electrochemical technique.

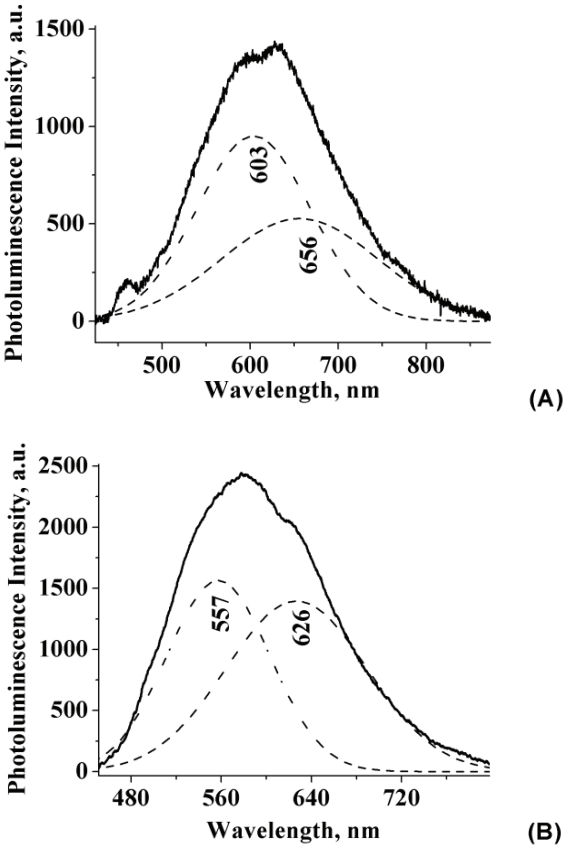

Fig. 7. Deconvoluted PL spectra of A) P3MT and B) P3OT, partially de-doped.

The changes in PL spectra as a function of laser irradiation time for the partially de-doped P3OT sample are shown in Fig 8. An unexpected increase in PL intensity with laser irradiation was observed. It was mentioned previously that the Raman spectrum of partially de-doped P3OT had a drastic intensity loss, probably due to the fluorescence effect. However, this behavior was not observed in P3MT, which presented a quite stable spectrum during the irradiation, and a Raman spectrum with good signal-to-noise ratio.

In general, an increase in polymer fluorescence observed in samples submitted to air photo-irradiation was explained by a model that predicted the creation of an energy profile along the film thickness due to the photodegradation process of the polymer chains.[28] In this case, the excitation was transferred from more conjugated to less conjugated segments, and the transfer process, assisted by a non-uniform distribution of photogenerated defects, led to a higher PL quantum efficiency. López-Elvira *et al.*[19] observed that in P3OT thin films, the polymer degradation was very sensitive to the illumination wavelength, blue light they

found to be more damaging than the UV light. They considered that the degradation induced by the blue light might be intimately related to photo-excitation.

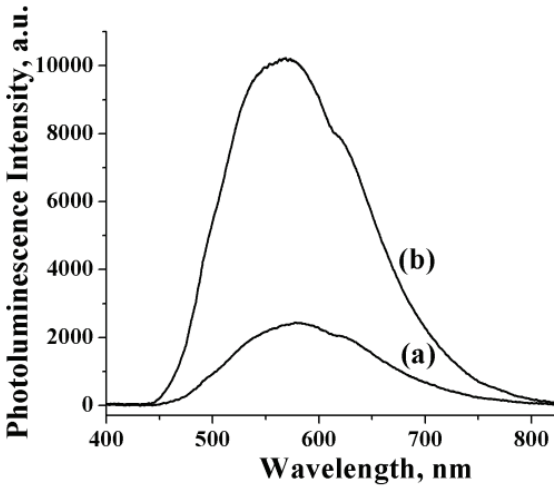

Fig, 8. PL Spectra of P3OT partially de-doped sample; a) 0 and b) 10 min.

Excitation radiation at 405 nm was used to obtain the PL spectrum, a frequency for which there is an increase due to a photochemical process. As it was observed only in P3OT and not in P3MT, it should also involve the participation of the alkyl side chains, destabilizing the chains containing the exciton species. As observed by Yoshino *et al.*[23] and Ohmori *et al.*,[24] the intensity of the luminescence band in P3ATs increased considerably depending on the nature of the alkyl chain, but this might have been influenced by the photochemical process. As discussed by López-Elvira *et al.*,[19] topographic variations were not observed until irradiation exposures of one to two orders of magnitude larger were adopted.

CONCLUSIONS

The present article dealt with the electrosynthesis of two P3ATs on platinum electrodes and their characterization by Raman and photoluminescence spectroscopic techniques. It brought some new insights into the procedure that yields thin polymer films and their detailed structural analysis and stability, which is intimately related to photo-excitation.

In order to explain the Raman spectra of P3MT and P3OT thin films, band-fitting was employed, which identified three structures (pristine, quinone and semi-quinone forms) as being the constituents of the polymeric chains. The PL spectra showed two main contributions: the emission of mixed chains (Gaussian of smaller wavelength) and the emission of the chains in the pristine form (Gaussian of larger wavelength).

In addition, this paper provided evidence that the luminescence intensity was inversely related to the conductivity. The luminescence quenching observed in

doped samples was due to the predominant quinone and semi-quinone segments presents in the polymer chains.

Acknowledgments. This work was supported by the Araucaria Foundation, Process Nos. 18.575 and 20.380, and CNPq, Process Nos. 470533/2009-9 and 301980/2011-0, and Elaine and Danielly are indebted to CAPES for the grant of a fellowship.

И З В О Д

СПЕКТРОСКОПСКА АНАЛИЗА СТРУКТУРЕ И СТАБИЛНОСТИ ДВА ЕЛЕКТРОХЕМИЈСКИ СИНТЕТИСАНА ПОЛИ(3-АЛКИЛТИОФЕНА)

ELAINE CRISTINA RODRIGUES MAIA[1], DANIELLY CRISTINA BENTO[1], EDSON LAURETO[2], DIMAS AUGUSTO MOROZIN ZAIA[1], ERALCI MOREIRA THERÉZIO[3], GREGORY J. MOORE[4] и HENRIQUE DE SANTANA[1]

[1]*Departamento de Química, Universidade Estadual de Londrina, 86051-990, Londrina, PR, Brazil,* [2]*Departamento de Física, Universidade Estadual de Londrina, 86051-990, Londrina, PR, Brazil,* [3]*Instituto de Física, Universidade Federal de Uberlândia, 38400-902, Uberlândia, MG, Brazil* и [4]*Yardney Technical Products, Inc. Pawcatuck, Stonington, CT, USA*

Поли(3-метилтиофен) (P3MT) и поли(3-октилтиофен) (P3OT) филмови електрохемијски су синтетисани коришћењем стандардне тро-електродне ћелије у ацетонитрилу са 0,100 mol L^{-1} $LiClO_4$. Полимерни танки филмови су депоновани на плочице од платине ради најбоље контроле квалитета процеса. Опажено је да овако припремљен материјал за анодну електрополимеризацију показује природни процес депротонизације у функцији времена. Такође, врста материјала, добијена у NH_4OH раствору, показује добру хемијску стабилност али, када је осветљена плавом светлошћу, поново постаје нестабилна. Филмови добијени овим методама су окарактерисани цикличном волтаметријом, раманском и фотолуминисцентном (PL) спектроскопијом. И Раманski и PL спектри омогућавају карактеризацију две структурне форме тиофенских прстенова који граде P3MT и P3OT полимерне ланце. На добијене резултате утиче стабилизација првобитних ланаца и мешаних ланаца, радикалских катјона и дикатјонских форми у полимерним филмовима. Њихове траке у Раманским и PL спектрима су широке и асиметричне па је њихово дефинисање Гаусовим функцијама било неопходно, што је указало на то да постоје три одвојена доприноса вибрационим и два емисионим спектрима у насталим једињењима.

(Примљено 27. марта, ревидирано 3. септембра 2012)

REFERENCES

1. K. Kaneto, K. Yoshino, Y. Inuishi, *Jpn. J. Appl. Phys.* **22** (1983) L412
2. S. Glenis, G. Horowitz, G. Tourillon, F. Garnier, *Thin Solid Films* **111** (1984) 93
3. H. Koezuka, A. Tsumura, T. Ando, *Synth. Met.* **18** (1987) 699
4. A. O. Patil, A. J. Heeger, F. Wudl, *Chem. Rev*. **88** (1988) 183
5. J. Roncali, *Chem. Rev*. **92** (1992) 711
6. J. H. Kaufman, T. C. Chung, A. J. Heeger, F. Wudl, *J. Electrochem. Soc*. **131** (1984) 2092
7. T. Yamamoto, *J. Chem. Soc., Chem. Commun*. **4** (1981) 187
8. H. Koizumi, H. Dougauchi, T. Ichikawa, *J. Phys. Chem., B* **109** (2005) 15288
9. G. A. dos Reis, I. F. L. Dias, H. de Santana, J. L. Duarte, E. Laureto, E. Di Mauro, M. A. T. da Silva, *Synth. Met.* **161** (2011) 340

10. E. M. Therézio, J. L. Duarte, E. Laureto, E. di Mauro, I. F. L. Dias, A. Marletta, H. de Santana, *J. Phys. Org. Chem.* **24** (2011) 640
11. A. J. Heeger, S. Livelson, J. R. Schrieffer, W.-P. Su, *Rev. Mod. Phys.* **60** (1988) 781
12. R. Singh, J. Kumar, R. K. Singh, S. Chand, V. Kumar, *J. Appl. Phys.* **100** (2006) 016106
13. G. Louarn, J. Y. Mevellec, J. P. Buisson, S. Lefrant, *J. Chim. Phys.* **89** (1992) 987
14. I. Villareal, E. Morales, J. L. Acosta, *Polymer* **42** (2001) 3779
15. G. Inzelt, *Electrochim. Acta* **34** (1989) 83
16. M. Lapkowski, J. Zak, M. Kolodziej-Sadlok, S. Guillerez, G. Bidan, *Synth. Met.* **119** (2001) 417
17. E. A. Bazzaoui, M. Bazzaoui, J. Aubard, J. S. Lomas, N. Félidj, G. Lévi, *Synth. Met.* **123** (2001) 299
18. V. Hernandez, F. J. Ramirez, T. F. Otero, J. T. Lopez Navarrete, *J. Chem. Phys.* **100** (1994) 114
19. E. López-Elvira, E. Escasaín, A. Baró, J. Colchero, E. Palacios-Lidón, *Polym. Degrad. Stab.* **96** (2011) 1279
20. H. de Santana, J. R. Matos, M. L. A. Temperini, *Polym. J.* **30** (1998) 315
21. H. de Santana, S. Quillard, E. Fayad, G. Louarn, *Synth. Met.* **156** (2006) 81
22. J. Casado, V. Hernández, S. Hotta, J. T. López Navarrete, *J. Chem. Phys.* **109** (1998) 10419
23. K. Yoshino, Y. Manda, K. Sawada, M. Onoda, R. Sugimoto, *Solid State Commun.* **69** (1989) 143
24. Y. Ohmori, M. Uchida, K. Muro, K. Yoshino, *Jpn. J. Appl. Phys.* **30** (1991) 1938
25. K. Yoshino, S. Nakajima, D. H. Park, R. Sugimoto, *Jpn. J. Appl. Phys.* **27** (1988) L716
26. R. Singh, J. Kumar, R. K. Singh, A. Kaur, K. N. Sooda, R. C. Rastog, *Polymer* **46** (2005) 9126
27. G. Wang, C. Yuan, Z. Lu, Y. Wei, *J. Lumin.* **68** (1996) 49
28. Y. G. Gobato, A. Marletta, R. M. Faria, F. E. G. Guimarães, J. M. Souza, E. Pereira, *Appl. Phys. Lett.* **81** (2002) 942.

Journal of the Serbian Chemical Society
JSCS-info@shd.org.rs • www.shd.org.rs/JSCS
J. Serb. Chem. Soc. 78 (4) 523–536 (2013) UDC 66.017+547.461.2:543.57:544.421.032.4
JSCS–4435 *Original scientific paper*

Thermal decomposition of a molecular material $\{N(n\text{-}C_4H_9)_4[Fe^{II}Fe^{III}(C_2O_4)_3]\}_\infty$ leading to ferrite: A reaction kinetics study

ASHIS BHATTACHARJEE[1]*, DEBASIS ROY[1], MADHUSUDAN ROY[2] and ARUNABHA ADHIKARI[3]

[1]*Department of Physics, Visva-Bharati University, Santiniketan, India,* [2]*Applied Material Science Division, Saha Institute of Nuclear Physics, Kolkata, India and* [3]*Department of Physics, West Bengal State University, Barasat, India*

(Received 19 May 2012)

Abstract: A multi-step thermal decomposition of a molecular precursor, $\{N(n\text{-}C_4H_9)_4[Fe^{II}Fe^{III}(C_2O_4)_3\}_\infty$ was studied using non-isothermal thermogravimetric (TG) measurements in the temperature range 300 to ≈800 K at multiple heating rates (5, 10 and 20 K min^{-1}). The thermal decomposition of the oxalate-based complex proceeded stepwise through a series of intermediate reactions. Two different isoconversional methods, namely, an improved iterative method and a model-free method were employed to evaluate the kinetic parameters: activation energy and rate of reaction. The most probable reaction mechanism of thermal decomposition was also determined. The different reaction pathways leading to different steps in the TG profile were also explored, which are supplemented by earlier experimental observations.

Keywords: molecular materials; oxalates; non-isothermal thermogravimetry; decomposition kinetics; model free methods.

INTRODUCTION

Among all nanomaterials, metal oxides are very attractive functional materials synthesized on the nanoscale. Their unique characteristics make them the most diverse class of materials with properties covering almost all aspects of solid-state physics and materials science. Metal oxides represent therefore essential constituents in technological applications such as magnetic storage,[1,2] gas sensing[3,4] and energy conversion,[5] to name but a few. Various physical or chemical synthetic approaches for the synthesis of metal oxide nanoparticles have been developed over the years.[6] Research was initiated aimed at the preparation of metal oxide nanoparticles using molecular metalorganic complexes as precur-

* Corresponding author. E-mail: ashis.bhattacharjee@visva-bharati.ac.in
doi: 10.2298/JSC120519145B

sors through the thermal decomposition route. The approach consisted of two steps: the synthesis of molecular metalorganic precursors in the first step and the oxidation of the precursor in a controllable manner in the second step. The precursors thermally degrade at different levels depending on the reaction conditions. It was conjectured that controlled oxidation through thermal decomposition of the precursors may lead to various metal oxide nanoparticles. Thus, by studying the solid-state thermal decomposition reaction kinetics of the precursors, the shape and size of the metal oxide nanoparticles could be monitored by externally controlling the different reaction kinetic parameters.

Polymeric bimetallic oxalate complexes of the general formula, $\{A[M^{II}M^{III}(C_2O_4)_3]\}_\infty$, (A: organic cation, M^{II} and M^{III}: di-/tri-valent transition metal ions; C_2O_4: oxalate ligand) have been important topics in the field of molecular magnetism.[7] Thermal decomposition of a ferromagnetic material of this family, $\{N(n\text{-}C_4H_9)_4[Mn^{II}Cr^{III}(C_2O_4)_3]\}_\infty$ results in a spinel compound, $Mn_{1.5}Cr_{1.5}O_4$ at ≈ 500 °C.[8] Recently, thermal decomposition of the molecular ferrimagnetic material $\{N(n\text{-}C_4H_9)_4[Fe^{II}Fe^{III}(C_2O_4)_3]\}_\infty$ was reported.[9,10] It was seen that thermal decomposition leads to the formation of nano-sized ferrites. These results suggested that $\{A[M^{II}M^{III}(C_2O_4)_3]\}_\infty$ type molecular materials may be suitable single-molecular precursors for the synthesis of metal oxides *via* the thermal decomposition route. Moreover, the synthesis of these molecular materials is quite easy and economic, and the desired metal oxides could be prepared from such homo/heterometallic complexes at relatively low temperatures.

In light of the above, it was thought worthy to undertake a systematic study of the kinetics of the solid state thermal decomposition reaction of $\{N(n\text{-}C_4H_9)_4[Fe^{II}Fe^{III}(C_2O_4)_3]\}_\infty$ to gain a comprehensive understanding of the process. The thermal decomposition of oxalate-based complexes is usually complicated and proceeds stepwise through a series of intermediate reactions.[11] In the present study, two different isoconversional methods, namely, an improved iterative method (to obtain a more accurate value for the activation energy of the reaction)[12] and a model-free method (to obtain reliable and consistent kinetic information from the non-isothermal data)[13] were employed to analyse the thermogravimetry results, as well as to estimate the kinetic parameters of the thermal decomposition of $\{N(n\text{-}C_4H_9)_4[Fe^{II}Fe^{III}(C_2O_4)_3]\}_\infty$. The kinetic parameters of a solid state thermal decomposition reaction have a physical meaning and could be used to study the solid state reaction mechanism *vis-à-vis* the reaction model. Modern kinetics investigation procedure using multi-heating rates for multi-step reactions are also used to determine the correct reaction mechanism function.[14] The variation of the activation energies with the extent of the reactions are discussed to reveal the complexity of the multi-step reactions observed for this material.

EXPERIMENTAL

The precursor material $\{N(n\text{-}C_4H_9)_4[Fe^{II}Fe^{III}(C_2O_4)_3]\}_\infty$, (BuFeFe) was prepared in a one-pot reaction according to a reported procedure.[15] The powdery deep green coloured sample thus obtained was used for the thermogravimetric (TG) study. The measurements were performed using an STA 449C Thermogravimetric analyzer (Netzsch, Germany) under a dry air atmosphere. The sample mass used for TG study was ~ 4 mg. UHP nitrogen (99.999 %) was used as protective gas in the instrument. All the kinetic parameters, namely, the activation energy, the pre-exponential factor, and the reaction model calculations, were performed using a program compiled in MATLAB.

RESULTS AND DISCUSSION

The thermal decomposition of BuFeFe was monitored by TG at three different heating rates (β) 5, 10 and 20 K min^{-1}. The TG curves of BuFeFe obtained at three different heating rates are shown in Fig. 1, from which different thermal decomposition steps can be seen. Thus, a very gradual loss of mass (m) for the three different heating rates commences at around 315 K. The thermal decomposition proceeds with rapid mass loss through three linear steps, indicating different stages of solid state reaction of BuFeFe. These linear steps, which appear in heating rate dependent temperature ranges, are indicated by arrows in Fig. 1, and denoted as Step-I, Step-II and Step-III, respectively, in Table I. It can be seen that the temperature range (ΔT) corresponding to the different steps were shifted

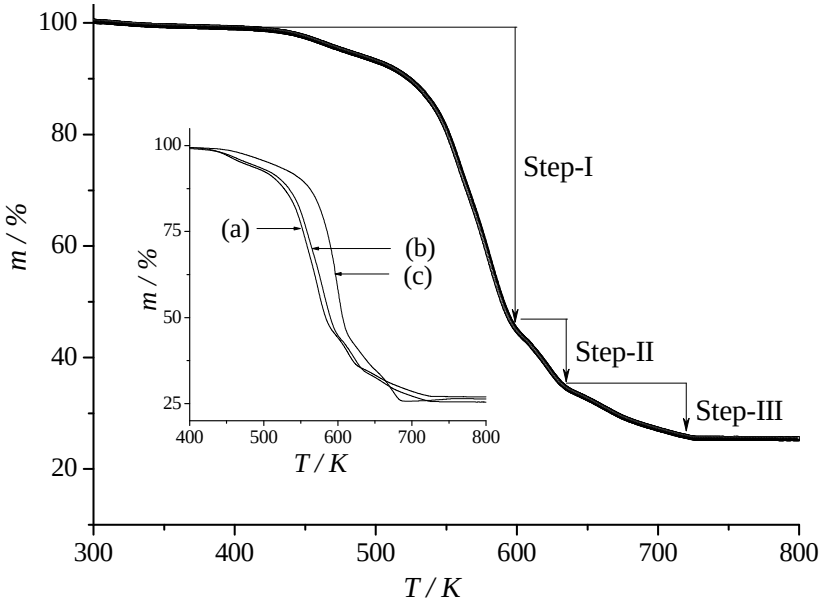

Fig. 1. Thermogravimetric profile of $\{N(n\text{-}C_4H_9)_4[Fe^{II}Fe^{III}(C_2O_4)_3]\}_\infty$ obtained at a heating rate of 10 K min^{-1}. The arrows indicate the different steps of the thermal decomposition. Inset represents the TG profiles of $\{N(n\text{-}C_4H_9)_4[Fe^{II}Fe^{III}(C_2O_4)_3]\}_\infty$ obtained under three different heating rates: a) 5, b) 10 and c) 20 K min^{-1}.

towards higher temperatures with increasing heating rate. For example, in case of Step-I, the loss of mass continues until ≈587 K for β = 5 K min^{-1}, until ≈598 K for β = 10 K min^{-1} and until 612 K for β = 20 K min^{-1}. The ΔT and m values corresponding to the different steps under different heating rates, along with the residual mass at 800 K in each case of heating rate are compared in Table I. Step-I corresponds to the largest mass loss in the TG profile. Thus, BuFeFe undergoes successive solid state reactions in three steps. Thermal decomposition becomes complete at ≈723, 718 and 685 K for heating rate 5, 10 and 20 K min^{-1}, respectively, with very similar residual masses. It was reported earlier that the decomposition of BuFeFe proceeds through a few intermediate phases and finally results in the formation of a powdery deep red product, which is nothing but the nano-sized ferrite particles (hematite and magnetite).[9,10]

TABLE I. The temperature range of the different steps and the corresponding mass loss values during the thermal decomposition of $\{N(n\text{-}C_4H_9)_4[Fe^{II}Fe^{III}(C_2O_4)_3]\}_\infty$ and associated residual mass values estimated under different heating rates; β = heating rate, ΔT = temperature range, m = loss of mass

β / K min^{-1}	Step-I		Step-II		Step-III		Residual mass, %
	ΔT / K	m / %	ΔT / K	m / %	ΔT / K	m / %	
5	315–587	52	587–625	12	625–723	9	27
10	315–598	54	598–633	11	633–718	9	26
20	315–612	54	612–648	11	648–685	10	25

Presently, the thermal decomposition mechanism of BuFeFe is analyzed considering the first two steps of the TG profile only, as it is impractical to consider Step-III. To describe the kinetics of thermal decomposition of BuFeFe reliably, isoconversional methods were used. In the isoconversional method, the reaction rate at constant extent of conversion is assumed to be a function of temperature only.[16] Two simplifying assumptions are used in this regard: *i*) the temperature at any point in the solid remains same and *ii*) the controlling step in the reaction rate does not alter throughout the transformation of a chemical process.[17] Under non-isothermal conditions where the temperature varies linearly with time, *i.e.*, the linear heating rate $\beta = \mathrm{d}T/\mathrm{d}t$ = const., the kinetic equation of solid state thermal decomposition is frequently described by the well-known differential rate equation:[18]

$$\beta \frac{\mathrm{d}\alpha}{\mathrm{d}T} = A\mathrm{f}(\alpha)\ \exp\left(-\frac{E^*}{RT}\right) \tag{1}$$

where $\alpha = (m_i - m_t)/(m_i - m_f)$ is the extent of reaction, *i.e.*, the fraction of the material that had reacted in time t, m_i and m_f are the initial and final masses in the particular decomposition step of interest, m_t is the mass at any instant of the reaction in this step, $\mathrm{d}\alpha/\mathrm{d}T$ is the rate of conversion (in K^{-1}), A is the pre-

exponential Arrhenius factor (in min^{-1}), f(α) is the differential conversion function depending on the mechanism of a kinetic reaction,[19] E^* is the activation energy (in kJ mol^{-1}) and R is the universal gas constant (in kJ mol^{-1} K^{-1}). The variations of the extent of reaction (α) with temperature during the thermal decomposition of BuFeFe during Step-I and Step-II are illustrated in Fig. 2.

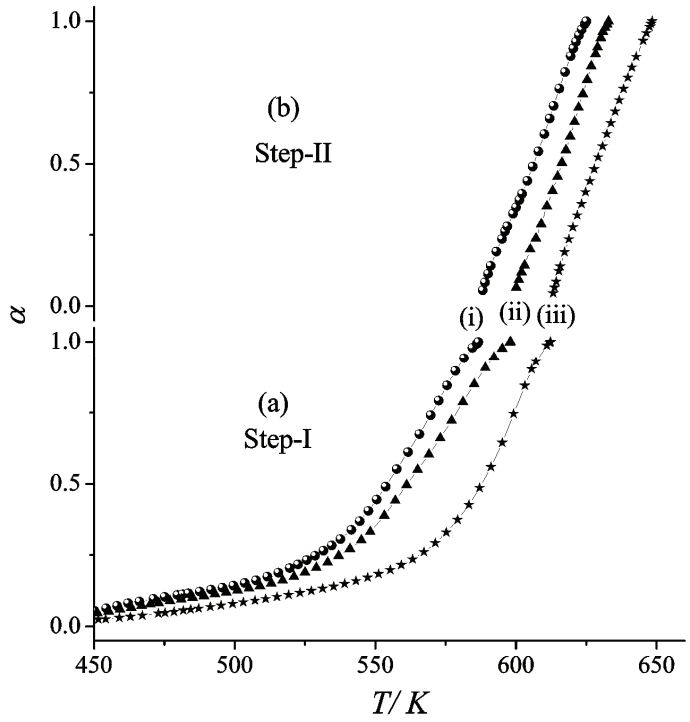

Fig. 2. Variation of the extent of conversion (α) with temperature during the thermal decomposition of $\{N(n\text{-}C_4H_9)_4[Fe^{II}Fe^{III}(C_2O_4)_3]\}_\infty$ for Step-I (a) and Step-II (b) under different heating rates: i) 5, ii) 10 and iii) 20 K min^{-1}.

The iterative procedure is used to calculate the activation energy, approximating the exact value of activation energy, according to the following equations:[12]

$$\ln\frac{\beta_i}{h(x)T_{\alpha,i}^2}=\ln\frac{A_\alpha R}{g(\alpha)E_\alpha^*}-\frac{E_\alpha^*}{RT_{\alpha,i}} \quad (2)$$

and

$$\ln\frac{\beta_i}{H(x)}=\ln\frac{0.0048A_\alpha E_\alpha^*}{g(\alpha)R}-1.0516\frac{A_\alpha E_\alpha^*}{RT_{\alpha,i}} \quad (3)$$

here h(x) is expressed as:[20]

$$h(x) = \frac{x^4 + 18x^3 + 88x^2 + 96x}{x^4 + 20x^3 + 120x^2 + 240x + 120} \quad (4)$$

and H(x) is expressed as:[14]

$$H(x) = \frac{\exp(-x)\mathrm{h}(x) / x^2}{0.0048\exp(-1.0516x)} \quad (5)$$

where $x = E_\alpha^* / RT_{\alpha\mathrm{i}}$. In performing the iterative procedure, the following steps are often used: Step 1 – the initial value of the activation energy $(E_\alpha^*)_1$ is estimated by fitting Eq. (2) or (3) with the assumption $h(x)$ = 1 or $H(x)$ = 1. Generally, the conventional isoconversional methods stop calculating at this step; Step 2 – using $E_\alpha^* = (E_\alpha^*)_1$, h($x$) and H($x$) are calculated and a new value of $E_\alpha^* = (E_\alpha^*)_2$ is calculated from the fit of the plot $\ln[\beta_\mathrm{i} / \mathrm{h}(x)T_{\alpha,\mathrm{i}}^2]$ *vs.* $1/T_{\alpha,\mathrm{i}}$ with Eq. (2) or of the plot $\ln[\beta_\mathrm{i} / \mathrm{H}(x)T_{\alpha,\mathrm{i}}^2]$ *vs.* $1/T_{\alpha,\mathrm{i}}$ with Eq. (3); Step 3 – repetition of Step 2 replacing $(E_\alpha^*)_1$ with $(E_\alpha^*)_2$ resulting in $E_\alpha^* = (E_\alpha^*)_3$ and so on until the absolute difference $[(E_\alpha^*)_\mathrm{i} - (E_\alpha^*)_{\mathrm{i}-1}]$ becomes less than 0.1 kJ mol^{-1}. The last value of $(E_\alpha^*)_\mathrm{i}$ thus obtained is considered to be the most accurate estimate of the activation energy (E_α^*) of a thermal reaction. The thus obtained E_α^* values for the present thermogravimetric data, based on Eqs. (2) and (3), are listed in Table II.

In the model-free isoconversional method for non-isothermal thermogravimetry experiments, the activation energy E_α^* can be evaluated at any particular value of α by minimizing the following objective function:[13,14]

$$\Omega(E_\alpha^*) = \sum_{i=1}^{n}\sum_{j=1}^{n} \frac{I\left(E_\alpha^*, T_{\alpha,i}\right)\beta_j}{I\left(E_\alpha^*, T_{\alpha,j}\right)\beta_i} \quad (6)$$

where $I\left(E_\alpha^*, T_{\alpha,\mathrm{i}}\right)$, the temperature integral, is given as:

$$I\left(E_\alpha^*, T_{\alpha,\mathrm{i}}\right) = \int_0^{T_{\alpha,\mathrm{i}}} \exp\left(-\frac{E_\alpha^*}{RT}\right) \mathrm{d}T \quad (7)$$

There are several methods and popular approximations to evaluate this temperature integral. However, the approximation as adopted by Cai *et al.*[21] is proved to be superior to any of the other approximations and is the most suitable solution for the evaluation of the activation energy, E_α^*, and other kinetic parameters from non-isothermal kinetic analyses. According to this approximation, the temperature integral is given as:[21]

$$\int_0^{T_{\alpha,\mathrm{i}}} \exp\left(-\frac{E_\alpha^*}{RT}\right) \mathrm{d}T = \frac{RT_{\alpha,\mathrm{i}}^2}{E_\alpha^*} \left[\frac{\frac{E_\alpha^*}{RT_{\alpha,\mathrm{i}}} + 0.66691}{\frac{E_\alpha^*}{RT_{\alpha,\mathrm{i}}} + 2,64943}\right] \exp\left(-\frac{E_\alpha^*}{RT_{\alpha,\mathrm{i}}}\right) \quad (8)$$

TABLE II. The activation energy, reaction rate and model of reaction mechanism for Step-I and Step-II of the thermal decomposition of $\{N(n\text{-}C_4H_9)_4[Fe^{II}Fe^{III}(C_2O_4)_3]\}_\infty$

Extent of conversion α / min^{-1}	Activation energy, E_a / kJ mol^{-1}						Reaction mechanism		Average value of A / min^{-1}	
	Step-I			Step-II			Step-I	Step-II	Step-I	Step-II
	Eq. (2)	Eq. (3)	Eq. (6)	Eq. (2)	Eq. (3)	Eq. (6)				
0.1	58.93	58.93	58.95	155.62	155.62	155.6	Nucleation[a]	Chemical reaction[b]	4.77×10^{4}	5.01×10^{12}
0.2	74.07	74.07	74.09	164.65	164.65	164.7	Chemical reaction		1.23×10^{6}	3.87×10^{13}
0.3	82.86	82.86	82.88	174.01	174.01	173.9			8.05×10^{6}	3.14×10^{14}
0.4	88.47	88.48	88.49	182.29	182.29	182.3			2.67×10^{7}	2.25×10^{15}
0.5	91.04	91.04	91.06	187.25	187.26	187.3			4.6×10^{7}	8.72×10^{15}
0.6	100.71	100.72	100.7	189.22	189.22	189.2			3.64×10^{8}	1.98×10^{16}
0.7	112.29	112.29	112.3	187.33	187.33	187.3			4.36×10^{9}	2.39×10^{16}
0.8	125.44	125.44	125.5	183.83	183.83	183.9			7.29×10^{10}	2.73×10^{16}
0.9	137.69	137.7	137.7	179.72	179.73	179.7			9.76×10^{11}	4.71×10^{16}

[a] $g(\alpha) = \ln \alpha, f(\alpha) = \alpha$; [b] $g(\alpha) = (1-\alpha)^{-2}-1, f(\alpha) = (1-\alpha)^{3}/2$

$$\int_0^{T_{\alpha,\mathrm{i}}} \exp\left(-\frac{E_\alpha^*}{RT}\right) \mathrm{d}T = \frac{RT_{\alpha,\mathrm{i}}^2}{E_\alpha^*} \left[\frac{\frac{E_\alpha^*}{RT_{\alpha,\mathrm{i}}} + 0.66691}{\frac{E_\alpha^*}{RT_{\alpha,\mathrm{i}}} + 2,64943}\right] \exp\left(-\frac{E_\alpha^*}{RT_{\alpha,\mathrm{i}}}\right) \quad (8)$$

The minimization procedure was repeated for each value of α from 0.1 to 0.9 for Step-I and Step-II (taking the data from Fig. 2) to determine the dependency of E_α^* on α during Step-I and Step-II of the thermogravimetry profile. The E_α^* values thus obtained for Step-I and Step-II are presented in Table II. The activation energy (E_α^*) values obtained by the three different methods are shown as a function of α in Fig. 3 for Step-I and Step-II. It is noticeable that the E_α^* values thus calculated by the three different methods (Eqs. (2), (3) and (6)) are remarkably similar.

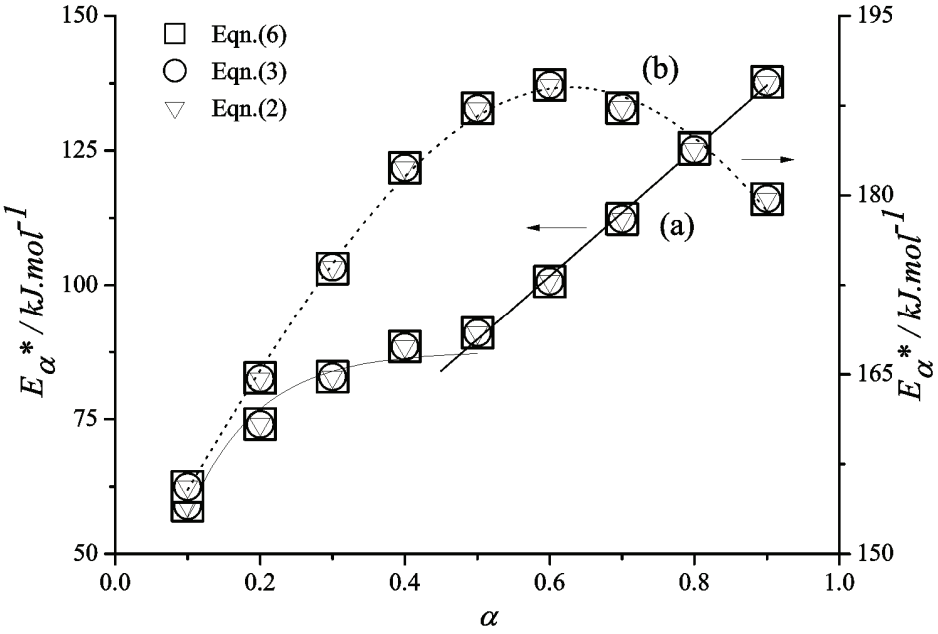

Fig. 3. Dependence of the activation energy on the extent of conversion (α) during the thermal decomposition of $\{N(n\text{-}C_4H_9)_4[Fe^{II}Fe^{III}(C_2O_4)_3]\}_\infty$ obtained using different isoconversional methods: a) Step-I and b) Step-II. The arrows indicate the scales used.

From Fig. 3, it is clear that in case of Step-I of the thermal reaction, the E_α^* value increased exponentially ($E_\alpha^* = a(1-e^{-b\alpha})$, a and b being two fit parameters) for $\alpha \leq 0.4$ and beyond that, E_α^* increased linearly with increasing α. Thus, at around $\alpha \approx 0.4$, the rate of reaction became almost saturated. However, the reaction was triggered at $\alpha \approx 0.5$, resulting in the linear E_α^* *vs.* α variation for the

remaining values of α. On the other hand, for Step-II of thermal reaction, the variation of E_α^* *vs.* α (Fig. 3b) was quite different from that observed for Step-I. Here, the E_α^* value increased with increasing α until $\alpha = 0.6$ and beyond that, the E_α^* value decreased with increasing α. The variation E_α^* with α observed for Step-II could be well-fitted with a Gaussian type distribution function, as shown by the dotted curve in Fig. 3. These different E_α^* *vs.* α variations, being either intra-step or inter-step thermal decomposition reactions, are the manifestations of different reaction rate control mechanisms involved along these steps.

The integral form of the reaction model describing the reaction mechanism[16,18] is given by:

$$g(\alpha) = \int_0^\alpha [f(\alpha)]^{-1} d\alpha$$

Some of the frequently used reaction mechanisms operating in solid-state reactions are given in the literature.[22] The equation which is mostly used to estimate the correct reaction mechanism, *i.e.*, the g(α) function, is:[14]

$$\ln g(\alpha) = \left[\ln \frac{A_\alpha E_\alpha^*}{R} + \ln \frac{e^{-x}}{x^2} + \ln h(x) \right] - \ln \beta_i \quad (9)$$

where the symbols have their usual meaning. The values of α corresponding to the multiple heating rates at the same temperature along the α *vs.* T plots (Fig. 2) were used to generate a plot of ln g(α) *vs.* ln β_i. For the determination of the correct mechanism function, the slope of the straight line ln $g(\alpha)$ vs. ln β_i, using linear regression, should be equal to –1.0000 and the square of the linear correlation coefficient, R^2, should be close to unity.[14] While finding the most probable reaction mechanism function $g(\alpha)$ involved in the present thermal decomposition reactions appearing in Step-I and Step-II, 35 types of mechanism functions given in literature[22] were used. Incidentally, a number of $g(\alpha)$ functions satisfied the conditions specified above when a particular temperature was used. To remove the confusion, different temperature values were used to arrive at a conclusion about the most probable reaction mechanism function. The most probable reaction mechanism functions, $g(\alpha)$, obtained for the solid state reactions corresponding to Step-I and Step-II of the thermal decomposition profile of BuFeFe according to Eq. (9) are $g(\alpha) = \ln \alpha$ and $g(\alpha) = (1- \alpha)^{-2} - 1$, respectively. Thus, Step-I of the TG profile corresponds to "nucleation" as the rate-controlling mechanism, whereas Step-II of the profile corresponds to "chemical reaction".[22]

Using the estimated value of the activation energy and the most probable reaction model, the value of the pre-exponential or frequency factor (A) can be evaluated from the following equation:[23,24]

$$A = -\frac{\beta_{x_p}}{Tf'(\alpha_p)} \exp(x_p) \tag{10}$$

where $x_p = E^*_\alpha / RT_p$ (T_p is the peak temperature on the corresponding differential thermogravimetric curve), $f'(\alpha_p)$ is the first derivative of the kinetic model function. The A values are thus determined for Step-I and Step-II of the TG profile of BuFeFe for different values of α under different heating rates. The variations of A with α under different heating rates are shown in Fig. 4. The effect of heating rate on the A values was found not to be remarkable. However, the dependence of A on the α values were quite noticeable and were different for Step-I and Step-II. For Step-I, the variation of $A(\alpha)$ was similar to that observed for the variation of E^*_α but for Step-II, the values of $A(\alpha)$ increased linearly up to $\alpha \approx 0.5$ and then become nearly independent of α, in contrast to the corresponding $E^*_\alpha(\alpha)$ variation in the same temperature region. The average values of A estimated for the different heating rates are presented in Table II as a function of

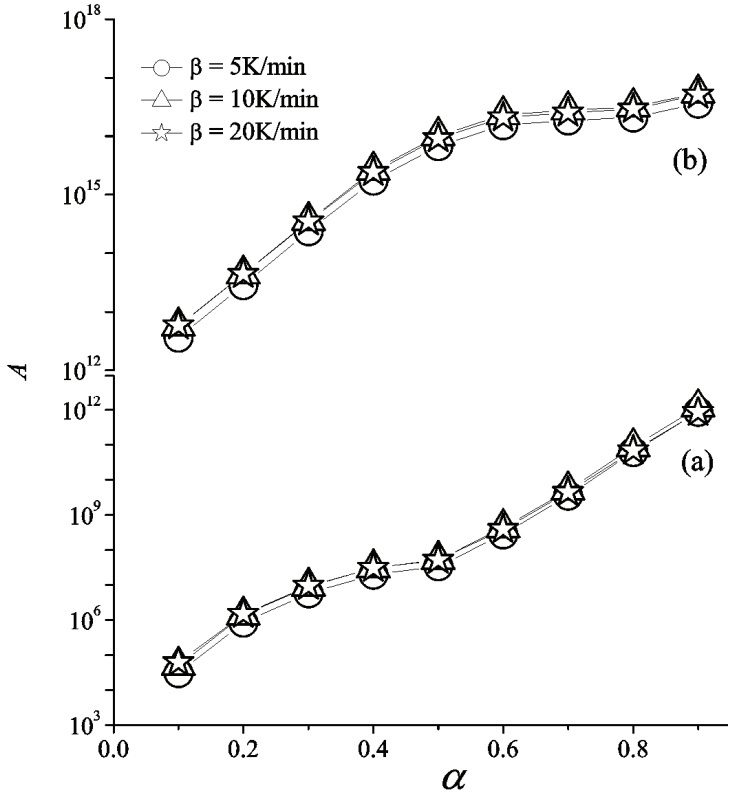

Fig. 4. Dependence of the frequency factor (A / min^{-1}) on the extent of conversion (α) during the thermal decomposition of $\{N(n\text{-}C_4H_9)_4[Fe^{II}Fe^{III}(C_2O_4)_3]\}_\infty$: a) Step-I and b) Step-II.

the α values. The rate of reaction for the decomposition of BuFeFe varied in the range of 10^3–10^{12} min^{-1} and 10^{12}–10^{18} min^{-1} for Step-I and Step-II, respectively. Thus, for both steps of the reaction, the A values varied by an order of 10^9 and 10^6 for Step-I and Step-II, respectively. This indicates that the reaction rate cannot be assumed to be a constant for the studied non-isothermal decomposition process. Interestingly, from Table II, it could be seen that the greatest number of A values were grouped about the order of 10^{15} min^{-1} in Step-II within a narrow E_α^* range, while for Step-I, the A values were distributed over a wide range of E_α^* values. The values of A in solid state reactions are expected to be in a wide range.[22] Low factors often indicate a surface reaction. If the reactions are not dependent on the surface area, a low A value indicates a "tight" complex, while a higher A value indicates a "loose" complex. Accordingly, in the present case, Step-I may involve loose and tight complexes, whereas Step-II involves a tight complex only.

Considering the mass loss values during the different thermal decompositions of BuFeFe, observed in the thermogravimetry profile, the reaction pathway(s) as well as the reaction product(s) at the end of the successive reaction step(s) of the thermal decomposition have already been reported by the authors.[9] The thermal decomposition process of BuFeFe was proposed as follows:

Reaction pathway for Step-I:

$$2\{N(n\text{-}C_4H_9)_4[Fe^{II}Fe^{III}(C_2O_4)_3]\}_\infty \rightarrow [Fe^{II}Fe^{III}(C_2O_4)_{3-x}] +$$
$$+ Fe_2O_3(s) + 2(n\text{-}C_4H_9)_3N(g) + 2C_4H_8(g) + (3+2x)CO_2(g) + 3CO(g) + H_2(g)$$

Reaction pathway for Step-II and Step-III:

$$6[Fe^{II}Fe^{III}(C_2O_4)_{3-x}] \rightarrow 3Fe_2O_3(s) + 2Fe_3O_4(s) + (19-12x)CO_2(g) + 17CO(g)$$

where g and s denote gaseous and solid substances, respectively and x is a positive number (< 3). The observed mass loss values compare well with the calculated mass loss values following the proposed reaction pathways. Thus, the proposed reaction pathways indicate the formation of either Fe_3O_4 (magnetite) or Fe_2O_3 (hematite) or a mixture of both as the end-product of the thermal decomposition of the molecular magnetic precursor BuFeFe. The formation of the proposed end products was supplemented by IR and powder XRD studies and confirmed by magnetic studies.[9] Incidentally, at present the authors have studied the reaction kinetics of Step-I and Step-II. An attempt to continue the calculation of kinetic parameters to Step-III was avoided because of practical difficulties as Step-III corresponds to very small mass loss, which, if considered, would have introduced an erroneous result due to the large error associated with the $\alpha(T)$ values.

Along the above-stated step-wise reaction pathways, during Step-I of the thermal decomposition, the bimetallic 3-dimensional network structure of $\{N(n\text{-}C_4H_9)_4[Fe^{II}Fe^{III}(C_2O_4)_3\}_\infty$ is disrupted completely. Here the organic cationic

part, $N(n\text{-}C_4H_9)_4^+$, decomposes giving rise to various gaseous substances, while the 2-dimensional Fe^{III}–oxalate–Fe^{II} anionic layers are partially degraded giving rise to Fe_2O_3. It is apparent that the former process may require a lower activation energy than the latter and will be completed faster due to the limited abundance. The partial decomposition of the Fe^{III}–oxalate–Fe^{II} anionic layers may be due to scission of the metal–oxalate linkages. In this way, the initial exponential growth in the E_α^* *vs.* α plot for Step-I may be due to the decomposition of $N(n\text{-}C_4H_9)_4^+$, while the steady linear E_α^* *vs.* α variation in the later part of Step-I may be due to decomposition of the bimetallic network and formation of metal oxides. The reaction mechanism responsible for this step of the thermal decomposition was resolved to be nucleation given by $g(\alpha) = \ln \alpha$, an acceleratory rate equation.[22]

The early stage of Step-II supposedly favours the gradual decomposition of the bimetallic network and formation of metal oxides, giving rise to a steady growth in the E_α^* *vs.* α variation. It should be noted that the activation energy required for the linear part of the E_α^* *vs.* α plot in Step-I and those for the initial growth part of the E_α^* *vs.* α plot in Step-II lie in the same range. The Gaussian type variation of E_α^* with α is certainly the manifestation of a reaction control mechanism owing to the residual amount of reactants, *i.e.*, the remaining amount of thermally degradable molecules as well as the *in situ* degraded gaseous products. It should be noted that the thermal decomposition of iron oxalate to hematite in an air atmosphere and to magnetite in presence of CO/CO_2 mixture was reported by other workers.[25] The thermal decomposition initially started in air atmosphere leading to the formation of hematite along with a profuse amount of CO_2 and subsequently, on further heating, it might have led to the formation of magnetite.[26] The reaction mechanism responsible for Step-II of thermal decomposition observed in the present study was resolved to be a chemical reaction type.[22]

CONCLUSIONS

The present study demonstrates the kinetics of solid state reaction of the thermal decomposition of $\{N(n\text{-}C_4H_9)_4[Fe^{II}Fe^{III}(C_2O_4)_3\}_\infty$ at multiple heating rates. The thermal decomposition proceeds through three different steps, indicating three reaction mechanisms. The reaction mechanism responsible for Step-I of the thermal decomposition was resolved to be nucleation whereas Step-II is of a chemical reaction type. Calculation of kinetic parameters for Step-III was avoided due to practical difficulties. Step-wise reaction pathways leading to ferrites were proposed. The rates of the reactions were in the range of 10^3–10^{12} and 10^{12}–10^{18} min^{-1} for Step-I and Step-II, respectively.

It would be of interest to know the nature of the dependence of the reaction kinetics and the reaction mechanism on the sample environment. The identi-

fication of the various reaction products at the end of each step of the TG profile is necessary and thereby the complete reaction pathway. These studies require an *in situ* FT-IR study and evolved gas analysis (EGA), which subjects of our present interest. These results would provide insight into the mechanism of external control of the solid state thermal reactions in order to yield interesting ferrite materials using molecular complex precursors through the thermal decomposition route.

И З В О Д

ТЕРМАЛНА ДЕКОМПОЗИЦИЈА МОЛЕКУЛАРНОГ МАТЕРИЈАЛА $\{N(\mathit{N}\text{-}C_4H_9)_4[Fe^{II}Fe^{III}(C_2O_4)_3]\}_\infty$ ДО ФЕРИТА: ИСПИТИВАЊЕ РЕАКЦИОНЕ КИНЕТИКЕ

ASHIS BHATTACHARJEE[1], DEBASIS ROY[1], MADHUSUDAN ROY[2] и ARUNABHA ADHIKARI[3]

[1]Department of Physics, Visva-Bharati University, Santiniketan, India, [2]Applied Material Science Division, Saha Institute of Nuclear Physics, Kolkata, India и [3]Department of Physics, West Bengal State University, Barasat, India

Термална декомпозиција молекуларног прекурсора, $\{\mathit{N}(\mathit{n}\text{-}C_4H_9)_4[Fe^{II}Fe^{III}(C_2O_4)_3\}_\infty$ која се одвија у више ступњева, испитивана је неизотермским термогравиметријским (ТГ) мерењима у температурском опсегу од 300 до ≈800 K при различитим брзинама грејања (5, 10 и 20 K min^{-1}). Термална декомпозиција комплекса на бази оксалата се одвија ступњевито кроз низ реакција. Коришћењем две различите изоконверзионе методе, тачније, унапређене итеративне методе и методе без модела одређени су кинетички параметри: енергија активације и брзина реакције, и највероватнији реакциони механизам термалне декомпозиције. Различити реакциони путеви који резултују у различитим ступњевима термогравиметријских профила су такође разматрани коришћењем ранијих експерименталних резултата истих аутора.

(Примљено 19. маја 2012)

REFERENCES

1. M. Winter, R. J. Brodd, *Chem. Rev.* **104** (2004) 4245
2. M. M. Thackeray, C. S. Johnson, J. T. Vaughey, N. Li, S. A. Hackney, *J. Mater. Chem.* **15** (2005) 2257
3. G. Eranna, B. C. Joshi, D. P. Runthala, R. P. Gupta, *Crit. Rev. Solid State Mater. Sci.* **29** (2004) 111
4. M. E. Franke, T. J. Koplin, U. Simon, *Small* **2** (2006) 36
5. K. L. Chopra, P. D. Paulson, V. Dutta, *Prog. Photovoltaics* **12** (2004) 69
6. M. L. Kahn, A. Glaria, C. Pages, M. Monge, L. Saint Macary, A. Maisonnat, B. Chaudret, *J. Mater. Chem.* **19** (2009) 4044
7. A. Bhattacharjee, S. Reiman, V. Ksenofontov, P. Gütlich, *J. Phys. Condens. Matter*. **15** (2003) 5103
8. K. E. Neo, Y. Y. Ong, H. V. Huynh, T. S. Andy Hor, *J. Mater. Chem.* **17** (2007) 1002
9. A. Bhattacharjee, D. Roy, M. Roy, *J. Therm. Anal. Calorim.* **109** (2012) 1423
10. A. Bhattacharjee, D. Roy, M. Roy, S. Chakraborty, A. De, J. Kusz, W. Hofmeister, *J. Alloy. Compd.* **503** (2010) 449
11. F. A. Cotton, G. Willkinson, C. A. Murillo, M. Bochmonn, *Advanced Inorganic Chemistry*, 6th ed., Wiley, New York, 1999

12. Z. Gao, M. Nakada, I. Amasaki, *Theromochim. Acta* **369** (2001) 137
13. S. Vyazovkin, D. Dollimore, *J. Chem. Inf. Comput. Sci*. **36** (1996) 42
14. L. Liqing, C. Donghua, *J. Therm. Anal. Calorim.* **78** (2004) 283
15. H. Ōkawa, N. Matsumoto, H. Tamaki, S. Kida, M. Ohba, *Mol. Cryst. Liq. Cryst.* **233** (1993) 257
16. S. Vyazovkin, in *The Handbook of Thermal Analysis & Calorimetry, Vol. 5: Recent Advances, Techniques and Applications*, M. E. Brown, P. K. Gallagher, Eds., Elsevier, Amsterdam, The Netherlands, 2008, p. 503
17. A. W. Coats, J. P. Redfern, *Nature* **201** (1964) 68
18. J. Farjas, P. Roura, *J. Therm. Anal. Calorim.* **105** (2011) 767
19. J. Šesták, *Thermophysical Properties of Solids, Their Measurements and Theoretical Analysis*, Vol. 12D, Elsevier, Amsterdam, The Netherlands, 1984
20. G. I. Senum, R. T. Yang, *J. Therm. Anal. Calorim.* **11** (1977) 445
21. J. Cai, F. Yao, W. Yi, F. He, *AIChE J.* **52** (2006) 1554
22. L. Vlaev, N. Nedelchev, K. Gyurova, M. Zagorcheva, *J. Anal. Appl. Pyrolysis* **81** (2008) 253
23. J. Málek, *Thermochim. Acta* **200** (1992) 257
24. B. Janković, S. Mentus, M. Janković, *J. Phys. Chem. Solids* **69** (2008) 1923
25. A. Angermann, J. Töffer, *J. Mater. Sci*. **43** (2008) 5123
26. I. S. Lyubutin, C. R. Lin, Yu. V. Korzhetskiy, T. V. Dmitrieva, R. K. Chiang, *J. Appl. Phys.* **106** (2009) 34311.

Journal of the Serbian Chemical Society
JSCS-info@shd.org.rs • www.shd.org.rs/JSCS
J. Serb. Chem. Soc. 78 (4) 537–548 (2013)
JSCS–4436
UDC 547.978+666.122.3:543.552+544.6.076.32–039.26
Original scientific paper

Differential pulse anodic stripping voltammetric determination of berberine using a nano-Na-montmorillonite clay-modified carbon paste electrode

WEN CHEN, MING-XIAO ZHANG*, CONG LI and YONG-LING LI

School of Chemistry and Chemical Engineering, Southwest University, 2 Rd Tiansheng, Beibei District, Chongqing, P. R. China

(Received 27 May, revised 16 July 2012)

Abstract: A simple and sensitive method is presented for the electrochemical determination of berberine based on a nano-Na-montmorillonite (nano-Na-MMT) clay-modified carbon paste electrode. The electrochemical oxidation and adsorption behavior of berberine was studied at the proposed electrode by linear sweep voltammetry in acetate buffer (0.2 M, pH 5.6). A differential pulse anodic stripping voltammetric procedure was developed for the determination of the drug. A good linear relationship between the oxidation peak current magnitude and the concentration of berberine was observed in the range from 1.0 to 18.0 μg mL^{-1} with a detection limit of 0.07 μg mL^{-1} and a quantification limit of 0.24 μg mL^{-1}. The proposed method was successfully applied to the determination of berberine in pharmaceutical tablets.

Keywords: berberine; nano-Na-montmorillonite clay; carbon paste electrode; modified electrode; electrochemical determination.

INTRODUCTION

Berberine, a well-known natural isoquinoline alkaloid, is mainly isolated from the roots and rhizomes of several plants, such as berberidaceae, ranunculaceae, menispermaceae, *etc*.[1] As a medicinal drug, it has drawn extensive attention for a long time due to its extensive biological activities, such as antibacterial,[2] antiparasitic,[3] antimicrobial,[4] antifungal,[5] hypotensive,[6] *etc*. Hitherto, numerous efforts focused on the research and development of berberine as an antimicrobial drug in the treatment of ocular trachoma infections and intestinal infections, such as acute gastroenteritis and bacillary dysentery.[4] In addition, the effects of berberine on human malignant brain tumor,[7] esophageal cancer,[8] leukemic cancer[9] and colon cancer[10] cell lines were tested and significant cell death

* Corresponding author. E-mail: pclab@swu.edu.cn
doi: 10.2298/JSC120527093C

effects were evidenced. Therefore, berberine research is becoming increasingly active with the aim of extending its possible potential in clinical practice.

Medicinal analysis plays an important role in quality control in medicine. The development of sensitive, simple, rapid and reliable methods for the determination of active ingredients is very important and interesting. At present, the methods of detection of berberine mainly include: supercritical fluid chromategraphy (SFC),[11] high performance capillary electrophoresis (HPCE),[12] thin layer chromatography (TLC),[13] electro-generated chemiluminescence (ECL),[14] resonance Raleigh scattering (RRS),[15] high performance liquid chromatography (HPLC)[16] or reverse phase liquid chromatography (RPLC)[17] and ^{1}H-NMR spectroscopy.[18] Most of these methods are costly and require expertise in addition to time-consuming pretreatment steps. The electrochemical properties of berberine have been known for a long time through studies concerned with the electrochemical reduction and adsorption of berberine at mercury electrodes.[19,20] The electrochemical reduction of berberine with a glassy carbon electrode was also reported.[21]

The carbon paste electrode (CPE), a mixture of conducting graphite powder and hydrophobic adhesive, has been extensively used in electro-analytical chemistry because of its excellent properties: wide potential range (from –1.40 to 1.30 V), easy preparation, convenient surface renewal, low residual current, porous surface, and low cost.[22] Recently, some new reports have appeared on the application of carbon paste electrodes for the analysis of drugs,[23,24] biomolecules,[25,26] and other important compounds.[27,28] These studies showed that the sensitivity of a bare CPE is relatively poor in trace assays. In order to improve its sensitivity, it is a fascinating and effective way to modify bare CPE by mixing with some other unique substances.

Nano-materials, defined as having one or more external dimension in the size range 1–100 nm, have received steadily growing interests because of their peculiar and fascinating properties, which include the quantum size effect, the small bulk effect, the surface effect and the macroscopic quantum tunneling effect.[29] Recently, some nano-materials were used as modifiers to improve the sensitivity of electrodes, such as carbon nanotubes,[23,24,27,30] gold nanoparticles,[31] SiO_2,[32] montmorillonite[33] and TiO_2.[30]

Montmorillonite belongs to the smectite group of clays and has a well-layered structure. Its predominant properties are its huge cationic exchange capacity, due to an excess negative charge on the surface of the clay, and a strong adsorptive ability, attributed to the expandability of its internal layers.[34] Therefore, montmorillonite has been widely used to modifying electrodes to improve their determination sensitivity towards anions,[35] cations,[33] and organic compounds,[36,37] and has been employed to fabricate biosensors.[38]

In this work, because of its positive charge in solution, the electrochemical oxidation and adsorption behavior of berberine were investigated using a carbon paste electrode modified with nano-Na-montmorillonite clay (nano-Na-MMT/ /CPE). A differential pulse anodic stripping voltammetric (DPASV) method was developed using acetate buffer (0.2 M, pH 5.6) as the supporting electrolyte. The proposed method was applied to the determination of the drug berberine in pharmaceutical tablets.

EXPERIMENTAL

Reagents and chemicals

Nano-Na-MMT clay (≈25 nm) was purchased from the Fenghong Clay Chemicals Co., Ltd. (Zhejiang, China). The content of montmorillonite was 96.0–98.0 %, and the apparent density and diameter thickness ratio of the material were 0.25–0.35 g cm^{-3} and 200, respectively. Berberine chloride was provided by the College of Pharmacy of the Southwest University (Chongqing, China). The analyzed formulation was "compound berberine tablets" labeling to contain 30 mg berberine chloride per tablet (Chongqing Tongjunge Pharmaceutical Factory Co., Ltd. of the Taiji Group, China).

A standard stock solution of 0.20 mg mL^{-1} berberine was prepared in ultra pure water. The desired concentration of berberine was obtained by direct dilution of the appropriate quantity of stock solution with the supporting electrolyte.

Britton–Robinson (B–R) universal buffer (pH 2–10) and acetate buffer (0.2 M, pH 3.7––5.6) were prepared in ultra pure water and were used as supporting electrolytes. All the employed chemicals were of analytical reagent grade and used without further purification.

Apparatus

All electrochemical measurements were performed on a LK2006AZ electrochemical analyzer (Lanlike Chemistry & Electron High Technology Co., Ltd. Tianjing, China). A conventional three-electrode system, including a nano-Na-MMT/CPE (3 mm in diameter), a saturated calomel reference electrode (SCE), and a platinum flat counter electrode, was employed. All potentials are referred to SCE.

Preparation of the nano-Na-MMT/CPE

Graphite powder (4.75 g) and nano-Na-MMT clay (0.25 g) were mixed uniformly by milling in a small agate mortar. Then 1.8 mL Nujol oil (d = 0.84 g mL^{-1}) and a little ethanol were added, and the mixture was milled again to obtain a homogenous 5 mass % nano-Na--MMT modified carbon paste after ethanol evaporation. Various modified carbon paste containing different mass percentages of nano-Na-MMT clay (0.0, 2, 4, 6, 8 and 10 mass %) were prepared in the same way. An amount of the prepared modified carbon paste was pressed into the end cavity of the electrode body. The surface of the constructed nano-Na-MMT/CPE was polished on clean paper before use.

General analytical procedure

Acetate buffer solution (10 mL, 0.2 M, pH 5.6) was introduced into the electrolysis cell and then a polished nano-Na-MMT/CPE was immersed in the supporting electrolyte. Then several cyclic voltammetric sweeps were applied to obtain a low background current. Then an analyte solution was introduced into the electrolysis cell, then at a selected preconcentration potential, accumulated to the developed nano-Na-MMT/CPE for a selected preconcentration time while the solution was stirred at 700 rpm. At the end of the preconcentration time, the

stirring was stopped 5 s for the solution becoming quiescent. The voltammograms were then recorded by scanning the potential in the positive direction using differential pulse voltammetry. After each measurement, the used carbon paste was carefully removed and a new nano--Na-MMT/CPE made again.

RESULTS AND DISCUSSION

Electrochemical behavior of berberine at CPE

Linear sweep voltammograms (LSV) of 10.0 μg mL^{-1} berberine were recorded at both a bare CPE and a 5 mass % nano-Na-MMT/CPE in B–R universal buffer (pH 2–10) and in acetate buffer (0.2 M, pH 3.7–5.6) at 50 mV s^{-1} before preconcentration and after preconcentration at 0.40 V for 150 s. The obtained LSVs are presented in Fig. 1. As shown, a very ill defined anodic peak was observed at the bare CPE before preconcentration (Fig. 1A, curve a), and a somewhat better peak was observed at the 5 mass % nano-Na-MMT/CPE (Fig. 1B, curve a) in acetate buffer (0.2 M, pH 5.6). The observed anodic peak corresponded to the oxidation of the methylenedioxy ring of berberine (Scheme 1).[39]

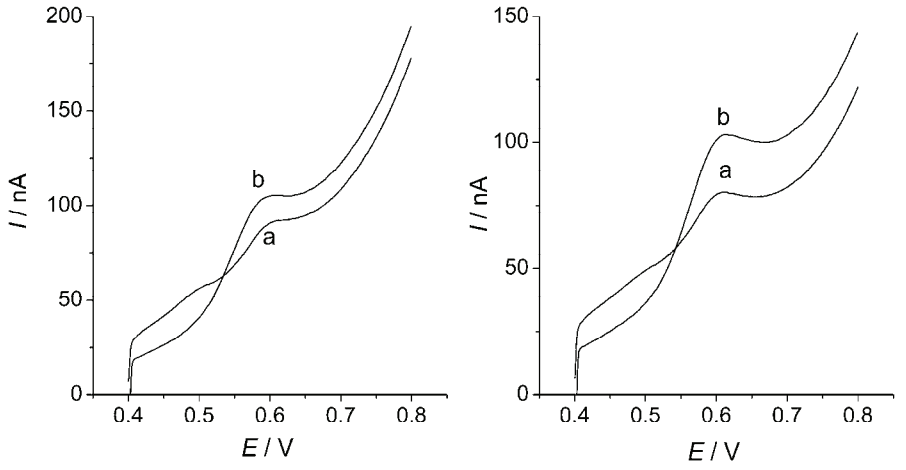

Fig. 1. Linear sweep voltammograms of 10.0 μg mL^{-1} berberine in acetate buffer (0.2 M, pH 5.6), recorded at a bare CPE (A) and at a nano-Na-MMT/CPE (B) before preconcentration (curves a) and after preconcentration at 0.40 V for 150 s (curves b), scan rate v = 50 mV s^{-1}.

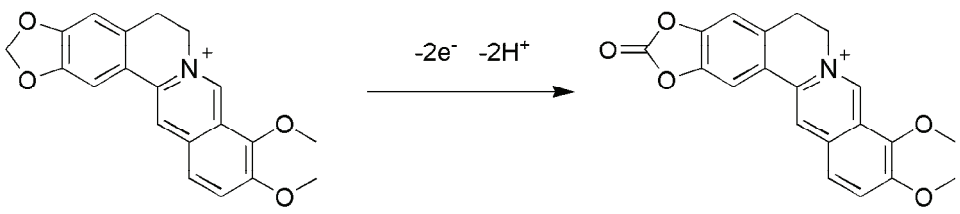

Scheme 1. Proposed mechanism for the electro-oxidation of berberine.

On the other hand, the voltammograms recorded after preconcentration at 0.40 V for 150 s showed a little enhanced peak at the bare CPE (Fig. 1A, curve b) and a better-defined enhanced peak at the 5 % (w/w) nano-Na-MMT/CPE (Fig. 1B, curve b). This enhancement of the peak current compared to that at the bare CPE indicated the strong enrichment behavior of berberine onto the modified CPE. This phenomenon may be attributed to cationic exchange and the adsorptive properties of the nano-Na-MMT clay, and consequentially the sensitivity of assay for berberine was remarkably improved. Therefore, nano-Na-MMT/CPE was used as the working electrode for the rest of the analytical study.

Further, linear sweep voltammograms of 10.0 μg mL^{-1} berberine were recorded at different scan rates, v (10–300 mV s^{-1}), at the developed 5 mass % nano-Na-MMT/CPE following preconcentration at 0.40 V for 150 s. The peak current (I_p) magnitude increased upon increasing the scan rate (v). According to the simplified Randles–Sevcik equation ($I_p = -\text{constant} \times v^{1/2}$),[40] a linear plot of log I_p *vs*. log v was obtained with corresponding equation:

$$\log I_p \text{ (nA)} = 0.614 \log v + 0.692 \ (r = 0.998 \text{ and } n = 7)$$

where v is in mV s^{-1}. The slope value of 0.614 is close to the expected theoretical value of 0.5, indicating that the oxidation process of berberine at a nano-Na-MMT/CPE is diffusion controlled. Moreover, as the scan rate was increased, the peak potential (E_p) shifted towards more positive potential, showing an irreversible oxidation process.[41] Since a slope value of 0.256 V dec^{-1} was found from the Tafel plot constructed from data of the rising part of the current–voltage curve recorded at a scan rate of 50 mV s^{-1}, it could be estimated that $\alpha n_a = 1.05$. The number of electrons, n_a, transferred in the rate-determining step of the removal of electrons from the methylenedioxy ring of the berberine moiety was 2.[39] Then, the transfer coefficient α should be 0.52.

Based on the electrochemical oxidation and the adsorption behavior of berberine onto the developed nano-Na-MMT/CPE surface, a differential pulse anodic stripping voltammetric (DPASV) method was optimized for its trace determination.

Composition and stability of the nano-Na-MMT/CPE

DPASV curves of 10.0 μg mL^{-1} berberine in acetate buffer (0.2 M, pH 5.6) at CPEs modified with various mass percentages (% w/w) of nano-Na-MMT clay were recorded after preconcentration at 0.20 V for 150 s. As shown in Fig. 2, the magnitude of the peak current (I_p) increased with increasing percentage of nano-Na-MMT clay in the modified CPE up to 5 mass %, and then decreased. Such an enhancement of the magnitude of stripping peak current (I_p) was expressed due to the strong adsorptive properties of the nano-Na-MMT clay. However, at higher percentage of nano-Na-MMT clay in the modified CPE, the decrease in the magnitude of the peak current (I_p) may be attributed to the decrease in conductivity of

the electrode with the increasing percentage of the nonconductive nano-Na-MMT clay, which hindered the electron transfer process and increased the background current. This status reflected the competitive relationship between the adsorption ability and the conductive ability of the electrode. As stated above, 5 mass % of nano-Na-MMT/CPE was used in the succedent analytical study.

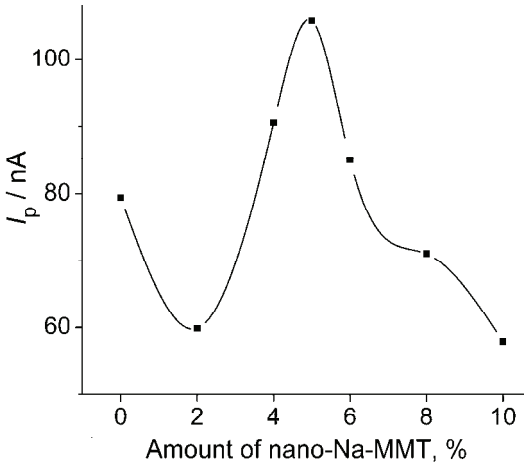

Fig. 2. Effect of the mass percentage (% w/w) of nano-Na-MMT clay on the DPASV peak current (I_p) of 10.0 μg mL^{-1} berberine in acetate buffer (0.2 M, pH 5.6); E_{acc} = 0.20 V, t_{acc} = 150 s, ΔE_s = 6 mV, E_a = 100 mV, t_w = 0.1 s and t_p = 0.5 s.

Moreover, the reproducibility of results utilizing 5 mass % nano-Na-MMT/ /CPE fabricated repeatedly was examined by comparing the DPASV oxidation peak current (I_p) of 10.0 μg mL^{-1} berberine. Nine repetitive analyses utilizing three separately fabricated 5 mass % nano-Na-MMT/CPE were obtained. It was found that the oxidation peak current (I_p) magnitude remained almost constant with a relative standard deviation of 4.2 %.

SEM characterization of the surface of the electrodes

Figure 3 depicts the typical images of scanning electronic microscope (SEM) based on different electrodes. Figure 3A shows an obvious image of the smooth graphite layer. After mixed nano-Na-MMT and graphite powder, a homogeneous morphology was obtained with a loose and porous layer (Fig. 3B).

Pulse parameters and preconcentration parameters

DPASV of 10.0 μg mL^{-1} berberine in acetate buffer (0.2 M, pH 5.6) following its preconcentration onto a developed 5 mass % nano-Na-MMT/CPE at 0.20 V for 150 s were recorded at the various pulse parameters (scan-increment ΔE_s = = 2–15 mV, pulse-amplitude E_a = 5–100 mV, pulse-width t_w = 0.01–1 s, and pulse-period t_p = 0.1–1 s). A developed, obvious and symmetrical voltammetric peak was obtained under the following pulse parameters: ΔE_s = 6 mV, E_a = 100 mV, t_w = 0.1 s and t_p = 0.5 s.

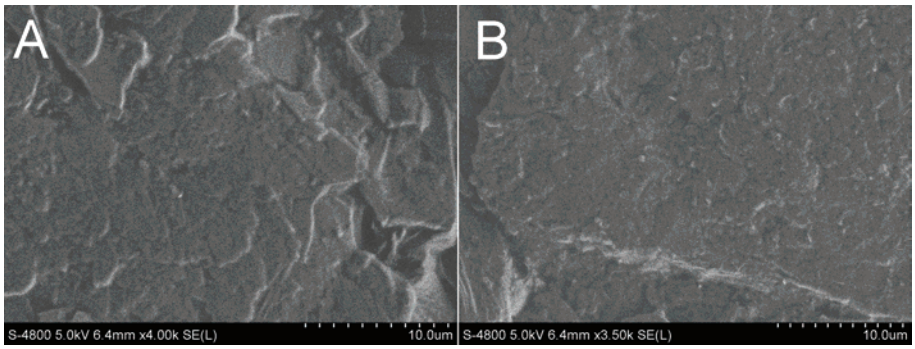

Fig. 3. SEM Images of a bare CPE (A) and a 5 mass % nano-Na-MMT/CPE (B).

The effect of various preconcentration potentials (E_{acc}) from −0.30 to 0.40 V on the magnitude of the peak current (I_p) of the DPASV of 10.0 μg mL^{-1} berberine in acetate buffer (0.2 M, pH 5.6) was evaluated at a 5 mass % nano-Na--MMT/CPE following preconcentration for 150 s (Fig. 4). The results showed that magnitude of the peak current (I_p) increased with increasing potential in the range from −0.30 to 0.20 V. At more positive preconcentration potentials, a significant decrease in the magnitude of the peak current (I_p) was observed. Therefore, a preconcentration potential of 0.20 V was the best and was applied in the present analytical study.

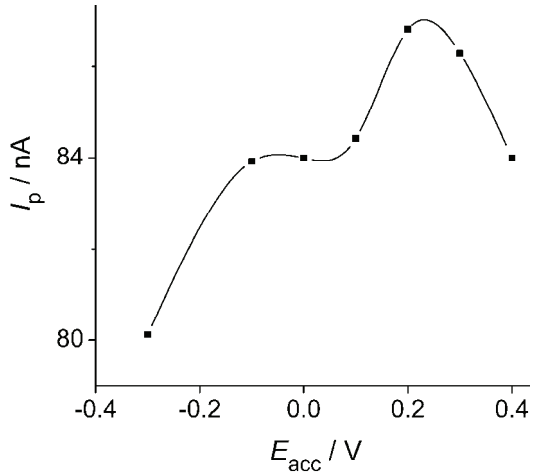

Fig. 4. Effect of preconcentration potential (E_{acc}) on the DPASV peak current (I_p) of 10.0 μg mL^{-1} berberine in acetate buffer (0.2 M, pH 5.6) after preconcentration onto a 5 mass % nano-Na-MMT/CPE for 150 s; ΔE_s = 6 mV, E_a = 100 mV, t_w = 0.1 s and t_p = = 0.5 s.

On the other hand, DPASV of 4.0 and 10.0 μg·mL^{-1} berberine were recorded at increasing preconcentration times (t_{acc}) under the foregoing optimal operational conditions. As shown in Fig. 5, in order to avoid the saturation of electrode surface, a preconcentration time of 150 s was applied in the present analytical study.

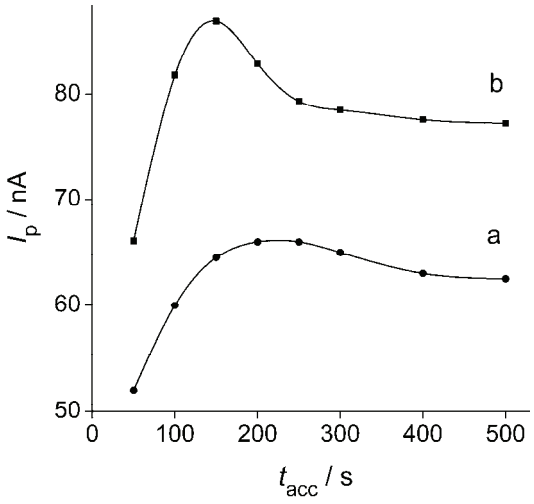

Fig. 5. Effect of preconcentration time (t_{acc}) on the DPASV peak current (I_p) of 4.0 (a) and 10.0 μg mL^{-1} (b) berberine in acetate buffer (0.2 M, pH 5.6) after preconcentration onto a 5 mass % nano-Na-MMT/CPE at 0.20 V; ΔE_s = 6 mV, E_a = 100 mV, t_w = 0.1 s and t_p = = 0.5 s.

According to the above results, the optimum operational conditions of the DPASV method utilizing 5 mass % nano-Na-MMT/CPE in acetate buffer (0.2 M, pH 5.6) were: E_{acc} = 0.20 V, t_{acc} = 150 s, ΔE_s = 6 mV, E_a = 100 mV, t_w = 0.1 s and t_p = 0.5 s.

Linearity

The relationship between the magnitude of the oxidation peak current (I_p) and the concentration of berberine (Fig. 6) was examined utilizing the developed 5 mass % nano-Na-MMT/CPE in acetate buffer (0.2 M, pH 5.6) by the developed DPASV method. A linear range from 1.0 to 18.0 μg mL^{-1} berberine was obtained with the following regression equation:

$$I_p \text{ (nA)} = 20.34c \text{ (μg mL}^{-1}\text{)} + 16.05 \ (r = 0.997 \text{ and } n = 6)$$

The limit of detection (*LOD*) and limit of quantification (*LOQ*) of berberine were estimated using the expression: kSD/b,[42] where k = 3 for the *LOD* and 10 for the *LOQ*, *SD* is the standard deviation of the blank and b is the slope of the calibration plot. The *LOD* and *LOQ* value were found to be 0.07 and 0.24 μg mL^{-1}, respectively.

Interference studies

The influence of various potentially interference species that are commonly found with berberine in pharmaceuticals on the determination of 10.0 μg mL^{-1} berberine were investigated to evaluate the selectivity of the proposed method. The tolerance limit was taken as the maximum concentration of the foreign substances that caused an approximately ±5 % relative error in the determination. The results after the experiments revealed that 800-fold of glucose, sucrose and citric acid, 500-fold of methanol, ethanol, Ca^{2+}, Mg^{2+}, Al^{3+}, Fe^{3+}, Fe^{2+}, NH^{4+},

PO_4^{3-}, SO_4^{2-}, SO_3^{2-}, CO_3^{2-}, NO_3^-, Cl^- and F^-, 300-fold of potassium sorbate, aqueous ethylcellulose and carboxymethyl cellulose, 50-fold of Tween 60 and Tween 80, and a saturated starch solution did not affect the selectivity. Although ascorbic acid showed interference in the determination of berberine, the interference could be minimized, if necessary, by using the ascorbic oxidase enzyme, which exhibits high selectivity to the oxidation of ascorbic acid. These results confirmed the suitable selectivity of the proposed method for the determination of berberine.

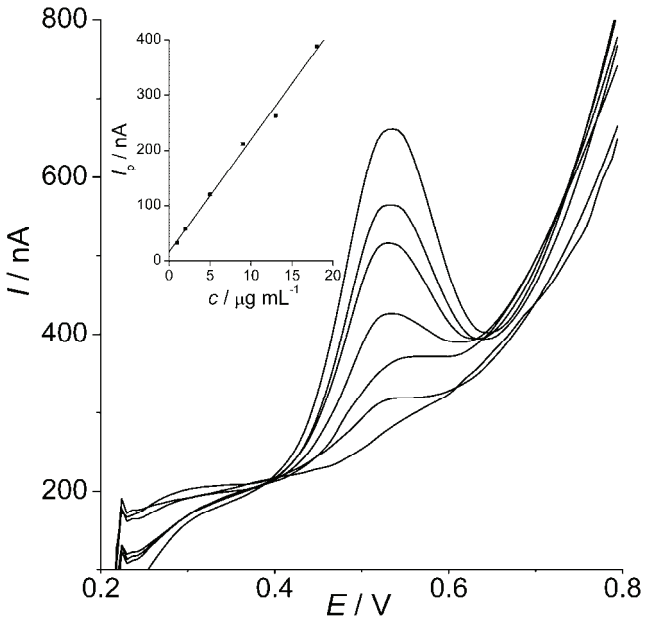

Fig. 6. DPASV recorded at a 5 mass % nano-Na-MMT/CPE for different concentration of berberine (1.0, 2.0, 5.0, 9.0, 13.0 and 18.0 μg mL^{-1}) in acetate buffer (0.2 M, pH 5.6). The inset shows a plot of peak current (I_p) *vs*. the concentration of berberine.

Analytical application

The sample powder was obtained from 10 tablets after the sugar-coating had been carefully removed. An accurately weighed amount of the power was dissolved in ultra pure water by ultrasonic sound for 30 min. After addition of an appropriate quantity of sample solution into 10 mL acetate buffer (0.2 M, pH 5.6), the DPASV was recorded.

The content of berberine was obtained by the standard addition method, and the results are listed in Table I. The recovery rates of standard solution of berberine were examined to detect the interference of excipients and co-formulated drugs. The value of recovery was at the range from 97.9 to 104.4 %, which

suggested that the excipients and co-formulated drugs have an acceptable interference on the determination. In addition, the average content of berberine in the selected tablets is 29.65 mg per tablet. The value of relative standard deviation and relative error were 1.02 and −1.16 %, respectively.

TABLE I. Results of berberine analysis in real samples (n = 5)

Sample	Detection result of sample μg mL^{-1}	Standard solution added μg mL^{-1}	Standard solution found μg mL^{-1}	Recovery %	Result of sample mg/tablet
1	9.785	5.000	5.220	104.4	29.64
2	9.659	5.000	5.119	102.4	29.26
3	9.746	5.000	4.965	99.3	29.52
4	9.824	5.000	5.050	101.0	29.76
5	9.932	5.000	4.893	97.9	30.08

CONCLUSION

In this work, a new method based on a nano-Na-montmorillonite clay modified carbon paste electrode was first developed for studying the direct electrochemical oxidation of berberine chloride. Simultaneously, a simple and sensitive differential pulse anodic stripping voltammetric method was developed and described in detail. This method was applied to the direct assay of berberine in pharmaceutical tablets without any precipitation, evaporation or extraction process, which were not necessary, as there was no interference from the excipients. The high precision, accuracy, sensitivity and selectivity of the method can foresee its promising application as a simple, convenient, and fast electrochemical method for the determination of berberine in clinical and pharmaceutical formulations.

Acknowledgements. The authors express their gratitude for the berberine drug provided by the College of Pharmacy of the Southwest University (Chongqing, China) and for the financial supports from the Doctor special fund for Basic Scientific Research of Southwest University (No. 104200-20710906).

ИЗВОД

ОДРЕЂИВАЊЕ БЕРБЕРИНА ДИФЕРЕНЦИЈАЛНОМ ПУЛСНОМ АНОДНОМ СТРИПИНГ ВОЛТАМЕТРИЈОМ НА ЕЛЕКТРОДИ ОД УГЉЕНИЧНЕ ПАСТЕ МОДИФИКОВАНЕ НАНОЧЕСТИЦАМА НАТРИЈУМ-МОНТМОРИЛОНИТА

WEN CHEN, MING-XIAO ZHANG, CONG LI и YONG-LING LI

School of Chemistry and Chemical Engineering, Southwest University, 2 Rd Tiansheng, Beibei District, Chongqing, P. R. China

Представљена је једноставна и осетљива електрохемијска метода одређивања берберина на електроди од угљеничне пасте модификоване наночестицама натријум-монтморилонита. На овој електроди је испитивана електрохемијска оксидација и адсорпција берберина помоћу волтаметрије са линеарно променљивим потенцијалом у ацетатном пуферу (0,2 M и pH 5,6). Развијена је процедура одређивања поменутог лека методом

диференцијалне пулсне анодне стрипинг волтаметрије. Добијена је добро дефинисана линеарна зависност максимума струје оксидације берберина од његове концентрације у опсегу од 1,0 до 18,0 μg mL^{-1} са границом детекције од 0,24 μg mL^{-1}. Предложена метода је успешно примењена за одређивање берберина у комерцијалним таблетама.

(Примљено 27. маја, ревидирано 16. јула 2012)

REFERENCES

1. T. C. Birdsall, G. S. Kelly, *Alter. Med. Rev*. **2** (1997) 94
2. K. A. Ettefagh, J. T. Burns, H. A. Junio, G. W. Kaatz, N. B. Czech, *Planta Med.* **77** (2011) 835
3. G. Monique, Q. L. Joelle, T. D. Pierre, B. Guy, A. Luc, *Planta Med*. **58** (1992) 276
4. S. Amritpal, D. Sanjiv, K. Navpreet, S. Jaswinder, *J. Nat. Prod.* **3** (2010) 64
5. K. Kang, F. K. Bhattacharyya, D. K. Ghosh, *Exp. Parasitol.* **60** (1985) 404
6. D. G. Kang, E. J. Sohn, E. K. Kwon, J. H. Han, H. Oh, H. S. Lee, *Vasc. Pharmacol.* **39** (2002) 281
7. D. Y. Wang, C. C. Yeh, J. H. Lee, C. F. Hung, J. G. Chung, *Neurochem. Res.* **27** (2002) 883
8. N. Iizuka, K. Miyamoto, K. Okita, A. Tangoku, H. Hayashi, S. Yosino, T. Abe, T. Morioka, S. Hazama, M. Oka, *Cancer Lett.* **148** (2000) 19
9. C. L. Kuo, C. C. Chou, B. Y. M. Yung, *Cancer Lett.* **93** (1995) 193
10. K. Fukuda, Y. Hibiya, M. Mutoh, M. Koshiji, S. Akao, H. Fujiwara, *J. Ethnopharmacol.* **66** (1999) 227
11. K. Suto, S. Kakinuma, Y. Ito, K. Sagara, H. Iwasaki, H. Ttokawa, *J. Chromatogr., A* **786** (1997) 371
12. Y. R. Chen, K. C. Wen, G. R. He, *J. Chromatogr., A* **866** (2000) 273
13. M. Matt, E. M. Galvez, V. L. Cebolla, L. Membrado, R. Bacaud, S. Pessayre, *J. Sep. Sci.* **26** (2003) 1665
14. L. Zhao, Y. Tao, X. Q. Yang, L. Y. Zhang, M. Oyama, X. Chen, *Talanta* **70** (2006) 104
15. J. D. Peng, S. P. Liu, Y. Shi, Z. F. Liu, *Anal. Sci*. **22** (2006) 1301
16. P. L. Tsai, T. H. Tsai, *Anal. Lett.* **35** (2002) 2459
17. J. Zhang, Y. Jin, Y. F. Liu, Y. S. Xiao, J. T. Feng, X. Y. Xue, X. L. Zhang, X. M. Liang, *J. Sep. Sci*. **32** (2009) 2084
18. P. L. Ding, L. Q. Chen, Y. Lu, Y. G. Li, *J. Pharmaceut. Biomed.* **60** (2012) 44
19. S. Komorsky-Lovric, M. Lovric, *Mikrochim. Acta* **1** (1989) 159
20. S. Komorsky-Lovric, *Electroanalysis* **12** (2000) 599
21. F. Wang, Y. Y. Gao, L. Gao, T. L. Xing, *J. Chin. Chem. Soc.-Taip.* **58** (2011) 450
22. W. Huang, S. Zhang, Y. Wu, Russ. *J. Electrochem.* **42** (2006) 153
23. H. Yaghoubian, H. Karimi-Maleh, M. A. Khalilzaden, F. Karimi, *J. Serb. Chem. Soc.* **74** (2009) 1443
24. A. Mokhtari, H. Karimi-Maleh, A. A. Ensafi, H. Beitollahi, *Sens. Actuators, B* **169** (2012) 96
25. S. Shahrokhian, H. R. Zare-Mehrjardi, H. Khajehsharifi, *J. Solid State Electrochem.* **13** (2009) 1567
26. J. B. Raoof, R. Ojani, M. Amiri-Aref, F. Chekin, *J. Appl. Electrochem.* **40** (2010) 1357
27. A. Ensafi, H. Karimi-Maleh, *J. Electroanal. Chem.* **640** (2010) 75
28. L. H. Liu, C. Q. Duan, Z. N. Gao, *J. Serb. Chem. Soc.* **77** (2012) 483

29. P. Ball, L. Garwin, *Nature* **355** (1992) 761
30. S. Kharian, N. Teymoori, M. A. Khalilzadeh, *J. Solid State Electrochem.* **16** (2012) 563
31. H. S. Yin, S. Y. Ai, W. J. Shi, *Sens. Actuators, B* **137** (2009) 747
32. C. L. Hong, R. Yuan, Y. Q. Chai, *Anal. Chim. Acta* **633** (2009) 244
33. B. H. Chen, L. S. Wang, X. J. Huang, P. X. Wu, *Microchim. Acta* **172** (2011) 335
34. S. J. Dong, G. L. Che, Y. W. Xie, *Chemically modified electrodes*, Science Press, Beijing, 2003, p. 279 (in Chinese)
35. M. Morigi, E. Scavetta, M. Berrettoni, M. Giorgetti, D. Tonelli, *Anal. Chim. Acta* **439** (2001) 265
36. B. Muralidharan, G. Gopu, C. Vedhi, P. Manisankar, *Appl. Clay Sci.* **42** (2008) 206
37. M. Beltagi, *J. Appl. Electrochem.* **39** (2009) 2375
38. X. J. Zhao, Z. B. Mai, Z. Dai, X. Y. Zou, *Talanta* **84** (2011) 148
39. V. C. Diculescu, T. A. Enache, P. J. Oliveira, A. M. Oliveira-Brett, *Electroanalysis* **21** (2009) 1027
40. J. Wang, *Analytical Electrochemistry*, Wiley, New York, 2006, p. 30
41. A. Bard, L. R. Faulkner, *Electrochemical Methods: Fundamentals and Applications*, Wiley, New York, 2001, p. 236
42. J. N. Miller, *Analyst* **116** (1991) 3.

Journal of the Serbian Chemical Society
JSCS-info@shd.org.rs • www.shd.org.rs/JSCS
J. Serb. Chem. Soc. 78 (4) 549–554 (2013)
JSCS–4437
UDC 546.714+544.478.1+
544.654.2:544.351–145.82
Extended abstract

EXTENDED ABSTRACT

Electrodeposition and characterization of Ni–MoO_2 composite coatings as cathodes for the hydrogen evolution reaction in alkaline solution•

UROŠ Č. LAČNJEVAC*#

Institute for Multidisciplinary Research, University of Belgrade, Kneza Višeslava 1, 11030 Belgrade, Serbia

(Received 15 December 2012)

Abstract: Composite Ni–MoO_2 coatings were prepared and characterized with respect to their possible application as electrocatalysts for the hydrogen evolution reaction (HER) in alkaline solution. The composites were electrodeposited onto Ni meshes from an ammonium chloride Ni solution with suspended MoO_2 particles under simulated industrial conditions for the production of commercial cathodes. The influence of the concentration of MoO_2 particles in the solution and deposition current density on the morphology, and chemical and phase composition of the obtained coatings were investigated by scanning electron microscopy (SEM), energy dispersive X-ray spectroscopy (EDS) and X-ray diffraction (XRD). Catalytic activity of the coatings for the HER was examined by polarization measurements in a 32 wt. % NaOH solution at 90 °C and compared to the activity of the commercial *De Nora*'s cathode (DN). It was shown that the most active Ni–MoO_2 coating exhibited better polarization characteristics for the HER than the DN cathode. The mechanism of the HER on the specified Ni–MoO_2 coating was investigated in 8 mol dm^{-3} NaOH at 30 °C by means of steady-state polarization measurements and an electrochemical impedance spectroscopy (EIS). Based on the theoretical interpretation of the experimental data, the rate constants of the three individual steps of the HER were determined and the source of catalytic activity of the coating was elucidated.

Keywords: hydrogen evolution; electrocatalysis; Ni–MoO_2 coating; morphology; electrochemical impedance spectroscopy.

* Correspondence. E-mail: uros.lacnjevac@imsi.rs
# Serbian Chemical Society member.
• Lecture given at the meeting of the Electrochemical Section of the Serbian Chemical Society held on 8 February, 2012.
doi: 10.2298/JSC121215160L

Chlor–alkali electrolysis is an industrial process of major importance since more than 95 % of chlorine and 99.5 % of sodium hydroxide are annually produced in the world by mercury, diaphragm and membrane chlor–alkali technologies.[1] One of the main obstacles to the future development of the chlor–alkali industry is the high cost of the consumed electrical energy,[1] partially associated with the inadequate efficiency of the hydrogen-evolving cathodes. Over the past years, great effort has been devoted to searching for cathode materials suitable for industrial application,[2–16] which have to meet several criteria, such as: high catalytic activity for the hydrogen evolution reaction (HER), large surface area, good mechanical, chemical and corrosion stability and low cost of the components. Nickel is used as the basic component of industrial cathodes due to its stability in alkaline media, moderate activity for the HER and low price.[17] In commercial zero-gap membrane cells of the *Industrie De Nora* (DN), a Ni–RuO_2 composite coating, characterized by the low overpotential for the HER, is employed as the cathode. However, regarding a high price of ruthenium compounds on the market, economic factors promote the tendency to replace the Ru-containing cathode with materials based on non-noble metals that show similar catalytic activity for the HER in alkaline solution as the commercial cathode.

In this lecture, the results of an investigation of the microstructure, chemical and phase composition and catalytic activity for the HER of Ni–MoO_2 composite coatings prepared by the simultaneous electrodeposition of Ni and MoO_2 were presented. The coatings were electrodeposited from suspensions composed of 0.2 mol dm^{-3} $NiCl_2$ + 2.0 mol dm^{-3} NH_4Cl solution (pH 3.6) and MoO_2 particles.[10] The average particle size of MoO_2 powder was determined to be 850 nm using the Scherrer formula.[10] The electrodeposition was performed in a test cell,[9] *i.e.*, a 20 dm^3 volume flow reactor, in which the suspension was circulating with a constant flow rate of 50 L min^{-1} and air bubbles were continually introduced at the bottom of the cell in order to prevent precipitation of the suspended MoO_2 particles and achieve their additional mixing. A Ni mesh 40 was used as the cathode substrate, while the anodes were two Ni plates. Dimensions of all three electrodes were 18 cm×22 cm. The catalytic activities of the obtained Ni–MoO_2 coatings were estimated by recording steady-state polarization curves for the HER in a 32 wt. % NaOH solution at 90 °C, and compared to the activity of the commercial DN electrode. The morphology, chemical and phase composition of the coatings were investigated by SEM, EDS and XRD analysis, respectively.

In order to establish the optimal conditions for the electrodeposition of Ni–MoO_2 coatings, preliminary experiments were conducted in a beaker cell (V = 0.5 dm^3) with much smaller electrodes (2 cm×3 cm).[10] The concentration of MoO_2 particles in the solution was varied in the range of 3–10 g dm^{-3}, whereas the deposition current density j_{dep} was varied from 50–1000 mA cm^{-2}. It was found that the coatings with larger content of Mo, electrodeposited from sus-

pensions with higher concentration of MoO_2 and at lower j_{dep}, exhibited the best catalytic activity for the HER, but were also characterized by the appearance of cracks and smaller and non-uniform thickness, implying a short service life under industrial conditions of exploitation. On the other hand, the coatings with a lower content of Mo, *i.e.*, a larger content of Ni, were thicker and had a developed surface area, but the overpotential for the HER was considerably larger. With respect to the catalytic activity for the HER, it appeared that for every applied j_{dep}, there is an optimal concentration of MoO_2 particles in the solution and *vice versa*.

Deposition of the coatings in the test cell was carried out at j_{dep} = –300 mA cm^{-2}, while the concentration of MoO_2 was varied in the range of 1 – 3 g dm^{-3}.[10] It was discovered that the morphology and composition of the Ni–MoO_2 coatings and, consequently, their activity for the HER, were crucially dependent on conditioning time of the deposition suspension. The coating electrodeposited from the suspension with 2 g dm^{-3} of MoO_2, conditioned for 1 h, was 2 μm thick and characterized by the presence of cracks and a uniform composition with 16 at. % Mo and 62 at. % O. The coating electrodeposited from the same suspension after 24 h conditioning had a thickness of about 40 μm and was composed of uniformly distributed Ni-rich (practically pure Ni) and MoO_2-rich (16 at. % Mo) parts, distinguishable from back-scatter electron micrographs of the cross section as the gray and white areas, respectively. The difference in the microstructure and composition of the two coatings was attributed to the sluggish occlusion of suspended MoO_2 particles by Ni^{2+} in the solution. The latter coating displayed a 60 mV lower overpotential for the HER at higher current densities compared to the former one.

The best polarization characteristics in 32 wt. % NaOH at 90 °C exhibited by the coating, deposited from a suspension with 3 g dm^{-3} of MoO_2 after 24 h conditioning.[10] At a current density of –300 mA cm^{-2}, the overpotential for the HER recorded on this sample was 15 mV lower in comparison to that of the commercial DN cathode. Its surface was found to be composed of two characteristic parts,[18] differing in composition and morphology. The Ni-rich parts (78. at. % Ni) consisted of agglomerates of ball-like grains of 2 μm in diameter, whereas the MoO_2-rich parts (76 at. % O) were characterized by the presence of mud-like cracks typical for electrodeposited Ni–Mo–O systems.[19,20] Cross section analysis of MoO_2-rich parts revealed that the cracks did not reach the Ni substrate, but extended only to the compact Ni-rich underlayer. Only two phases, Ni and MoO_2, were detected by XRD analysis, confirming that the MoO_2 particles were incorporated into the Ni matrix during the electrodeposition process. It was concluded that the coating prepared from the suspension containing 3 g dm^{-3} of MoO_2 after 24 h of aging represents the most promising candidate for replacement of the commercial DN cathode since it exhibits better polarization characteristics for the HER than the DN cathode and has a satisfactory microstructure.

The kinetics and mechanism of the HER on this coating were examined in an 8 mol dm^{-3} NaOH solution at 30 °C by means of steady-state polarization measurements and the electrochemical impedance spectroscopy (EIS).[18] The polarization curve was characterized by only one well-defined Tafel slope of b = –122 mV dec^{-1} in the overpotential range $|\eta| \geq 70$ mV. The impedance spectra recorded at four different overpotentials corresponding to the Tafel region consisted of two overlapped semicircles on the complex plane diagrams. The so-called 1CPE equivalent circuit[21,22] was successfully fitted to the impedance spectra, providing the values for the circuit parameters. Based on the theoretical model for the HER,[23,24] the polarization curve and the overpotential dependences of the circuit parameters were simultaneously simulated using the non-linear least squares method. The fitting procedure produced values of the rate constants of the three elementary steps of the HER. In the range of low overpotentials, $0 < |\eta| < 50$ mV, the rates of the Heyrovsky and Tafel steps were approximately the same, indicating that the reaction equally proceeds through both possible reaction pathways, the Volmer–Heyrovsky and the Volmer–Tafel. At $|\eta| > 150$ mV, the rate of the Tafel step was approaching the limiting value and the reaction dominantly proceeded through the Volmer–Heyrovsky reaction pathway, with the Heyrovsky step being the rate determining one.[18]

At the most negative overpotential studied by EIS, the roughness factor was calculated to be 125. In order to separate the contribution of surface roughness to the catalytic activity for the HER, the intrinsic activity of examined Ni-MoO_2 coating was determined and compared to the intrinsic activity of a flat polycrystalline Ni electrode reported in literature.[25,26] Considering that the intrinsic activity for the Ni–MoO_2 electrode was an order of magnitude higher in comparison with the one for a polycrystalline Ni, it was concluded that the synergetic effect on the catalytic activity for the HER in alkaline solution could be assigned to a Ni + MoO_2 combination.

Acknowledgements. The work presented in the lecture was financially supported by the Ministry of Education, Science and Technological Development of the Republic of Serbia through Project No. 172054. The author would also like to express his gratitude to the Department for Research and Development of the Industrie De Nora S.p.A. for providing the necessary equipment and chemicals.

И З В О Д

ЕЛЕКТРОХЕМИЈСКО ТАЛОЖЕЊЕ И КАРАКТЕРИЗАЦИЈА КОМПОЗИТНИХ Ni–MoO_2 ПРЕВЛАКА КАО КАТОДА ЗА РЕАКЦИЈУ ИЗДВАЈАЊА ВОДОНИКА У АЛКАЛНИМ РАСТВОРИМА

УРОШ Ч. ЛАЧЊЕВАЦ

Институт за мултидисциплинарна истраживања, Универзитет у Београду, Кнеза Вишеслава 1, 11030 Београд

Композитне Ni–MoO_2 превлаке су припремљене и окарактерисане са становишта њихове могуће примене као катализатора за реакцију издвајања водоника у алкалним растворима. Композити су електрохемијски исталожени на Ni мрежице из амонијум-хлоридног раствора никла са суспендованим MoO_2 честицама у симулираним индустријским условима за производњу комерцијалних катода. Утицај концентрације честица MoO_2 у раствору и густине струје таложења на морфологију и хемијски и фазни састав добијених превлака испитиван је методама скенирајуће електронске микроскопије, енергетски дисперзивне спектроскопије X-зрачења и рендгенске дифракције. Каталитичка активност превлака за издвајање водоника испитивана је поларизационим мерењима у 32 мас. % NaOH на 90 °C и упоређена са активношћу комерцијалне катоде (De Nora). Најактивнија Ni–MoO_2 превлака показује боље поларизационе карактеристике него комерцијална катода. Механизам издвајања водоника на наведеној Ni–MoO_2 превлаци у 8 mol dm^{-3} NaOH на 30 °C испитан је помоћу стационарних поларизационих мерења и методе спектроскопије електрохемијске импеданције. На основу теоријске интерпретације експерименталних података одређене су вредности константи брзина појединачних ступњева реакције и разјашњена природа каталитичке активности превлаке.

(Примљено 15 децембра 2012)

REFERENCES

1. T. F. O'Brien, T. V. Bommaraju, F. Hine, *Handbook of Chlor–Alkali Technology, Volume I: Fundamentals*, Springer Science + Business Media, Inc., New York, USA, 2005, pp. 37–47
2. I. Arul Raj, K. I. Vasu, *J. Appl. Electrochem.* **22** (1992) 471
3. L. B. Albertini, A. C. D. Angelo, E. R. Gonzalez, *J. Appl. Electrochem.* **22** (1992) 888
4. J. Divisek, H. Schmitz, B. Steffen, *Electrochim. Acta* **39** (1994) 1723
5. J. Fournier, H. Menard, L. Brossard, *J. Appl. Electrochem.* **25** (1995) 923
6. Th. Borucinsky, S. Rausch, H. Wendt, *J. Appl. Electrochem.* **27** (1997) 762
7. R. K. Shervedani, A. R. Madram, *Electrochim. Acta* **53** (2007) 426
8. A. L. Antozzi, C. Bargioni, L. Iacopetti, M. Musiani, L. Vasquez-Gomez, *Electrochim. Acta* **53** (2008) 7410
9. N. V. Krstajić, Lj. Gajić-Krstajić, U. Lačnjevac, B. M. Jović, S. Mora, V. D. Jović, *Int. J. Hydrogen Energy* **36** (2011) 6441
10. N. V. Krstajić, U. Lačnjevac, B. M. Jović, S. Mora, V. D. Jović, *Int. J. Hydrogen Energy* **36** (2011) 6450
11. U. Č. Lačnjevac, V. D. Jović, B. M. Jović, *Zaštita materijala* **52** (2011) 153
12. V. D. Jović, U. Lačnjevac, B. M. Jović, Lj. Karanović, N. V. Krstajić, *Int. J. Hydrogen Energy* **37** (2012) 17882
13. V. D. Jović, U. Lačnjevac, B. M. Jović, N. V. Krstajić, *Electrochim. Acta* **63** (2012) 124

14. B. M. Jović, U. Č. Lačnjevac, V. D. Jović, Lj. M. Gajić-Krstajić, N. V. Krstajić, *J. Serb. Chem. Soc.* **77** (2012) 211
15. V. D. Jović, U. Č. Lačnjevac, B. M. Jović, Lj. M. Gajić-Krstajić, N. V. Krstajić, *J. Serb. Chem. Soc.* (2012), doi: 10.2298/JSC120831112J.
16. G. Tasić, B. Jović, U. Lačnjevac, N. Krstajić, V. Jović, *J. Electrochem. Sci. Eng.* **3** (2013) 29
17. M. Wang, Z. Wang, Z. Guo, Z. Li, *Int. J. Hydrogen Energy* **36** (2011) 3305.
18. U. Č. Lačnjevac, B. M. Jović, V. D. Jović, N. V. Krstajić, *J. Electroanal. Chem.* **677**–**680** (2012) 31.
19. U. Lačnjevac, V. D. Jović, B. M. Jović, Z. Baščarević, M. G. Pavlović, *Zaštita materijala* **49** (2008) 41.
20. U. Lačnjevac, B. M. Jović, Z. Baščarević, V. M. Maksimović, V. D. Jović, *Electrochim. Acta* **54** (2009) 3115.
21. C. Hitz, A. Lasia, *J. Electroanal. Chem.* **500** (2001) 213.
22. L. Birry, A. Lasia, *J. Appl. Electrochem.* **34** (2004) 735.
23. R. D. Armstrong, M. Henderson, *J. Electroanal. Chem.* **39** (1972) 81.
24. D. A. Harrington, B. E. Conway, *Electrochim. Acta* **32** (1987) 1703.
25. A. Lasia, A. Rami, *J. Electroanal. Chem.* **294** (1990) 123.
26. N. V. Krstajić, M. Popović, B. Grgur, M. Vojnović, D. Šepa, *J. Electroanal. Chem.* **512** (2001) 16.

Journal of the Serbian Chemical Society
JSCS-info@shd.org.rs • www.shd.org.rs/JSCS
J. Serb. Chem. Soc. 78 (4) 555–564 (2013)
JSCS–4438
UDC 637.12+520.8.07+546.226+547.867.2:543.4/.5
Original scientific paper

Genetic algorithm-based wavelength selection in multicomponent spectrophotometric determinations by partial least square regression: application to a sulfamethoxazole and trimethoprim mixture in bovine milk

MOHAMMAD HADI GIVIANRAD*, MOHAMMAD SABER-TEHRANI and SABER ZARIN

Department of Chemistry, Science and Research Branch, Islamic Azad University, Tehran, Iran

(Received 3 March, revised 26 May 2012)

Abstract: The simultaneous determination of sulfamethoxazole (SMX) and trimethoprim (TMP) mixtures in bovine milk by spectrophotometric method is, due to spectral interferences, a difficult problem in analytical chemistry. By means of multivariate calibration methods, such as partial least square (PLS) regression, it is possible to obtain a model adjusted to the concentration values of the mixtures used in the calibration range. A genetic algorithm (GA) is a suitable method for selecting the wavelengths for PLS calibration of mixtures with almost identical spectra without the loss of prediction capacity using a spectrophotometric method. In this study, a calibration model based on the absorption spectra in the 200–400 nm range for 25 different mixtures of SMX and TMP. Calibration matrices were formed from samples containing 0.25–20 and 0.3–21 μg mL^{-1} for SMX and TMP, at pH 10, respectively. The root mean squared error of deviation *(*RMSED*)* for SMX and TMP with PLS and genetic algorithm partial least square (GAPLS) were 0.242 and 0.066 μg mL^{-1}, and 0.074 and 0.027 μg mL^{-1}, respectively. This procedure allowed the simultaneous determination of SMX and TMP in synthetic and real samples and good reliability of the determination was proved.

Keywords: sulfamethoxazole; trimethoprim; partial least square; simultaneous determination; bovine milk.

INTRODUCTION

Sulfamethoxazole, 4-amino-*N*-(5-methylisoxazol-3-yl)-benzenesulfonamide, (SMX) is a sulfonamide antibiotic that is a highly effective chemotherapeutic agent, which competitively inhibits the bacterial enzyme dihydropteroate synthetase.[1,2] Trimethoprim, 5-(3,4,5-trimethoxybenzyl)pyrimidine-2,4-diamine,

* Corresponding author. E-mail: givianradh@yahoo.com
doi: 10.2298/JSC120303080G

(TMP), is one of the most widely used antibacterial additive. In addition, TMP is a dihydrofolat-reductase inhibitor.[3] A combination of TMP/SMX is an effective antimicrobial agent that is commonly used in dairy cattle for the treatment or prevention of respiratory infections and mastitis.[4] The use of this combination may lead to the presence of residual levels in milk and meat. Residues of this combination can cause several risks for human health, such as allergic reaction in hypersensitive individuals and induction of resistance of strains of pathogenic bacteria. Various methods have been published for the determination of SMX and TMP in milk and biological fluids.[5–14] Most of these methods employ separation methods, such as online solid phase extraction–liquid chromatography with UV (SPE-LC–UV) and mass spectrometry detection (SPE-LC–MS/MS),[3] a HPLC method using an on-line clean-up column coupled with amperometric detection employing a boron-doped diamond (BDD),[4] or micellar electrokinetic capillary chromatography.[6] The majorities of these methods are expensive and time consuming. Besides these methods, UV–Vis spectrophotometry could be considered a rapid method. Moreover, a flow-through optosensor combined with photochemically induced fluorescence was used for the simultaneous determination of binary mixtures of sulfonamides in pharmaceuticals, milk and urine.[15] However, spectrophotometric methods are sensitive and a hand scanner is inexpensive, available in most work offices and is easy to operate by non-skilled users. The simultaneous determination of SMX and TMP in milk by this method could be a difficult task, because their absorption spectrums overlap in this region and superimposed curves are not suitable for quantitative evaluation. Hence, multivariate calibration methods are playing an important role in the multicomponent analysis of mixtures SMX/TMP by UV–Vis spectrophotometry.[8]

In the present study, a multivariate calibration method, *i.e.*, partial least square (PLS) regression, was applied to the simultaneous spectrophotometric determination of SMX and TMP in milk. The major advantage of multi-component analysis using PLS are speed and expense. A genetic algorithm (GA) is a very useful technique with variable selection problems, because the relationship between the presence/absence of the variables in a calibration model and the prediction ability of the model, specifically for PLS models, is very complex and the mathematical properties are unknown.

EXPERIMENTAL

Apparatus and software

The spectra were obtained with an Agilent UV–Vis spectrophotometer, PerkinElmer (Lambda 25) in the wavelength range of 200 to 400 nm. A 1-cm path length quartz cell was used. The spectra were blank-corrected. The pH values of the solutions were measured with a Metrohm, model 827 instrument, using a combined glass electrode. All the absorbance spectra were digitized and stored at wavelengths from 200 to 350 nm in steps of 1 nm and transferred (in ASCII format) to a Pentium IV computer with Windows XP operating system. Data

processing (GAPLS) was performed by a laboratory-written program in MATLAB, version 7.8.0 (R2009a).

PLS and GA

The application of quantitative chemometrics methods, particularly partial least squares (PLS), to multivariate chemical data is becoming more widespread, owing to the availability of digitized spectroscopic data and commercial software for laboratory computers. The advantage of multicomponent analysis along with the partial least squares method in mixtures is the demonstration of fast separation steps. The theory and application of partial least squares (PLS) in spectrometry were previously discussed by several workers.[16,17] Genetic algorithm (GA) is a very useful technique in variable selection problems, because of the relationship between the presence/absence of the variables in the calibration model and the prediction ability of the model. The algorithm used in this paper is an evolution of the algorithm described in the literature,[18] the parameters of which are tabulated in Table I.

TABLE I. Parameters of the genetic algorithms

Parameter	Value
Population size	30 Chromosomes; on average, 5 variables per chromosome in the original population
Regression method	PLS
Response	Cross-validated percent explained variance (5 deletion groups; the number of components is determined by cross-validation)
Maximum number of variables selected in the same chromosome	30
Probability of mutation	1 %
Probability of cross-over	50 %
Maximum number of components	Determined by cross-validation on the model containing all the variables (not more than 15)
Number of runs	100, backward elimination after every 100th evaluation and at the end (if the number of evaluation is not a multiple of 100)
Window size for smoothing	3

Reagents and solutions

All experiments were performed with analytical grade reagents and used directly without further purification. Methanol was obtained from Merck. Doubly distilled deionized water was used to prepare the reagent solutions. The pharmaceutical substances (SMX and TMP) were of analytical grade and were obtained from Sigma. The stock solutions (50 ppm) of SMX and TMP were prepared by dissolving the sample powders in NaOH 0.001 M and deionized water, respectively. Universal buffer solutions (pH 2–12) were prepared by mixing 50 mM phosphoric acid, 50 mM boric acid, 50 mM acetic acid and a sufficient amount of CO_2-free NaOH solution.

One-component calibration

For each component, the linear dynamic concentration range was found by one-component calibration. For the preparation of each solution, different volumes of SMX and TMP stock solutions (50 μg mL^{-1}) were added to 2 ml universal buffer (pH 10) in a 10 ml volu-

metric flask and then diluted to the mark with deionized water. The concentration ranges of SMX and TMP for the construction of the calibration graphs were 5–40 μg mL^{-1}. The absorbance spectra were achieved over the 200–400 nm spectral range *vs.* the solvent blank. The linear dynamic range for SMX (0.25–20 μg mL^{-1}) and TMP (0.3–21 μg mL^{-1}) was determined by regression of the absorbance at the corresponding λ_{max} *vs.* concentration.

Binary standard solution

Two set of solutions (calibration and prediction sets) were prepared (Table II). The calibration set contained 25 standard mixtures, and 6 mixtures were used as the validation set. Concentrations of SMX and TMP in the standard mixtures were 1–15 μg mL^{-1} and 0.2–8.0 μg mL^{-1}, respectively. For preparation of each solution, the required volumes of stock solution and 2 mL universal buffer were added to 10 mL volumetric flask and diluted to the mark with 0.001 M NaOH. Then absorbance spectra of the mixture were recorded *vs.* the blank solvent in the wavelength range of 200–400 nm (at 1.0 nm intervals).

TABLE II. Concentration data of the different mixtures used in the calibration (M1–M25) and the prediction (M26–M31) set for the determination of SMX and TMP

Mixture	SMX[a]	TMP[b]	Mixture	SMX	TMP	Mixture	SMX	TMP
M1	1.0	0.2	M14	8.0	6.0	M27	5.0	1.0
M2	1.0	1.6	M15	8.0	8.0	M28	6.0	1.6
M3	1.0	3.0	M16	11.0	0.2	M29	8.0	5.0
M4	1.0	6.0	M17	11.0	1.6	M30	10.0	6.0
M5	1.0	8.0	M18	11.0	3.0	M31	15.0	2.4
M6	5.0	0.2	M19	11.0	6.0			
M7	5.0	1.6	M20	11.0	8.0			
M8	5.0	3.0	M21	15.0	0.2			
M9	5.0	6.0	M22	15.0	1.6			
M10	5.0	8.0	M23	15.0	3.0			
M11	8.0	0.2	M24	15.0	6.0			
M12	8.0	1.6	M25	15.0	8.0			
M13	8.0	3.0	M26	4.0	0.8			

[a]Concentrations of sulfamethoxazole in μg mL^{-1}; [b]concentrations of trimethoprim in μg mL^{-1}

Preparation of real samples

In this study, milk was selected as a real sample. In order to determine concentration of SMX and TMP in milk, an extraction method was applied. In this case, the binary standard solutions were prepared in skimmed milk. The milk samples were filtered through a filter paper to remove solid particles. Then 10 ml of filtered milk and 15 g of anhydrous sodium sulfate were transferred into a 50 mL polypropylene centrifuge tube, blended with 15 ml of ethyl acetate for 1 min using a high-speed blender, and then centrifuged for 2 min at 3000 rpm. The organic phase was collected into clean centrifuge tubes, and the same amount of organic phase was added to the remainder of the sample in the centrifuge tubes and the extraction process was repeated. The combined extracts were evaporated to dryness under reduced pressure at 40 °C. The residue was dissolved in 2 ml of 0.001M NaOH and used for spectrophotometric analysis. An average extraction recovery in the range of 92–98 % was achieved using this developed method. The blank sample was prepared in the same method as for the analytes except that no analyte was added to the milk.

RESULTS AND DISCUSSION

The absorbance spectra of 15 mg L^{-1} SMX and TMP under certain experimental condition were recorded.[8] It could be inferred that the spectra of SMX and TMP were highly overlapped. Therefore, these compounds cannot be determined in presence of each other and it is necessary to use a chemometrics method to solve this problem. This problem alleviated by use of multivariate calibration methods.

Effect of pH

The influence of the medium pH on the absorption spectra of the two compounds was studied over the range of 2 to 10. The optimum pH (pH 10) was selected at which value the minimum overlap between two species, higher selectivity and maximum sensitivity were evidenced as mentioned previously.[8]

Variable selection

In this work, the calibration set had 121 variables. GA was run for these 121 variables (in the 200–320 nm range), using a PLS regression method. The maximum number of factors which, determined by cross-validation on the model consisted of all the variables. To find optimum the wavelength set for the determination of SMX and TMP, the GA procedure was repeated 10 times. Finally, a wavelength was selected if the percent of selection for that variable exceeded a critical value. The wavelengths selected by GA were 277, 239, 240, 241, 242, 217, 216 and 215 nm for SMX and 238, 237, 236, 235, 234, 256, 255 and 312 nm. Selected variables were used for PLS modeling.

Data processing and PLS modeling

PLS and GAPLS regression was run on the calibration data, and the concentrations of the analytes were predicted at the optimum number of factors. The selection of the number of factors in factor analysis-based methods is very important for achieving the best prediction. The model refinement procedure used the predicted residual errors sum of squares (PRESS) of the leave-one-out cross-validation to select the optimal number of PLS factors. In the case of each number of factors used, given 25 calibration standards, n–1 solutions were used in the model-building step (calibration) and the resulting model was used to predict the concentration of the desired analyte in the solution. This procedure was repeated n times until the concentrations of the analyte in all solutions were predicted. When each number of factors was entered, *PRESS* was calculated by comparing the predicted concentration of compounds in each sample with a known concentration of compounds in the standard solutions, (Eq. (1)):

$$PRESS = \left[\sum_{i=1}^{N} \left(\hat{c}_i - c_j \right) \right]^2 \quad (1)$$

where N is the total number of calibration samples; c_j the reference concentration for the j^{th} sample; $\hat{c}_i$ represents the estimated concentration. The GAPLS and PLS *PRESS* values are minimum in a number of factors for TMP and SMX, respectively. Then these numbers of factors were selected as the optimum for the calibration models (Figs. 1 and 2).

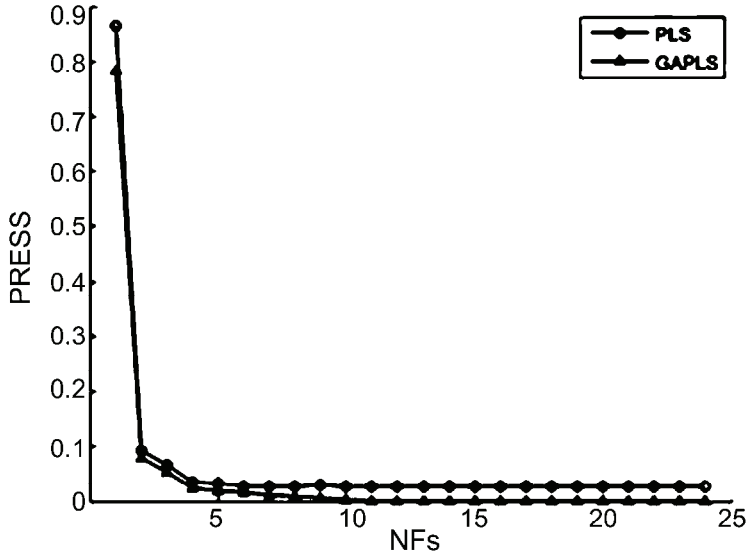

Fig. 1. Plots of *PRESS vs.* number of factors (NFs) by PLS and GAPLS for SMX.

Statistical parameters

For the constructed models, two parameters were selected to evaluate the prediction ability of the models for the simultaneous determination of TMP and SMX, *i.e.*, the root mean square error of deviation *(RMSED)* (Eq. (2)) and the relative error of prediction *(REP)* (Eq. (3)), calculated for each component as follows:

$$RMSED = \sqrt[2]{\frac{\sum_{i=1}^{n} \left(\hat{c}_i - c_i \right)^2}{n}} \quad (2)$$

$$REP(\%) = \frac{100}{\bar{c}} \sqrt[2]{\frac{1}{n} \sum_{i=1}^{n} (\hat{c}_i - c_i)^2} \quad (3)$$

where c_i is the true analyte concentration in the sample i, $\hat{c}_i$ represents the estimated analyte concentration in the sample i, $\overline{c}$ is the mean of the true concentration in the prediction set and n is the total number of samples used in the prediction set.

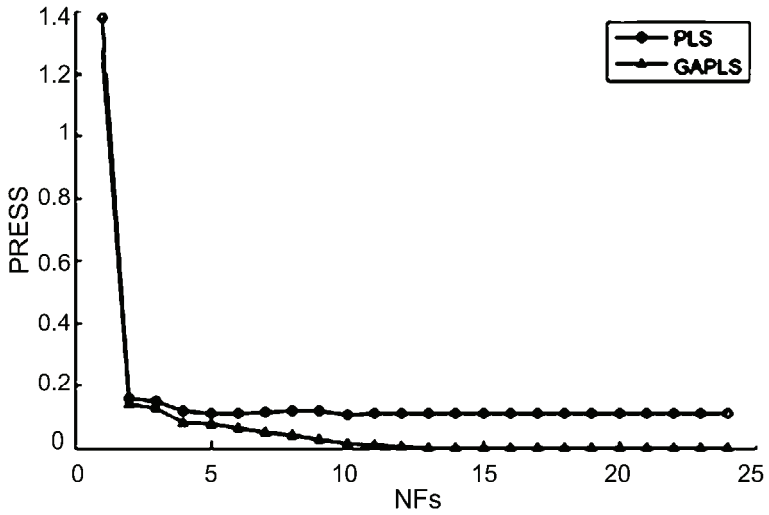

Fig. 2. Plots of *PRESS vs.* number of factors (NFs) by PLS and GAPLS for TMP.

Determination of SMX and TMP in the test set mixtures

The PLS and GAPLS methods were applied to the spectrophotometric concurrent monitoring of SMX and TMP. The predictive abilities of the methods were determined using 6 test mixtures (Tables III and IV). It can be seen that the values of *PRESS*, *RMSED* and *REP* (%) for the GAPLS method were lower than those for the PLS method.

TABLE III. Prediction results for SMX in the synthetic samples using the PLS and GAPLS methods

Sample	PLS[a]			GAPLS[b]	
	Added[c]	Predicted[c]	Recovery, %	Predicted	Recovery, %
1	4.00	3.88	97.00	3.98	99.50
2	5.00	5.35	107.00	5.11	102.20
3	6.00	6.15	102.50	6.03	100.50
4	8.00	8.19	102.37	7.90	98.75
5	10.00	10.39	103.90	9.98	99.80
6	15.00	14.94	99.60	15.05	100.33
RMSED[d]	–	0.242	–	0.066	–
REP[e] / %	–	3.023	–	0.829	–

[a]Partial least square regression; [b]genetic algorithm partial least square; [c]concentrations of sulfamethoxazole in μg mL^{-1}; [d]root mean squared error of deviation in μg mL^{-1}; [e]relative error of prediction

TABLE IV. Prediction results for TMP in the synthetic samples using the PLS and GAPLS methods

Sample	PLS[a]			GAPLS[b]	
	Added[c]	Predicted[c]	Recovery, %	Predicted	Recovery, %
1	0.80	0.74	92.50	0.81	101.25
2	1.00	1.03	103.00	1.01	101.00
3	1.60	1.51	94.37	1.59	99.37
4	5.00	5.03	100.60	4.98	99.6
5	6.00	6.13	102.16	6.06	101.00
6	2.40	2.35	97.91	2.39	99.58
RMSED[d]	–	0.074	–	0.027	–
REP[e] / %	–	2.648	–	0.964	–

[a]Partial least square regression; [b]genetic algorithm partial least square; [c]concentrations of trimethoprim in μg mL^{-1}; [d]root mean squared error of deviation in μg mL^{-1}; [e]relative error of prediction

Determination of SMX and TMP in bovine milk samples

The real samples in this study were bovine milk from the Kadkhoda dairy, Iran. Three spiking levels (3, 6 and 10 μg mL^{-1} for SMX, and 3, 5 and 8 μg mL^{-1} for TMP) in bovine milk samples were determined, based on the GAPLS and PLS methods. Accordingly, the accuracy of the GAPLS method was recognized as being better than that of the PLS method. Each measurement was repeated 6 times and the obtained mean recovery values are tabulated in Table V (found values calculated based on $\bar{X} \pm (tS.D.)/\sqrt{N}$, for N = 6 measurements and $t_{(N-1=5)}$ = = 2.571). The obtained values for the recovery rate varied between 98 and 108 % and the obtained values for the *RSD* ranged from 1.2 to 5.5 %. It could be observed that for all mixtures, the calculated values were in satisfactory agreement with those of the declared values. Consequently, the performance characteristics are recognized as acceptable and therefore the method is considered suitable for the intended purpose.

TABLE V. Recovery yields and relative standard deviations at different spiking levels in bovine milk samples

Sample	PLS[a]			GAPLS[b]	
	Spiking level[c]	Recovery, %	*RSD*[d] / %	Recovery, %	*RSD*[d] / %
SMX[e]	3.00	108.10	4.10	101.90	3.50
	6.00	100.40	3.80	99.60	1.20
	10.00	97.50	2.50	98.20	1.60
TMP[f]	3.00	84.40	4.80	108.40	4.70
	5.00	101.10	5.90	100.70	5.50
	8.00	105.40	4.80	101.80	3.90

[a]Partial least square regression; [b]genetic algorithm partial least square; [c] different spiking levels in bovine milk samples in μg mL^{-1}; [d]relative standard deviation; [e]sulfamethoxazole; [f]trimethoprim

CONCLUSIONS

This was the first spectrophotometric determination study that was accomplished on bovine milk in this manner. For overcoming the high spectral overlap observed between the absorption spectra, PLS was successfully applied to the absorption spectra for the concurrent analysis of SMX and TMP in their synthetic mixtures. In addition, the present study showed that GA could be regarded as a good method for feature selection in the spectral data sets. The proposed techniques are precise, inexpensive, simple to perform and do not require separation steps. The resulting data for the TMP and SMX mixture data set demonstrated that the predictive ability of the models, obtained with the wavelengths selected by the algorithm, was frequently enhanced. The good agreement between the obtained and spiked results demonstrated the utility of this procedure for the simultaneous detection of SMX and TMP in complex synthetic and bovine milk samples without tedious pretreatment. The superiority of the developed GAPLS method, which included the application of a chemometric method to milk samples and biological fluid samples, as well as the selection of wavelength by the GA method, over other official methods was demonstrated. In addition, it is very simple and accurate.

Acknowledgement. The authors are so grateful to the Laboratory Complex of I.A.U. for valuable technical assistance.

И З В О Д

ИЗБОР ТАЛАСНИХ ДУЖИНА БАЗИРАН НА ГЕНЕТИЧКОМ АЛГОРИТМУ У ВИШЕКОМПОНЕНТНОМ ОДРЕЂИВАЊУ МЕТОДОМ НАЈМАЊИХ КВАДРАТА: ПРИМЕНА НА СМЕШИ СУЛФАМЕТОКСАЗОЛА И ТРИМЕТОПРИМА У МЛЕКУ ГОВЕДА

MOHAMMAD HADI GIVIANRAD, MOHAMMAD SABER-TEHRANI И SABER ZARIN

Department of Chemistry, Science and Research Branch, Islamic Azad University, Tehran, Iran

Истовремено одређивање сулфаметоксазола и триметоприма у смеши, у бивољем млеку, сектрофотометријском методом представља велики проблем у аналитичкој хемији због спектралних сметњи. Коришћењем мултивариантне калибрационе методе, као што је парцијална регресија најмањих квадрата (PLS), могуће је добити модел прилагођен концентрацијама у смеши, коришћеним у калибрационом опсегу. Генетички алгоритам (GA) је погодна метода за селектовање таласних дужина за PLS калибрацију смеша са скоро идентичним спектрима, без губитка капацитета предвиђања, при коришћењу спектрофотометријске методе. У овом раду је калибрациони модел базиран на апсорпционом спектру у опсегу 200–400 nm за 25 различитих смеша сулфаметоксазола и триметоприма range. Калибрационе матрице су формиране за узорке који садрже 0,25–20 и 0,3–21 μg mL^{-1} сулфаметоксазола и триметоприма на pH 10. Вредности *RMSED* за сулфаметоксазол и триметоприм, базиране на PLS и GAPLS, износиле су 0,242 и 0,066 μg mL^{-1}, и 0,074 и 0,027 μg mL^{-1}. Ова процедура омогућава истовремено одређивање сулфаметоксазола и триметоприма у синтетичким и реалним узорцима и потврђена је доба поузданост методе.

(Примљено 3. марта, ревидирано 26 маја 2012)

REFERENCES

1. G. L. Mandel, W. A. Petri, *Goodman and Gilman's the Pharmacological Basis of Therapeutics*, 11th ed, McGraw Hill, New York, USA, 2006, p. 1057
2. AOAC, method 993.32, *Multiple sulfonamide residues in raw bovine milk, Handbook of analytical methods of analysis*, 16th ed., V. A. Arlington, USA, 1995, p. 13
3. L. S. Andrade , M. C. de Moraes, R. C. Rocha-Filho, O. Fatibello-Filho, Q. B. Cass, *Anal. Chim. Acta* **654** (2009) 127
4. D. C. G. Bedor, T. M. Gonçalves, M. L. L. Ferreira, C. E. M. de Sousa, A. L. Menezes, E. J. Oliveira, D. P. de Santana, *J. Chromatogr., B* **863** (2008) 46
5. S. E. Hismiogullar, E. Yarsan, *Hacet. Univ. J. Fac. Pharm.* **29** (2009) 95
6. R. Injac, J. Kac, K. Ovic-Rajic, B. Strukelj, *J. Food Drug Anal*. **16** (2008) 18
7. M. L. Fernández de Córdova, P. Ortega Barrales, G. Rodríguez Torné, A. Molina Díaz, *J. Pharm. Biomed. Anal*. **31** (2003) 669
8. M. H. Givianrad, M. Saber-Tehrani, P. Abroomand Azar, M. Mohagheghian, *Spectrochim. Acta* **78** (2011) 1196
9. V. Srivatsan, A. K. Dasgupta, P. Kale, R. R. Datla, D. Soni, M. Patel, R. Patel, C. Mavadhiya, *J. Pharm. Biomed. Anal.* **1031** (2007) 307
10. M. Goodarzi, P. Shahbazikhah, M. R. Sohrabi, M. Fathabadi, A. Hassannouri, *J. Chil. Chem. Soc.* **54** (2009) 309
11. F. E. Silva, M. F. Ferrao, G. Parisotto, E. I. Müller, E. M. Flores, *J. Pharm. Biomed. Anal.* **49** (2009) 800
12. Y. Wen, M. Zhang, Q. Zhao, Y. Q. Feng, *J. Agric. Food Chem.* **53** (2005) 8468
13. H. Amini, A. Ahmadiani, *J. Pharm. Biomed. Anal*. **43** (2007) 1146
14. F. C. C. R. de Paula, A. C. de Pietro, Q. B. Cass, *J. Chromatogr., A* **1189** (2008) 221
15. J. L. Flores, M. L. F. de Cordova, A. M. Diaz, *Anal. Chim. Acta* **600** (2007) 164
16. S. Wold, M. Sjostrom, L. Eriksson, *Chemometr. Intell. Lab*. **58** (2001) 109
17. R. G. Brereton, *Analyst* **125** (2000) 2125
18. R. Leardi, A. L. Gonzalez, *Chemometr. Intell. Lab.* **41** (1998) 195.

Journal of the Serbian Chemical Society
JSCS-info@shd.org.rs • www.shd.org.rs/JSCS
J. Serb. Chem. Soc. 78 (4) 565–577 (2013)
JSCS–4439
UDC 669.214:54.064:543.4:669.015.5
Original scientific paper

Determination of trace elements in refined gold samples by inductively coupled plasma atomic emission spectrometry

MIRJANA STEHARNIK[1], MARIJA TODOROVIĆ[2], DRAGAN MANOJLOVIĆ[2#], DALIBOR STANKOVIĆ[2#], JELENA MUTIĆ[2*] and VLASTIMIR TRUJIĆ[1]

[1]*Mining and Metallurgy Institute Bor, Department of Chemical Investigations, 19210 Bor, Serbia and* [2]*Faculty of Chemistry, University of Belgrade, Studentski trg 12–16, 11000 Belgrade, Serbia*

(Received 5 May, revised 24 September 2012)

Abstract: This paper presents a method for the determination of trace contents of silver, copper, iron, palladium, zinc and platinum in refined gold samples. A simultaneous inductively coupled plasma atomic emission spectrometer in the radial torch position and with a cross flow nebulizer was used for the determinations. In order to compare the different calibration strategies, two sets of calibration standards were prepared. The first set was based on matrix matched calibration standards and the second was prepared without the addition of matrix material. The detection limits for the matrix-matched calibrations were higher for some elements than those without matrix matching. In addition, the internal standardization method was applied and experiments indicated that indium was the best option as the internal standard. The obtained results for gold samples with matrix matched and matrix free calibrations were compared with the results obtained by the standard addition method. The accuracy of the methods was tested by performing a recovery test. The recoveries for the spiked sample were in the range of 90–115 %. The accuracy of the methods was also tested by analysis of a certified reference material of high purity gold AuGHP1. The best results were achieved by matrix free calibration and standard addition method using indium as the internal standard at a wavelength of 230 nm.

Keywords: refined gold samples; trace elements; ICP-AES; certified reference material of high purity gold AuGHP1.

INTRODUCTION

Gold, one of the most important precious metals, is widely used in different fields of science, mostly in microelectronic and medicine. During the last few years, gold has found extensive application in diagnostics and therapy of diffe-

* Corresponding author. E-mail: jmutic@chem.bg.ac.rs
# Serbian Chemical Society member.
doi: 10.2298/JSC120505135S

rent types of cancer. The application of gold mostly depends on its purity. The presence of trace impurities could significantly affect its physical and chemical properties. Therefore, it is very important to find a rapid and accurate technique for the determination of trace elements in refined gold samples. In the Mining and Metallurgy Institute Bor, high purity gold is produced from different materials, mostly from anode slime and electrical waste by a long process of purification and finally by reduction of gold with SO_2 gas or by electrolytic separation of gold. The American Society for Testing and Materials established the maximum allowed concentrations of some elements in 99.99 % purity gold (ASTM B562-95) standard,[1] as shown in Table I.

TABLE I. Maximum allowed concentrations of the investigated elements according to the requirements ASTM B562-95 standard1 for 99.99 % purity gold

Element	Concentration, mg kg^{-1}
Ag	90
Cu	50
Pd	50
Fe	20

A detailed study of the literature revealed that there are not many published papers that present results for the determination of trace elements in pure gold. The determination of major constituents in precious metals is mostly realized by fire assay and trace elements are determined using different spectrometric methods. During the 1960s and 1970s, the determination of trace elements in pure gold was performed by the emission spectrographic technique with different excitation sources, such as arc and glow discharge lamp.[2,3] Atomic absorption spectrophotometry with a graphite furnace (ETAAS) or flame (FAAS) was used for the determinations of some elements in pure gold during 1990s.[4–11] In the last few years, inductively coupled plasma atomic emission spectrometry (ICP--AES)[12,13] and especially inductively coupled plasma mass spectrometry (ICP--MS)[14–21] and laser ablation inductively coupled plasma mass spectrometry (laser ablation-ICP-MS)[22] have been extensively applied. Electrochemical techniques were also used for the determination of some trace elements in pure gold, in particular, stripping voltammetry was used for the determination of arsenic(III) and silver.[23,24] Trace elements in gold and its alloys samples were determined by synchrotron radiation X-ray fluorescence spectrometry (SR-XRF)[25,26] and energy dispersive X-ray spectrometry (EDXRF).[27]

In order to improve the sensitivity and to reduce matrix effects, many researchers used a combination of different pre-concentration methods or matrix separation with instrumental analysis, mostly by FAAS, ETAAS, AES-ICP or ICP-MS for the determination of trace elements in pure materials. Procedures that involve separation steps for the complete removal of the matrix are often

tedious and complicated, thereby increasing the risk of contamination with the resulting worsening of the detection limits. On the other hand, the direct determination of trace elements has some advantages, such as minimizing sample preparation, reducing the potential risk of sample contamination, simplicity of use and rapidity.

In this paper, a direct determination of silver, copper, iron, palladium, zinc and platinum in refined gold samples was realized by application of simultaneous inductively coupled plasma atomic emission spectrometry.

EXPERIMENTAL

Apparatus

All measurements were performed using a Spectro Ciros Vision simultaneous inductively coupled plasma atomic emission spectrometer (Germany) and controlled by Smart Analyser Vision software. This device is provided with a radial torch position and a cross flow nebulizer, a double grating spectrometer with 22 linear CCDs as detectors situated on a Rowland circle, allowing a spectral range of 125–770 nm. The energy for the plasma was obtained by a free-running 27.12 MHz generator.

In the present investigations, the most sensitive and recommended wavelengths[28] of the analyzed elements were selected as much as possible free from spectral interferences from the gold matrix and other elements present in the samples (Table II). Emission peaks of analytes were symmetrical and well resolved from the gold peaks. The appropriate spline or polynomial corrections were applied for subtraction of background intensities from the analytical line of calibration standards and unknown samples.

TABLE II. Wavelengths used for the determination of the trace elements in refined gold

Element	Wavelength, nm
Ag	328.068
Cu	324.754
Pd	340.458
Fe	259.941
Pt	214.423
Zn	213.856

Preparation of calibration standard solutions

All chemicals and acids were of analytical grade. Calibration solutions of the elements Ag, Cu, Pd, Fe, Pt and Zn were prepared. They were prepared from the corresponding 1 g L^{-1} stock solutions (Accu Standards, USA). Ultra pure deionized water was used for the dilution and preparation of the calibration standards at the desired concentration.

Two sets of calibration standards were prepared, *i.e.*, matrix-matched with and without internal standard and aqueous calibration standards also with and without internal standard. Fresh calibration standards were prepared before each analysis. This procedure was applied to reduce the possibility of precipitation the analyte elements that could occur if the diluted solutions were kept for some time.

Matrix-matched calibration standards were prepared so that all the calibration standards had the same concentration of matrix as the unknown samples. To this aim, 0.1000 g of pure gold powder, obtained from the laboratory of the Mining and Metallurgy Institute Bor, was

weighed and dissolved in 8 mL *aqua regia*. After complete dissolution, the gold solution was cooled and quantitatively transferred into a 10 mL volumetric flask. Then 1 mL of a solution containing all the mentioned trace elements at a concentration of 10 mg L^{-1} was added and diluted with ultra pure deionized water to the final volume (10 mL); hence, the individual concentration of each element was 1 mg L^{-1}. This procedure was repeated for lower concentrations of the calibration samples. Indium was used as the internal standard at a concentration of 1 mg L^{-1}.

The concentration of the elements both with the internal standard and with standard additions were calculated according to Skoog.[29]

In order to compare the obtained results by different calibration strategies and to conclude which is the best, different sets of calibration standard solutions were made. All six strategies are present in Table III.

TABLE III. Name of the analytical program, type of calibration standard and wavelength of the internal standard

Analytical program name	Type of calibration standard	Internal standard, nm
Au–H_2O	Matrix free	None
Au–Au	Matrix matching	None
Au–In230–H_2O	Matrix free	In II 230.606
Au–In230	Matrix matching	In II 230.606
Au–In325–H_2O	Matrix free	In I 325.609
Au–In325	Matrix matching	In I 325.609

Preparation of the samples and the certified reference material

Refined gold samples of unknown composition were weighed (0.5000 g) and dissolved in 40 mL *aqua regia*. After complete dissolution, the gold solutions were cooled, quantitatively transferred into 50 mL volumetric flasks. Indium was added as the internal standard in a concentration of 1 mg L^{-1}.

The certified reference material of high pure gold AuGHP1 (Order No. IA/7075/10, Rand Refinery Ltd., South Africa) was prepared in the same manner.

For the standard addition method, the gold samples and certified reference material were prepared as follows: after weighing (0.5000 g), they were dissolved in 40 mL *aqua regia*. After complete dissolution, the gold solutions were evaporated to a smaller volume, cooled, and quantitatively transferred into 25 mL volumetric flasks. Three aliquots of gold solution of 5 ml were transferred into 10 mL volumetric flasks. The first was diluted to the final volume with ultra pure deionized water. The appropriate volumes of standard solution from 10 mg L^{-1} of analyzed elements were added to the second and third volumetric flask. Indium was added as the internal standard to all prepared solutions. The final concentration of indium was 1 mg L^{-1}.

RESULTS AND DISCUSSION

It is a well-known fact that a matrix element can change the intensities of the analytical lines of impurity elements in different matrix materials. A matrix element modifies almost all steps the sample undergoes, from its introduction into the system to light emission. Easily and non-easily ionized elements are responsible for changes in the analytical signals because they modify the state in which the analyte is introduced into the plasma, the plasma thermal characteristics, the

excitation efficiency of an analyte and the spatial distribution of the emitting species.[30–32]

Matrix effects can be reduced using robust operating conditions that lead to efficient energy transfer between the plasma and sample.[33,34] The ideal robust conditions would result in the absence of variation in the signal intensities of analytes for any change in the matrix or reagent composition.[35] Under robust conditions, an increase in the matrix concentration or acid leads to signal depression for ionic lines. Usually, this depression is similar for every line, regardless of the ionization energy and the line excitation energy. The use of robust conditions results in a flat response for all elements, contrary to non-robust conditions when the response is element dependent.[36] Under non-robust conditions, the plasma is more sensitive to any small change in the forward power or the amount of aerosol delivered to the plasma. Therefore, non-robust conditions should be avoided for analytical application; they can be useful to enhance the matrix effects.[37–40]

The most effective way to eliminate matrix effects is the separation of the matrix element but this is not practical in daily work, as it is time consuming and demands working with ultra pure chemicals in order to avoid contamination of the samples. Direct analysis has the advantages of minimizing the sample preparation procedure and reducing the potential risk of sample contamination. Thus, the possibility for direct determination of trace elements in pure gold was investigated with and without matrix matching and with internal standardization methods. Such results were compared with those obtained by the standard addition method.

Choice of the internal standard

In order to apply the internal standardization method, some potential internal standard elements were investigated. Preliminary experiments indicated that most of the commonly investigated elements (Sc, Mo, Y, Ge, Sr, V and Zr) had significant spectral overlap with some of the sensitive analytical lines of the analyzed elements. However, as indium did not show spectral interferences with the analyzed elements, it was employed as the internal standard in further experiments. The most sensitive wavelengths of indium, *i.e.*, 230 nm and 325 nm, were tested as the internal standard. Internal standardization is effective if the characteristics of the internal standard and analyte elements are similar in the plasma and they strongly depend on the operating conditions.[41–43]

Selection of the optimal experimental parameters

The optimal experimental parameters for all analyzed elements and internal standard were obtained by pumping a working solution containing 0.5 mg L^{-1} of the analytes through the carrier line and optimizing one parameter while fixing

all the other parameters. The optimal experimental parameters were selected as a compromise for multi-element analysis and they are given in Table IV.

TABLE IV. Optimal experimental parameters for ICP-AES

Parameter	Value
Generator power, W	1450
Relative torch position, mm	5
Diameter of injector bore, mm	1.8
Coolant flow rate, L min^{-1}	12
Auxiliary flow rate, L min^{-1}	0.6
Nebulizer flow rate, L min^{-1}	0.75
Sample uptake rate, mL min^{-1}	1.5
Measurement processing mode	Peak height
Background correction	Manual selection

Investigation the influence of relative torch position on the intensity of all analytical and internal standard lines showed that the maximum intensities were achieved by observation 5 mm above the induction coil. In particular, satisfactory results could be obtained under robust operating conditions when a high generator power (Figs. 1 and 2) is combined with a long residence time, which could be achieved with lower carrier gas flow rates (Figs. 3 and 4). It may be seen in Figs. 1–4 that indium could be an adequate internal standard for the efficient compensation of changes in the amount of formed aerosol and analyte residence time at a carrier gas flow rate of 0.75 L min^{-1} and a high generator power of 1450 W.

The change in the behavior of the ionization and excitation conditions of plasma as a function of operating conditions was monitored through the MgII280/MgI285 intensity ratio in order to obtain its highest value.[33,35,36,38] An increase in the generator power from 1000 to 1500 W led to an increase in the values of MgII280/MgI285 ratio. Generator power of 1500 W had slightly higher value for this ratio, but *RSD* value of the measurements was higher under this condition. The effect of nebulizer flow rate on the MgII280/MgI285 ratio from 0.5 to 1 L min^{-1} showed that the highest values for MgII280/MgI285 ratio were obtained for a nebulizer flow rate in the range from 0.7 to 0.85 L min^{-1}, but the lowest *RSD* value of the measurements was obtained with a nebulizer flow rate of 0.75 L min^{-1}.

Determination of trace elements in gold samples

Using the establish experimental conditions, as given in Table IV, the achievable detection limits for the investigated elements, defined as the analyte concentration giving a signal that is three times the standard deviation (n = 6) of the blank, are given in Table V.

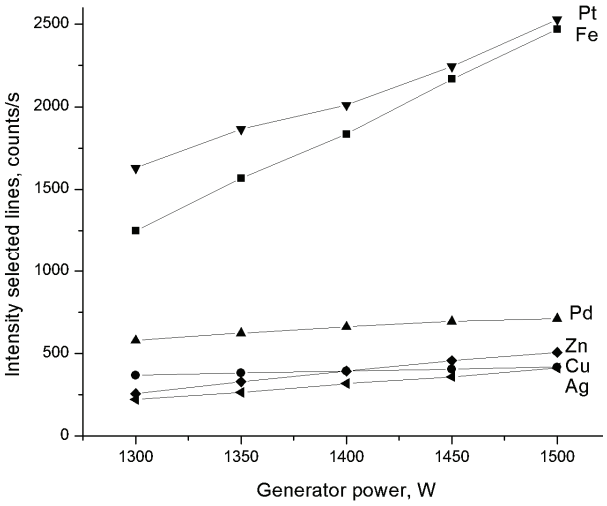

Fig. 1. The effect of the generator power on the intensity of the analytical lines.

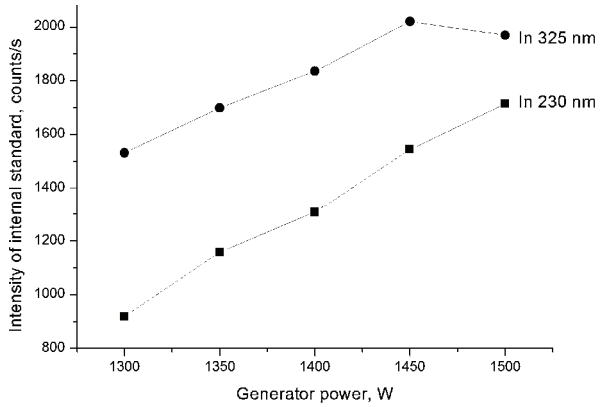

Fig. 2. The effect of the generator power on the intensity of the internal standard lines.

A refined gold sample of unknown composition was analyzed using the previously defined analytical programs and experimental parameters. The obtained results for different calibration strategies are presented in Table VI. Since the detection limits for most of the analyzed elements were slightly higher with the matrix matching calibrations than without matrix matching, especially for copper and iron, the contents of such elements could not be quantified with the former technique. Similar results for a decrease in sensitivity for matrix matching calibration were obtained by Hinds,[9] Baucells[13] and Kogan.[22] These results could be explained by the fact that high purity gold free from all the analyzed elements, which should be used for the preparation of calibration solutions as the matrix material, is not readily available. Inhomogeneous distributions of these trace elements present in the matrix material lead to higher standard deviation of blank and higher detection limits. Therefore, matrix free calibration and standard addi-

tion methods are more convenient for analyte contents lower than 10 mg kg^{-1} in solid samples.

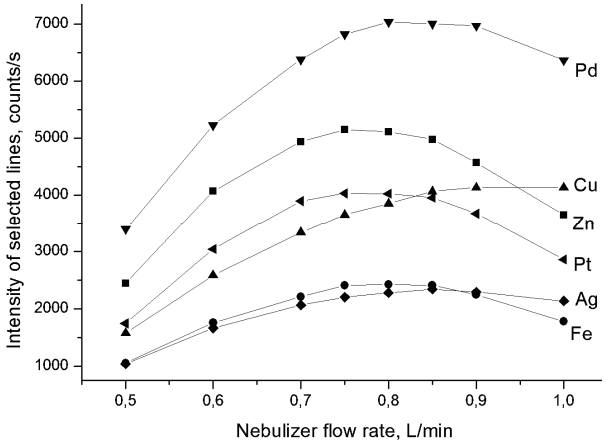

Fig. 3. The effect of the nebulizer flow rate on the intensity of the analytical lines.

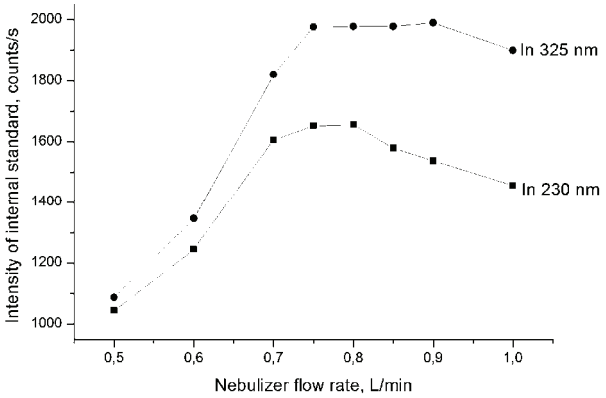

Fig. 4. The effect of the nebulizer flow rate on the intensity of the internal standard lines.

TABLE V. Detection limits for the determination of trace elements in gold

Analyte	Matrix matching calibration, mg/L			Matrix free calibration, mg/L		
	No IS	In 230 nm	In 325 nm	No IS	In 230 nm	In 325 nm
Ag	0.006	0.006	0.009	0.006	0.004	0.007
Cu	0.014	0.019	0.014	0.007	0.004	0.006
Fe	0.020	0.022	0.020	0.005	0.003	0.004
Pd	0.017	0.018	0.018	0.017	0.018	0.016
Pt	0.039	0.027	0.035	0.016	0.010	0.014
Zn	0.004	0.008	0.008	0.003	0.001	0.002

In general, matrix matching is certainly a better way to overcome matrix effects. However, this matching requires perfect knowledge of the sample composition, which is not always possible. In the case of analysis of ultra pure materials, matrix-matching calibration requires using a matrix material with as low

possible concentrations of the investigated elements. The gold matrix used in the present investigation did not contain significant amounts of Ag, Pt and Pd but involved some contents of Cu, Fe and Zn. Therefore, the results for Cu, Fe and Zn were better using internal standardization without the addition of the matrix material and standard addition methods, while, the results for Ag, Pt and Pd were in accordance with all calibration strategies and standard addition methods.

TABLE VI. The results of the analysis of the gold sample (mean ±*SD*, mg kg^{-1}); the results for zinc were lower than the limit of quantification of the employed ICP-AES

Analytical program	Ag	Pd	Pt	Cu	Fe
Au–H_2O	88.80±1.30	10.84±0.22	13.70±0.34	2.80±0.17	6.52±0.31
Au–Au	91.55±2.14	12.06±0.62	12.27±0.55	ND	ND
Au–In230–H_2O	91.97±1.13	13.06±0.28	14.64±0.28	3.57±0.20	6.60±0.22
Au–In230	83.05±3.12	11.93±0.53	12.45±0.51	ND	ND
Au–In325–H_2O	102.17±2.34	12.38±0.26	14.90±0.55	3.57±0.35	7.05±0.57
Au–In325	85.60±3.31	11.47±0.66	12.07±0.73	ND	ND
Standard addition method					
No-Is	79.02±2.30	12.79±0.52	12.79±0.53	3.01±0.03	7.23±0.41
Is–In230	82.78±3.67	11.29±0.28	13.55±0.63	3.39±0.18	6.77±0.25
Is–In325	82.78±4.99	12.04±0.61	13.55±0.75	3.76±0.13	8.28±0.81

The precision of the methods, expressed as *RSD* values for four replicate determinations from the same sample solution, was apparently better using matrix free calibration standards, especially when indium at wavelength of 230 nm was used as the internal standard. The obtained *RSD* values were within 5 % for all analyzed elements, except for copper. The main reason for higher *RSD* values for copper compared to other investigated elements was its lower concentration, which is close to the limit of quantification. The precision of the obtained results by matrix matching and matrix free calibration for silver, palladium and platinum was also compared through the *F* test. As the ratios of the variances $F_{experiment}$ were smaller than F_{table}, this indicated that there were no significant differences in precision of the methods at the 95 % confidence level.

As no pure gold certified reference material containing all analyzed elements was available, the accuracy of the methods was realized by performing the recovery test for all the analyzed elements. The recoveries were evaluated by analysis of trace elements in unspiked and spiked samples using the described methods. The results from Table VII indicated spike recoveries in the range 90–115 % and there was no evidence of interferences of the gold matrix in the described AES--ICP analysis. The accuracy expressed as the percent of the spike recoveries shows good agreement for all calibration strategies.

TABLE VII. Spike recoveries, %, of the trace elements in the pure gold sample

Analytical program	Ag	Pd	Pt	Cu	Fe	Zn
Au–H_2O	109.8	93.6	103.2	95.3	93.5	93.2
Au–Au	115.3	90.9	99.3	92.2	98.3	93.5
Au–In230–H_2O	102.2	101.0	109.7	99.6	99.0	99.2
Au–In230	112.1	89.8	100.3	92.2	94.0	95.7
Au–In325–H_2O	108.2	100.1	107.0	97.0	99.2	99.9
Au–In325	110.8	91.3	102.0	95.4	101.1	95.6

Analysis of certified reference material of high purity gold

The internal standardization and the standard addition method were further validated by analyzing a certified reference material of high purity gold AuGHP1. The determination results of the certified reference material by the internal standardization and the standard addition methods, together with the certified values, are given in Table VIII.

TABLE VIII. The results of analysis the certified reference material of highly pure gold AuGHP1 (mean ±*SD*, mg/kg)

Analytical program	Fe	Cu	Zn	Pt
Au–H_2O	8.62±0.30	4.67±0.07	4.30±0.08	ND
Au–In230–H_2O	10.27±0.26	4.78±0.21	5.01±0.19	ND
Au–In325–H_2O	10.74±0.27	4.43±0.10	5.25±0.33	ND
Certified value	8.90	4.40	4.30	1.80
Standard addition method				
No–Is	8.13±0.26	4.69±0.25	4.69±0.26	1.56±0.39
Is–In230	8.75±0.40	4.38±0.09	4.69±0.11	1.56±0.29
Is–In325	10.31±0.56	4.38±0.29	5.00±0.41	2.50±0.50

The results of the analysis of the certified reference material obtained by the internal standardization and the standard addition methods were in accordance with certified values, with the exception of platinum. The obtained results for platinum using matrix-matching and matrix free calibrations with and without internal standard were lower than the limit of quantification, but the recoveries obtained by standard addition methods were in the range from 86.67 to 138.89 %. Thu sensitivity enhancement is essential for the determination of low concentrations of platinum by inductively coupled plasma atomic emission spectrometry. This can be achieved using a more efficient sample introduction technique, such as ultrasonic nebulizer or electrothermal vaporizer, as well as using more sensitive techniques such as inductively coupled plasma mass spectrometry or electrothermal atomizer atomic absorption spectrophotometry. The internal standardization and standard addition method were proved effective ways of overcoming matrix effects. Comparison of the results obtained using the two

wavelengths for indium, employed as an internal standard, indicated better results were obtained using the 230 nm wavelength.

CONCLUSIONS

A rapid and simple method for the determination of trace contents of silver, copper, iron, palladium, zinc and platinum in refined gold samples was developed. Indium was used as the internal standard. Two sets of calibration standards were prepared. In the first set of matrix matched calibration standards, the concentration of the gold matrix was the same as in the samples, while in the second set, the matrix material was not present. The detection limits of some elements for matrix matching calibrations were higher than those obtained without the addition of matrix material. The precision of the methods, expressed through the RSD values, was better using matrix free calibration standards using the indium 230 nm line as the internal standard or without using the internal standard. The accuracy of methods was confirmed by performing the recovery test and by analysis of a certified reference material of high purity gold AuGHP1. Therefore, simultaneous inductively coupled plasma atomic emission spectrometry with a radial torch position and a cross flow nebulizer can be successfully applied for the determination the trace elements in refined gold samples. The best results were achieved by matrix free calibration and the standard addition method using the indium 230 nm line as an internal standard.

Acknowledgements. This research was supported by the Project No. 34024 funded by the Ministry of Education, Science and Technological Development of the Republic of Serbia: "Development of Technologies for Recycling of Precious, Rare and Associated Metals from Solid Waste in Serbia to High Purity Products".

ИЗВОД

ОДРЕЂИВАЊЕ ТРАГОВА ЕЛЕМЕНАТА У УЗОРЦИМА РАФИНИСАНОГ ЗЛАТА АТОМСКОМ ЕМИСИОНОМ СПЕКТРОМЕТРИЈОМ СА ИНДУКТИВНО КУПЛОВАНОМ ПЛАЗМОМ

МИРЈАНА ШТЕХАРНИК[1], МАРИЈА ТОДОРОВИЋ[2], ДРАГАН МАНОЈЛОВИЋ[2], ДАЛИБОР СТАНКОВИЋ[2], ЈЕЛЕНА МУТИЋ[2] и ВЛАСТИМИР ТРУЈИЋ[1]

[1]*Институт за рударство и металургију Бор, Сектор за хемијска испитивања, 19210 Бор,и*
[2]*Универзтет у Београду, Хемијски факултет, 11000 Београд*

Овај рад приказује методу за одређивање ниских садржаја сребра, бакра, гвожђа, паладијума, цинка и платине у узорцима рафнисаног злата. За испитивања је коришћен атомски емисиони спектрометар са индуктивно куплованом плазмом, радијално постављеним пламеником са унакрсним распршивачем. Да би се упоредиле различите стратегије калибрације припремљена су два сета калибрационих стандарда. Први сет калибрационих стандарда са и други сет стандарда без додатка матрикса. Границе детекције добијене при коришћењу стандарда са додатком матрикса су више за неке елементе од калибрација без додатка матрикса. Такође, примењена је и метода унутрашње стандардизације, експерименти су показали да је индијум најбољи избор за унутрашњи стандард. Резултати анализа узорка злата добијених коришћењем стандарда са и без додатка

матрикса упоређени су са методом стандардног додатка. Тачност метода испитана је приносом стандардног додатка и добијене су вредности у опсегу од 90 до 115 %. Тачност методе, такође, је проверена коришћењем сертификованог референтног материјала високочистог злата AuGHP1. Најбољи резултати постигнути су употребом калибрационих стандарда без додатка матрикса и методом стандардног додатка употребом индијума као унутрашњег стандарда на таласној дужини од 230 nm.

(Примљено 5. маја, ревидирано 24. септембра 2012)

REFERENCES

1. The American Society for the Testing and Materials, ASTM B562-95, *Standard specification for refined gold*, West Conshohocken, PA, USA, 2005
2. B. Zmbova, M. Marinkovic, *Talanta* **20** (1973) 647
3. H. Jager, *Anal. Chim. Acta* **60** (1970) 303
4. G. Muller-Vogt, A. Huwe, W. Wendl, *Spectrochim. Acta, B* **51** (1996) 1191
5. M. W. Hinds, *Spectrochim. Acta, B* **53** (1998) 1063
6. E. Ivanova, I. Havesov, H. Berndt, G. Schaldach, *Fresenius J. Anal. Chem*. **336** (1990) 320
7. E. Ivanova, N. Jordanov, I. Havesov, M. Stoimenova, S. Kadieva, *Fresenius J. Anal. Chem*. **336** (1990) 501
8. M. W. Hinds, G. N. Brown, D. L. Styris, *J. Anal. Atom. Spectrom*. **9** (1994) 1411
9. M. W. Hinds, V. V. Kogan, *J. Anal. Atom. Spectrom*. **9** (1994) 451
10. M. W. Hinds, I. Shuttler, C. P. Bosnak, *J. Anal. Atom. Spectrom*. **12** (1997) 833
11. I. Karadjova, S. Arpadjan, L. Jordanova, *Fresenius J. Anal. Chem*. **367** (2000) 146
12. S. D. Dan, *Spectrosc. Spect. Anal*. **21** (2001) 849
13. M. Baucells, G. Lacort, M. Roura, *J. Anal. Atom. Spectrom.* **2** (1987) 645
14. G. H. Lee, S. R. Yang, C. J. Park, K. W. Lee, *Bull. Korean Chem. Soc*. **14** (1993) 696
15. S. M. Graham, R. V. D. Robert, *Talanta* **41** (1994) 1369
16. P. Becotte-Haigh, J. F. Tyson, E. Denoyer, M. W. Hinds, *Spectrochim. Acta, B* **51** (1996) 1823
17. Y. C. Sun, C. H. Hsieh, T. S. Lin, J. C. Wen, *Spectrochim. Acta, B* **55** (2000) 1481
18. H. Xie, K. Huang, X. Nie, L. Fu, *J. Wuhan. Univ. Technol*. **24** (2009) 608
19. L. Xiangsheng, Z. Anding, L. Yulong, L. Yiqiang, *Chin. J. Anal. Chem*. **28** (2000) 322
20. C. Younghong, H. Rui, C. Feifei, Z. Yu, *Gold* **4** (2009) 43
21. Y. C. Sun, C. H. Hsieh, *J. Anal. Atom. Spectrom*. **17** (2002) 94
22. V. V. Kogan, M. W. Hinds, G. I. Ramendik, *Spectrochim. Acta, B* **49** (1994) 333
23. C. Billing, D. R. Root, J. F. van Staden, *Anal. Chim. Acta* **453** (2002) 201
24. S. Glodowski, Y. Kublik, *Anal. Chim. Acta* **175** (1985) 37
25. M. F. Guerra, M. Radtke, I. Reiche, H. Riesemeier, E. Strub, *Nucl. Instr. Meth. Phys. Res., B* **266** (2008) 2334
26. M. Kasamatsu, Y. Suzuki, T. Nakanishi, O. Shimoda, Y. Nishiwaki, N. Miyamoto, S. Suzuki, *Anal. Sci*. **21** (2005) 785
27. I. Calliari, M. Dabalá, M. Magrini, *X-Ray Spectrom*. **29** (2000) 438
28. R. K. Winge, V. A. Fassel, V. J. Peterson, M. A. Floyd, *Inductively coupled plasma atomic emission spectroscopy-An atlas of spectral information, Prominent lines emitted by AES-ICP,* Appendix B, Elsevier, 1985

29. D. A. Skoog, F. James, T. A. Neiman, *Principles of instrumental analysis*, Saunders College, New York, 1998
30. J. L. Todoli, L. Gras, V. Hernandis, J. Mora, *J. Anal. Atom. Spectrom.* **17** (2002) 142
31. M. Iglésias, T. Vaculovic, J. Studynkova, E. Poussel, J. M. Mermet, *Spectrochim. Acta, B* **59** (2004) 1841
32. H. Kola, P. Perämäki, *Spectrochim. Acta, B* **59** (2004) 231
33. A. Fernandez, M. Murillo, N. Carrion, J. M. Mermet, *J. Anal. Atom. Spectrom.* **9** (1994) 217
34. C. Dubuisson, E. Poussel, J. L. Todoli, J. M. Mermet, *Spectrochim. Acta, B* **53** (1998) 593
35. X. Romero, E. Poussel, J. M. Mermet, *Spectrochim. Acta, B* **52** (1997) 495
36. C. Dubuisson, E. Poussel, J. M. Mermet, *J. Anal. Atom. Spectrom.* **13** (1998) 1265
37. I. Novotny, J. C. Farinas, W. Jia-Liang, E. Poussel, J. M. Mermet, *Spectrochim. Acta, B* **51** (1996) 1517
38. J. M. Mermet, *Anal. Chim. Acta* **250** (1991) 85
39. C. Dubuisson, E. Poussel, J. M. Mermet, J. L. Todoli, *J. Anal. Atom. Spectrom.* **13** (1998) 63
40. X. Romero, E. Poussel, J. M. Mermet, *Spectrochim. Acta, B* 52 (1997) 487
41. J. Mutic, D. Manojlovic, R. Kovacevic, J. Trifunovic, N. R. Amaizah, Lj. Ignjatovic, *Microchem. J*. **98** (2011) 11
42. M. Carre, E. Poussel, J. M. Mermet, *J. Anal. Atom. Spectrom.* **7** (1992) 791
43. N. S. Mokgalak, R. I. McCrindle, B. M. Botha, Lj. Marjanovic, *S. Afr. J. Chem*. **55** (2002) 72.

Journal of the Serbian Chemical Society
JSCS-info@shd.org.rs • www.shd.org.rs/JSCS
J. Serb. Chem. Soc. 78 (4) 579–590 (2012)
JSCS–4440
UDC 549.623.9–033.62+621.927+
541.12–116:66.017
Original scientific paper

Mechanochemical treatment of Serbian kaolin clay to obtain a highly reactive pozzolana

ALEKSANDRA MITROVIĆ[1] and MIODRAG ZDUJIĆ[2*#]

[1]*Institute for Testing of Materials, Bulevar vojvode Mišića 43, 11000 Belgrade, Serbia and* [2]*Institute of Technical Sciences of the Serbian Academy of Sciences and Arts, Knez Mihailova 35, 11000 Belgrade, Serbia*

(Received 29 August, revised 11 October 2012)

Abstract: Mechanochemical treatment of Serbian kaolin clay was performed in a planetary ball mill using two different milling media, hardened steel or zirconia vials and balls. The samples obtained after various milling times were characterized by particle size laser diffraction (PSLD), X-ray diffraction (XRD), differential scanning calorimetry/thermogravimetry (DTA/TGA) and Fourier-transform infrared (FTIR) analyses. The mechanochemical treatment induced amorphization of the kaolinite phase accompanied by dehydroxylation. It was found that for given milling parameters, amorphization mainly occurred in the milling period up to 15 min, and was completed after about 30 min of milling for both employed milling media. The pozzolanic activities were determined by the Chapelle method. Milling in the hardened steel milling medium had no significant influence on pozzolanic activity, even though there was accumulated iron contamination. For both milling media, a pozzolanic activity of 0.79 was obtained for the samples milled for 15 min and it remained almost unchanged with prolonged milling. The determined pozzolanic activity values were similar to those of commercial metakaolinite or metakaolinite obtained by calcination of the same clay, thereby, indicating that highly reactive pozzolana could be obtained by mechanochemical treatment of Serbian kaoline clay.

Keywords: kaolin clay; kaolinite; metakaolinite; mechanochemical treatment; pozzolana.

INTRODUCTION

Kaoline clays are important industrial materials, used in engineering and construction applications, ceramic processing, environmental remediation and in many other miscellaneous applications.[1] There is an ongoing interest in the utilization of kaolin clays as raw materials for the manufacture of metakaolin

* Corresponding author. E-mail: miodrag.zdujic@itn.sanu.ac.rs
# Serbian Chemical Society member.
doi: 10.2298/JSC120829107M

(MK), a dehydroxylated form of the clay mineral kaolinite, as a pozzolanic additive for cement and concrete. MK usage can be found in many aspects of obtaining concrete and can have beneficial effects on the ultimate compressive strength, permeability and chemical durability, as well as economic and ecological advantages.[2] Bearing this in mind, as well as the lack of traditional pozzolanic materials (*e.g.*, fly ash and silica fume), great effort has been given to improving the technical characteristics MK as well as its production using kaolin clay as the raw material.[3–5]

Metakaolinite ($Al_2Si_2O_7$) is an X-ray amorphous reactive aluminosilicate, commercially obtained by heat treatment of kaolinite ($Al_2Si_2O_5(OH)_4$) clay.[6,7] The heat treatment involves the use of fossil fuels that produce CO_2 and other gases (NO_x and SO_x types), all of which are air pollutants. Recently, there has been an effort to reduce the emissions of greenhouse gases, and to develop processes less aggressive to the environment. One of these processes is mechanical treatment, widely applied for the modification and synthesis of various classes of materials.[8–10] The mechanochemical treatment of kaolinite has also been reported in several papers.[11–21].

In Serbia, there are several high-quality kaolin clay deposits: the Aranđelovac Basin, the Kolubara Basin, and the Vranje and Kriva Reka Basin. Certain quantities of the kaolin clays from these deposits are used in the ceramic industry and for the production of refractory materials. In order to find other possible applications, a process of metakaolin production by heat treatment (calcination) of Serbian kaolin clay was developed.[22] Good pozzolanic activity, as well as mechanical and physical characteristics of the cements with the addition of metakaolin produced by calcination and subsequent milling,[23] gave substantial reason to try to produce reactive pozzolana with a process less aggressive to the environment, *i.e.*, mechanochemical treatment.

Although a lot of work on milled kaolinite has been reported in recent years,[11–21] there seem to be only one report on the pozzolanic activity of amorphous kaolinite obtained by mechanochemical treatment.[19] Furthermore, it should be born in mind that the mineral composition of natural kaolin clays from different locations usually differ remarkably, thus influencing the physical and chemical properties of produced kaolinite.

In this work, the results of mechanochemical treatment of Serbian kaolin clay, performed using either hardened steel or zirconia vial and balls as the milling media, are presented. The investigations were focused on how milling influences the pozzolanic activity and whether contamination arising from balls and vial debris affects the properties of the final product. The results obtained enable a better understanding of kaolinite preparation by milling and its properties as a pozzolanic additive.

EXPERIMENTAL

Material

Kaolin clay from the Aranđelovac Basin in Serbia was used for mechanochemical treatment. Before characterization and mechanochemical treatment, clay was dried to less than 0.5 % moisture content, crushed and then ground in ball mill for 10 min (sample denoted as 0 h).

The chemical composition of the starting clay expressed in mass % of oxides was SiO_2, 48.00; Al_2O_3, 31.75; Fe_2O_3, 4.38; CaO, 1.00; MgO, 0.48; Na_2O, 0.16; K_2O, 1.50 and loss on ignition 12.33 %. The main physical characteristics of the starting clay were given previously.[23]

The semi quantitative estimation, namely chemical analysis in combination with X-ray diffraction (XRD) analysis was used to determine the kaolinite and quartz contents of 80 and 10.6 mass %, respectively.

Milling procedure

The powders were milled without any additives (dry milling) in a planetary ball mill – Fritsch Pulverisette 5 – using either hardened steel 500 cm^3 vials and 13.4 mm diameter balls or 500 cm^3 zirconia vials (yttrium oxide added ZrO_2) vials and 10.0 mm diameter balls, in an air atmosphere. The masses of the powders were 25 and 20 g for milling in the hardened steel and zirconia vials, respectively, giving a balls-to-powder mass ratio of about 25 for both sets of milling. The angular velocity of the supported (basic) disc, measured by a tachometer, varied between 340 and 350 rpm (35.6 and 36.7 rad s^{-1}) throughout the milling. Thus, the milling parameters were such that the same milling intensity may be expected for both milling media.[24,25] Due to contamination arising from ball and vial debris, the color of the powders milled in the hardened steel vials gradually darkened from almost white to black. Prolonged milling up to 5 h was deliberately performed in order to investigate the possible effect of contamination on the properties of the clay prepared by mechanochemical treatment. Thus, chemical analysis of the powder milled for 5 h revealed an iron contamination of 5.6 %. Milling in zirconia was performed for up to 2 h of milling. Determination of the ZrO_2 contamination by chemical analysis was not performed but since the XRD analysis did not reveal a ZrO_2 phase, it should be no greater than a few percent.

Experimental techniques

The particle size distribution was measured by laser particle size analyzer on Mastersizer 2000 (Malvern Instruments Ltd., UK), which covers the particle size range of 0.02–2000 μm.

The X-ray powder diffraction data were collected on a Philips PW1710 diffractometer using Cu-Kα graphite-monochromatized radiation (λ = 1.5418 Å) in the 2θ range 4−65° (step-length: 0.02° 2θ, scan time: 5 s).

The thermal behavior of the staring clay and powders milled for 15 and 30 min and for 1 and 2 h was investigated from room temperature up to 1100 °C using an SDT Q600 simultaneous DSC–TGA instrument (TA Instruments) with a heating of 20 °C min^{-1} under a dynamic (100 cm^3 min^{-1}) N_2 atmosphere.

The Fourier-transform infrared (FTIR) spectra were recorded using Nicolet 6700 Thermo Scientific spectrometer. Measurements were conducted in the wave number range 4000–400 cm^{-1}, with 4 cm^{-1} resolution.

The pozzolanic activity was evaluated according to the Chapelle test.[26] Kaolinite clay of a mass of 1 g was mixed with 1 g $Ca(OH)_2$ and 200 cm^3 boiling water. The suspension was subsequently boiled for 16 h and the free $Ca(OH)_2$ was determined by the means of sucrose extraction and titration with HCl solution.

RESULTS AND DISCUSSION

Particle size distribution

Particle size measurements revealed that mechanochemical treatment using either hardened steel or zirconia vials and balls induced only a moderate powder change compared to the kaolin clay pre-milled for 10 min (Fig. 1). Mean particle size slightly increased from 9.85 to 11.34 μm after 15 min, because of particle agglomeration, and remained almost unchanged for milling times up to 30 min in the hardened steel vial. Such an observation is in an agreement with previously reported results.[15] Particle size reduction of the fraction of coarse powder particle size could also be noticed. The powder behaved in a similar manner during milling in the zirconia vial.

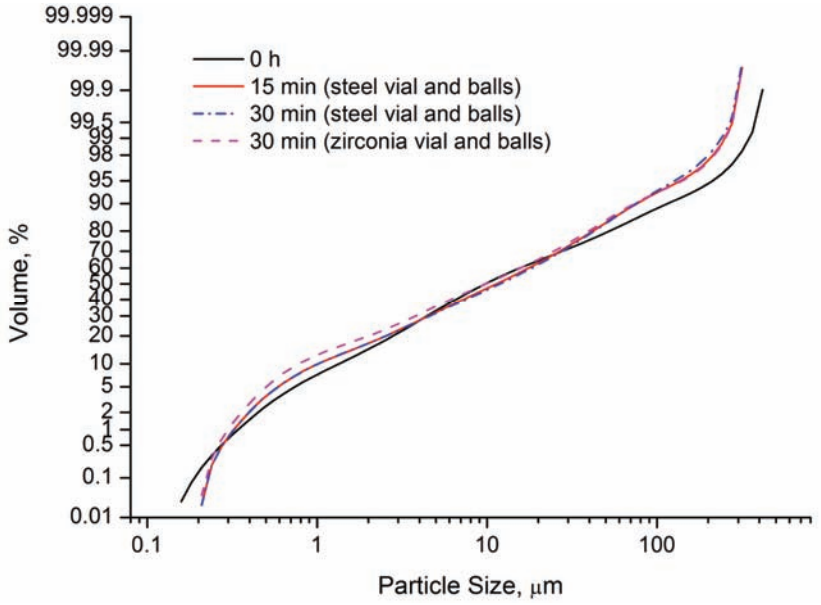

Fig. 1. Particle size distribution of the kaolin clay pry-milled for 10 min (0 h) and milled for 15 and 30 min using hardened steel balls and vial and milled for 30 min using zirconia balls and vial.

XRD structural analysis

The XRD patterns of the starting clay and samples milled for various milling times, for both milling media, are presented in Figs. 2 and 3. XRD analysis of the starting clay identifies kaolinite ($Al_2Si_2O_5(OH)_4$) by basal reflections at about 2θ 12.4, 20.0, 21.0 and 25.0° (JCPDS card No. 89-6538), quartz at 2θ 20.9 and 26.7° (JSPDS card No. 89-8934) and mica at 2θ 8.9 and 17.9° (JCPDS card No. 88-0791). In the XRD pattern of the sample milled for 15 min, the peaks of kaolinite had almost vanished (or can hardly be resolved) as the result of deterioration of

the kaolinite structure. The loss of peak intensity at 2θ 12.4° suggests breaking of the bonds between the kaolinite layers (001).[15] Mechanochemical treatment induces dehydroxylation, and the consequential transformation of kaolinite to a very disordered (amorphous) structure. It was already demonstrated that during milling, the kaolinite phase becomes gradually distorted and amorphous.[13–16] For the thermally induced transformation of kaolinite to metakaolin, a molecular dynamic study showed that the loss of crystallinity was governed by the loss of hydroxyl groups at the surface of the inter-layer spacing and the migration of the aluminum into the vacant sites.[7]

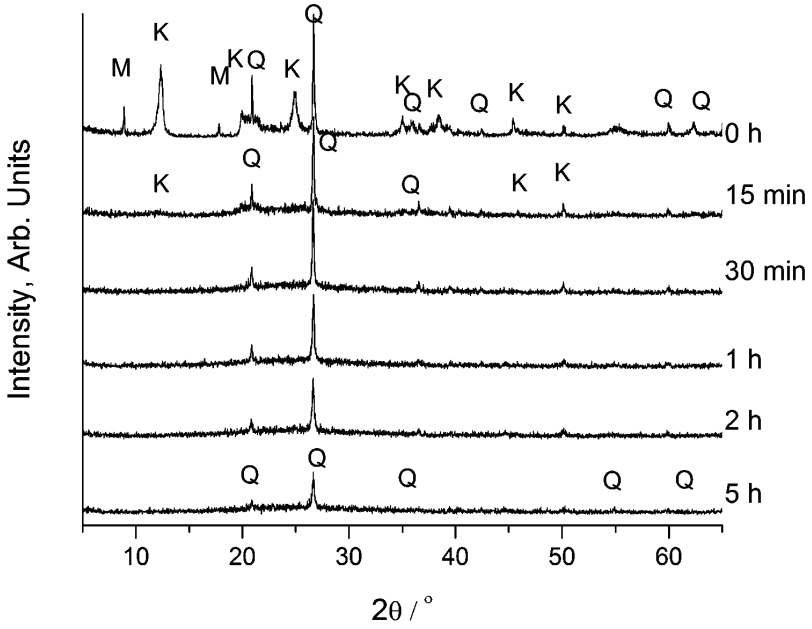

Fig. 2. XRD Patterns of the kaolin clay milled for various milling times using hardened steel balls and vial (K – kaolinite, Q – quartz, M – mica).

The XRD patterns of the samples milled for longer milling times (30 min, 1, 2 and 5 h) are similar (Figs. 2 and 3), indicating that with prolonged milling structural changes occurred very slowly. The XRD patterns suggest that the quartz phase was not altered because the position of peaks at 2θ 21.2 and 27.4° remained almost unchanged. However, their intensities gradually decreased, perhaps as the result of very slow dissolution of quartz into the disordered (amorphous) matrix. XRD analysis of mechanically treated samples during either hardened steel or zirconia milling medium indicated fast deterioration of the kaolinite structure during milling, mainly within the first 15 min. The results obtained in this study are consistent with previous investigations.[11–19]

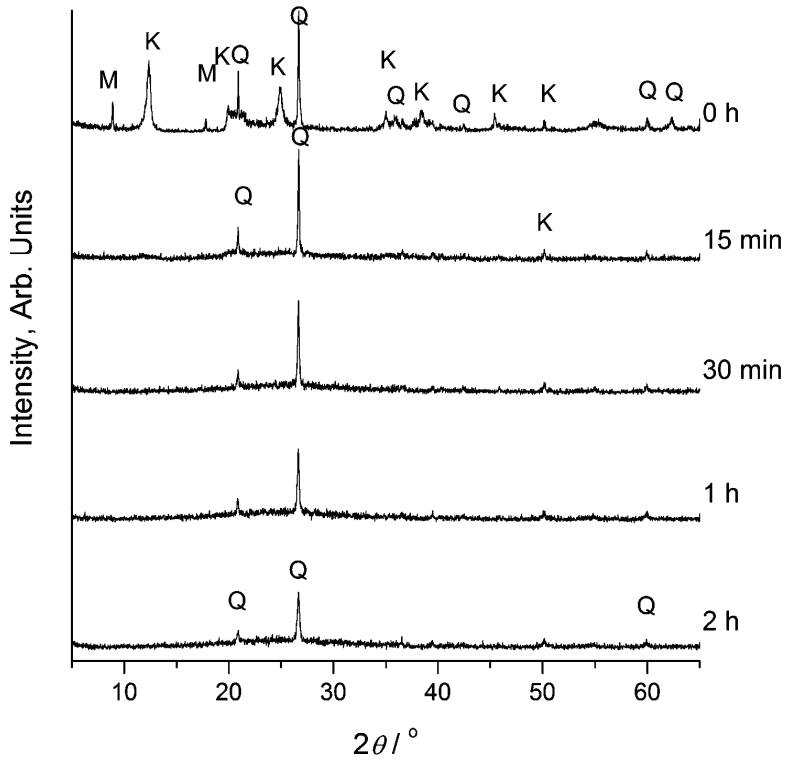

Fig. 3. XRD Patterns of the kaolin clay milled for various milling times using zirconia balls and vial (K – kaolinite, Q – quartz, M – mica).

The observation that almost identical results were obtained in both milling media suggests that specific energy dose defined as cumulative mechanical energy transferred to the powder during milling time is responsible for the kinetics and final phase formation, in spite of different milling parameters such as impact energy and frequency.[27]

DTA/TGA thermal analysis

Thermal analysis of the samples milled for various milling times further supports the XRD findings. On the DTA curve (Fig. 4a) of the pre-milled clay (milling time 0 h), two heat effects could be identified. A well-developed endothermic peak at a temperature of about 511 °C, assigned to the process of dehydroxylation, was accompanied with a weight loss of about 12 % during heating up to temperatures of about 800 °C (Fig. 4b). At higher temperatures, the exothermic heat effect at about 982 °C could be assigned to the crystallization of spinel and/or mullite phases.[12]

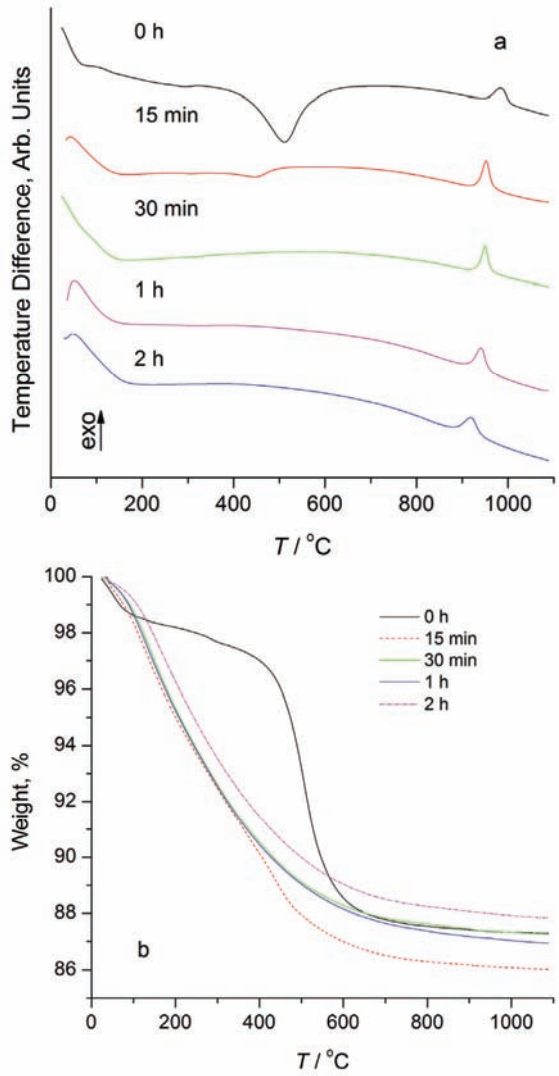

Fig. 4. DTA (a) and TGA (b) curves of the kaolin clay milled for various milling times using hardened steel balls and vial.

For the sample milled for 15 min, the endothermic heat effect had almost disappeared, indicating that mechanochemical treatment induced breaking of O–H bonds. It should also be noted that this peak was shifted to a lower temperature of about 460 °C. Thus, mechanochemical treatment through the generation of lattice defects decreased the dehydroxylation temperature by about 50 °C. For prolonged milling times, such a heat effect could not be detected, implying that the process of dehydroxylation was completed in up to about 30 min of milling. The exothermic peak shifted to lower temperatures with milling time (from 982 to 920 °C for 0 and 2 h, respectively), which is in agreement with

previously reported results.[12] DTA results (Fig. 4b) show that water release was facilitated in the milled samples in comparison to the unmilled sample.

DTA/TGA curves of the samples milled in the zirconia-milling medium along with metakaolinite sample prepared by heat treatment (calcination) of the kaoline clay at 650 °C for 90 min,[22] are given in Fig. 5. As can be seen, milled samples exhibited a very similar thermal behavior to that milled in hardened steel, suggesting contamination had no significant effect on the dehydroxylation process. Therefore, the weight loss between 100 and 300 °C (Figure 4b and 5b) may be attributed to the liberation of coordinated water, which is formed from

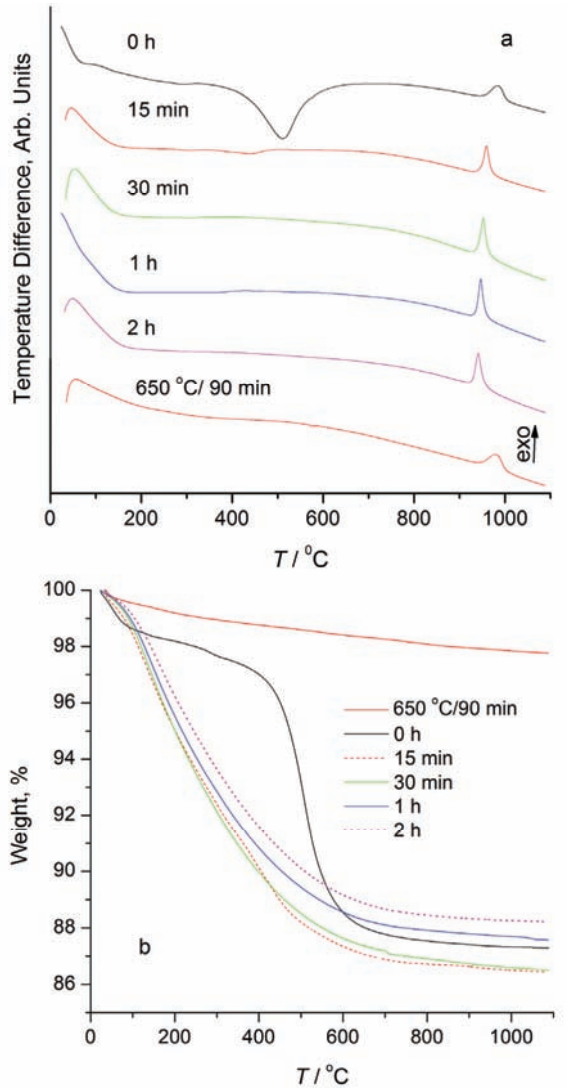

Fig. 5. DTA (a) and TGA (b) curves of the kaolin clay milled for various milling times using zirconia steel balls and vial.

the OH groups because of mechanochemical dehydroxylation of kaolinite. The difference in the thermal behavior of amorphous kaolinite and of metakaolinite is obvious from Fig. 5. The metakaolinite sample was characterized by the absence of a dehydroxylation heat effect (Fig. 5a), while the TGA measurement did not reveal any significant weight loss (Fig. 5b).

Infrared analysis

The FTIR spectra of the pre-milled kaolin clay and those of the kaolin clay milled for 15 and 30 min, and 1 and 2 h in the zirconia-milling medium are shown in Fig. 6. The characteristic bands at 3697, 3651 and 3620 cm^{-1}, assigned to SiO–H stretching vibrations, were markedly decreased in intensity in the spectra of the mechanochemically treated samples, indicating the scission of O–H bonds. The appearance of a broad band at 3443 cm^{-1} may be assigned to the hydroxyl vibrations of interlayer and adsorbed water.[11,19–21,28] The very weak but detectable bands at 3697 and 3624 cm^{-1} indicate that after 30 min of milling, some OH groups still remained bonded between the adjacent kaolin layers, evidencing that some residual kaolinite phase still existed. However, on prolonging the milling time up to 1 h, these bands completely disappeared, implying completion of the dehydroxylation process. No significant difference could be observed between samples milled for 1 and 2 h.

FTIR spectra of the samples milled in hardened steel milling media (not given) exhibited almost identical features as presented in Fig. 6.

Pozzolanic activity

Determination of pozzolanic activity, and in particular lime reactivity, of various materials is essential for their efficient application in cement and concrete. The influence of milling time of the kaolin clay on the pozzolanic activity is given in Table I. It is evident that after 15 min of milling, the pozzolanic activity reached its highest value of 0.79 g $Ca(OH)_2$ per g pozzolana. Prolonged milling slightly decreased the pozzoloanic activity. The values obtained were similar to those of metakaolinite obtained by calcination[22] and subsequent milling[23] for the same kaolinite clay, as well as commercial metakaolinite, implying that mechanochemical treatment could be applied to produce highly reactive pozzolana.

It is known that the lime reactivity of a pozzolanic material depends on its particle size and surface area as well as its mineralogical composition.[29] High reactivity pozzolans are those that contain large proportions of amorphous aluminosilicates, have particles of small average mean diameter and relatively high specific surface. Therefore, taking the structural changes of the starting clay during milling into the account, it could be presumed that amorphization of the studied kaolinite was the main factor responsible for the obtained pozzolanic activity.

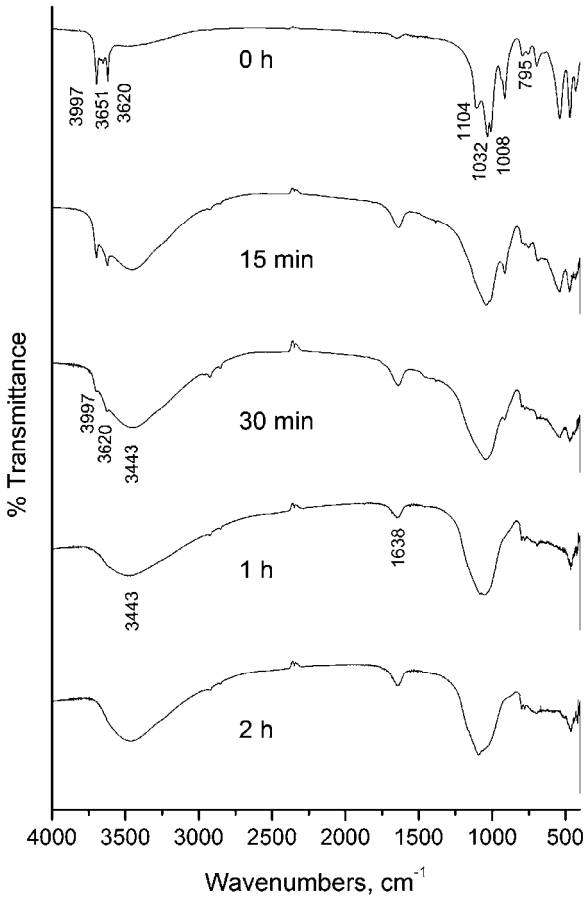

Fig. 6. FTIR Spectra of a kaolin clay pre-milled for 10 min (0 h) and milled for various milling times using zirconia steel balls and vial.

TABLE I. Pozzolanic activity of the kaolinite clay milled for various milling times in either hardened steel or zirconia milling medium (balls and vial), and obtained by calcination and subsequent milling in comparison to commercial metakaolinite

Milling time	Pozzolanic activity, g $Ca(OH)_2$ per g pozzolana	
	Hardened steel	Zirconia
0 h (pre-milled for 10 min)	0.59	
15 min	0.79	0.79
30 min	0.75	0.74
2 h	–	0.73
5 h	0.76	–
Metakaolinite obtained by calcination[21]	0.65	
Metakaolinite obtained by calcination and subsequent milling[22]	0.76	
Commercial metakaolinite	0.78	

CONCLUSIONS

The results obtained in this study show the feasibility of obtaining highly reactive pozzolan by mechanochemical treatment. The results could be summarized as follows:

Milling in a hardened steel or zirconia medium has no significant effect on the pozzolanic activity beyond a milling time of 15 min.

Contamination arising from ball and vial debris during milling in hardened steel also had significant effect on the pozzolanic activity.

Milling of the pre-milled clay induces only moderate changes in the particle size distribution.

XRD and DTA/TGA analyses of mechanically treated clays indicated a fast deterioration of the kaolinite structure (amorphization) occurred mainly within the first 15 min.

The absence of a signal at 913 cm^{-1} arising from Al–O–H bonds in the IR spectra of milled samples confirmed mechanochemical dehydroxylation and transformation to amorphous kaolinite.

Milling for more than 30 min was unnecessary, as further milling has no significant effects on the characteristics of the pozzolan.

In conclusion, mechanochemical treatment instead of the heat treatment could be employed for the production of pozzolan with the same activity.

Acknowledgements. This work was financially supported by the Ministry of Education, Science and Technological Development of the Republic of Serbia (Grants Nos. TR 36017 and 45001). The authors are grateful to their colleagues Smilja Marković and Zoran Stojanović for the particle size measurements.

ИЗВОД

РЕАКТИВНИ ПУЦОЛАН ДОБИЈЕН МЕХАНОХЕМИЈСКИМ ТРЕТМАНОМ ДОМАЋЕ КАОЛИНСКЕ ГЛИНЕ

АЛЕКСАНДРА МИТРОВИЋ[1] и МИОДРАГ ЗДУЈИЋ[2]

[1]Институт за испитивање материјала, Булевар војводе Мишића 43, 11000 Београд и [2]Институт техничких наука Српске академије наука и уметности, Кнез Михаилова 35, 11000 Београд

Домаћа каолинска глина је механохемијски третирана у планетарном млину коришћењем челичних или ZrO_2 посуда и куглица. Узорци добијени после различитих времена млевења испитивани су рендгенском структурном (XRD) и диференцијално термијском и термогравиметријском (DTA/TGA) анализом, инфрацрвеном спектроскопијом са Фуријеовом трансформацијом (FTIR), као и ласерском дифракцијом расподеле величине честица ((PSLD). Механохемијски третман проузрокује аморфизацију каолинске фазе праћену дехидроксилацијом. Нађено је да је аморфизација интезивна током почетних 15 min млевења, а да је готово у потпуности завршена након 30 min млевења. Пуцоланска активност је одређивана *Chapelle* методом. Млевење у челичним посудама у трајању од 5 h нема битног утицаја на пуцоланску активност, иако је током млевења дошло до запрљања праха гвожђем. Вредност пуцоланске активности од 0,79 добијана је за узорак млевен 15 min у челичним као и за онај млевен у ZrO_2 посудама, и остаје го-

тово непромењена за дужа времена млевења. Одређене пуцоланске активности блиске су вредностима за комерцијални метакаолинит, као и за метакаолинит добијен калцинацијом каолинске глине истог хемијског састава. На основу овога, може се закључити да је механохемијски третман погодна метода за добијање рекативног пуцолана.

(Примљено 29. августа, ревидирано 11. октобра 2012)

REFERENCES

1. H. H. Murray, *Occurrences, Processing and Application of Kaolins, Bentonites, Palygorskite-Sepiolite, and Common Clays*, 1st ed., Elsevier, Oxford, 2007, pp. 1–179
2. R. Siddique, J. Klaus, *Appl. Clay Sci.* **43** (2009) 392
3. C. Fortes-Revilla, S. Martínez-Ramírez, M. T. Blanco-Varela, *Cement Concrete Comp.* **28** (2006) 458
4. H. Kim, L. Lee, H. Moon, *Constr. Build. Mater.* **21** (2007) 1229
5. T. Ramochlan, M. Thomas, K. Gruber, *Cement Concrete Res.* **30** (2000) 339
6. C. E. White, J. L. Provis, T. Proffen, D. P. Riley, J. S. J. van Deventer, *J. Phys. Chem., A* **114** (2010) 4988
7. S. Sperinck, P. Raiteri, N. Marks, K. Wright, *J. Mater. Chem.* **21** (2011) 2118
8. E. Avvakumov, M. Senna, N. Kosova, *Soft Mechanochemical Synthesis*, Kluwer, Boston, USA, 2001
9. V. V. Boldyrev, *Russ. Chem. Rev.* **75** (2006) 177
10. P. Baláž, *Mechanochemistry in Nanoscience and Minerals Engineering*, Springer, Berlin Heidelberg, 2008
11. E. Kristóf, A. Z. Juhász, I. Vassány, *Clay Clay Miner.* **41** (1993) 608
12. K. Sugiyama, J. M. Filio, F. Saito, Y. Waseda, *Mineral. J.* **17** (1994) 28
13. G. Suraj, C. S. P. Iyer, S. Rugmini, M. Lalithambika, *Appl. Clay Sci.* **12** (1997) 111
14. M. Miyazaki, M. Kamitan, T. Nagai, J. Kano, F. Saito, *Adv. Powder Technol.* **11** (2000) 235
15. P. J. Sánchez-Soto, M. C. Jiménez de Haro, L. A. Pérez-Maqueda, I. Varona, J. L. Pérez--Rodríguez, *J. Am. Ceram. Soc.* **83** (2000) 1649
16. R. L. Frost, E. Mako, J. Kristof, E. Horvath, J. T. Kloprogge, *J. Colloid Interface Sci.* **239** (2001) 458
17. R. L. Frost, E. Mako, J. Kristof, E. Horvath, J, T. Kloprogge, *Langmuir* **17** (2001) 4731
18. F. Dellisanti, G. Valde, *Int. J. Miner. Process.* **88** (2008) 94
19. C. Vizcayno, R. M. de Gutiérrez, R. Castello, E. Rodriguez, C. E. Guerrero, *Appl. Clay Sci.* **49** (2010) 45
20. M. Valášková, K. Barabaszová, M. Hundáková, M. Ritz, E. Plevová, *Appl. Clay Sci.* **54** (2011) 70
21. F. Dellisanti, G. Valde, *Int. J. Miner. Process.* **102–103** (2012) 69
22. B. R. Ilić, A. A. Mitrović, Lj. Miličić, *Hem. Ind.* **64** (2010) 351
23. A. Mitrović, D. Jevtić, Lj. Miličić, B. Ilić, *Materijali i Konstrukcije* **53** (2010) 32
24. A. Iasonna, M. Magini, *Acta Mater.* **44** (1996) 1109
25. M. Magini, C. Colella, A. Iasonna, F. Padella, *Acta Mater.* **46** (1998) 2841
26. R. Largent, *Bulletin de Liaison des Laboratoires Routiers des Ponts et Chaussées* **93** (1978) 61
27. F. Delogu, L. Schiffini, G. Cocco, *Philos. Mag., A* **81** (2001) 1917
28. E. Makó, R. L. Frost, J. Kristóf, E. Horváth, *J. Colloid Interface Sci.* **244** (2001) 359
29. J. Cabrera, M. F. Rojas, *Cement Concrete Res.* **31** (2001) 177.

Journal of the Serbian Chemical Society
JSCS-info@shd.org.rs • www.shd.org.rs/JSCS
J. Serb. Chem. Soc. 78 (4) 591–602 (2013)
JSCS–4441
UDC 628.3+546.171.6:628.161.2:
546.47/.49'56'815
Original scientific paper

Polyaza macroligands as potential agents for heavy metal removal from wastewater

PERLA ELIZONDO MARTÍNEZ[1]*, BLANCA NÁJERA MARTÍNEZ[1], NANCY PÉREZ RODRÍGUEZ[1], LAURA HINOJOSA REYES[1] and ISABEL GÓMEZ del RÍO[2]

[1]*Universidad Autonoma de Nuevo Leon, UANL, Chemistry School of Sciences, Avenida Universidad S/N, Cd. Universitaria, 66451 San Nicolas de los Garza, NL, Mexico and* [2]*Universidad Nacional de Educación a Distancia, Madrid, España, Paseo Senda del Rey # 9, 28040 Madrid, Spain*

(Received 28 February, revised 9 April 2012)

Abstract: Two polyaza macroligands *N,N´*-bis(2-aminobenzyl)-1,2-ethanediamine (**L1**) and 3,6,9,12-tetraaza-4(1,2),11(1,2)-dibenzo-1(1,3)-pyridinacyclotridecaphane (**L2**) were characterized and investigated for their metal ion extraction capabilities. The nature of all complexes was established by spectroscopic techniques. The equilibrium constants were determined by spectrophotometric and potentiometric techniques and the residual concentration of metals in the solutions by atomic absorption spectrometry (AAS). The capacity of the ligands to remove heavy metals such as Cu(II), Ni(II), Cd(II), Zn(II) and Pb(II) as insoluble complexes was evaluated in wastewater from industrial effluents. These agents showed high affinity for the studied metals. The values of the equilibrium constants of the isolated complexes (between 1×10^4 and 2×10^7) demonstrated the feasibility of applying these chelating agents as alternatives for the removal of heavy metals from industrial effluents.

Keywords: polyaza macroligands; pollutant removal; wastewater; heavy metals.

INTRODUCTION

The removal of heavy metals from aqueous solutions is an important issue faced by industries discharging wastewater. Due to rapid industrialization, an alarming amount of toxic heavy metals has been released into the environment, endangering natural ecosystems and public health.[1] In recent years, a wide range of treatment technologies, such as chemical precipitation, solvent extraction, adsorption, membrane filtration, and electrodialysis, have been developed for the removal of heavy metals from contaminated wastewater.[2] The use of organic-

* Corresponding author. E-mail: perla.elizondomr@uanl.edu.mx
doi: 10.2298/JSC120228050E

based ligands that produce stable coordination compounds has been proposed as an alternative procedure for the selective extraction and removal of dissolved heavy metals from contaminated water.[3,4]

Some of the main features of a suitable extracting agent are high affinity toward the target metals and their ability to form stable insoluble compounds. In this context, Schiff base macroligands show great potential to act as extracting agents.[5–7] Schiff base condensation reactions have been used to produce a large number of macroligands or receptors that form metal complexes with different stabilities according with the nature of the ligands and the preferences of the metal ions to coordinate.[5,8–14]

The synthesis of new polyaza macrocyclic and their potential applications in areas such as environmental protection for the removal of heavy metals from contaminated effluents are themes of great interest. The synthesis of a polyaza receptor incorporating five nitrogens and a pyridyl unit to obtain the cyclic macroligand 3,6,9,12-tetraaza-4(1,2),11(1,2)-dibenzo-1(1,3)-pyridinacyclotridecaphane (**L2**) was previously reported. This ligand was capable of binding metal ions such as Ni(II), Pb(II) and Zn(II) to give high yields of fairly stable complexes at room temperature with 1:1 (metal:ligand) stoichiometry that were insoluble in water.[9,10,16]

As part of the ongoing development of new ligands, the goal of this work was to investigate the potential extracting properties of the acyclic and cyclic macroligands **L1** (*N*,*N*′-bis(2-aminobenzyl)-1,2-diaminoethane) and **L2** toward Cu(II), Ni(II), Cd(II), Zn(II) and Pb(II). These metals are usually reported in wastewater samples from some industries and creeks in Monterrey, Mexico. The capabilities of these ligands to minimize the metal concentration below the allowed limits by the Official Mexican Regulations for treated water discharge[17] were evaluated. The spectral characterization (infrared and MS), elemental analysis and the equilibrium constants determined by UV-vis and potentiometric titration of the complexes of Cu(II), Ni(II), Cd(II), Zn(II) and Pb(II) with **L1** and **L2** are also reported herein.

MATERIALS AND METHODS

All reagents of the highest available purity were obtained from Aldrich and used without further purification.

The UV–Vis spectra were recorded on a GBC Scientific Cintra 6 spectrometer and the IR spectra on an IR-FT Nicolet 550 Magna-IR spectrometer or an ATR-FT Perkin Elmer Spectrum 1. The ESI-TOF mass spectra were obtained using a Bruker Daltonics Data Analysis 3.3 instrument. The elemental analysis for C, H and N were performed using a Perkin Elmer 2400 Series II CHNS/O elemental analyzer. The metal ion concentrations were estimated using a GBC Scientific 932 AA atomic absorption spectrometer.

Synthesis of the macroligands and their complexes

The receptors **L1** and **L2** (Fig. 1) were synthesized according to published procedures.[15] Briefly, **L1** was synthesized by condensation reaction between 2-nitrobenzaldehyde and ethane-1,2-diamine followed by the selective reduction of the imine and nitrate groups using $NaBH_4$ in methanol and $NH_2NH_2 \cdot H_2O$ in ethanol, respectively. The **L2** cyclic ligand was produced in the template reaction between **L1** and 2,6-diformyl pyridine (DFP) using Mn(II) ions as the templating agent.

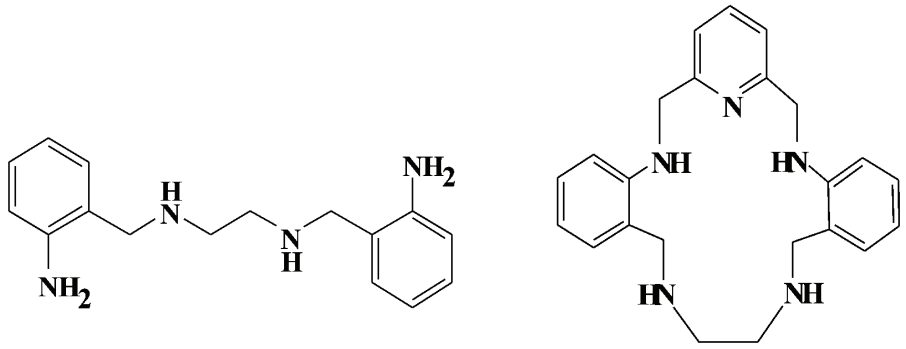

L1 **L2**

Fig. 1. Polyaza macroligand structures.

The complexes were prepared at room temperature by direct reaction between an ethanolic solution of the required ligand and an ethanolic solution of the appropriate metallic salt (either the nitrate or perchlorate) in a 1:1 mole ratio (M:L) (Eq. (1)):

$$mM + nL \rightarrow M_mL_n \quad (1)$$

where L is **L1** or **L2** and M is Cu(II), Ni(II), Zn(II), Cd(II) or Pb(II).

Ligand 1. A solution of **L1** (274 mg, 1 mmol) in EtOH (5 mL) was added to 5 mL of an EtOH solution of Ni(II), Cu(II), Zn(II), Cd(II) or Pb(II) (1 mmol) and the mixture was stirred for 30 min. The resulting product was then recrystallized from hot ethanol and finally dried in a vacuum desiccator.

Ligand 2. A solution of **L2** (373 mg, 1 mmol) in EtOH (4 mL) was added to 5 mL metal solution of Ni(II), Cu(II), Zn(II), Cd(II) and Pb(II) (1 mmol), and this mixture was stirred for 30 min. The resulting product was then recrystallized with hot ethanol and finally dried in a vacuum desiccator.

Elemental analysis, infrared and mass spectrometry studies were used to characterize the compounds. The stability constants of the colored complexes were determined at 25 °C by UV–Vis spectrophotometry with application of the Job Method.[18] Potentiometric titrations were used to characterize the uncolored complexes at 25 °C.[19]

Affinity studies and equilibrium constants.

The affinity of **L1** and **L2** toward the metals was determined based on the mole percentage of bound metallic ions.

The obtained complexes were filtered, washed with ethanol and after drying, the solids were weighed and a decimal part of each one was dissolved in the minimum amount of HNO_3 and the sample volume was made up to 50 mL with deionized water. A 1-mL aliquot of the

samples was taken and the volume adjusted to 25 or 100 mL with deionized water. The resulting solutions were analyzed by AAS in order to determine the mole percentage of bound metallic ion. All assays were performed in triplicate and the results are presented as mean values.

Application to the removal of heavy metals from water samples

The metals and their concentrations in synthetic water samples were based on previous analysis performed on real water samples.[20] The synthetic samples were a mixture of 0.0001 moles of one or more metal. With respect to the real waters, four samples were selected, two from industry, the third from the Topo Chico Creek, and the fourth from the Boca Lake, which is the main source of drinking water in Monterrey, Mexico. These samples were previously treated by ozonization to eliminate organic matter and, in the cases where this procedure failed, to acid digestion.[21] The pH of the solutions was adjusted to 5.5 before the addition of an excess of the corresponding receptor. The results of the characterization of the water samples are given in Table I. The concentrations of free metal ions were determined by AAS.

TABLE I. Characterization of crude water samples. Average value of the three determinations; "± confidence interval (P = 0.05; n = 3); Cd concentrations were below < 0.10 mg L^{-1}; ND: not detected

Sample	pH	Concentration, mg L^{-1}			
		Cu(II)	Ni (II)	Zn(II)	Pb(II)
Topo Chico	5.9	3.01±0.19	3.35±0.21	3.49±0.22	ND
San Juan River	6.1	2.96±0.23	2.20±0.18	2.65±0.21	ND
Industrial water 1	5.1	6.63±0.39	12.5±0.66	2.02±0.17	5.37±0.31
Industrial water 2	5.2	ND	24.0±1.20	72.0±3.6	ND

RESULTS AND DISCUSSION

All products were characterized by UV–Vis, IR and MS spectroscopy. The yields, colors, elemental analyses and mass spectrometry data of the ligands and their complexes are given in Table II. The receptors formed stable complexes with Cu(II), Ni(II), Zn(II), Cd(II) and Pb(II) at room temperature. The complexes were isolated in high yield (71–96 %) as colored crystalline mononuclear solids. The complexes of Cd(II) and Pb(II) with **L1** and **L2** were found to be soluble in methanol. The complexes of Cu(II), Ni(II) and Zn(II) with **L1** were soluble in acetonitrile and methanol while the complexes of Cu(II), Ni(II) and Zn(II) with **L2** were soluble in acetonitrile. Mass spectroscopy was used for the structural characterization of the solid products (Table II). The mass spectral data indicated complex formation since all the products showed a characteristic molecular ion (M^+) that represented the molecular ion peak of the complex. The mass spectra of **L1** and **L2** also showed a parent peak at m/z 271.4 and 374, respectively, corresponding to protonated **L1** and **L2**. Each of the complexes had a 1:1 (ligand:metal) stoichiometry. The formula is in agreement with the mass spectral data.

TABLE II. Physical properties, elemental analysis and mass spectrometry data of the ligands and their complexes

Compound	Yield %	Color	Elemental analysis			Mass spectrometry	
			Found (Calcd.), %			Molecular mass	Ion molecular fragment
			C	H	N		
L1	54	Pale	70.9	8.2	20.5	270.1	$[L1+H]^+$ (271)
$C_{16}H_{22}N_4$		yellow	(70.1)	(8.2)	(20.7)		
$[CuL1](NO_3)_2$	95	Dark	42.01	4.93	18.15	457.5	$[CuL1-2H]^+$
$C_{16}H_{22}N_6CuO_6$		blue	(41.92)	(4.84)	(18.30)		(332)
$[NiL1](NO_3)_2$	90	Lilac	41.86	4.81	18.28	453.1	$[NiL1-2H]^+$
$C_{16}H_{22}N_6NiO_6$			(42.42)	(4.89)	(18.44)		(327)
$[ZnL1](ClO_4)_2{\cdot}2H_2O$	93	Creamy	34.41	4.62	10.23	$[ZnL1](ClO_4)_2{\cdot}H_2O$	$[ZnL1]^+$ (335)
$C_{16}H_{22}N_4ZnO_8Cl_2$			(34.77)	(4.38)	(10.14)	(552.7)	$[ZnL1CLO_4-H]^+$ (433)
$[CdL1](NO_3)_2$	75	Creamy	38.20	4.38	16.43	–	–
$C_{16}H_{22}N_6CdO_6$			(37.92)	(4.30)	(16.58)		
$[PbL1](NO_3)_2$	90	White	31.40	3.62	13.83	601.6	$[PbL1-H]^+$
$C_{16}H_{22}N_6PbO_6$			(31.94)	(3.69)	(13.97)		(477)
L2	57	White	73.5	7.4	19.1	373.0	$[L2+H]^+$ (374)
$C_{23}H_{27}N_5$			73.6)	7.9)	(18.6)		
$[CuL2](NO_3)_2{\cdot}EtOH$	94	Green	49.43	5.50	16.49	607.1	$[CuL2-H]^+$
$C_{25}H_{33}CuN_7O_7$			(49.46)	(5.48)	(16.15)		(435)
$[NiL2](NO_3)_2{\cdot}EtOH$	88	Purple	49.43	5.50	16.49	602.3	$[ZnL2-H]^+$
$C_{25}H_{33}NiN_7O_7$			(49.86)	(5.52)	(16.28)		(436)
$[ZnL2](ClO_4)_2$	96	White	43.54	3.72	10.47	637.9	$[CdL2-H]^+$
$C_{23}H_{27}ZnN_5O_8Cl_2$			(43.31)	(4.27)	(10.98)		(484)
$[PbL2](NO_3)_2$	77	White	39.40	3.10	13.76	704.7	$[PbL2-H]^+$
$C_{23}H_{27}PbN_7O_6$.			(39.20)	(3.86)	(13.91)		(579)
$[CdL2](NO_3)_2{\cdot}EtOH$	71	Creamy	45.40	4.78	14.36	$[CdL2](NO_3)_2{\cdot}$	$[CdL2-H]^+$
$C_{25}H_{33}CdN_7O_7$			(45.77)	(5.07)	(14.95)	$\cdot EtOH$ (639.9)	(484)

Elemental analysis data were also obtained. The results were in good agreement with the formula. The structures of the ligands (**L1** and **L2**) and their complexes were also determined from their FT-IR spectra (Table III). The IR spectra of the free ligands were compared with those of the metal complexes to determine the bonding mode of the ligands to the metal in the complexes. In the IR spectral data of the ligands, strong bands for **L1** (3398 and 3316 cm^{-1}) and for **L2** (3420 and 3249 cm^{-1}) belong to the ν(N–H) vibration of the aromatic amine groups. In the spectra of complexes, these bands were shifted to lower frequencies. The IR spectra confirmed the existence of cyclic ligands in the complexes, by the presence of strong absorption bands at *ca*. 1600–1608 cm^{-1} and 1412––1510 cm^{-1}, expected for the two highest-energy pyridine or benzene ring vibrations.[22] All complexes showed weak to medium intensity bands in the region 710–1380 cm^{-1}, which were absent in the spectra of the free ligands; these can be attributed to (M–N). The absorptions of the counter ions (NO_3^- or ClO_4^-) pro-

vided some useful structural information. The IR spectra of the nitrate complexes showed bands at 1342–1322 cm^{-1} and *ca*. 1034 cm^{-1}, suggesting the presence of coordinated nitrate groups, as well as a band at *ca*. 1384 cm^{-1} attributable to NO_3^-. Thus, the IR spectra gave evidence that that the nitrate groups are involved in the coordination sphere of the metal ion. The IR spectra of the perchlorate complexes exhibited bands attributable to the asymmetric Cl–O stretching mode at 1088 cm^{-1} and the asymmetric Cl–O bending mode at 627 cm^{-1}.[23] The bands of the perchlorate complexes did not suggest interaction of perchlorate anions with the metal.[23] Therefore, it could be concluded that the **L1** and **L2** ligands bound to the metal ions through nitrate N groups. Spectroscopic studies and elemental analysis suggested a 1:1 metal–ligand ratio for all the formed complexes.

TABLE III. Frequencies of significant bands in the IR spectra of the ligands and their complexes; ν_s – symmetric stretching and ν_{as} – asymmetric streching

Compound	ν_s(N–H) and ν_{as} cm^{-1}	ν_s(C–N) cm^{-1}	ν_s(ArC=C) cm^{-1}	ν(free or coordinate anion) cm^{-1}
L1	3398, 3316	1627, 1502	1496, 1459	–
$[CuL1](NO_3)_2$	3266, 3195	1620,1581	1498, 1464	1381, 1334, 1094, 851, 826, 765 $\nu(NO_3^-)$
$[NiL1](NO_3)_2$	3311, 3260	1615, 1574	1497, 1412	1308, 1088, 1034, 852, 819 $\nu(NO_3^-)$
$[ZnL1](ClO_4)_2$	3333, 3295	1620, 1585	1499, 1460	1091, 624 $\nu(ClO_4^-)$
$[CdL1](NO_3)_2$	3430, 3293	1618	1498, 1458	1384, 1272, 1037, 843, 820 $\nu(NO_3^-)$
$[PbL1](NO_3)_2$	3350, 3264	1608	1496, 1456	1330, 1052, 825, 752 $\nu(NO_3^-)$
L2	3420, 3249	1604	1510,1433	–
$[CuL2](NO_3)_2 \cdot EtOH$	3150	1612	1500,1475	1359, 1332, 826, 740 $\nu(NO_3^-)$
$[CuL2](ClO_4)_2$	3262, 3251	1600	1501,1456	1090, 622 $\nu(ClO_4^-)$
$[NiL2](NO_3)_2 \cdot EtOH$	3278, 3230	1605	1471,1451	1388, 1322, 839,732 $\nu(NO_3^-)$
$[ZnL2](ClO_4)_2$	3290, 3250	1609	1497,1460	1094 $\nu(ClO_4^{-1})$
$[CdL2](NO_3)_2 \cdot EtOH$	3254, 3235	1603	1505,1470	1387, 1324, 1287, 828, 736 $\nu(NO_3^-)$
$[PbL2](NO_3)_2$	3283, 3215	1600	1504,1460	1372,1342, 1035, 740, 710 $\nu(NO_3^-)$

*Affinity of **L1** and **L2** toward Cu(II), Ni(II), Zn(II), Cd(II) and Pb(II)*

The interactions of **L1** and **L2** and the metal ions were studied by AAS (Table IV). The results suggested that these complexing agents have high affinity for the analyzed metals.

The order of affinity of **L1** toward the metals follows the Irving Williams series.[24] The affinity series took the following order: Cu(II) > Ni(II) > Zn(II) > > Cd(II) > Pb(II). With respect to the cyclic ligand **L2**, its selectivity and the

stability of its complexes could be related to the ionic radius of the metal[25] and the size of the ligand cavity. The highest stability of complexes was previously described as being when the ionic radius best fitted into the ligand cavity.[26] The affinity series took the following order for **L2**: Cd(II) > Cu(II) > Zn(II) > Ni(II) > > Pb(II).

TABLE IV. Percentage of metallic ion bounded to **L1** and **L2** receptors

Metallic ion	Ionic radii[24], Å	Ion to **L1**, %	Ion to **L2**, %
Cu(II)	0.73	99.2	98.6
Ni(II)	0.69	98.7	94.8
Zn(II)	0.78	97.9	97.1
Cd(II)	0.95	96.3	99.1
Pb(II)	1.55	92.7	85.4

Equilibrium constants

The equilibrium constants of the colored complexes were determined at 25 °C and pH 6.5 by UV–Vis spectrometry applying the Job method, and by potentiometric titration for the uncolored complexes under the same conditions. The constants reported in Table V (coefficient of variation (*CV*) < 5 %) indicated high stability for all complexes. so the receptors show potential usefulness as extracting agents for Cu(II), Ni(II), Zn(II), Cd(II) and Pb(II). Metal–ligand ratio was confirmed to be 1:1 in all cases, as shown in Fig. 2 for CuL1 and CdL1.

TABLE V. Equilibrium constants of complexes with L1 and L2; average value of the three determinations

Complex	$K_{fML} \times 10^{-5}$	*CV*
[CuL1]	166	4.0
[NiL1]	158	4.43
[ZnL1]	11.5	3.63
[CdL1]	1.76	4.44
[PbL1]	0.291	4.47
[CuL2]	226	4.2
[NiL2]	15.4	4.26
[ZnL2]	73.7	4.07
[CdL2]	97.0	4.03
[PbL2]	1.66	4.00

***L1** and **L2** as extracting agents*

The study of macroligands **L1** and **L2** as extracting agents was performed on synthetic and real water samples based on triplicate analyses. Synthetic water samples with a mixture of two, three or four heavy metals were prepared according to the concentration reported in a previous analysis performed on real waters (data not shown). The initial metal concentrations were 29.0, 23.4, 36.5, 22.2 and 39.0 mg L^{-1} for Cu(II), Ni(II), Cd(II), Zn(II) and Pb(II), respectively; the pH of

the solutions was in the range of 4.9–6.5. The complexing agents were added in excess. On increasing the metal ions concentration, the ligands functioned efficiently over a wide range of concentrations up to 100 mg L^{-1} for Cu(II), Ni(II), Cd(II), Zn(II) and Pb(II) ions (data not shown). The free metal ion concentrations in solution after treatment with the macroligands **L1** and **L2** were determined by AAS (*CV* < 5%). The receptor tendencies to bind each metal ion are shown in Figs. 3a–3d. In all cases, the ligands were able to minimize the metal concentration to below the limit allowed by the Official Mexican Regulation for treated water discharge (daily averages, in mg L^{-1} are: Cu, 1.5; Ni, 6; Zn, 9; Cd, 0.75 and Pb, 1.5).[17]

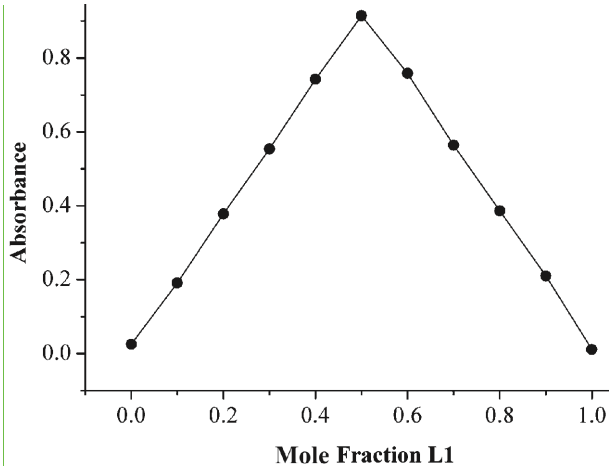

(a)

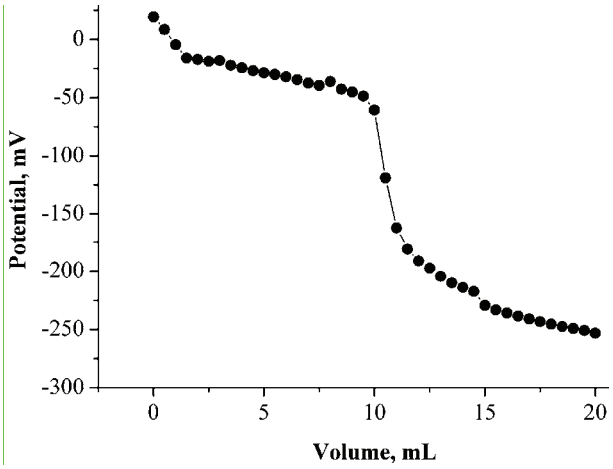

(b)

Fig. 2. a) Job's method for CuL1 complex and b) potentiometric titration for CdL1.

L1 and **L2** were essentially similar in the efficiency of metals affinity to bond complexes in both single and multiple metal solutions. Ligand **L1** was associated with a higher effectiveness for the removal of the evaluated metal ions compared with ligand **L2**, especially for Ni(II) and Pb(II) (Fig. 3). Thus, even without direct evidence, it could be suggested that one ion is too large and the other is too small for the cavity of ligand **L2**, reducing slightly the stability of such complexes.

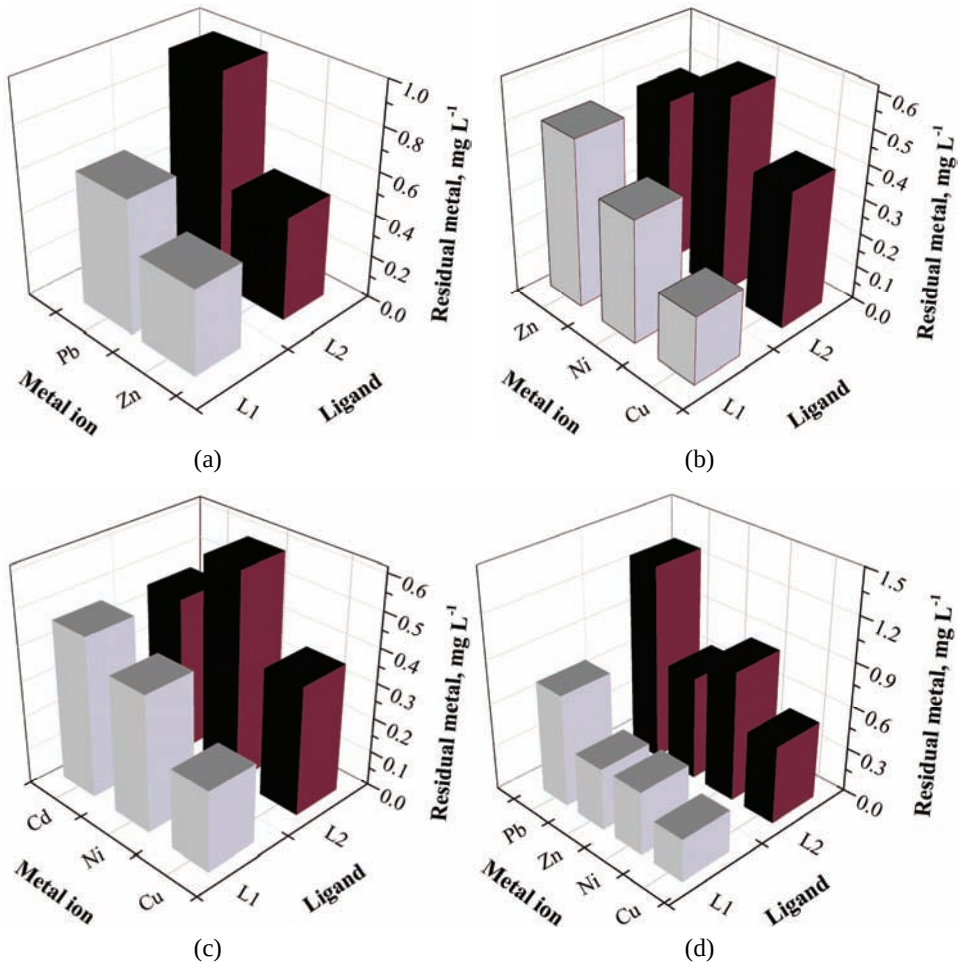

Fig. 3. Residual metal concentration in the synthetic water samples containing mixture of metals treated with receptors **L1** and **L2**: a) two metals, b–c) three metals and d) four metals.

The ligands **L1** and **L2** were evaluated for their ability as extracting agents to remove Cu(II), Ni(II), Zn(II) and Pb(II) from real water samples. Cadmium was not considered in this study since the initial concentration of Cd(II) in the

real water samples was below the detection limit. There were no significant differences in the results obtained for the real water samples (Table VI) compared to synthetic water samples (Table IV).

TABLE VI. Residual concentration of metals in crude water samples after adding **L1** and **L2**; the receptor was added in excess; confidence interval (P = 0.05; n = 3); ND: not detected

Sample	Concentration, mg L^{-1}			
	Cu(II)	Ni (II)	Zn(II)	Pb(II)
L1–Topo Chico	0.38±0.04	0.46±0.04	0.50±0.05	ND
L1–San Juan River	0.38±0.03	0.42±0.04	0.44±0.04	ND
L1–Industrial water 1	0.33±0.03	0.43±0.04	0.59±0.05	0.91±0.09
L1–Industrial water 2	ND	0.42±0.04	0.42±0.04	ND
L2–Topo Chico	0.39±0.03	0.41±0.04	0.47±0.04	ND
L2–San Juan River	0.39±0.04	0.45±0.04	0.43±0.04	ND
L2–Industrial water 1	0.40±0.04	0.60±0.05	0.54±0.05	1.54±0.12
L2–Industrial water 2	ND	0.42±0.04	0.44±0.04	ND

These findings indicated that **L1** is a better extracting agent than **L2**. In addition, ligand **L1** was efficiently synthesized in a relatively simple procedure compared to **L2** since **L1** was the precursor of **L2**.

CONCLUSIONS

Elemental analyses, and spectroscopic data of the metal complexes confirmed that the metal:ligand ratio of the complexes with **L1** and **L2** were 1:1. The IR data of both the Schiff bases and their metal complexes showed that the **L1** and **L2** were coordinated to the metal ion through the nitrogen atom of the nitrate group. The complexing agents **L1** and **L2** were demonstrated to be efficient extraction agents for lowering metal ion concentrations of Cu(II), Ni(II), Cd(II), Zn(II) and Pb(II) in real water samples. The results demonstrated that the receptors minimized the concentrations of the metals to below the allowed limits of the Official Mexican Regulations[17] for treated water discharge. **L1** seemed to be better agent because it minimized the concentration of all metals to lower values than **L2** did. The results showed that a high removal efficiency of heavy metals from wastewaters could be achieved by receptors **L1** and **L2**. These extraction experiments will serve as an initial evaluation of the capabilities of polyaza receptors for the removal of heavy metals from environmental water samples.

ИЗВОД

ПОЛИАЗНИ МАКРОЛИГАНДИ КАО ПОТЕНЦИЈАЛНИ АГЕНСИ ЗА УКЛАЊАЊЕ ТЕШКИХ МЕТАЛА ИЗ ОТПАДНИХ ВОДА

PERLA ELIZONDO MARTÍNEZ[1], BLANCA NÁJERA MARTÍNEZ[1], NANCY PÉREZ RODRÍGUEZ[1], LAURA HINOJOSA REYES[1] и MA. ISABEL GÓMEZ DEL RÍO[2]

[1]Universidad Autonoma de Nuevo Leon, UANL, Chemistry School of Sciences, Avenida Universidad S/N, Cd. Universitaria, 66450 San Nicolas de los Garza, NL, Mexico, и [2]Universidad Nacional de Educación a Distancia, Madrid, España Paseo Senda del Rey # 9, 28040 Madrid, Spain

Два полиазна макролиганда *N,N*′-бис(2-аминобензил)-1,2-етандиамин (L1) и 3,6,9,12-тетрааза-4(1,2),11(1,2)-дибензо-1(1,3)-пиридинациклотридекафано (L2) карактерисани су и испитивани на способности екстракције металног јона. Природа свих комплекса установљена је спектроскопским техникама. Константе равнотеже су одређене спектрофотометријски и потенциометријски, а концентрација остатка метала у раствору атомском апсорпционом спектрометријом (ААС). Капацитет лиганада да уклоне тешке метале као што су Cu(II), Ni(II), Cd(II), Zn(II) и Pb(II) као нерастворне комплексе испитан је у отпадној води индустријских ефлуената. Ови агенси су показали висок афинитет према испитиваним металима. Вредности константи равнотеже изолованих комплекса (од 1×10^4 до 2×10^7) показали су употребљивост ових хелатних агенаса као једну од алтернатива за уклањање тешких метала из индустријских ефлуената.

(Примљено 28. фебруара, ревидирано 9. априла 2012)

REFERENCES

1. S. Babel, T. A. Kurniawan, *J. Hazard. Mater.* **97** (2003) 219
2. T. A. Kurniawan, G. Y. S. Chan, W. H. Lo, S. Babel, *Chem. Eng. J.* **118** (2006) 83
3. Z. X. Quan, H. J. La, Y. G. Cho, M. H. Hwang, L. S. Kim, S. T. Lee, *Environ. Technol.* **24** (2003) 369
4. B. Dede, F. Karipcin, M. Cengiz, *J. Chem. Sci.* **121** (2009) 163
5. A. Freiría, R. Bastida, L. Valencia, A. Macías, C. Lodeiro, H. Adams, *Inorg. Chim. Acta* **359** (2006) 2383
6. V. Gasperov, S. G. Galbraith, L. F. Lindoy, B. R. Rumbel, B. W. Skelton, P. A. Tasker, A. H. White, *Dalton Trans. 1* (2005) 139
7. C. B. Squires, W. Christopher, J. Campbell, L. F. Lindoy, H. McNab, A. Parkin, S. Parsons, P. A. Tasker, W. Gang, D. J. White, *Dalton Trans.* **16** (2006) 2026
8. C. Núñez, R. Bastida, A. Macías, L. Valencia, J. Ribas, J. L. Capelo, C. Lodeiro, *Dalton Trans.* **39** (2010) 7673
9. H. Adams, B. Nájera, *J. Coord. Chem.* **56** (2003) 1215
10. J. R. Anacona, R. Durán, B. Nájera, C. Rodríguez, *J. Coord. Chem.* **58** (2005) 1395
11. J. R. Anacona, T. Martell, I. Sanchez, *J. Chil. Chem. Soc.* **50** (2005) 375
12. M. C. Fernández-Fernández, R. Bastida, A. Macías, L. Valencia, P. Pérez-Lourido, *Polyhedron* **25** (2006) 783
13. M. C. Fernández-Fernández, R. Bastida, A. Macías, L. Valencia, P. Pérez-Lourido, *Polyhedron* **27** (2008) 2301
14. S. G. Galbraith, Q. Wang, L. Li, A. J. Blake, C. Wilson, S. R. Collinson, L. F. Lindoy, P. G. Plieguer, M. Schroder, P. A. Tasker, *Chem. Eur. J.* **13** (2007) 6091
15. S. Kulaksizoğlu, R. Gup. *Chem. Pap.* **66** (2012*)* 194

16. P. Elizondo, *PhD Thesis*, Digital journals UNED, Madrid, Spain, 2007, http://e--spacio.uned.es/fez/view.php?pid=bibliuned:19848 (accessed 17 February 2012).
17. Mexican Official Norm; NOM-002-SEMARNAT-1996, *On the limits of polluting agents in residual unloadings to the sewage system*, Federal Office of the Judge Advocate General for the Protection of the Atmosphere, 1998
18. L. L. Lu, Y.-H. Li, X. Y. Lu, *Spectrochim. Acta, A* **74** (2009) 829
19. M. S. Brandon, A. J. Paszczynski, R. Korus, R. L. Crawford, *Biodegradation* **14** (2003) 73
20. E. Soto, R. C. Miranda, C. A. Sosa, J. A. Loredo, *Inf. Technol.* **17** (2006) 33
21. L. S. Clesceri, A. E. Greenberg, A. D. Eaton (Ed). *Standard Methods for Examination of Water and Wastewater*, 20th ed., American Public Health Association, Washington DC, 1998, p. 6
22. C. Lodeiro, R. Bastida, E. Bértolo, A. Macías, A. Rodríguez, *Transition Met. Chem.* **28** (2003) 388
23. L. De Cola, D. L. Smailes, L. M. Vallarino, *Inorg. Chem.* **25** (1986) 1729
24. F. Li, R. Delgado, J. Costa, M. G. B. Drew, V. Félix, *Dalton Trans. 1* (2005) 82
25. R. D. Shannon, *Acta Crystallogr., A* **32** (1976) 751
26. M. G. Drew, J. Nelson, S. M. Nelson, *J. Chem. Soc., Dalton Trans.* **8** (1981) 1685.

Journal of the Serbian Chemical Society
JSCS@tmf.bg.ac.rs • www.shd.org.rs/JSCS
J. Serb. Chem. Soc. 78 (4) 603–609 (2013)
UDC 543+061.3(4)
EuCheMS news

DIVISION OF ANALYTICAL CHEMISTRY
EUROPEAN ASSOCIATION FOR CHEMICAL AND MOLECULAR SCIENCES

EUCHEMS NEWS

European Analytical Column No. 41

JENS E.T. ANDERSEN[1], WOLFGANG BUCHBERGER[2]* and PAUL WORSFOLD[3]

[1]Department of Chemistry, Technical University of Denmark, Kemitorvet building 207, DK-2800 Kgs. Lyngby, Denmark (jeta@kemi.dtu.dk), [2]Analytische Chemie, Universität Linz, Altenbergerstrasse 69, A-4040 Linz, Austria and [3]School of Geography, Earth and Environmental Sciences, Plymouth University, Plymouth PL4 8AA, UK (pworsfold@plymouth.ac.uk)

1. A PERSONAL VIEW ON QUALITY ASSURANCE

Jens E.T. Andersen

1.1. Scientific results

The European Commission's EURAMET and IMEP programmes,[1–2] together with IRMM,[3] have elucidated the challenges related to reaching compliance between results for the same sample obtained in different laboratories (industrial and/or academic). Inter-laboratory comparisons showed that costumers had a high risk of receiving significantly different results from independent professional laboratories, which should not happen given the advanced technologies available in contemporary analytical chemistry laboratories. It was further demonstrated that results differed significantly not only when samples were analysed by different instruments and procedures but also when analysed by identical methodologies. It seemed that this was a genuine scientific issue that needed attention from scientists able to evaluate accepted statistical procedures. As a first approach the celebrated EURACHEM/CITAC guide[4] to quantify uncertainty in analytical measurements and the VIM guide[5] allowed scientists to check the traceability of measurements by establishing uncertainty budgets for their methods. The introduction of the concept 'uncertainty' is now a key factor in experimental work. Secondly, the concept of certified reference materials was introduced and is now an integral aspect of analytical chemistry and a growing in-

* Corresponding author. E-mail: wolfgang.buchberger@jku.at

dustry where certificated values for many analytes in various mixtures (matrices) are available. The latter approach has provided much greater confidence in many analytical methods. The philosophy of measurement is that the true amount of an analyte in a sample is not known but everyone makes a reliable estimate of the amount and the uncertainty of measurement is also estimated correctly. The result obtained as the mean value from results submitted by several laboratories is then announced as the consensus value. Right or wrong, the result represents the combined effort of all laboratories and all results have the same eligibility since they belong to the same distribution. With this philosophy of 'consensus science' in mind it becomes possible to arrive at compliance or agreement between analytical results; an idea which also has significance beyond the analytical community itself. Consensus science should be discussed as a future framework for scientific methodology.

1.2. Operational calibrations

Construction of calibration lines or regression lines is a key operation in analytical chemistry; it is widely believed that the operational calibration takes care of day-to-day variations of the apparatus sensitivity, which allows one to eliminate the influence of the apparatus on the result. Although some variations of the apparatus are eliminated by the operational calibration, it is still not possible to explain large uncertainties observed for results obtained on different days as compared with the uncertainty predicted by the parent uncertainty budget. There are several explanations as to these discrepancies, one of which is related to systematic errors. It is a well-known fact that no apparatus displays a linear response. The response is always non-linear, and analytical chemists frequently identify the linear range of calibrations by means of an intuitive feeling. Since the full extension of the regression line must be evaluated on the basis of uncertainty, the extension of the calibration line could be estimated by considering the difference, in terms of uncertainty of fitting parameters, between using a straight line and, for example, a second order polynomial. However, differences and decisions can only be made when the data set has a certain magnitude. It is recommended that the central limit theorem is strictly followed during method validations, which means that at least one hundred repetitions are required in order to provide a reliable estimate of standard deviation. In fact two hundred repetitions are required to obtain a standard deviation that is correct with 95 % probability. Another reason for systematic deviations is related to ordinary-linear regression (ODL) as opposed to orthogonal-linear regression (OLR).[6] The former is nearly always used in analytical chemistry because it is an option available in most software packages and spread sheets. It is anticipated that systematic differences introduced by using ODL instead of OLR is not a serious problem in comparison with other systematic errors that follow routine work in the laboratory. The ODL

proposed by Currie and Danzer[6] predicts a centroid value at which concentration the confidence band has a minimum that has not been verified experimentally; a peculiarity of the model. Weighted-linear regression (WLR) relies on the assumption that variance is uniform and independent of concentration, which has never been verified experimentally. Therefore WLR cannot be recommended; not only for this reason but also because the outcome of WLR is weighted uncertainty that is impossible to report to costumers unless the data are re-calculated using an un-weighting scheme. This makes WLR laborious, inconvenient and an unsuitable alternative as it does not provide results different from those of OLR.[7] These examples indicate that some of the systematic errors associated with the straight line are of relatively minor importance to accuracy in analytical chemistry, and they cannot explain the large variations in results found by inter-laboratory exercises.

1.3. Uncertainty and outliers

Uncertainty of measurement has replaced the concept of error of measurement because errors are not supposed to influence the result; rather they should be discarded. In addition, the term "random errors" creates an incorrect impression and the term "uncertainty" is therefore recommended. Despite the importance of the concept of uncertainty it is considered an inconvenience to many scientists because there are many ways to approach it and it can greatly increase the amount of work involved in evaluating the results.

For the sake of simplification only two schools of estimating uncertainty are considered: The IUPAC method and the method introduced by EURACHEM/ /CITAC. The majority of professional laboratories follow the directives of the IUPAC methodology[6] that is represented in ISO standards, ISO 5725, ISO 17025 and others. These guidelines and standards have many positive aspects and include several examples but some of the concepts and procedures are outdated, such as error of measurement and true value, and the issue of sampling is not considered. Further, ISO recommends outlier rejection and the guidelines introduce procedures for outlier testing which may be a cause for concern. Rejection of outliers requires that two laboratories comparing independent measurements on the same sample must reject any observed outliers in such a manner that neither the mean value nor the standard deviations are influenced by the rejection. Otherwise they will inevitably arrive at significantly different results. This situation is very likely, particularly when a low number of repetitive measurements are made. The main reason to retain outliers rather than rejecting them is that outliers inherently possess important information about the actual performance of the method with respect to accuracy. In brief, it can be stated that rejection of outliers promotes disagreement and it is recommended never to reject outliers. Errors should be reported and discarded from a data set but outliers must

be left unaltered. Rejection of outliers depends on uncertainty of measurement; a concept that is treated by both the ISO guides and by the EURACHEM/CITAC guide.[4] An uncertainty budget and expanded uncertainty are the main concepts introduced by the EURACHEM/CITAC guide[4] with the intention of ensuring traceability and reliability and creating an overview of all uncertainty contributions. The combined uncertainty obtained by the uncertainty budget is multiplied by a factor of two, referring to student's *t*-value at a very high number of repetitions, to yield the expanded uncertainty. The expanded uncertainty corresponds to the 95 % confidence range and it covers 95 % of all measurements, which is an advantage when reporting results to customers. In an extension of the efforts by EURACHEM and CITAC, it is suggested that statistical control is obtained when the uncertainty of calibrations corresponds to the uncertainty of repetitions, and hence is a worthwhile addition to the protocol.

1.4. Statistics revisited

A potential problem with the application of statistical methods in Analytical Science is related to the concept of short-term precision *versus* long-term precision. Many scientists assume that one type of precision prevails but this is nowhere near the truth. Contemporary digital-data acquisition can be performed at very high rates; under normal laboratory conditions sampling rates of millions of samples per second are possible. Sampling data at very high rates allows the collection of large amounts of data within a short period of time, which in terms of the central-limit theorem of statistics, fulfills all the requirements to produce a valid and reliable value of precision; a precision that may be expressed in terms of a measurement uncertainty. This type of precision we denote as the short-term precision whereas the long-term precision is of a completely different nature, with a much higher uncertainty than that of short-term precision. The long-term precision is determined on the basis of multiple independent series of measurements where a shut-down and turn-on sequence is performed between each series. Such an operation challenges the apparatus in a manner much different from that of short-term precision. Although operational calibrations are performed on a daily basis there is no guarantee that the apparatus produces the same concentration of the unknown every day. The concentration of the unknown is, to some extent, un-correlated with the characteristic parameters of the calibration curve, *e.g.*, with the slope of a calibration line. That is within certain limits of long-term precision. Statistics works equally well for both short-term precision and long-term precision but statistics cannot account for accuracy; the true concentration is an unknown quantity that can only be estimated by multiple independent measurements. The true value is a matter of consensus and not statistics. Manipulation of data in science is not allowed but removal of outliers from a data set is an option that is sustained by ISO. This can be a serious problem in Analytical Che-

mistry. Certificates of certified reference materials show those outliers of "poor laboratories" that were removed in order to arrive at the final consensus value. The question is: How can the manufacturer of the reference material make sure that the laboratory using the product removes the same number of outliers when it tries to reproduce the results? Some manufacturers of CRMs supply information about the data set both before and after the removal of outliers and they also clearly state the number of results used for calculation of the certified value, making it easy to compare laboratory result to the certified value. Reporting data sets before and after the selection of outliers should be general practice in science or, alternatively, a comment should be made in the text if no outliers have been removed from the data set. Both outlier rejection and confusion between short-term precision and long-term precision may help to explain the large deviations observed in inter-laboratory tests.

1.5. Conclusions

The search for compliance, both with respect to consensus values and with respect to uncertainty of measurement, is not yet complete. There are several peculiarities in Analytical Science that can lead scientists in the wrong direction when they search for accuracy of measurements. Eventually, customers and colleagues are interested in accuracy in preference to precision. Generally, a customer cares less about the performance of the apparatus but focuses on the validity of the result. It has been proven by inter-laboratory tests that independent laboratories produce different results and different uncertainties. It is a challenge to Analytical Chemistry, as well as to related fields of science, to promote scientific methodology in order to reach compliance. Two sets of apparatus of the same type measuring the same measurand can produce significantly different results and the discrepancy increases when more repetitions are performed simply because the confidence band narrows as a function of the inverse-square root of the number of repetitions. This is a scientific paradox that originates from small differences between sets of apparatus that lead to a difference in accuracy. This paradox needs be resolved before we can explain all of the deviations of inter-laboratory tests. Such actions benefit Analytical Chemistry and it is much more rewarding to scientists to discuss genuine topics related to mechanisms of nature rather than focusing on differences that may readily be explained by uncertainty of measurement. Consensus science might be the way ahead.[8–9]

2. INFORMATION FROM THE **EU**C**HE**M**S** DIVISION OF ANALYTICAL CHEMISTRY (DAC)

Wolfgang Buchberger

The DAC Annual Meeting 2012 was held in Prague on 26 August, 2012. It coincided with the 4th EuCheMS Chemistry Congress in Prague. Many thanks are

due to Jiri Barek, who hosted the Annual Meeting and was also a member of the local organizing committee of the EuCheMS conference.

Within this Meeting, the „DAC Tribute“ was awarded to Prof. Yuri Zolotov (Moscow State University) for his long, committed involvement in DAC and his professional contributions to various DAC working groups and Euroanalysis conferences.

DAC activities, together with strategic planning, are coordinated by the DAC Steering Committee. In 2012 it consisted of Paul Worsfold (Chair of DAC, UK), Jens Andersen (Secretary of DAC, Denmark), Wolfgang Buchberger (Austria), Slavica Razic (Serbia), Jiri Barek (Czech Republic) and Majiej Jarocz (Poland). The Annual Meeting delegates endorsed the proposal that Wolfgang Buchberger takes over as Secretary in 2013. DAC is indebted to Jens for his efficient work as Secretary during the last five years. The vacant position on the Steering Committee will be taken by Christian Rolando (France) who will be co-organiser of the Euroanalysis 2015 conference in Bordeaux. Further details of DAC activities can be found at http://www.euchems.eu/divisions/analytical-chemistry.html.

In 2012 the Steering Committee had meetings in Warsaw, 27 April (together with a meeting of the Euroanalysis Presidium), and in Prague (25 August). Another meeting of the Chair and the Secretaries took place in Copenhagen (5 July). Among other things, the DAC strategy for the years 2012–2014 has been drafted which has been accepted by the delegates at the Annual Meeting.

For 2013, DAC has the following Study Groups: Education in Analytical Chemistry (R.Salzer), Quality Assurance and Accreditation (J. Andersen, H. Emons as liaison person to CITAC), History (D.T.Burns), Bioanalytics (G. Horvai), Chemometrics (R.Tauler). It was decided to close the Study Group European Analytical Chemistry on the Web, which had been headed by B. Karlberg. Efforts have been made to establish a new task force on Archaeometry and Cultural Heritage in Analytical Chemistry.

Several events have been organized in cooperation with DAC-EuCheMS during the year 2012; Isranalytica, 24–25 Januray (Tel-Aviv, Israel), 12th Eurasia Conference on Chemical Sciences, 16–20 April (Corfu, Greece), Analysdagarna, 11–13 June (Uppsala, Sweden), 1st International Congress on Analytical Chemistry, 18–21 September (Targoviste, Romania), and the European Chemistry and Chemical Engineering Education Network EC2E2N.

One of the main activities of DAC in 2013 will be the promotion and support of the Euroanalysis conference 2013, 25–29 August, Warsaw. The Chairpersons Maciej Jarosz and Ewa Bulska are working hard to provide a perfect environment for a high-quality analytical conference. Further details can be found at www.euroanalysis2013.pl. We invite all analytical chemists to participate in this event, to present their scientific work, and to strengthen the network in Analytical

Sciences. Euroanalysis 2013 will also be the event at which the Annual Meeting 2013 of DAC will be held.

REFERENCES

1. S. Davidson, *Metrologi*a, **48** (2011) Suppl. S, Article Number: 07005, DOI: 10.1088/ /0026-1394/48/1A/07005.
2. A. Lamberty, P. de Bievre, J.R. Moody, *At. Spectr*. **15** (1994) 107
3. European Commission's Joint Research Centre, Institute of Reference Materials and Measurements, http://irmm.jrc.ec.europa.eu/ (accessed on March 5, 2013)
4. A. Williams, S. Ellison, R. Bettencourt da Silva, W. Bremser, A. Brzyski, P. Fodor, R. Kaarls, R. Kaus, B. Magnusson, E. Amico di Meane, P. Robouch, M. Rösslein, A. van der Veen, M. Walsh, W. Wegsheider, R. Wood, P. Yolci Omeroglu, A. Squirrell, I. Kuselman, A. Fajgelj, M. Golze, *EURACHEM/CITAC Guide CG 4, Quantifying Uncertainty in Analytical Measurements*, 3rd ed.,. http://www.citac.cc/QUAM2012_P1.pdf (accessed on March 5, 2013)
5. http://www.bipm.org/utils/common/documents/jcgm/JCGM_200_2012.pdf (accessed on March 5, 2013)
6. K. Danzer, L.A. Currie, *Pure Appl. Chem.* **70** (1998) 993
7. A. C. Raffalt, J. E.T. Andersen and S. Christgau, *Anal. Bioanal. Chem.* **391** (2008) 2199
8. http://www.analytisk.kemi.dtu.dk/ (accessed on March 11, 2013)
9. J. E.T. Andersen, M. Mikolajczak, K. O. Wojtachnio-Zawada and H. V. Nicolajsen, *J. Chromatogr*., *B* **908** (2012) 122.